STUDIES OF RHODIUM, PLATINUM AND PALLADIUM DERIVATIVES OF SOME ARSENA-, CARBA- AND TELLURABORANES

by

Denis Patrick O'Connell, B.Sc., MICI, CChem, MRSC,
Department of Chemistry,
University College,
Cork.

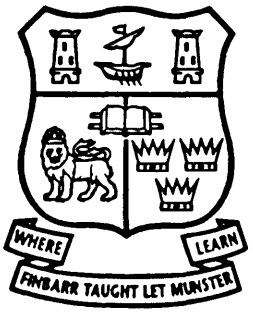

Being a thesis submitted for the degree of

DOCTOR OF PHILOSOPHY

to

THE NATIONAL UNIVERSITY OF IRELAND

Based on research carried out under the direction of

Professor T. R. Spalding
Department of Chemistry
University College
Cork

August 1994

ABSTRACT

The research described in this thesis involved the synthesis and characterisation of rhodium, platinum and palladium derivatives of arsena-, carba- and telluraboranes.

Chapter One summarises the chemistry of group V/15 (excluding nitrogen) heteroboranes and their metal derivatives.

Chapter Two describes a theoretical investigation of the electronic structure and bonding of the closely related eleven-vertex *nido*-heteroborane dianions [7,8-$C_2B_9H_{11}]^{2-}$, [7,9-$C_2B_9H_{11}]^{2-}$, [1,7-$C_2B_9H_{11}]^{2-}$, [4,7-$C_2B_9H_{11}]^{2-}$, [7,8-$P_2B_9H_9]^{2-}$, [7,9-$P_2B_9H_9]^{2-}$ and [7-$SB_{10}H_{10}]^{2-}$. These compounds were studied with MNDO calculations in which the geometries were optimised with no restriction on the (3N-6) degrees of freedom of the molecules. In all the *nido* systems studied the calculated bond lengths were in good agreement with the related experimental data. The heats of formation were calculated. The MNDO calculations showed that, as expected, there were thirteen *i.e.* n+2, cluster molecular orbitals in each cage. On the basis of the charge distribution, all seven *nido* anions would be expected to react at the open face with $[ML_n]^{2+}$ electrophiles. Both the nature of the homo or shomo and the energy difference between them have significance in determining the configurations of metal units such as $Pt(PR_3)_2$ and $Rh(PR_3)_2H$ above the heteroatom faces to which they are attached in twelve atom *closo* complexes. The orientation of the $Pt(PR_3)_2$ or $Rh(PR_3)_2H$ metal unit above the top face of the molecule may be predicted for complexes of all seven dianions.

Chapter Three is concerned with microwave heating effects and their application to synthetic metallaborane chemistry. This chapter initially reviews the relatively new area of the application of microwave heating effects to synthetic chemistry. Subsequently the modifications required to enable the safe adaptation of a conventional microwave oven for chemical reactions is described in detail for both low and high pressure systems. In sealed vessel reactions which generally occur at high pressure, microwave dielectric heating techniques have the ability to reduce the reaction time by a factor of up to 10^3. Chapter Four is concerned with the synthesis of platinum derivatives of $C_2B_9H_{11}$, $As_2B_9H_9$ and $TeB_{10}H_{10}$ ligands. Reactions were carried out under normal (thermal) conditions and in the high-pressure microwave

apparatus described in chapter three. The products synthesised were three new platinacarboranes, *closo*-[3,3-$(PMe_2Ph)_2$-3,1,2-$PtC_2B_9H_{11}$] (1), *closo*-[2,2-$(PMe_2Ph)_2$-2,1,8-$PtC_2B_9H_{11}$] (2) and *closo*-[8-Ph-2,2-$(PMe_2Ph)_2$-2,1,8-$PtC_2B_9H_{10}$], and the previously known compounds, *closo*-[3,3-$(PMe_2Ph)_2$-3,1,2-$PtAs_2B_9H_9$] and *closo*-[2,2-$(PMe_2Ph)_2$-2,1-$PtTeB_{10}H_{10}$]. Where previously the direct reaction between simple starting materials has been kinetically slow *eg.* in the present case six days for the reaction of *nido*-$[7,8\text{-}C_2B_9H_{12}]^-$ and *cis*-$[Pt(PMe_2Ph)_2Cl_2]$, the microwave technique speeds up the process to 30 minutes. This leads not only to a considerable saving in time but also to a marked improvement in the overall reaction yield in certain reactions. In the present study isomeric products (1) and (2) from *nido*-$[7,8\text{-}C_2B_9H_{12}]^-$ and *cis*-$[Pt(PMe_2Ph)_2Cl_2]$ and the rearrangement product *closo*-[8-Ph-2,2-$(PMe_2Ph)_2$-2,1,8-$PtC_2B_9H_{10}$], from *nido*-$[7\text{-Ph-}7,8\text{-}C_2B_9H_{11}]^-$ and *cis*-$[Pt(PMe_2Ph)_2Cl_2]$ were formed from reactions performed under microwave irradiation. Experiments carried out on the parent carborane starting materials show that these materials do not isomerise under the conditions used for the microwave syntheses. The compounds were characterised by IR and NMR spectroscopy and the compounds (1) and (2) were studied by X-ray diffraction methods. An important feature of the NMR spectra of both (1) and (2) were that both compounds were fluxional. Single crystal X-ray analyses of (1) and (2) showed that both compounds had a *closo* twelve vertex PtC_2B_9 geometry based on a distorted dodecahedron. From the X-ray determined crystal structure of (1) there were two molecules present in the unit cell which differed primarily in the platinum-carborane cage bond lengths and in the orientation of the platinum phosphine unit above the C_2B_3 faces. The small $\Delta G^{\ddagger}$ for the rotational process in (1) is of the same order of magnitude as crystal packing forces. With this low barrier any rotamer could in principle be observed in the solid state. The compound *closo*-[2,2-$(PMe_2Ph)_2$-2,1,8-$PtC_2B_9H_{11}$] (2) is only the third platina-carborane with non-directly bonded carbons in adjacent rings to be fully characterised. Compounds (1) and (2) provide a useful insight into the mechanism of the thermal rearrangement of icosahedral metallacarboranes and a detailed discussion of possible mechanisms based on data for rearrangements of carboranes is presented.

Chapter Five describes the syntheses and characterisation of three new metallaheteroborane complexes with metal halide bonds and two new cationic

complexes. The two rhodium chloride complexes *closo*-[3,3-$(PMePh_2)_2$-3-Cl-3,1,2-$RhC_2B_9H_{11}$] (3) and *closo*-[3,3-$(PMePh_2)_2$-3-Cl-3,1,2-$RhAs_2B_9H_9$] were synthesised from the reactions between $PMePh_2$, CH_2Cl_2 and *closo*-[3-{η^2-SC(H)NPh}-3-PPh_3-3,1,2-$RhC_2B_9H_{11}$] or *closo*-[3-{η^2-SC(H)NPh}-3-PPh_3-3,1,2-$RhAs_2B_9H_9$]. When the reaction of *closo*-[3-{η^2-SC(H)NPh}-3-PPh_3-3,1,2-$RhC_2B_9H_{11}$] was carried out with irradiation provided by a 60 Watt light there was a marked increase in the yield. The reaction of Tl[9-SMe_2-7,8-$C_2B_9H_{10}$] and [$Pd(PPh_3)_2I_2$] in refluxing CH_2Cl_2 resulted in the formation of *closo*-[3-PPh_3-3-I-4-SMe_2-3,1,2-$PdC_2B_9H_{10}$] (4). Two cationic metallacarboranes, *closo*-[3-PPh_3-3-Bu^tNC-4-SMe_2-3,1,2-$PdC_2B_9H_{10}$][BF_4]and *closo*-[3,3-$(PMePh_2)_2$-3-Bu^tNC-3,1,2-$RhC_2B_9H_{11}$][BF_4], were synthesised from reactions of *closo*-[3-PPh_3-3-I-4-SMe_2-3,1,2-$PdC_2B_9H_{10}$] and *closo*-[3,3-$(PMePh_2)_2$-3-Cl-3,1,2-RhC_2-B_9H_{11}]. Both reactions were carried out at ambient temperature in toluene with one equivalent of Ag[BF_4]. A slight excess of Bu^tNC was added immediately after precipitation of Ag[X] to stabilise the cationic products. Neither of the cationic compounds were stable in solution for more than 8 hours. Single crystal X-ray analyses of (3) and (4) were carried out to confirm the exact nature of the cluster and *exo*-cluster ligand bonding. All the above compounds were characterised by spectroscopic methods and elemental analysis.

In Chapter Six ten new isothiocyanate derivatives of rhodaheteroboranes were prepared. The synthesis and reactivity of twelve-vertex rhodaheteroborane clusters is reviewed. A brief introduction to the reactions of transition metal complexes with RNCS is given. Reactions between RNCS (R=Ph, *p*-tol and Bz) and Rh-H bonds in *closo*-[3,3-$(PPh_3)_2$-3-H-3,1,2-$RhAs_2B_9H_9$], *closo*-[2,2-$(PPh_3)_2$-2-H-2,1-$RhTeB_{10}H_{10}$] and *closo*-[3,3-$(PPh_3)_2$-3-H-3,1,2-$RhC_2B_9H_{11}$]were studied. The rhodaarsenaborane *closo*-[3,3-$(PPh_3)_2$-3-H-3,1,2-$RhAs_2B_9H_9$] was reacted with RNCS (R=Ph, *p*-tol and Bz) in CH_2Cl_2 to form three dithiocarbamato rhodaarsenaboranes *closo*-[3-{η^2-$S_2CN(H)R$}-3-(PPh_3)-3,1,2-$RhAs_2B_9H_9$] {R=Ph (5), *p*-tol and Bz} and three thioformamido rhodaarsenaboranes *closo*-[3-{η^2-SC(H)NR}-3-(PPh_3)-3,1,2-$RhAs_2$-B_9H_9] {R=Ph (6), *p*-tol and Bz}. Reaction of the rhodatelluraborane *closo*-[2,2-$(PPh_3)_2$-2-H-2,1-$RhTeB_{10}H_{10}$], and the rhodacarborane *closo*-[3,3-$(PPh_3)_2$-3-H-3,1,2-$RhC_2B_9H_{11}$] respectively with PhNCS afforded the two new rhodatelluraboranes, *closo*-[2-{η^2-$S_2CN(H)Ph$}-2-(PPh_3)-2,1-$RhTeB_{10}H_{10}$] (7) and *closo*-[2-{η^2-SC(H)NPh}-2-(PPh_3)-2,1-$RhTeB_{10}H_{10}$], and two new rhodacarboranes *closo*-[3-{η^2-SC(H)NPh}-3-(PPh_3)-

3,1,2-$RhC_2B_9H_{11}$] and *closo*-[3-{η^2-$S_2CN(H)Ph$}-3-(PPh_3)-3,1,2-$RhC_2B_9H_{11}$]. The reaction conditions were varied in order to maximise the yields of either the thioformamido or dithiocarbamato complexes. Under thermally induced reflux conditions, the reaction between the rhodium hydride complexes and RNCS (R=Ph, *p*-tol and Bz) in a 1:1 mole ratio afforded thioformamido {η^2-SC(H)NR} complexes as the major products. If an excess of isothiocyanate was used the major product was the dithiocarbamate {η^2-$S_2CNH(R)$} complex. Subjecting the reaction between the rhodacarborane *closo*-[3,3-(PPh_3)$_2$-3-H-3,1,2-$RhC_2B_9H_{11}$] and PhNCS in a 1:1 mole ratio in CH_2Cl_2 to microwave irradiation for 5 minutes produced *closo*-[3-{η^2-SC(H)NPh}-3-(PPh_3)-3,1,2-$RhC_2B_9H_{11}$] in 98.8% yield. Clearly the reaction carried out in the microwave oven afforded a marked improvement in the yield, fewer side products and required much less time. All of the new compounds were yellow/orange in colour and air-stable and were characterised by spectroscopic methods. In three cases, compounds (5), (6) and (7), the structures were elucidated by single crystal X-ray analyses. The successful solution and refinement of the molecular structures *closo*-[3-{η^2-SC(H)NPh}-3-(PPh_3)-3,1,2-$RhAs_2B_9H_9$] (6), *closo*-[3-{η^2-$S_2CN(H)Ph$}-3-(PPh_3)-3,1,2-$RhAs_2B_9H_9$] (5) and *closo*-[2-{η^2-$S_2CN(H)Ph$}-2-(PPh_3)-2,1-$RhTeB_{10}H_{10}$] (7) showed that all three compounds had a *closo* twelve-vertex geometry based on a distorted dodecahedron. Compounds (5) and (6) are the first reported X-ray crystal structures of rhodaarsenaboranes. Compound (6) appears to be the first reported {η^2-SC(H)NPh}Rh-containing structure. Infrared spectra of the compounds contained characteristic bands for the dithiocarbamate complexes which could be distinguished from thioformamido complexes. ^{13}C NMR spectroscopy clearly distinguishes the dithiocarbamate complexes from thioformamido complexes.

The X-ray analyses were carried out by Professor George Ferguson and Dr. John Gallagher, University of Guelph, Canada. The NMR data was collected by Mr. D. O'Leary, University College, Cork and by Dr. J. D. Kennedy, University of Leeds.

ACKNOWLEDGEMENTS

I would like to take this opportunity of saying a general "thank you" to all my friends at UCC and everyone who supported me during the last few years in completing this thesis. It is impossible to include everybody by name but I hope that as many people as possible are mentioned.

The first person to be thanked is my supervisor Professor Trevor Spalding for all his help and encouragement during the last few years. I would like to thank Prof. Hathaway for the use of his laser printer and for his help during my years at UCC. I would also like to acknowledge my research director Professor M.A. McKervey.

I am very grateful to Prof. George Ferguson and Dr. John Gallagher, University of Guelph, Ontario, Canada for all my crystal structures. I would also like to thank Dr. J.D. Kennedy, University of Leeds, England for recording NMR spectra.

Lab 343 has been my home away from home for some time now and it is only right to thank all my labmates that have passed through in the last few years, Anna, Anne-Marie, Brian, Carmel, Denis, Donogh, Ger, Jenny, Jim, Michael, Ros, Seamus, Siobhán, Susan and Trish.

A special mention is required for my proof readers Anne-Marie and Denis for all the time they have given to reading and correcting this thesis.

Most of the class of 89 have left UCC but I had a lot of friends that I would like to mention especially all "the lads", Colm O'Sullivan, Darragh, Denis, Kieran, Michael Moore, Michael Murphy, Neal, Noel and Phil. I would also like to thank my fellow postgraduate students for all their friendship during my time at UCC, Kevin Crowley, Pat Field, Liz Horne, Margaret O'Leary, Kevin Manley and Dave Mulcahy.

The staff of the chemistry department have all been of great help and assistance to me over the years. I would like to thank all the staff in the office, Karen and Olive for typing, Mary for all my supplies, Eileen for organising my demonstrating and Denis O'Donoghue for organising some repairs. Thank you to the staff in microanalysis, Barry, Helen and John Meehan. I would like to thank Donal for running my NMR spectra. Thanks to two men that I have kept busy during the last few years, Liam for looking after all my post and Dave for supplying me with PLC plates. Thanks to the technical staff especially for all their help with my

microwave, Tony, Johnny, Mick and Derry. Thanks to Terry and Rose in helping many an afternoon demonstrating pass that little bit quicker with their company. Pat O'Connell, John Caffrey, Agnes and Rita always have a friendly word to say whenever I met them in the corridor or in the lab and they all make the chemistry department a pleasant place to work in.

A special thank you for my 45 partner Jim Allen for all his help.

One man who is always in the best of form and has been a friend since second year inorganic practicals deserves a special thank you, the friendliest person in the chemistry department, Sean Downey. Sean is always a great person for a chat and if you need anything Sean is the man to get it (anything from a spin home to All Ireland tickets). Thank you Sean.

Chrissey also deserves a special mention, only for Chrissey my desk would always be covered in a layer of silica but when Chrissey comes in, she literally brings a shine to the lab and brightens up the chemistry department with her pleasant personality.

On a personal level I would like to thank my friend Harry, and all the members of the Ballyphehane and District Pipe Band for their support.

My family have been a great support and have encouraged me for all my years in college especially my father (who would be a very proud man now if he was alive to see me get my Ph.D., I remember him telling everybody about me when I got my B.Sc. "with honours"). I would like to thank my mother who deserves a medal for putting up with me all this time and as there are no plans for leaving home I am afraid that she is stuck with me. I would like to thank my family, Donal, Eileen, Rosarie and Billy who have always been there for me.

Finally I would just like to say that I have enjoyed my years at UCC and I would like to thank everybody who helped me in any way.

Donnacha O'Connell 29/8/94

Donnacha O'Connell

To my mother and family
and in memory of
my father and godmother

TABLE OF CONTENTS

CHAPTER TWO: THEORETICAL INVESTIGATION OF THE ELECTRONIC STRUCTURE AND BONDING OF ELEVEN-VERTEX *NIDO*-HETEROBORANE DIANIONS $[7,8\text{-}C_2B_9H_{11}]^{2-}$, $[7,9\text{-}C_2B_9H_{11}]^{2-}$, $[1,7\text{-}C_2B_9H_{11}]^{2-}$, $[4,7\text{-}C^2B_9H_{11}]^{2-}$ $[7,8\text{-}P_2B_9H_9]^{2-}$, $[7,9\text{-}P_2B_9H_9]^{2-}$ AND $[7\text{-}SB_{10}H_{10}]^{2-}$

CHAPTER THREE: MICROWAVE HEATING EFFECTS AND THEIR APPLICATION TO SYNTHETIC METALLABORANE CHEMISTRY

CHAPTER FOUR: SYNTHESIS AND CHARACTERISATION OF SOME PLATINUM DERIVATIVES OF $C_2B_9H_{11}$, $As_2B_9H_9$ AND $TeB_{10}H_{10}$

CHAPTER FIVE: SYNTHESIS AND CHARACTERISATION OF METAL HALIDE COMPLEXES OF $C_2B_9H_{11}$ AND $As_2B_9H_9$ AND THEIR REACTIONS WITH $Ag[BF_4]$

CHAPTER SIX: SYNTHESIS AND CHARACTERISATION OF SOME ISOTHIOCYANATE DERIVATIVES OF RHODAHETEROBORANES

CHAPTER ONE

AN INTRODUCTION TO MAIN GROUP V/15 HETEROBORANES AND THEIR METAL DERIVATIVES

1.1 INTRODUCTION

Twelve-vertex metal derivatives of the arsenaborane $[7,8\text{-}As_2B_9H_9]^{2-}$ and carborane $[7,8\text{-}C_2B_9H_{11}]^{2-}$ anions are the main subjects of this thesis and some metallatelluraborane chemistry is also discussed. In cluster electron counting terms, a group V/15 atom is isoelectronic with a CH group. Therefore one would expect that substitution of a group V/15 element for a CH unit in carboranes would yield compounds with similar structures. Generally this has been found to be true.[1] The chemistry of carboranes and their metal derivatives is vast and well documented,[2] and metal derivatives of telluraboranes have been recently reviewed.[3,4] This chapter introduces the general area of group V/15 heteroborane chemistry and their reactions with metal complexes. Thus the following sections 1.2-1.4 describe the synthesis and characterisation of the arsenaboranes, stibaboranes and bismaboranes reported to date. Section 1.5 is an account of the preparation and characterisation of related phosphaboranes. Azaboranes have not been part of the work described in this thesis and will not be discussed.

1.2 ARSENABORANES

Arsenaboranes can be classified by the number of arsenic atoms present as either monoarsenaboranes or diarsenaboranes. Virtually all arsenaboranes (except the As_2SB_7- ligand as discussed in section 1.2.3.3) are either eleven or twelve atom systems. This section begins by discussing eleven atom mono-arsenaboranes and their derivatives. Later twelve atom anion mono-arsenaboranes are reviewed, then other twelve atom arsenaboranes are discussed including diarsenaboranes and their derivatives.

1.2.1 Arsenaboranes of the AsB_{10}-, As_2B_9-, AsB_{11}- and As_2B_{10}- type

Little and co-workers first reported the formation of heteroboranes containing arsenic in 1974.[5] The synthesis of *nido*-$[7\text{-}AsB_{10}H_{12}]^-$ involved the addition of $AsCl_3$ and NaH (or $Na[BH_4]$) to decaborane in diethylether. The anion was precipitated as

the salt $Me_4N[7\text{-}AsB_{10}H_{12}]$ (1) in 34% yield. If the same reaction was carried out with triethylamine as base, zinc powder as the reducing agent and thf as solvent, much purer $[7\text{-}AsB_{10}H_{12}]^-$ was formed, albeit in lower yield (15%). In a detailed NMR study of (1) the ^{11}B assignments were made on the basis of relative intensity and [^{11}B-^{11}B]-COSY correlations and the ^1H assignments followed from the results of $^1H\{^{11}B$ (selective)$\}$ experiments.[6] The ^{11}B NMR spectrum of (1) showed a 1:1:2:2:2:2 intensity pattern. From the NMR study it was suggested that the configuration of (1) has the (8,9;10,11) doubly bridged configuration, Figure 1.1, which is typical of other *nido*-$[XB_{10}H_{12}]$ systems.

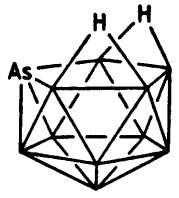

Figure 1.1 Proposed structure of $[7\text{-}AsB_{10}H_{12}]^-$ (1).[5,6]

Addition of methyl iodide to $[7\text{-}AsB_{10}H_{12}]^-$ gave $(AsMe)B_{10}H_{12}$ (2) in 76% yield.[5] The ^{11}B NMR spectrum of (2),[6] was strikingly similar to that of (1) which suggested that the arsenic atoms contribute similarly to the electronic character of both these clusters. Compound (2) readily loses a proton in dilute aqueous ammonia to form $[(AsMe)B_{10}H_{11}]^-$ which was precipitated as $Me_4N[(AsMe)B_{10}H_{11}]$ (3) in 90% yield.[5] A detailed NMR study of (3) has suggested that it has a singly hydrogen-bridged configuration, Figure 1.2.[6] Facile conversion of $[(AsMe)B_{10}H_{11}]^-$ to $(AsMe)B_{10}H_{12}$ (2) was achieved by acidification in acetonitrile/water as solvent and extraction of (2) with diethylether. Demethylation of (2) with sodium in liquid ammonia afforded $[7\text{-}AsB_{10}H_{12}]^-$ in 90% yield.[5]

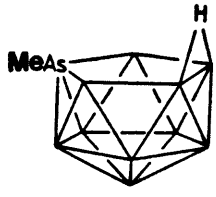

Figure 1.2 Proposed structure of $[(AsMe)B_{10}H_{11}]^-$ (3).[6]

Attempts to prepare $(AsPh)B_{10}H_{12}$ (4) by routes analogous to those used to prepare $(AsMe)B_{10}H_{12}$ (2) failed. However an alternative reaction of $[AsCl_2Ph]$ with decaborane in thf in the presence of two equivalents of triethylamine produced $(AsPh)B_{10}H_{12}$ (4) in 5% yield.[5] Compound (4) is acidic and could be deprotonated to give $[(AsPh)B_{10}H_{11}]^-$ which was precipitated as $Me_4N[(AsPh)B_{10}H_{11}]$ (5) in 90% yield.[5]

The addition of a BH unit to $[7\text{-}AsB_{10}H_{12}]^-$ by reaction with triethylamine-borane gave $[AsB_{11}H_{11}]^-$ which was precipitated as $Me_4N[AsB_{11}H_{11}]$ (6) in 52% yield.[5] Excess triethylamineborane had to be used if pure $[AsB_{11}H_{11}]^-$ was to be isolated. The formation of $[AsB_{11}H_{11}]^-$ also occurs but in low yield (13%) from the thermal decomposition of $Cs[AsB_{10}H_{12}]$ under nitrogen at 648K.[5] Certain oxides of arsenic are known to insert arsenic into boranes and carboranes.[7] For example treatment of $Et_4N[B_{11}H_{14}]$[8] with As_2O_3 in aqueous KOH formed $[AsB_{11}H_{11}]^-$ (6) in 48% yield.[9]

Little and co-workers reported the preparation of *closo*-1,2-$As_2B_{10}H_{10}$ (7) from $B_{10}H_{14}$ and $AsCl_3$ in the presence of triethylamine in refluxing thf in 29% yield.[5] The ^{11}B NMR spectrum is consistent with a C_{2v} cage symmetry, Figure 1.3, with a 2:2:4:2 pattern of doublets.[6] The ^{11}B and ^1H signals were assigned using [^{11}B-^{11}B]-COSY correlations and $^1H\{^{11}B$ (selective)$\}$ experiments.[6] If a four fold excess of triethylamine and arsenic trichloride were used, none of compound (7) was formed. {It is noteworthy that (7) was also isolated from the reactions used to prepare $[7\text{-}AsB_{10}H_{12}]^-$. For instance, when $Na[BH_4]$ was used, (7) was isolated in 1% yield and when triethylamine was substituted as base, (7) was isolated in 30% yield}. Isomerisation of 1,2-$As_2B_{10}H_{10}$ (7) to its 1,7 isomer required relatively high temperatures (*ca.* 848K) and gave only 35% yield of 1,7-$As_2B_{10}H_{10}$.[10]

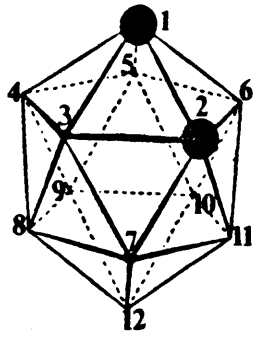

Figure 1.3 Proposed structure of *closo*-1,2-$As_2B_{10}H_{10}$ (7).[5,6,9]

Like other icosahedral heteroboranes containing two heteroatoms,[11,12] the removal of a boron atom can be accompanied by reaction with base (piperidine). Thus reaction of 1,2-$As_2B_{10}H_{10}$ afforded [7,8-$As_2B_9H_{10}$]$^-$ (8) in 86% yield.[9,11] The ^{11}B NMR spectrum of (8) showed a 2:2:1:2:1:1 pattern of doublets[6] and in general the spectrum was very similar to the carborane analogue [7,8-$C_2B_9H_{12}$]$^-$,[10] hence one would expect (8) to have a similar structure, Figure 1.4.[13,14]

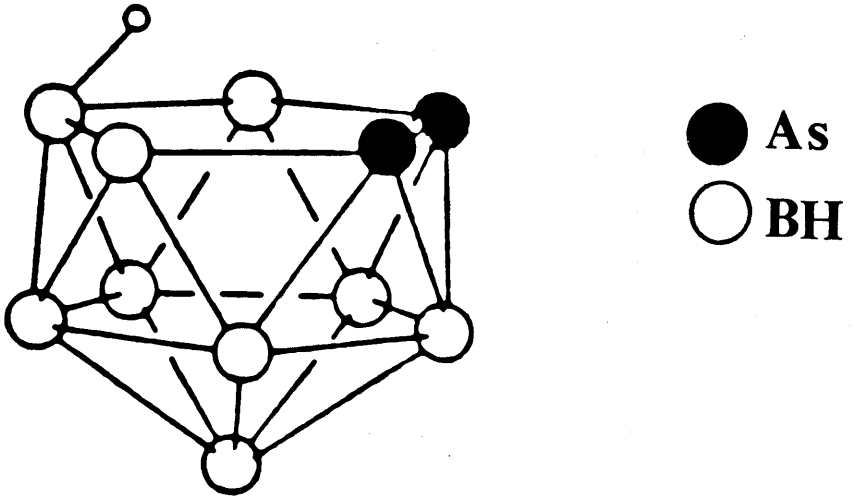

Figure 1.4 Proposed Structure of *nido*-[7,8-$As_2B_9H_{10}$]$^-$ (8).[5,6,11,12,13]

1.2.1.1 Structural chemistry of *closo*-$As_2B_{10}H_8I_2$ (9)

Since no arsenaborane had been structurally characterised prior to this work it was decided to undertake a single crystal X-ray study of a diarsenaborane compound. After trying to crystallise *closo*-1,2-$As_2B_{10}H_{10}$ (7) without success it was decided to make a derivative of (7) for X-ray analysis. The diiodinated complex $As_2B_{10}H_8I_2$ (9) was prepared in 26% yield by reacting 1,2-$As_2B_{10}H_{10}$ (7) with a ten fold excess of iodine at room temperature in CH_2Cl_2 in the presence of $AlCl_3$ catalyst for 16 h. The experimental details are given in chapter 4 section 4.3.12 with the X-ray details in 4.3.13. The X-ray analysis of (9) showed that the reaction of $As_2B_{10}H_{10}$ with I_2 had produced two distinct 9,12- and 8,12-diiodo isomers which had co-crystallised during post reaction work-up.[15] Because the 12-atom cage is essentially

spherical, the two isomers packed in such a way that the coordinates of the adjacent I atoms remain identical, but the As atoms appeared to be disordered over four sites. The ORTEP plot shown in Figure 1.5 has the correct numbering scheme for the 9,12 isomer {site occupancies for atoms at sites 1,2,3 (refined as As atoms) were 0.921(2), 0.681(2) and 0.492(2) respectively. The occupancy factor for site 6 (refined as a boron atom) was 1.655(23)}; the disorder caused by the co-crystallisation of the two isomers only appears to affect these four sites. A somewhat similar problem (with iodination occurring at two sites) has also been encountered in an electron-diffraction study of the product obtained by diiodinating 1,7-$C_2B_{10}H_{12}$, where a 1:1 mixture of 9,10- and 5,12-diiodo isomers was assumed in the analysis of the structure.[16]

Because the $As_2B_{10}H_{10}$ reagent had the two As atoms immediately adjacent, only models which have the two As atoms directly bonded are physically reasonable in interpreting the disorder in the crystals of (9). The main isomer present was the 9,12 one, with As-As 2.435(2) Å. A "normal" range of 2.43-2.46 Å for two electron As-As single bonds has been suggested.[17] The distances between As(1) and the 100% boron sites B(4) and B(5) are 2.157(7) and 2.131(8) Å respectively. For those sites which are 100% boron, the range of B-B distances in $As_2B_{10}H_8I_2$ (9) is notably narrow, 1.763(10)-1.852(11) Å, with a mean value 1.786 Å; a much broader range of B-B distances was found in the selenaborane derivative *closo*-12-I-1-$SeB_{11}H_{10}$ 1.715(12)-1.934(13), mean 1.762(12) Å.[18] The B-I distances in (9) {2.161(7) and 2.170 (7) Å} span the B-I distance found in 12-I-1-$SeB_{11}H_{10}$ of 2.167(7) Å and are also similar to the value found in 1-I-$B_{10}H_{13}$ {2.17(I) Å}.[19]

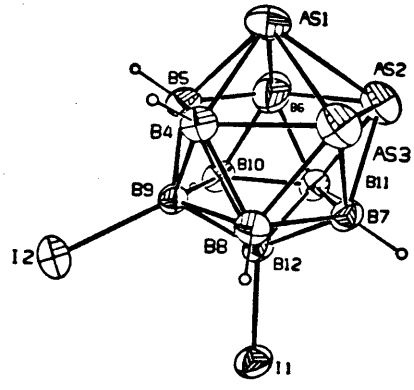

Figure 1.5 View of the $As_2B_{10}H_8I_2$ (9) molecule showing the numbering scheme for the 9,12-diiodo isomer.

1.2.2 Arsenaboranes containing other elements (C, S, Se) as cluster atoms

In this section monocarbaarsenaboranes are first discussed (section 1.2.2.1) which is followed by a discussion of dicarbaarsenaboranes (section 1.2.2.2) and finally group VI/16 (S, Se) arsenaboranes are discussed in section 1.2.2.3.

1.2.2.1 Monocarbaarsenaboranes

The 1,2- 1,7- and 1,12- $CAsB_{10}H_{12}$ isomers form the basis of this section. Initially these three isomers are discussed. The following paragraphs then discuss the derivatives of the 1,2- isomer followed by derivatives of the 1,7- and 1,12- isomers with the final paragraph in this section comparing these arsenacarboranes with carboranes and phosphacarboranes.

The first compounds of this type which were prepared were the isomers 1,2-$CAsB_{10}H_{11}$ (10), 1,7-$CAsB_{10}H_{11}$ (11) and 1,12-$CAsB_{10}H_{11}$ (12).[11] Reaction of arsenic trichloride with $Na_3[B_{10}H_{10}CH]\cdot(thf)_2$[20] in thf gave 1,2-$CAsB_{10}H_{11}$ (10) in 25% yield.[11,21] Compound (10) was also obtained in low yield by reaction of $Na[CB_{10}H_{13}]$ with solid As_2O_3 in an aqueous KOH-heptane mixture.[7]

The thermolysis of 1,2-$CAsB_{10}H_{11}$ (10) in a sealed tube at 495°C for 22h produced 1,7-$CAsB_{10}H_{11}$ (11) in 65% yield.[11] Heating 1,2-$CAsB_{10}H_{11}$ (10) at 575°C for 13h in a sealed tube gave a 1:1 mixture of 1,7-$CAsB_{10}H_{11}$ (11) and 1,12-$CAsB_{10}H_{11}$ (12). The 1,7- and 1,12- isomers (11) and (12) could be obtained in 15% yield by a complex work up procedure.[11]

Metallation of the C-H bond of 1,7-$CAsB_{10}H_{11}$ (11) by phenylithium in ether gave 1,7-$C(Li)AsB_{10}H_{10}$ (13).[22] Compound (13) has been used to prepare several C-substituted derivatives, as illustrated in Table 1.1.[23,24]

Table 1.1: List of C-substituted derivatives of 1,7-$CAsB_{10}H_{11}$ (11)

No.	Compound	Reactants
(13)	1,7-C(Li)$AsB_{10}H_{10}$	1,7-$CAsB_{10}H_{11}$ (10) +PhLi
(14)	1,7-C(CO_2H)$AsB_{10}H_{10}$	(13) + 1 CO_2 + 2 H_3O^+
(15)	1,7-C(COCl)$AsB_{10}H_{10}$	(14) + PCl_5
(16)	1,7-C(COPh)$AsB_{10}H_{10}$	(15) + C_6H_6, $AlCl_3$
(17)	1,7-C(HgMe)$AsB_{10}H_{10}$	(13) + MeHgCl

Treatment of 1,2-$CAsB_{10}H_{11}$ (10) or 1,7-$CAsB_{10}H_{11}$ (11) with piperidine at reflux gave [7,8-$CAsB_9H_{11}$]$^-$ (18) and [7,9-$CAsB_9H_{11}$]$^-$ (19). These were isolated as their tetramethylammonium salts in 70% and 80% yields respectively.[11] Reaction of (19) with methyl iodide in refluxing thf solution produced 7,9-C(AsMe)B_9H_{11} (20) in 96% yield.[11] Methylation of (18) gave a mixture of products which were difficult to separate and were not fully characterised.[11]

The compound 1,12-$CAsB_{10}H_{11}$ (12) was reduced by sodium/naphthalene to give a rearranged species formulated as the ion [1,7-$CAsB_{10}H_{11}$]$^{2-}$ (21).[11] Oxidation of (21) with [$CuCl_2$] produced 1,7-$CAsB_{10}H_{11}$ (11).[22] A *nido* twelve-atom complex, $Me_3NC(AsPh)B_{10}H_{10}$ (22), isoelectronic with [$CAsB_{10}H_{11}$]$^{2-}$ (21) has been prepared.[25] Reduction of 1,12-$CAsB_{10}H_{11}$ (12) with sodium in liquid ammonia followed by acid hydrolysis produced the carborane [$CB_{10}H_{11}$]$^-$.[26]

Comparison of the relative ease of monochlorination of isomers of $CAsB_{10}H_{11}$, $CPB_{10}H_{11}$ and $C_2B_{10}H_{12}$ compounds showed that for a particular isomeric type, the CAs- species were most reactive, then the carboranes followed by the CP-compounds.[25] Polarographic reduction of the isomeric 1,2-, 1,7-, 1,12- arsena- and phosphacarboranes showed that the electron affinity of the cage system increases when a CH unit in the equivalent $C_2B_{10}H_{12}$ carboranes is replaced by either an arsenic or phosphorus atom.[27]

1.2.2.2 Dicarbaarsenaboranes

A number of arsenacarboranes containing two carbon atoms have been prepared.[28,29,30,31] The dicarbaarsenaboranes can be divided into three groups, $(AsY)C_2B_9H_9R_2$ (Y=Ph, Bu, Me, Pr^i, Br, Cl, R=H, Me), $(Me_2As)_2C_2B_9H_9R_2$ (R=H, Me) and $As_2C_2B_7H_9$ which will be discussed sequentially in this section.

The *nido* compound $(AsPh)C_2B_9H_{11}$ (23) was the first reported example of this class of heteroborane.[30] Addition of phenyldichloroarsine to a suspension of $Na_2[1,2\text{-}C_2B_9H_{11}]$ in toluene afforded yellow, sublimable $(AsPh)C_2B_9H_{11}$ (23) in low yield. The CC′-dimethyl analogue, $(AsPh)C_2B_9H_9Me_2$ (24) was also prepared.[30,32] Reaction of $Tl_2[7,8\text{-}C_2B_9H_{11}]$ with $RAsX_2$ (R=Ph, *n*-Bu, X=Cl; R=Me, X=Br) in diethylether afforded $(AsR)C_2B_9H_{11}$ {R=Ph (23), *n*-Bu (25), Me (26)} in 15%, 38% and 30% yields respectively. Similarly, reaction of $Tl_2[7,8\text{-}C_2B_9H_9Me_2]$ with $MeAsBr_2$ in diethylether at 0°C afforded $(AsMe)C_2B_9H_9Me_2$ (27) but in very low yield (3.5%). Treatment of $(AsPh)C_2B_9H_{11}$ (23) with a dilute solution of boron tribromide in carbon tetrachloride gave $(AsBr)C_2B_9H_{11}$ (28) in 95% yield.[29] Prolonged exposure of compounds (23), (25), or (26) to air resulted in extensive decomposition but the bromo-derivative (28) was considerably more stable than the organo-substituted compounds. Treatment of compounds (23), (25), (26) and (28) with ethanolic potassium hydroxide rapidly produced $K[7,8\text{-}C_2B_9H_{12}]$ in quantitative yield.[29]

The lithium salt $Li_2[Me_2C_2B_9H_9]$ was reacted with $AsCl_3$ in diethylether at -90°C to give the arsenadicarbollyl compound $(AsCl)C_2B_9H_9Me_2$ (29) in 21% yield.[33] The ^{11}B spectrum of (29) consisted of six doublets in a 1:2:1:2:2:1 intensity ratio consistent with the solid state molecular structure of (29) which is shown in Figure 1.6. It may be described as a *closo* compound with a distorted *nido* structure because of the η^3-coordination of the AsCl unit to the B(1a), B(1b) and B(1c) atoms on the open face of the $C_2B_9H_9Me_2$ fragment, Figure 1.6.

Reaction of (29) with the Grignard reagent Pr^{i}MgCl afforded the compound $(AsPr^i)C_2B_9H_9Me_2$ (30) in 40% yield.[33] Reaction of (29) in CH_2Cl_2 at -78 °C with $AlCl_3$ afforded the adduct $[(AsCl)C_2B_9H_9Me_2]\cdot AlCl_3$ (31) in 45% yield.[33]

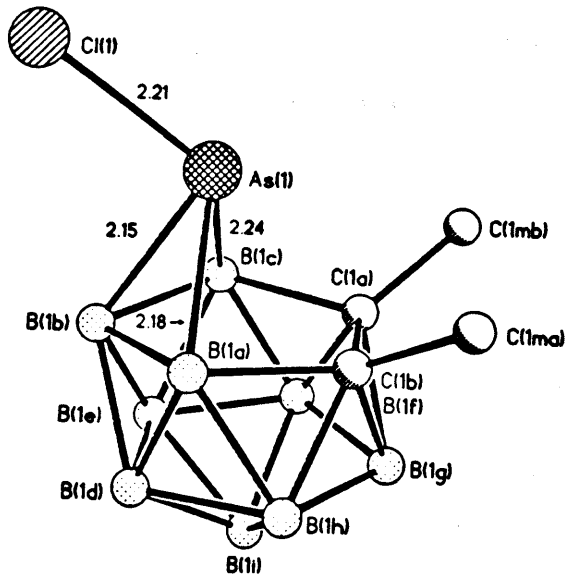

Figure 1.6 Molecular structure of $(AsCl)C_2B_9H_9Me_2$ (29).[33]

Attempts to effect the synthesis of $(AsMe)C_2B_9H_{11}$ (26) in a similar manner to that used for the *closo*-aluminacarborane $AlC_2B_9H_{11}Me$,[32] *i.e.* by the addition of Me_2AsBr to a hot benzene solution of $Li[7,8\text{-}C_2B_9H_{12}]$ in a 1:1 molar ratio, failed.[29] Instead, the major product was the carborane $7,8\text{-}C_2B_9H_{13}$. The residue after sublimation of $7,8\text{-}C_2B_9H_{13}$ showed the presence of a species with a mass spectral cut off at m/z 340, corresponding to the $^{75}As_2{}^{11}B_9{}^{12}C_6{}^{1}H_{23}{}^{+}$ ion, and this was tentatively identified as $(Me_2As)_2C_2B_9H_{11}$ (32). The possible overall stoichiometry of the reaction is illustrated in equation 1.

$$2Me_2AsBr + 2Li[7,8\text{-}C_2B_9H_{12}] \longrightarrow (Me_2As)_2C_2B_9H_{11} + 7,8\text{-}C_2B_9H_{13} + 2LiBr \quad (1)$$

However, reaction of $Tl_2[C_2B_9H_{11}]$ with Me_2AsBr in benzene in a 1:2 molar ratio afforded $(Me_2As)_2C_2B_9H_{11}$ (32) as the major product (70% yield).[29] The CC′-dimethyl analogue $(Me_2As)_2C_2B_9H_9Me_2$ (33) was prepared in a similar fashion. The analogous reaction of $Tl_2[C_2B_9H_{11}]$ with Ph_2AsCl in refluxing toluene did not give $(Ph_2As)_2C_2B_9H_{11}$. Instead the starting materials were recovered. Compounds (32) and (33) decomposed to boric acid on exposure to the atmosphere. Treatment of an acetone solution of $(Me_2As)_2C_2B_9H_{11}$ (32) with ethanolic potassium hydroxide in the absence of air produced a white volatile crystalline solid in 72% yield. This exhibited a mass spectral cut off at m/z 284 which corresponds to the $^{75}As^{11}B_9{}^{12}C_6{}^{16}O^{1}H_{22}{}^{+}$ ion,

in which ethoxide has replaced one Me_2As unit. The ^{11}B NMR spectra of (32), (33) and the "ethoxy derivative" of (28) were apparently very similar. Two possible structures for $(Me_2As)_2C_2B_9H_{11}$ (32) which were consistent with the spectral data are shown in Figure 1.7.

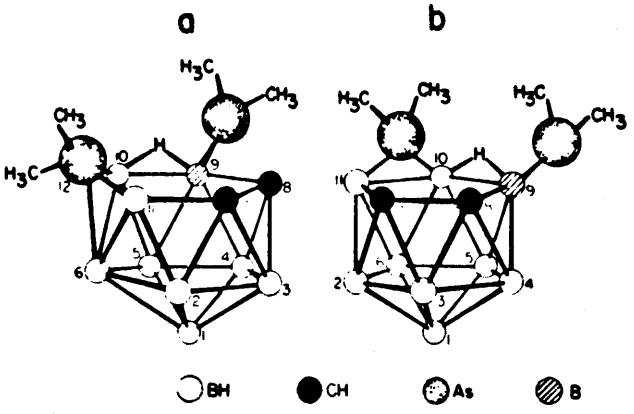

Figure 1.7 Possible structures of $(Me_2As)_2C_2B_9H_{11}$ (32).[29]

In Figure 1.7 (a) the cage has been expanded to include one arsenic atom while the other is located as a terminal Me_2As group to a boron atom, while structure (b) has separate terminal and bridging dimethylarsino groups. In view of the ready replacement of one but not both of the arsenic functions and the fact that no $[C_2B_9H_{12}]^-$ was formed by the prolonged action of concentrated base, the proposed structure (a) was preferred.[10]

The synthesis of $As_2C_2B_7H_9$ (34) has been reported.[28] Reaction of $C_2B_7H_{13}$ in thf with triethylamine and then AsI_3 in thf gave (34) in 33% yield. The proposed *nido* structure, containing two contiguous arsenic atoms, is shown in Figure 1.8. This molecule is isoelectronic with $C_4B_7H_{11}$, a member of the tetracarbon carborane series.[34]

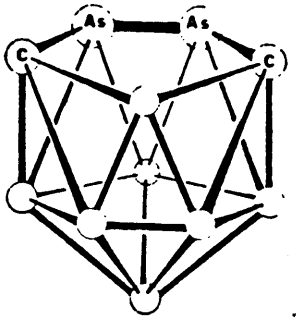

Figure 1.8 Proposed structure of *nido*-$As_2C_2B_7H_9$ (34).[28]

1.2.2.3 Arsenaboranes containing group VI/16 elements

Mixed eleven atom arsenaborane clusters of the general formula $As_2EB_8H_8$, containing main Group VI/16 elements have been synthesised where E=S,[8,30] or Se.[30,35] Reaction of $Cs[SB_9H_{12}]$ with $AsCl_3$ in an acetonitrile solution gave a white sublimable air-sensitive compound, $As_2SB_8H_8$ (35) in low yield.[30] The ^{11}B NMR spectrum of (35) gave a pattern of doublets of the ratio 2:1:2:2:1 which is consistent with either the *nido*-8-S-7,9-$As_2B_8H_8$ structure shown in Figure 1.9, or the 10-S-7,8-$As_2B_8H_8$.

Treatment of $K[B_9H_{12}X]$ (X=S or Se), with As_2O_3 in basic solution afforded $As_2SB_8H_8$ (35) and $As_2SeB_8H_8$ (36) respectively.[28] Compound (36) was yellow and was obtained in "much lower" yield, than the $As_2SB_8H_8$ (35) analogue (the actual yields were not reported).

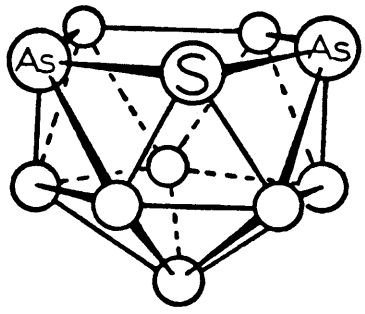

Figure 1.9 Proposed structure of $As_2SB_8H_8$ (35).[30]

1.2.3 Metal derivatives of arsenaboranes

Like section 1.2.2 the metal derivatives will be classified according to the type of cage structure. Section 1.2.3.1 contains metal derivatives of the eleven atom monoarsenaborane AsB_{10}- ligand. Section 1.2.3.2 discusses metal and metalloid derivatives of the eleven atom arsenacarborane $AsCB_9$- ligand and section 1.2.3.3 contains a metal derivative of the arsenathiaborane As_2SB_7- ligand. Section 1.2.3.4 reviews metal derivatives of the eleven atom As_2B_9- diarsenaborane ligand and a metal derivative of the ten atom As_2B_8- ligand is also discussed. Section 1.2.3.4, being a

large section, will be sub-divided according to the metal present and a short discussion on the types of compounds present will be given at the start of section 1.2.3.4.

1.2.3.1 Metal derivatives of the monoarsenaborane AsB_{10}- ligand

This section contains metal derivatives of the eleven atom monoarsenaborane AsB_{10}- ligand. The first compound discussed is one in which the metal atom is σ-bonded to the arsenic atom, in all the other compounds in this section the metal atoms form part of the cluster structure. Initially transition metal derivatives are discussed. Main group derivatives of AsB_{10} are reviewed at the end of the section.

The iron complex, $[Fe(CO)_2(\eta^5\text{-Cp})(AsB_{10}H_{12})]$ (37) formed from the reaction of the cationic complex $[Fe(CO)_2(\eta^5\text{-Cp})(\textit{cyclo}\text{hexene})]^+$ with the arsenaborane anion $[AsB_{10}H_{12}]^-$ in acetone was the first reported arsenaborane-metal complex.[36] There was no evidence from the ^{11}B NMR spectrum of (37) of any singlet resonance which would be indicative of a boron-iron σ bond. Furthermore (37) had the two expected B-H-B bridging hydrogens suggesting that there was no B-Fe-B bridge in the molecule. It was proposed that in (37) the iron atom was σ-bonding to the arsenic atom with a structure that is shown in Figure 1.10.

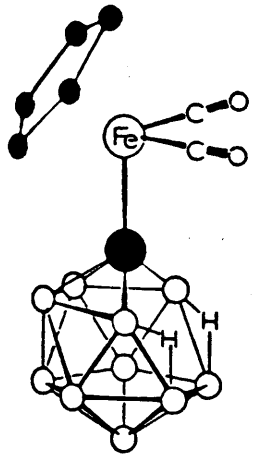

Figure 1.10 Proposed structure of $[Fe(CO)_2(\eta^5\text{-Cp})(AsB_{10}H_{12})]$ (37).[36]

Some nickel and cobalt derivatives of arsenaboranes have been synthesised.[9,37] In aqueous sodium hydroxide solution, cobalt or nickel chloride reacted with $[AsB_{10}H_{12}]^-$ to give the anionic "sandwich" type compounds, $[Co(AsB_{10}H_{10})_2]^{3-}$ and $[Ni(AsB_{10}H_{10})_2]^{2-}$ respectively. These were precipitated as the tetramethylammonium salts, $[Me_4N]_3[Co(AsB_{10}H_{10})_2]\cdot H_2O$ (38) and $[Me_4N]_2[Ni(AsB_{10}H_{10})_2]$ (39) in 93% and 52% yield, respectively.[37] Little and co-workers were unsuccessful in an attempt to synthesise $[Fe(AsB_{10}H_{10})_2]^{3-}$ from $Cs[AsB_{10}H_{12}]$ and ferrous ammonium sulphate.[37]

The reaction of $(AsMe)B_{10}H_{12}$ (2), *cyclo*pentadiene and cobalt chloride in a KOH solution in ethanol afforded a 43% yield of the twelve atom anionic cluster $Me_4N[Co(\eta^5\text{-}Cp)(AsB_{10}H_{10})]$ (40).[9,37] None of the expected compound $[Co(\eta^5\text{-}Cp)(\{AsMe\}B_{10}H_{10})]$ was isolated. Attempts to synthesise (40) from the $[AsB_{10}H_{12}]^-$ anion gave no product even though the analogous carborane complex $[Co(\eta^5\text{-}Cp)(CB_{10}H_{11})]^-$ has been successfully prepared from a salt of $[CB_{10}H_{13}]^-$.[38] Attempts to alkylate (40) were also unsuccessful.[37]

In 1987, Todd *et al* successfully synthesised the first example of main group derivatives of $AsB_{10}H_{10}$, namely $[1,2\text{-}AsMB_{10}H_{10}]^-$ (M = Sn, Pb).[9] Deprotonation of the $[AsB_{10}H_{12}]^-$ anion with excess *n*-BuLi followed by treatment with $SnCl_2$ or $PbCl_2$ in thf afforded $Li[1,2\text{-}AsSnB_{10}H_{10}]$ (41) and in the case of M = Pb, after precipitation with tetramethylammoniumchloride, $Me_4N[1,2\text{-}AsPbB_{10}H_{10}]$ (42) in moderate yields. Compound (42) was fully characterised both spectroscopically and analytically but only ^{11}B NMR evidence was presented for (41).

1.2.3.2 Metal derivatives of the arsenacarborane $AsCB_9^-$ ligand

Initially in this section metal derivatives of the $AsCB_9^-$ ligand where the metal atom forms part of the cluster are discussed. Compounds where the metal atom is not part of the cluster but is sigma-bonded through the arsenic atom are then discussed and finally arsenacarborane derivatives of germanium are reported.

Reaction of $[7,9\text{-}AsCB_9H_{11}]^-$ with sodium hydride followed by reaction with anhydrous $FeCl_2$ afforded $[Fe(7,9\text{-}AsCB_9H_{10})_2]^{2-}$ (43).[39] Oxidation of the Fe(II) complex (43) with anhydrous $FeCl_2$ afforded the paramagnetic complex $[Fe(7,9\text{-}AsCB_9H_{10})_2]^-$ (44). Treatment of (43) with excess methyl iodide formed [(7,9-

$CAsB_9H_{10})Fe(7,9\text{-}C\{AsMe\}B_9H_{10})]^-$ (45) as the major product. No neutral dimethylated complex was obtained from this reaction. Reaction of 7,9-$C(AsMe)B_9H_{11}$, $FeCl_2$, C_5H_6, and triethylamine gave a low yield of $[Fe(\eta^5\text{-}Cp)(7,9\text{-}C\{AsMe\}B_9H_{10})]$ (46). A manganese compound $[Mn(CO)_3(7,9\text{-}CAsB_9H_{10})]$ (47) was also prepared using the $[7,9\text{-}CAsB_9H_{10}]^{2-}$ ligand.[39]

Deprotonation of $[7,8\text{-}CAsB_9H_{11}]^-$ (18) and $[7,9\text{-}CAsB_9H_{11}]^-$ (19) using sodium hydride or triethylamine in thf followed by reaction with manganese or cobalt compounds afforded metallaarsenacarborane $MXCAsB_9H_{10}$ {M=Mn X=$(CO)_3$ or M=Co X=$(\eta^5$-Cp)} complexes.[39] An X-ray diffraction study of $[Co(\eta^5\text{-}Cp)(1,2\text{-}CAsB_9H_{10})]$ (48) has been completed, Figure 1.11.[39]

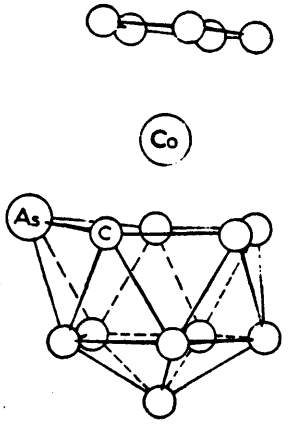

Figure 1.11 Molecular structure of $[Co(\eta^5\text{-}Cp)(7,8\text{-}CAsB_9H_{10})]$ (48).[39]

A thf solution of $Me_4N[7,8\text{-}CAsB_9H_{11}]$ and $Mo(CO)_6$ in a 1:1 mole ratio was irradiated with a high-pressure mercury-vapour lamp and afforded the sigma-bonded (through the arsenic atom) $[7,8\text{-}B_9H_{11}CAs\cdot Mo(CO)_5]^-$ (51).[39] Similar complexes involving the $[7,9\text{-}CAsB_9H_{11}]^-$ ion and chromium or tungsten carbonyls were also prepared. The photochemically induced reaction of $[Fe(7,9\text{-}CAsB_9H_{10})_2]^{2-}$ (43) with $Cr(CO)_6$ in thf led to the formation of $[\{7,9\text{-}B_9H_{10}CAs\cdot Cr(CO)_5\}_2Fe]^{2-}$ (52). It was proposed that each heteroborane ligand is π-bonded to the iron atom and σ-bonded through the arsenic atom to a $Cr(CO)_5$ unit.[39]

The addition of germanium diiodide to the $[7,9\text{-}AsCB_9H_{10}]^{2-}$ ion (generated as the disodium salt in refluxing benzene) resulted in insertion into the vacant icosahedral position forming $[1,2,7\text{-}AsCGeB_9H_{10}]$ (49).[40] By employing a similar method with the $[7,8\text{-}AsCB_9H_{10}]^{2-}$ ion, $[1,2,3\text{-}AsCGeB_9H_{10}]$ (50) was synthesised.[40]

These compounds were identified by elemental analyses and high resolution mass spectrometry. The 1,2,7 isomer (49) is thermally more stable than the 1,2,3 isomer.

1.2.3.3 Metal derivatives containing the arsenathiaborane ligand $As_2SB_7H_7$

Only one metal derivative of the arsenathiaborane ligand $As_2SB_7H_7$ has been reported. Reaction of $As_2SB_8H_8$ (35) with KOH in methanol followed by addition of triethylamine, *cyclo*pentadiene and cobalt chloride in thf afforded [Co(η^5-Cp)$As_2SB_7H_7$] (53) in very low yield characterised by NMR and high resolution mass spectroscopy.[28]

1.2.3.4 Metal derivatives of diarsenaboranes

The most common arsenaborane ligand used to form metallaarsenaboranes has been the [7,8-$As_2B_9H_9$]$^{2-}$ anion. The majority of compounds in this section are twelve atom compounds based on a MAs_2B_9- cluster. The exceptions to this are an iron compound in which the iron is sigma-bonded to an arsenic atom and two cobalt complexes which are based on $Co(As_2B_9)_2$ and $Co_2As_2B_{10}$ structures. This section is divided into groups of metals ranging from group 8 to group 11 complexes. Each group is subdivided into individual metals starting with the lightest metals at the top of a group and then proceeding down the group.

(A) Group 8 complexes

The first metal derivative of [7,8-$As_2B_9H_{10}$]$^-$ reported was the compound [Fe$(CO)_2$(η^5-Cp)($As_2B_9H_{10}$)] (54).[36] This was prepared in 45% yield by the reaction of [Fe$(CO)_2$(η^5-Cp)(*cyclo*hexene)]PF_6 with [7,8-$As_2B_9H_{10}$]$^-$ in acetone. Compound (54) was characterised with IR, ^{1}H and ^{11}B NMR spectroscopies and by elemental analysis. There were no NMR signals which would be indicative of a boron-iron σ

bond, but there was a B-H-B bridge hydrogen at δ -4.2. It was proposed that (54) contained an iron atom σ bonded to an arsenic atom, Figure 1.12. No arsenaborane complexes of ruthenium or osmium have been reported.

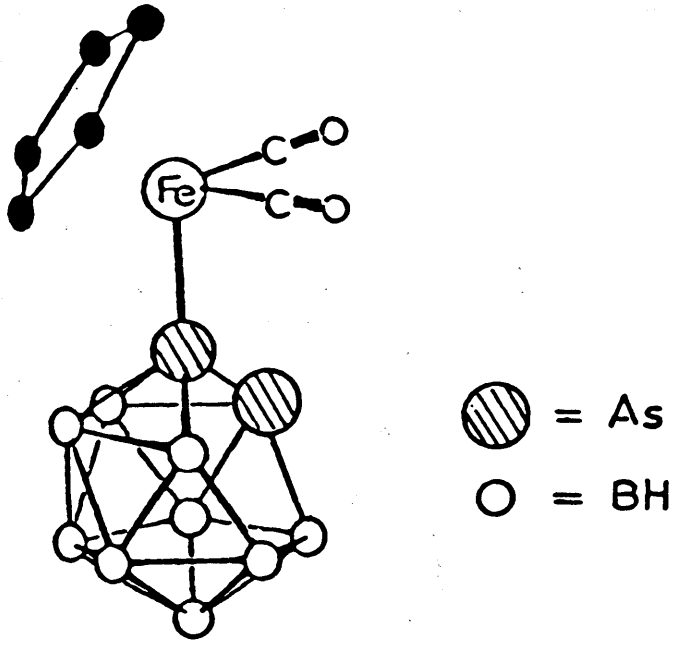

Figure 1.12 Proposed structure of $[Fe(CO)_2(\eta^5\text{-}Cp)(As_2B_9H_{10})]$ (54).[36]

(B) Group 9 complexes of diarsenaboranes

(i) Cobaltadiarsenaboranes

The piperidinium salt of $[7,8\text{-}As_2B_9H_{10}]^-$ has been found to be useful in the preparation of cobalt and nickel diarsenaboranes.[11,37] Reaction of $[C_5H_{10}NH_2][As_2B_9H_{10}]$ and $[CoCl_2]$ in aqueous NaOH solution followed by precipitation with $[Me_4N]Cl$ afforded $Me_4N[Co(As_2B_9H_9)_2]$ (55) in 46% yield.[37] The analogous carborane derivative $Me_4N[Co(C_2B_9H_{11})_2]$ is also known.[41]

The reaction between the piperidinium salt of $[7,8\text{-}As_2B_9H_{10}]^-$, freshly prepared *cyclo*pentadiene, Et_3N and $[CoCl_2]$ in thf afforded $[3\text{-}(\eta^5\text{-}Cp)\text{-}3,1,2\text{-}CoAs_2B_9H_9]$ (56) in 46% yield.[37] Prolongation of the reaction gave red air-stable crystals of $[3,6,1,2\text{-}\{Co(\eta^5\text{-}Cp)\}_2As_2B_8H_8]$ (57), in very low yield (0.3%).[9] The isoelectronic carborane derivatives of (56) and (57) i.e. $[3,1,2\text{-}Co(\eta^5\text{-}Cp)(C_2B_9H_{11})]$ and $[3,6,1,2\text{-}\{Co(\eta^5\text{-}$

Cp)}$_2$C$_2$B$_8$H$_{10}$] respectively are known.[42] The ^{11}B NMR spectrum of (57) consisted of three doublets in a 1:2:1 intensity ratio, and the proposed structure (57) as a [3,6,1,2-{(η^5-Cp)Co}$_2$As$_2$B$_8$H$_8$] dodecahedral species is shown in Figure 1.13. It was the first example of a diarsenaborane complex containing less than nine boron atoms. The complex [Co(η^5-Cp)As$_2$SB$_7$H$_7$] (53) has also been synthesised (see section 1.2.3.3).[28]

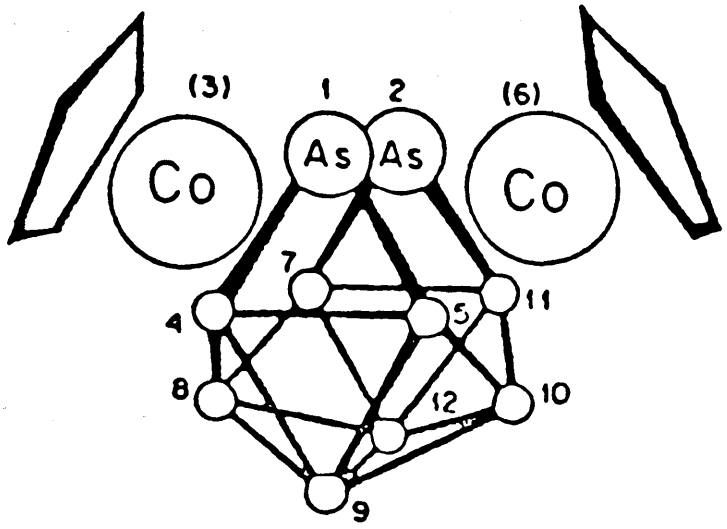

Figure 1.13 Proposed structure of [3,6,1,2-{Co(η^5-Cp)}$_2$As$_2$B$_8$H$_8$] (57).[9]

(ii) Rhodadiarsenaboranes

Until quite recently no rhodium derivatives containing diarsenaborane ligands had been reported. However, the reaction of equimolar amounts of [Rh(PPh$_3$)$_3$Cl] and Me$_4$N[As$_2$B$_9$H$_{10}$] in ethanol at room temperature for 24h gave a yellow precipitate of *closo*-[3,3-(PPh$_3$)$_2$-3-H-3,1,2-RhAs$_2$B$_9$H$_9$] (58) in 98% yield.[6,22] The infrared spectrum of (58) contained a Rh-H band at 2020 cm^{-1} and signals due to Rh-H were characteristic features of the ^{1}H NMR spectrum. The measured ^{11}B NMR features were all confirmatory of the *closo*-[3,3-(PPh$_3$)$_2$-3-H-3,1,2-RhAs$_2$B$_9$H$_9$] (58) formulation, Figure 1.14. The analogous rhodacarborane *closo*-[3,3-(PPh$_3$)$_2$-3-H-3,1,2-RhC$_2$B$_9$H$_{11}$] (59) is known and has been the subject of a considerable amount of research.[43]

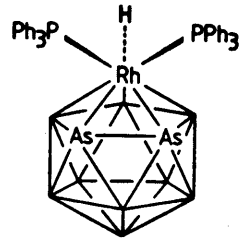

Figure 1.14 Proposed structure of *closo*-[3,3-$(PPh_3)_2$-3-H-3,1,2-$RhAs_2B_9H_9$] (58).[6]

A second rhodaarsenaborane *closo*-[3-(η^5-Cp^*)-3,1,2-$RhAs_2B_9H_9$] (60) has also been reported.[22] Reaction of the dimeric rhodium species [(η^5-Cp^*)$RhCl_2]_2$ with $Me_4N[As_2$-$B_9H_{10}]$ in a 1:2 molar ratio in CH_2Cl_2 in the presence of a ten fold excess of triethyl-amine at room temperature for 4d and then at reflux for 20 min, afforded (60) in 51% yield. To date compounds (58) and (60) are the only reported rhodaarsenaboranes.

(C) Group 10 derivatives of diarsenaboranes

(i) Nickeldiarsenaboranes

Only three nickel complexes of $[7,8$-$As_2B_9H_{10}]^-$ have been reported.[9,44] Treatment of a solution of the piperidinium salt of $[7,8$-$As_2B_9H_{10}]^-$ in thf with excess triethylamine and [Ni(dppe)Cl_2] afforded dark green plates of [3-(dppe)-3,1,2-$NiAs_2B_9H_9$] (61), {dppe=[1,2-bis(diphenylphosphino)ethane]}.[9] Compound (61) was characterised spectroscopically as a twelve atom *closo* structure.

The reaction of *nido*-$[7,8$-$As_2B_9H_{10}]^-$ with *n*-butyllithium followed by [$Ni(PMe_2Ph)_2Cl_2$] in thf at room temperature for 2h led to the formation of *closo*-[3,3-$(PMe_2Ph)_2$-3,1,2-$NiAs_2B_9H_9$] (62) in 27% yield.[44] In addition *closo*-[3-Cl-3,8-$(PMe_2Ph)_2$-3,1,2-$NiAs_2B_9H_8$] (63) was isolated in 6% yield. The C_s symmetry of the icosahedral configuration expected for *closo*-[3,3-$(PMe_2Ph)_2$-3,1,2-$NiAs_2B_9H_9$] (62) would lead to three signals of intensity 2 and three signals of unit intensity in the ^{11}B spectrum. The actual spectrum has a 1:3:2:2:1 intensity ratio due to an unresolved overlap. The single ^{31}P resonance in (62) suggests that at 21 °C there is rapid rotation of the metal vertex in the icosahedral structure relative to the pentagonal bonding face

of the diarsenaborane ligand.

Compound (63), *closo*-[3-Cl-3,8-$(PMe_2Ph)_2$-3,1,2-$NiAs_2B_9H_8$] was suggested to be formed by a phosphine-hydride interchange to give [3-H-3,8-$(PMe_2Ph)_2$-3,1,2-$NiAs_2B_9H_8$] which then underwent hydrogen-chlorine exchange. This type of phosphine-hydride interchange reaction has been previously reported for a number of (phosphine)metallacarborane complexes containing nickel,[45,46] platinum,[47] rhodium,[48] and ruthenium.[49,50,51] Compound (63) exhibits a 1:2:2:1:3 intensity ratio in it's $^{11}B\{^1H\}$ NMR spectrum, which is consistent with C_s symmetry. One signal of the area 1 was a doublet in the proton-decoupled ^{11}B NMR spectrum, which indicated that there was a B-P bond and this was confirmed in the $^{31}P\{^1H\}$ NMR spectrum. Furthermore, the phosphine attached to the cage must be located on the plane of symmetry in order to maintain the C_s symmetry of the molecule. The X-ray structure of the Pd analogue *i.e closo*-[3-Cl-3,8-$(PMe_2Ph)_2$-3,1,2-$PdAs_2B_9H_8$] (64) demonstrated that the phosphine was attached to the B(8) cage atom,[22,44] and it was assumed that the phosphine is on B(8) in (63) as well. The ^1H NMR spectrum of (63) contained two doublets in the methyl region of the spectrum, which suggests that the two methyl groups on each phosphine are chemically equivalent on the NMR time scale at 21°C. This in turn suggests that there is rapid rotation about (a) the *pseudo*-five-fold axis through nickel and the B_3As_2 face and (b) the B-P bond. Rotational behaviour such as this is quite common in metallaboranes (see section 4.2.3), and variable temperature proton NMR studies have been used to determine the energy of activation associated with this rotational process.[52] These studies have not yet been attempted for the compounds (62) and (63).

(ii) Palladadiarsenaboranes

The first palladadiarsenaboranes reported were *closo*-[3,3-$(PMe_2Ph)_2$-3,1,2-$PdAs_2B_9H_9$] (65), *closo*-[3,3-$(PPh_3)_2$-3,1,2-$PdAs_2B_9H_9$] (66) and *closo*-[3-Cl-3,8-$(L)_2$-3,1,2-$PdAs_2B_9H_8$] {L=PPh_3 (67); PMe_2Ph (64)}.[22,53] Treatment of a thf solution of *nido*-[7,8-$As_2B_9H_{10}$]$^-$ with a ten fold excess of triethylamine followed by an equimolar suspension of $[Pd(PPh_3)_2Cl_2]$ in thf afforded two different products, depending on the

reaction conditions. If the reaction was stirred at room temperature for 48h, the major product was *closo*-[3,3-$(PPh_3)_2$-3,1,2-$PdAs_2B_9H_9$] (66) in 31% yield. However, if the reaction mixture was stirred at ambient temperature for 16h and then at reflux for 20 min, the major product isolated was *closo*-[3-Cl-3,8-$(PPh_3)_2$-3,1,2-$PdAs_2B_9H_8$] (67) in 27% yield. Interestingly, the reaction between the *nido*-$[7,8\text{-}As_2B_9H_{10}]^-$ anion and $[Pd(PMe_2Ph)_2Cl_2]$ in thf in the presence of excess triethylamine at room temperature for 36h produced two compounds which were characterised as *closo*-[3,3-$(PMe_2Ph)_2$-3,1,2-$PdAs_2B_9H_9$] (65) in 40% yield and *closo*-[3-Cl-3,8-$(PMe_2Ph)_2$-3,1,2-$PdAs_2B_9H_8$] (64) in 19% yield. The migration of the PR_3 group (R_3=Ph_3, Me_2Ph) observed in the formation of (67) and (64) had precedence in the formation of [9-H-9,10-$(PEt_3)_2$-7,8,9-$C_2PtB_8H_9$],[54] and *closo*-[3-(μ-CO)-8-PPh_3-3,1,2-$NiC_2B_9H_{10}$]$_2$.[46]

Compound (65) has also been prepared by the reaction of *nido*-$[7,8\text{-}As_2B_9H_{10}]^-$ with *n*-butyllithium followed by $[Pd(PMe_2Ph)_2Cl_2]$ in thf for 45 min.[22,53] The structures of *closo*-[3,3-$(PMe_2Ph)_2$-3,1,2-$PdAs_2B_9H_9$](65) and *closo*-[3-Cl-3,8-$(PPh_3)_2$-3,1,2-$PdAs_2B_9H_8$] (67) were confirmed by single crystal X-ray analyses, Figures 1.15 and 1.16 respectively.[22,44,53]

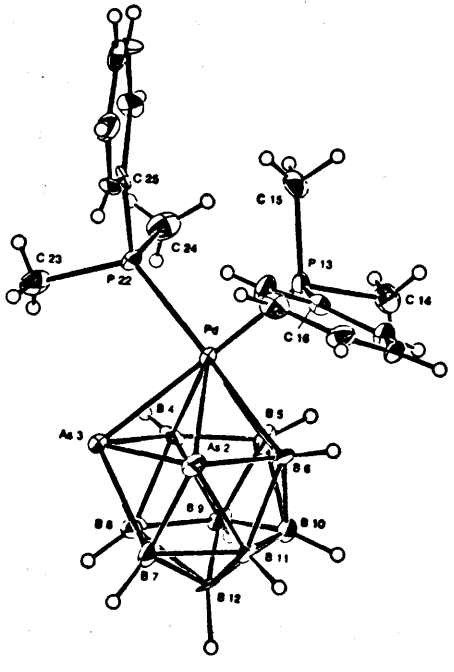

Figure 1.15 ORTEP diagram of *closo*-[3,3-$(PMe_2Ph)_2$-3,1,2-$PdAs_2B_9H_9$] (65).[1*,44]

[1*] The numbering scheme used in the diagram is the actual numbering used by Todd *et al*, in the crystal structure determination of (65). To label the compound according to the diagram it would be *closo*-[1,1-$(PMe_2Ph)_2$-1,2,3-$PdAs_2B_9H_9$].[44]

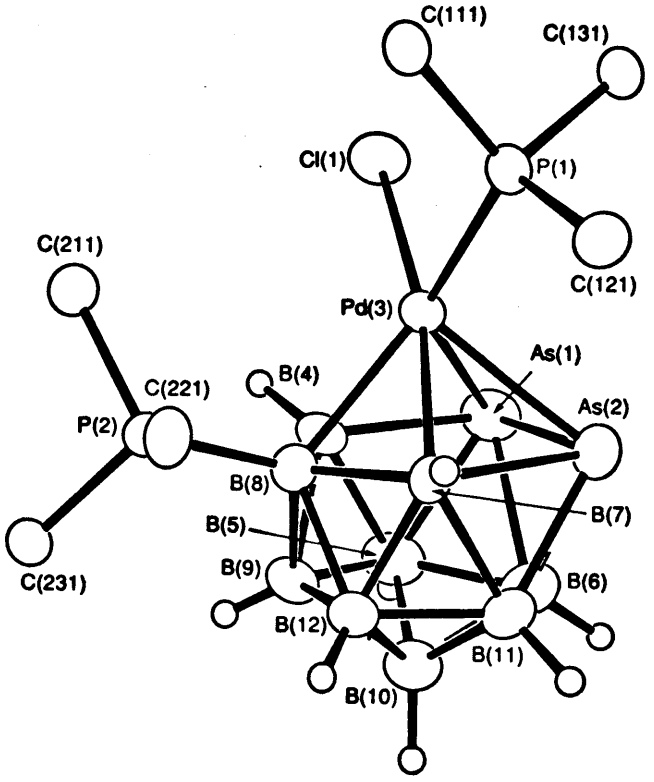

Figure 1.16 ORTEP-type plot of *closo*-[3-Cl-3,8-$(PPh_3)_2$-3,1,2-$PdAs_2B_9H_8$] (67).[53]

The compounds (65) and (67) are twelve atom *closo* systems and are both clearly distorted. In (65) the bonding of the Pd atom is markedly asymmetric *i.e.* off the *pseudo*-five-fold rotational axis of symmetry. This is seen in the bonding distances Pd-As(2) 2.6835(18) Å, Pd-As(3) 2.530(4) Å, Pd-B(4) 2.298(11) Å, Pd-B(5) 2.283(12) Å and Pd-B(6) 2.309(10) Å. In (67) different Pd-As and Pd-B distances may be expected in each Pd-B-As face since the Pd-Cl bond is *trans* to Pd-As(2)-B(7) whilst the Pd-P bond is *trans* to Pd-As(1)-B(4). However, in (67) the Pd-B distances are only significantly different at the "three times esd level" being 2.218(8) Å for Pd-B(7) and 2.291(8) Å for Pd-B(4).

Although the two chlorinated complexes *closo*-[3-Cl-3,8-$(PPh_3)_2$-3,1,2-$PdAs_2B_9H_8$] (67) and *closo*-[3-Cl-3,8-$(PMe_2Ph)_2$-3,1,2-$PdAs_2B_9H_8$] (64) are asymmetric and would therefore be expected to have nine separate ^{11}B resonance positions, the ready contrarotational fluxionality of the $\{Cl(PR_3)\}$ *versus* the $\{As_2B_9H_8(PR_3)\}$ $\{R_3=Ph_3$ (67); Me_2Ph (64)$\}$ ligand about the palladium atom confers a time-average mirror-plane symmetry on the molecules at room temperature in solution so that a 1:1:2:2:2:1 relative intensity is observed.

The reaction between *closo*-[3,3-$(PMe_2Ph)_2$-3,1,2-$PdAs_2B_9H_9$] (65) and [Pd(P-$Me_2Ph)_2Cl_2$] in a mixture of CH_2Cl_2/thf (2:1) for 12 days afforded the green compound *closo*-[3,4-Cl_2-3,8-$(PMe_2Ph)_2$-3,1,2-$PdAs_2B_9H_7$] (68) in 17% yield.[44] The previously reported *closo*-[3-Cl-3,8-$(PMe_2Ph)_2$-3,1,2-$PdAs_2B_9H_8$] (64) was also isolated from the reaction in 19% yield.[22,53] Compound (68) has a distinctive ^{11}B NMR spectrum since all nine boron atoms are chemically inequivalent because the molecule has C_1 symmetry. One of the $^{11}B\{^1H\}$ signals is a doublet due to ^{31}P coupling.[46,49] A single crystal X-ray diffraction study of (68) was undertaken to establish the structural details, Figure 1.17. As in the parent molecule (65), the $PdAs_2B_9$ cage is significantly distorted from a regular icosahedron due primarily to the large As and Pd atoms in the cage.[55]

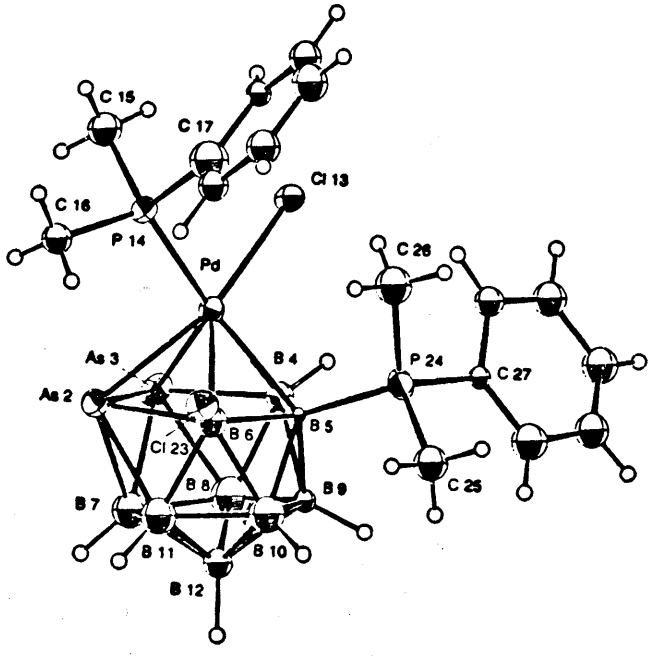

Figure 1.17 ORTEP diagram of *closo*-[1,6-Cl_2-1,5-$(PMe_2Ph)_2$-1,2,3-$PdAs_2B_9H_7$] (68)[44] (The original numbering scheme is used here).[2*]

[2*] The more conventional numbering scheme for this compound would be *closo*-[3,4-Cl_2-3,8-$(PMe_2Ph)_2$-3,1,2-$PdAs_2B_9H_7$]

(iii) Platinadiarsenaboranes

Until recently no platinadiarsenaboranes had been reported although many platinum containing MC_2B_9-cages were known.[56,57] Reaction between *closo*-1,2-$As_2B_{10}H_{10}$ and $[Pt(PPh_3)_4]$ in absolute alcohol at room temperature for 18h followed by refluxing for 24h gave *closo*-[3,3-$(PPh_3)_2$-3,1,2-$PtAs_2B_9H_9$] (69) in 9% yield.[22,53] Reaction of *nido*-[7,8,-$As_2B_9H_{10}$]$^-$ and $[Pt(PMe_2Ph)_2Cl_2]$ in thf in the presence of a ten fold excess triethylamine at room temperature for 2d and then at reflux for 6h produced *closo*-[3,3-$(PMe_2Ph)_2$-3,1,2-$PtAs_2B_9H_9$] (70) in 45% yield.[22,53] The molecular structure of *closo*-[3,3-$(PPh_3)_2$-3,1,2-$PtAs_2B_9H_9$] (69) was established using a single crystal X-ray analysis and is shown in Figure 1.18. One of the arsenic atoms is exchange-disordered with a BH group over two sites {labelled As/B(2) and As/B(4) in Figure 1.18}. Thus, the crystal contained both conformations of PtP_2 above the As_2B_3 face, Figure 1.19.

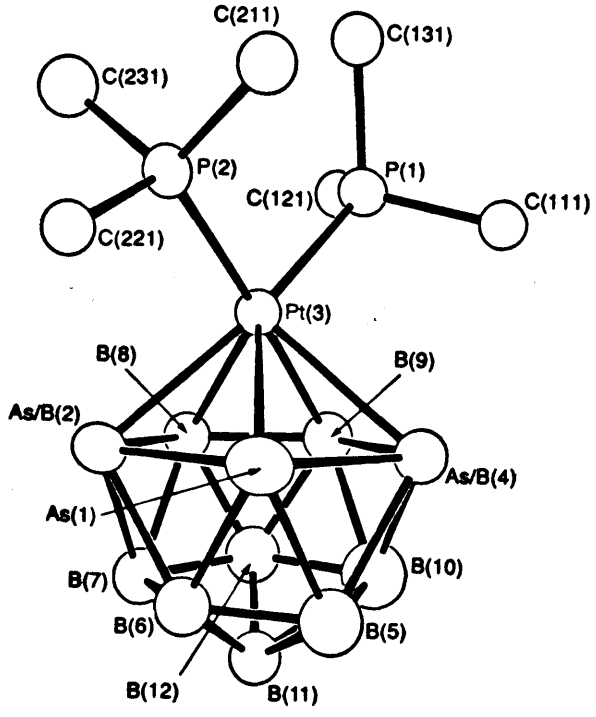

Figure 1.18 An ORTEP-type diagram of *closo*-[3,3-$(PPh_3)_2$-3,1,2-$PtAs_2B_9H_9$] (69).[53]

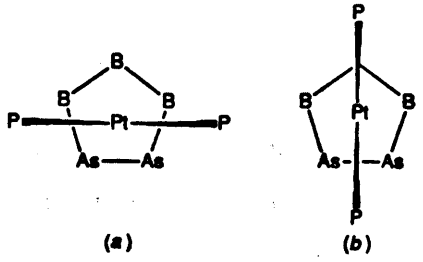

Figure 1.19 Possible conformations of the PtP_2 unit above the As_2B_3 face of the $\{As_2B_9H_9\}$ ligand: (a) As_2/PtP_2 "parallel", (b) As_2/PtP_2 "perpendicular".

The molecular structure of *closo*-[3,3-$(PMe_2Ph)_2$-3,1,2-$PtAs_2B_9H_9$] (70) is shown in Figure 1.20. The platinum-arsenic distances are significantly different, Pt-As(1) and Pt-As(2) being 2.655(4) and 2.545(4) Å respectively.[53] The conformation of the PtP_2 unit above the As_2B_3 face of the arsenaborane ligand in the solid state of (70) is the As_2/PtP_2 "parallel" one shown in Figure 1.19 (a) above. However, from variable temperature ^1H NMR spectroscopy an upper limit on free energy of rotation of $\Delta G^{\ddagger}$ *ca.* 30 kJ mol^{-1} was calculated.

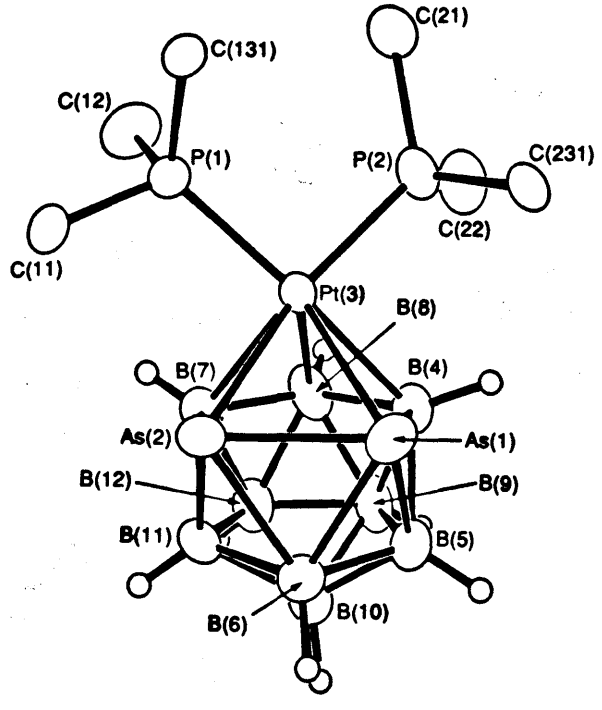

Figure 1.20 An ORTEP-type diagram of *closo*-[3,3-$(PMe_2Ph)_2$-3,1,2-$PtAs_2B_9H_9$] (70).[53]

(D) Group 11 derivatives of diarsenaboranes

Cupraarsenaboranes

Two cupraarsenaboranes have been synthesised and characterised.[58] Both are twelve vertex *closo*-species of the general formula [8-{OPr^{i}R}-3-PPh$_3$-3,1,2-CuAs$_2$B$_9$H$_8$] {R=Et (71), Me (72)}. Reaction of *nido*-[7,8-As$_2$B$_9$H$_{10}$]$^-$ with [CuNO$_3$(PPh$_3$)$_2$] in a 1:1 ratio in a mixed solvent, ethanol/acetone (1:1), at reflux for 2.5 h gave *closo*-[8-{OPr^i(Et)}-3-PPh$_3$-3,1,2-CuAs$_2$B$_9$H$_8$] (71) in 19% yield, Figure 1.21. Similarly, reaction of equimolar amounts of *nido*-[7,8-As$_2$B$_9$H$_{10}$]$^-$ with [CuNO$_3$(PPh$_3$)$_2$] in methanol/acetone gave *closo*-[8-{OPr^i(Me)}-3-PPh$_3$-3,1,2-CuAs$_2$B$_9$H$_8$] (72) in 23% yield. Compounds (71) and (72) were fully characterised by ^{11}B and ^{1}H NMR and IR spectroscopies and in the case of (71) by X-ray crystallography, Figure 1.21.

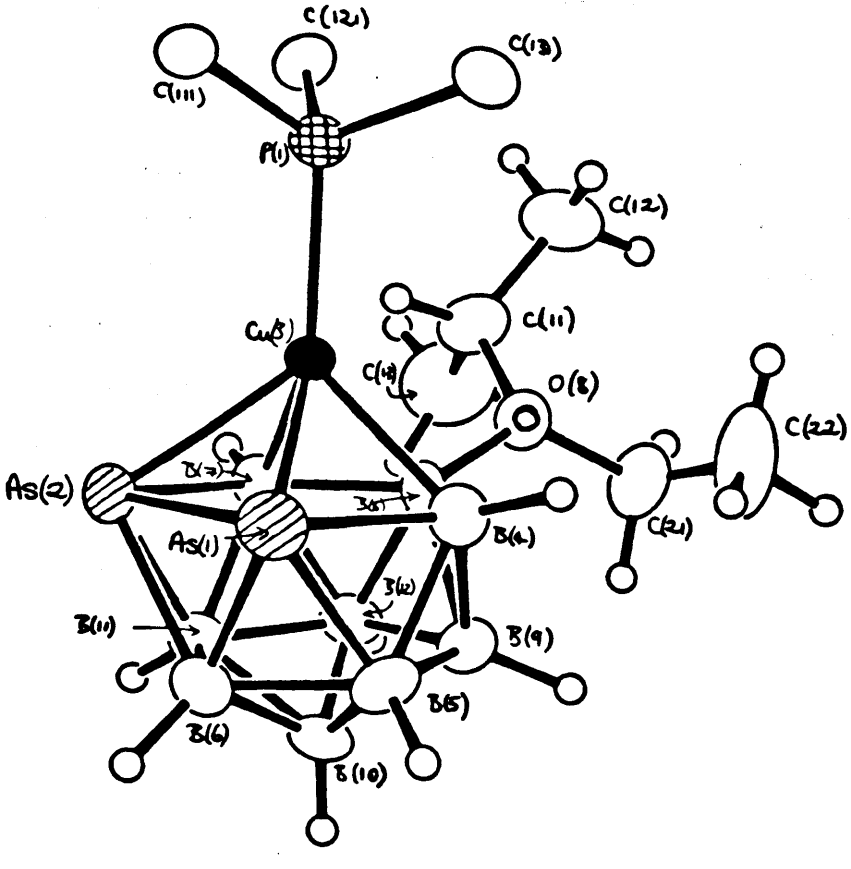

Figure 1.21 Molecular structure of *closo*-[8-{OPr^i(Et)}-3-PPh$_3$-3,1,2-CuAs$_2$B$_9$H$_8$] (71).[58]

The ^{11}B NMR spectra of (71) and (72) exhibited relative intensity patterns of 1:2:2:1:1:2 which were consistent with *closo*-cage geometries. The single X-ray crystal analysis of (71) confirmed the *closo*-geometry based on a distorted $CuAs_2B_9$ icosahedron in which the copper and both arsenic atoms were adjacent. The copper-arsenic bond lengths were identical 2.462(3) and 2.463(3) Å. The Pr^iOEt ether was directly bound to the boron atom in position (8) and the boron-oxygen distance was 1.561(10) Å. The formation of (71) and (72) are unique in metallaheteroborane chemistry. No arsenaborane complexes of silver or gold have been reported.

1.3 STIBABORANES

Relatively few stibaboranes have been reported.[44,59] In section 1.3 three stibaboranes are noted. In section 1.3.1 three stibacarboranes are discussed and in section 1.3.2 three metal derivatives of stibaboranes are reviewed. The mixed bismuth/stibaborane 1,2-$SbBiB_{10}H_{10}$ will be discussed in section 1.4 on bismaboranes.[60]

By reacting $Me_4N[7\text{-}AsB_{10}H_{12}]$ (1),[5,9] with triethylamine and $SbCl_3$ in thf an antimony atom was inserted in the AsB_{10} cage to give 1,2-$AsSbB_{10}H_{10}$ (73) in 46% yield.[59] Compound (73) was the first known mixed heteroatom group V/15 borane. It has one of the highest melting points of any heteroatom borane, (>500°C) and was structurally characterised by ^{11}B NMR spectroscopy.

Reaction of $B_{10}H_{14}$ in thf with Zn/triethylamine/$SbCl_3$ afforded 1,2-$Sb_2B_{10}H_{10}$ (74) in 11% yield, Figure 1.21. The ^{11}B and ^1H NMR spectra were assigned.[6]

Figure 1.22 Suggested structure of 1,2-$Sb_2B_{10}H_{10}$ (74).[6]

The reaction of $Me_4N[B_{11}H_{14}]$ in thf with triethylamine and $SbCl_3$ gave $Me_4N[SbB_{11}H_{11}]$ (75) in 13% yield.[59] As in the case of $Me_4N[AsB_{11}H_{11}]$ (6),[5] attempts to quaternise the antimony in (75) led to cage destruction. Resonances in the ^{11}B spectrum of (75) appeared as a 1:5:5 pattern.

1.3.1 Stibacarboranes

To date only three antimony containing carboranes have been reported and characterised.[11] These include the 1,2- and 1,7- isomers of the twelve atom *closo* compound $CSbB_{10}H_{10}$ and the eleven atom *nido* anion $[CSbB_9H_{11}]^-$.

Addition of antimony triiodide to $Na_3[B_{10}H_{10}CH] \cdot (thf)_2$ in thf at 0°C gave 1,2-$CSbB_{10}H_{11}$ (76) in 41% yield.[11,21] The measured NMR data for 1,2-$CSbB_{10}H_{11}$ (76) were assigned to a *closo*-1,2-$XYB_{10}H_{10}$ configuration (X=CH, Y=Sb) on the basis of relative intensities and [^{11}B-^{11}B]-COSY correlations, Figure 1.23. The ^{11}B NMR spectrum of this molecule was very similar to the ^{11}B NMR spectra of the phosphacarborane compound 1,2-$CPB_{10}H_{11}$ (77)[12] and the arsena-analogue 1,2-$CAsB_{10}H_{11}$ (10).[11] Compound (76) decomposed above 240°C without melting.

Figure 1.23 Proposed structure of 1,2-$CSbB_{10}H_{11}$ (76).[6]

Heating 1,2-$CSbB_{10}H_{11}$ (76) at 450 °C for 13h produced a 20% yield of 1,7-$CSbB_{10}H_{11}$ (78). Thermolysis of (76) at 500 °C for 10h in a sealed tube afforded a very small quantity of sublimable products. Gas chromatographic analysis of these indicated the presence of (78) and another component with a shorter retention time

as would be expected for 1,12-$CSbB_{10}H_{11}$. However attempts to increase the yield of the 1,12-isomer were unsuccessful and it was not characterised fully.

Treatment of 1,2-$CSbB_{10}H_{11}$ (76) with neat piperidine at reflux gave mainly $[CB_{10}H_{13}]^-$ which was identified by comparison of its infrared and ^{11}B NMR spectra with those of an authentic sample.[11] However, reaction of (76) with piperidine in a 1:4 molar ratio in a dilute solution of benzene at reflux produced $[7,8\text{-}CSbB_9H_{11}]^-$ (79). This was isolated as the tetramethylammonium salt in 74% yield. Attempted methylation of (79) under the conditions used with the phosphorus and arsenic derivatives gave no observable reaction.

1.3.2 Metal derivatives of Stibaboranes

Only three metal derivatives of stibaboranes have been reported. Two contained the $Sb_2B_9H_9$ ligand and one was an $AsSbB_9H_9$ derivative.[44,59,61]

Reaction of 1,2-$Sb_2B_{10}H_{10}$ (74) or 1,2-$AsSbB_{10}H_{10}$ (73) with piperidine at 50-70 °C gave ionic products that were precipitated from aqueous solutions as Me_4N^+ salts. On attempted recrystallisation the salts slowly decomposed.[59] Addition of freshly prepared *cyclo*pentadiene and anhydrous cobalt chloride to the piperidine solution afforded twelve-vertex clusters as $[Co(\eta^5\text{-}Cp)(7,8\text{-}Sb_2B_9H_9)]$ (80) and $[Co(\eta^5\text{-}Cp)(7,8\text{-}AsSbB_9H_9)]$ (81) in 22% and 25% yields respectively.[59] Compounds (80) and (81) were characterised spectroscopically and by elemental analyses.

The reaction of $[PdCl_2(PMe_2Ph)_2]$ with the *nido*-$[7,8\text{-}Sb_2B_9H_9]^{2-}$ ion in thf at room temperature for 2h led to the formation of *closo*-$[3,3\text{-}(PMe_2Ph)_2\text{-}3,1,2\text{-}PdSb_2B_9H_9]$ (82) in 25% yield, Figure 1.24, which was characterised spectroscopically and by an X-ray crystallographic study.[44] The most striking feature of the solid state structure of (82) is the distortion of the 12-membered cage that results from the inclusion of the relatively large Sb and Pd atoms. This was more marked than in the corresponding compound *closo*-$[3,3\text{-}(PMe_2Ph)_2\text{-}3,1,2\text{-}PdAs_2B_9H_9]$ (65).

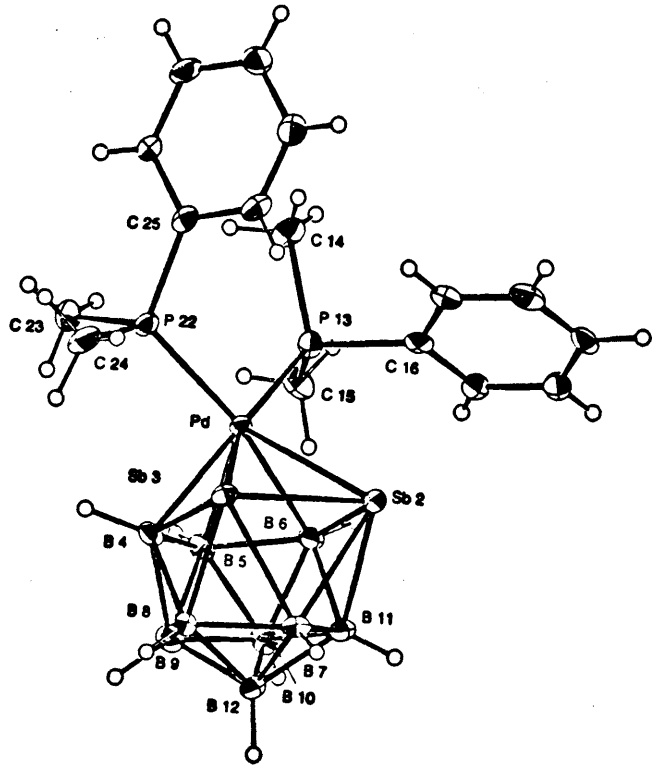

Figure 1.24 ORTEP diagram of *closo*-[1,1-$(PMe_2Ph)_2$-1,2,3-$PdSb_2B_9H_9$] (82) (Using original numbering scheme).[3*,44]

1.4 BISMABORANES

Only five bismaboranes have been synthesised and characterised.[60] The first bismaboranes have been recently prepared and characterised, and have been found to be surprisingly heat-stable. None of the compounds melt before 500 °C.[60] Four of the bismaboranes are twelve atom *closo* structures, 1,2-$EBiB_{10}H_{10}$ {E=Bi, P, As, Sb} and the fifth compound is the anion $[BiB_{11}H_{11}]^-$. These five compounds will be discussed in this section.

The reaction of decaborane with excess triethylamine and $BiCl_3$ at room temperature in thf gave 1,2-$Bi_2B_{10}H_{10}$ (83) in 8% yield.[60] The structure of (83) was

---

3* The more conventional numbering scheme for (82) would be *closo*-[3,3-$(PMe_2Ph)_2$-3,1,2-$PdSb_2B_9H_9$]

obtained from a single-crystal X-ray structure study. An ORTEP plot of (83) is given in Figure 1.25, in which the highly distorted icosahedral geometry is confirmed. The average Bi-Bi distance in the four molecules which exist in the unit cell is 2.957 Å.

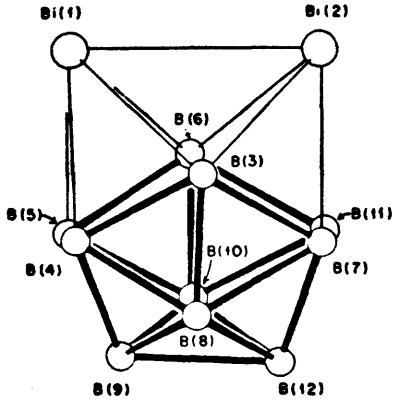

Figure 1.25 ORTEP plot of 1,2-$Bi_2B_{10}H_{10}$ (83).[60]

The mixed compound 1,2-$PBiB_{10}H_{10}$ (84) was synthesised in 9% yield from the reaction of a ten fold excess of $BiCl_3$ with $Me_4N[PB_{10}H_{12}]$ and triethylamine in thf.[60] The mixed compounds 1,2-$AsBiB_{10}H_{10}$ (85) and 1,2-$SbBiB_{10}H_{10}$ (86) were both synthesised in 1% yields by reaction of decaborane, triethylamine, $AsCl_3$ or $SbCl_3$, and $BiCl_3$.[60] The compounds were characterised spectroscopically and all had the same type of structure, Figure 1.26.

Treating $B_{11}H_{14}^-$ with *n*-butyllithium and adding solid $BiCl_3$ gave a black solution from which $Me_4N[BiB_{11}H_{11}]$ (87) was isolated in 25% yield.[60] The ^{11}B NMR spectrum for compound (87) consists of resonances in a 1:5:5 ratio.

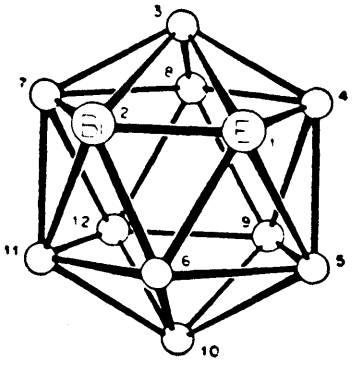

Figure 1.26 Proposed structure and numbering of the bismaboranes of the general formula 1,2-$EBiB_{10}H_{10}$ {E=Bi(83), P(84), As(85), Sb(86)}.[60]

1.5 PHOSPHABORANES

Section 1.5 reviews the known phosphaboranes and section 1.5.1 contains metal derivatives of phosphaboranes. Section 1.5.2 discuses phosphacarboranes and their metal derivatives.

Many phosphaboranes are known and for the purpose of this section they have been arranged in the following order. First the twelve-atom phosphaborane $(PPh)B_{11}H_{11}$ is discussed. This is followed by compounds containing the $(RP)B_{10}$- cage. The next section discusses the synthesis of $P_2B_{10}H_{10}$ compounds and their derivatives and include a short discussion on twelve atom *closo* phosphaboranes containing other group V atoms and also the eleven-atom $PB_{10}H_{10}$ which is a minor product in the formation of $P_2B_{10}H_{10}$. Derivatives of the PB_{11}- cage are then discussed and *closo*-diphosphahexaborane $P_2B_4Cl_4$ is mentioned. Borane compounds containing phosphorus units in bridging positions are discussed next.

The first phosphaborane cluster which contained a cage phosphorus atom was $(PPh)B_{11}H_{11}$ (88).[62] This was formed from the reaction of $[B_{11}H_{13}]^{2-}$ with phenylphosphorus dichloride in low yield. The ^1H NMR and ^{11}B NMR data suggested an icosahedral structure.

Deprotonation of decaborane with sodium hydride in diethylether followed by slow addition of $RPCl_2$ (R=Ph, Me) afforded $(PPh)B_{10}H_{12}$ (89) or $(PMe)B_{10}H_{12}$ (90) in moderate yield.[61] The ^{11}B NMR spectra of (89) and (90) did not distinguish between 7-$(PR)B_{10}H_{12}$ and 2-$(PR)B_{10}H_{12}$ isomers. Assuming, however, that the decaborane framework has not rearranged under the mild reaction conditions, the 7-$(PR)B_{10}H_{12}$ isomer would be the expected product of a simple phosphorus insertion reaction. The X-ray analysis of (90) was reported recently.[63] This confirmed the earlier proposed structure based upon an icosahedron with one vertex removed, Figure 1.27.[61]

One bridging proton can be removed from (89) or (90) by a base such as aqueous ammonia. Both bridging hydrogens can be removed by a strong base such as NaH. Addition of tetramethylammonium chloride solution to aqueous ammonia solutions of (89) or (90) precipitated Me_4N[7-$(PPh)B_{10}H_{11}$] (91) and Me_4N[7-$(PMe)B_{10}H_{11}$] (92).[62]

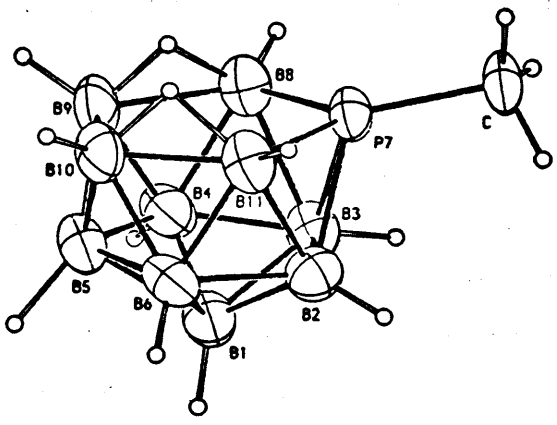

Figure 1.27 Molecular structure of 7-(PMe)$B_{10}H_{12}$ (90).[63]

In 1976, Little reported the synthesis of a number of other phosphaboranes of the type [7-(PR)$B_{10}H_{12}$] and Me_4N[7-(PR)$B_{10}H_{11}$] in addition to (89)-(92).[64] In the presence of 4 equivalents of NaH, decaborane in diethylether reacts with $RPCl_2$ (R = Ph, Me, Et, *n*-Pr) to give [7-(PR)$B_{10}H_{11}$]$^-$ which on protonation afforded 7-(PR)$B_{10}H_{12}$ {R = Ph (89), Me (90), Et (93), *n*-Pr (94)}.[61,64] Unlike 7-(AsMe)$B_{10}H_{12}$ (2),[5] 7-(PMe)$B_{10}H_{12}$ (90) was not demethylated by sodium in liquid ammonia or by sodium hydride in refluxing thf. Deprotonation of 7-(PR)$B_{10}H_{12}$ with dilute ammonia and subsequent precipitation with tetramethylammonium chloride solution gave Me_4N[7-(PR)$B_{10}H_{11}$] {R=Ph (91), Me(92), Et(95), *n*-Pr (96)}.[61,64]

Reaction of $B_{10}H_{14}$ in thf with Zn/triethylamine/PCl_3 gave 1,2-$P_2B_{10}H_{10}$ (97) in 12% yield.[65] A high resolution mass spectrum verified the molecular formula as $P_2B_{10}H_{10}$. Compound (97) exhibited a ^{11}B NMR spectrum which is consistent with an icosahedral structure similar to the twelve atom *closo* compound 1,2-$As_2B_{10}H_{10}$ (7). The thermal conversion of 1,2-$P_2B_{10}H_{10}$ (97) to 1,7-$P_2B_{10}H_{10}$ (98) occurred at 560-590 °C in a sealed tube. The molecular composition of (98) was confirmed by high-resolution mass spectroscopy.

From the product mixture in the synthesis of 1,2-$P_2B_{10}H_{10}$ (97) the phosphaborane anion [2-PB_9H_9]$^-$ (99) was isolated in 0.3% yield.[66] The anionic compound (99) was isolated as the tetramethylammonium salt and its ^{11}B NMR spectrum was consistent with a *closo*-[2-PB_9H_9]$^-$ structure for the anion.

Aqueous base rapidly removed one phosphorus atom from 1,2-$P_2B_{10}H_{10}$ (97) to form the 7-$PB_{10}H_{12}^-$ (100) ion in 27% yield.[65] It was suggested that (100) has the

nido 11-atom icosahedral fragment structure resulting from abstraction of one phosphorus atom from 1,2-$P_2B_{10}H_{10}$ (97). The ^{11}B NMR spectrum of (100) is consistent with the suggested structure. Treatment of [7-$PB_{10}H_{12}$]$^-$ (100) with methyl iodide afforded the previously reported 7-(PMe)$B_{10}H_{12}$ (90) in 16% yield.

In an anhydrous, oxygen-free, environment, 1,2-$P_2B_{10}H_{10}$ (97) reacted with piperidine in chloroform solution to give [7,8-$P_2B_9H_{10}$]$^-$ (101) in 76% yield.[66] It was suggested that (101) has a *nido* 11-vertex structure resulting from abstraction of a boron atom adjacent to both phosphorus atoms of 1,2-$P_2B_{10}H_{10}$ (97) and the ^{11}B NMR spectrum was consistent with such a *nido* structure with the two phosphorus atoms in adjacent positions on the open face as in [7,8-$As_2B_9H_{10}$]$^-$ (8) (see figure 1.4).[6] The ^{11}B spectrum of [7,8-$As_2B_9H_{10}$]$^-$ (8) (as discussed in section 1.2) was quite similar to that of (101).

The phosphaborane (PMe)$B_{11}H_{11}$ (102) was produced in 4% yield from the reaction of $[B_{11}H_{13}]^{2-}$ with $PMeCl_2$ in thf.[63] The same reaction in diethylether gave (PMe)$B_{10}H_{12}$ (90) in 12% yield which had been prepared previously by a different route (see above).[64] The ^{11}B NMR spectrum of (102) is consistent with an icosahedral *closo*-PB_{11} framework in solution. A single-crystal X-ray analysis showed the molecular structure to be a slightly distorted icosahedron in the solid state, Figure 1.28.[63]

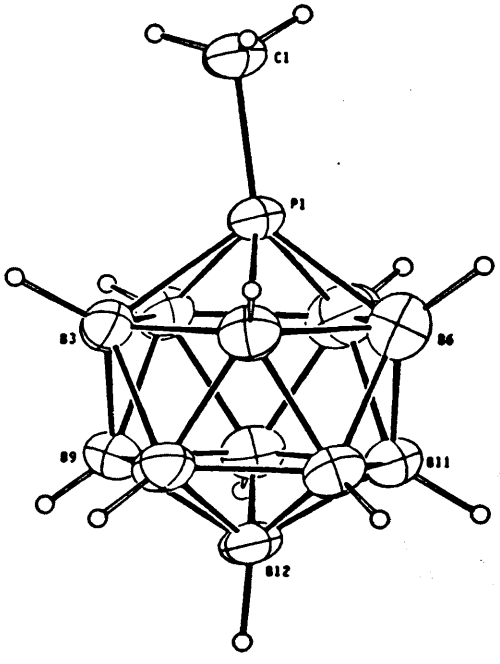

Figure 1.28 Molecular structure of (PMe)$B_{11}H_{11}$ (102).[63]

Recently, a series of phosphaboranes have been reported.[66] The mixed heteroboranes 1,2-$PAsB_{10}H_{10}$ (103) and 1,2-$PSbB_{10}H_{10}$ (104) were prepared in 4% and 3% respectively by reaction of decaborane in thf with triethylamine and mixtures of PCl_3 and $AsCl_3$ or PCl_3 and SbI_3, respectively {the synthesis of the bismuth compound 1,2-$PBiB_{10}H_{10}$ (84) has been discussed in section 1.4}. The individual boron atoms in 1,2-$PEB_{10}H_{10}$ were assigned, (E =As, Sb or Bi), Figure 1.29.

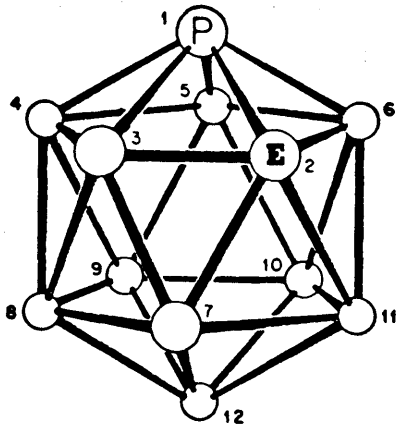

Figure 1.29 Numbering scheme for 1,2-$PEB_{10}H_{10}$ {E =As(103), Sb(104) or Bi(84)}.[66]

The reaction leading to the preparation of 1,2-$PB_{10}H_{10}$ (97) gave several products, one of which was formed in very low yield (0.5%) and identified as the *closo*-phosphaborane, 6-Et_3N-2-PB_9H_8 (105).[65] The ^{11}B NMR spectrum of (105) exhibited nine resonances all of unit area indicating a total lack of symmetry in the molecule. The structure of (105) was determined by a single-crystal X-ray study, Figure 1.30.[65]

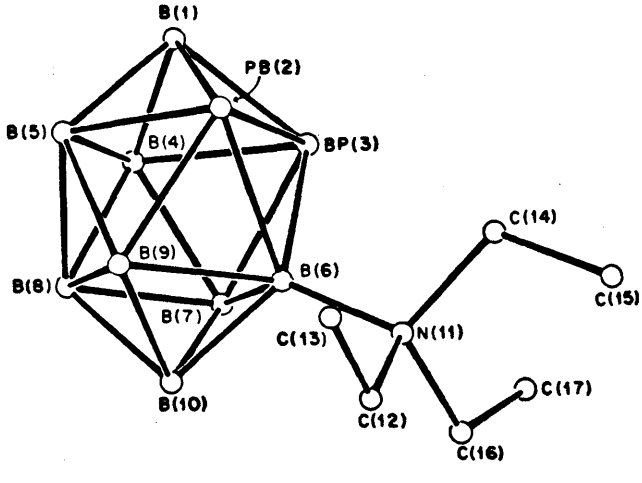

Figure 1.30 Molecular structure of 6-Et_3N-2-PB_9H_8 (105).[65]

The structural results of (105) are complicated by the fact that two different molecules are present in the asymmetric unit, each of which exists as an enantiomeric pair. The enantiomers cause the PB(2) and PB(3) positions to be disordered. Because of the complexities of this structure, all P-B bond distances can only be considered as approximate values.

When freshly prepared $Me_3NH[B_{11}H_{14}]$ was reacted in thf with 4 equivalents of *n*-butyllithium followed by reaction with an excess of PCl_3 in thf solution, 2-NMe_3-1-$PB_{11}H_{10}$ (106) was formed in 29% yield.[66] The ^{11}B NMR spectrum of (106) is consistent with an icosahedral phosphaborane having a Me_3N substituent at either B(2) or B(7). A single-crystal X-ray study of (106) clearly showed that the trimethylamine is attached to B(2) as illustrated in Figure 1.31, and the phosphorus atom causes a local distortion of the icosahedron.

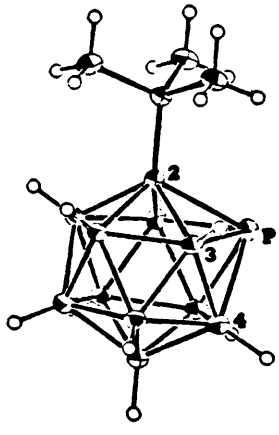

Figure 1.31 ORTEP drawing of 2-NMe_3-1-$PB_{11}H_{10}$ (106).[66]

Treatment of $Me_3NH[B_{11}H_{14}]$ with excess *n*-butyllithium and PCl_3 afforded both $[PB_{11}H_{11}]^-$ (107) (in 14% yield) and 2-NMe_3-1-$PB_{11}H_{10}$ (108) (in 29% yield).[66] The ^{11}B NMR spectrum of (107) had a 1:5:5 pattern of doublet resonances expected for this icosahedral ion.

Pyrolysis of a mixture of B_2Cl_4 and PCl_3 at 330 °C gave $P_2B_4Cl_4$ (109), the first *closo*-diphosphahexaborane derivative, as a hygroscopic, colourless, crystalline solid.[67] The X-ray determined structure, shown in Figure 1.32 is based on an

octahedron, which is considerably distorted by the large phosphorus atoms which are adjacent to each other. The P(1)-P(2) distance, 2.222(3) Å corresponds to a single bond.

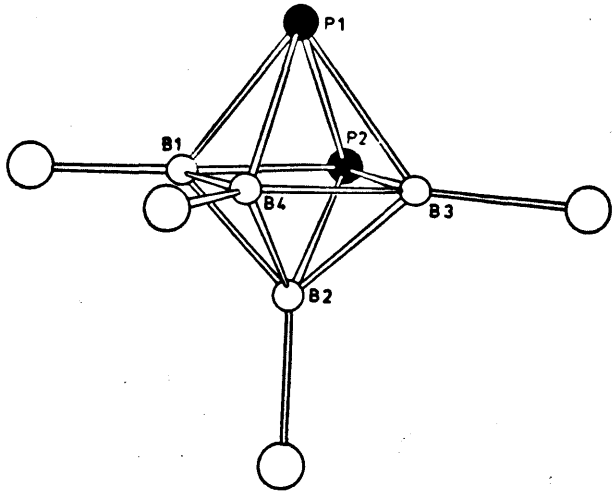

Figure 1.32 Molecular structure of *closo*-$P_2B_4Cl_4$ (109).[67]

Bridging phosphaboranes

The borane $B_{10}H_{12}(SMe_2)_2$ reacts with the phosphaalkyne P≡CBu^t in a 1:2 mole ratio to form the product $[B_{10}H_{12}(SMe_2)][CBu^t\text{-}PH](B_{10}H_{12})$ (110) in 78% yield. This contains two B_{10} units linked by HP and CBu^t bridges, Figure 1.33.[68]

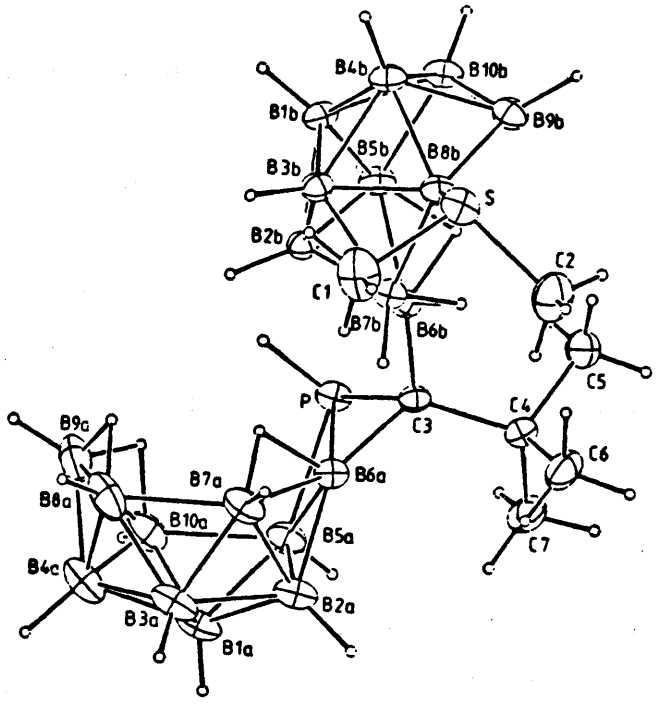

Figure 1.33 Molecular structure of $[B_{10}H_{12}(SMe_2)][CBu^t\text{-}PH](B_{10}H_{12})$ (110).[68]

The structure was determined by X-ray analysis, Figure 1.33. The ^{11}B spectrum was assigned.

The above compound (110) is not the only cluster compound known where a phosphorus atom occupies a μ^2-bridging position. The structure of the *nido*-compound 5,6-μ-$PPh_2B_{10}H_{13}$ (111) has been determined by single crystal X-ray analysis, Figure 1.34.[69] There is also a unique 6,9-B_{10}-bridged phosphido species *arachno*-$[PPh_2B_{10}H_{12}]^-$ (112).[70]

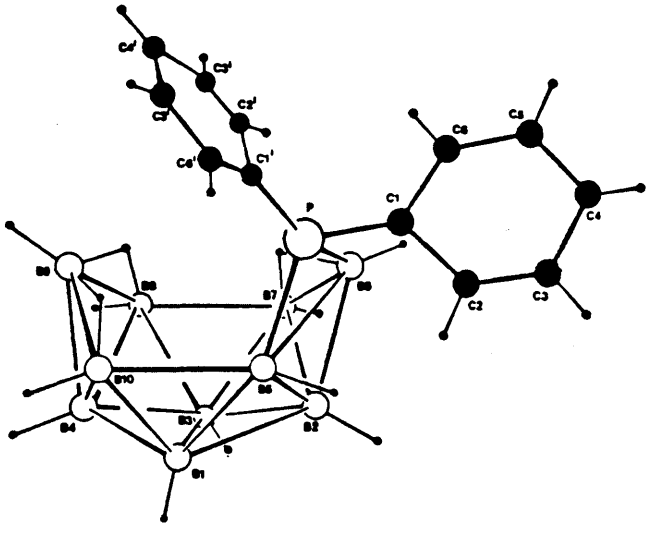

Figure 1.34 Molecular structure of 5,6-μ-$PPh_2B_{10}H_{13}$ (111).[69]

In 1986, Gaines reported the first *nido*-methylenephosphahexaboranes, $CPB_5H_8R_2$ {R=Me_3Si (113), Ph (114)}, Figure 1.35.[71] Two routes were developed for the preparation of this new class of heteroborane cluster. Reaction of R_2CHPCl_2 (R=Me_3Si, Ph) with $[B_5H_8]^-$ in diethylether at -196 °C afforded a reaction mixture containing the phosphino-bridged derivatives (μ-$R_2CHPCl)B_5H_8$, as well as B_5H_9 and traces of $R_2CPB_5H_8$. Addition of 2,7-dimethylpyridine to the reaction mixture resulted in nearly quantitative formation of $R_2CPB_5H_8$ {R=Me_3Si (113), Ph (114)}. Compound (113) was also synthesised directly by the reaction of $[B_5H_8]^-$ with the phosphaalkene $(Me_3Si)_2C{=}PCl$ in diethylether at -196 °C. The ^{11}B NMR spectra of compounds (113) and (114) differ considerably from those of the (μ-$R_2CHPCl)B_5H_8$ (R=Me_3Si, Ph) derivatives. It was thought, based on ^{31}P NMR data, that the bonding

about the phosphorus atoms in (113) and (114) was similar to that in the phosphorus ylides $R_3P{=}CR^1_2$. A proposed structure for *nido*-methylenephosphahexaboranes (113) and (114) is illustrated in Figure 1.35.

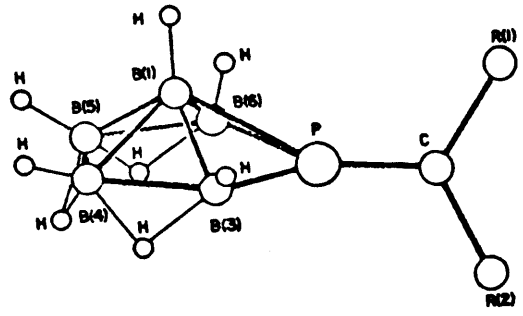

Figure 1.35 Proposed structure of $R_2CPB_5H_8$.[71]

Recently a series of small bridging phosphaboranes of the type [μ{R(Me$_3$SiO)HCPX}B_5H_8] (R = Bu^t or adamantyl) (X = SiMe$_3$, H or D) in excellent yields, have been reported.[72,73] These will not be discussed in detail in this work since the phosphorus atom is not considered part of the cluster.

1.5.1 Metal derivatives of phosphaboranes

In this section eleven metal derivatives of phosphaboranes are discussed. The first three complexes are derivatives of eleven atom PB_{10}- containing phosphaboranes. Six cobalt derivatives of phosphaboranes and platinum and rhodium derivatives of the *nido* anion [7-(PPh)$B_{10}H_{11}$]$^-$ are discussed.

The first reported metallaphosphaborane was Me$_4$N[Mn(CO)$_3${(PPh)$B_{10}H_{10}$}] (115).[61] This was prepared by reacting 7-(PPh)$B_{10}H_{12}$ (89) with two equivalents of NaH and one equivalent of [Mn(CO)$_5$Br] in thf. Compound (115) was a pale yellow, air-sensitive solid which was characterised only by elemental analyses and its IR spectrum.

In 1974 Todd *et al.* prepared some iron and molybdenum complexes of eleven-atom PB_{10}- containing heteroboranes.[36] Reaction between [Fe(CO)$_2$(η^5-Cp)*cyclo*-hexene]PF_6 and [7-$PB_{10}H_{12}$]$^-$ (100) in acetone gave [Fe(CO)$_2$(η^5-

Cp)($PB_{10}H_{12}$)] (116) in moderate yield. It was proposed from ^{11}B and ^{31}P NMR studies that (116) contained the iron atom σ-bonded to the phosphorus atom, Figure 1.36. Treatment of [$Mo(CO)_3(\eta^7$-$C_7H_7)$] with [7-$PB_{10}H_{12}$]$^-$ (100) in acetone at reflux produced [$Mo(CO)_3(\eta^7$-$C_7H_7)(PB_{10}H_{12})$] (117). The ^{11}B NMR spectrum of (117) was quite similar to that of compound (116), consequently it was proposed that the [7-$PB_{10}H_{12}$]$^-$ (100) anion was σ-bonded to the molybdenum atom *via* the phosphorus atom.

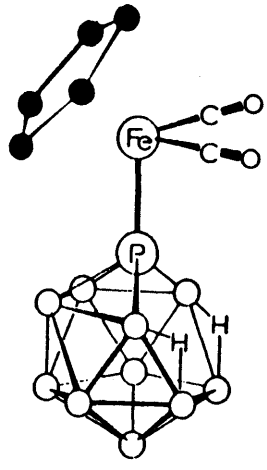

Figure 1.36 Proposed structure of [$Fe(CO)_2(\eta^5$-Cp)($PB_{10}H_{12}$)] (116).[36]

A number of *cyclo*pentadienylcobalt(III) complexes of phosphaboranes have been synthesised.[64] Reacting anhydrous cobalt chloride, *cyclo*pentadiene, 7-(PR)$B_{10}H_{12}$ and excess KOH in anhydrous ethanol gave low to moderate yields of [$Co(\eta^5$-Cp){7-(PR)}$B_{10}H_{10}$)] {R = Me (118), Et (119), *n*-Pr (120) and Ph (121)}. Compound (118) was obtained in the lowest yield 9% and (307) in the highest yield 60%. A by-product was Me_4N[$Co(\eta^5$-Cp)($PB_{10}H_{10}$)] (122).[64] Treating (122) with MeI, EtI, or *n*-PrI gave (118), (119) and (120) respectively in high yields. Compounds (118)-(121) were characterised by elemental analyses, IR, ^1H NMR and ^{11}B NMR spectroscopy.

The first metallaphosphaborane to be structurally characterised was based on the seven-vertex Co_4B_2P unit.[74] Reaction of BH_3·thf with [$Co(\eta^5$-Cp)(PPh_3)$_2$] in a 2.5:1 molar ratio produced *closo*-[2-Ph-1,3,6,7,2-{(η^5-Cp)Co_4}PB_2H_2] (123) in 5%

yield. The single-crystal X-ray determined structure of (123) is shown in Figure 1.37. It was based on a pentagonal bipyramid containing four cobalt, one phosphorus and two boron atoms in the cluster core.

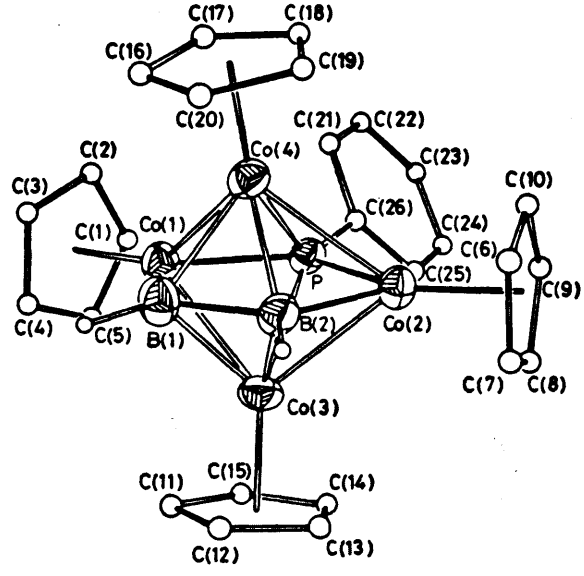

Figure 1.37 Molecular structure of *closo*-[2-Ph-1,3,6,7,2-{(η^5-Cp)Co$_4$}PB$_2$H$_2$] (123).[74]

The preparation, molecular structure and NMR study of *closo*-[1,1-(PMe$_2$Ph)$_2$-2-Ph-1,2-PtPB$_{10}$H$_{10}$] (124) and some related chemistry has been reported.[22,75] Reaction between [Pt(PMe$_2$Ph)$_2$Cl$_2$] and Et$_4$N[*nido*-7-(PPh)B$_{10}$H$_{11}$] in refluxing CH$_2$Cl$_2$ solution for one hour gave (124) as a yellow air-stable solid in 43% yield. Compound (124) was characterised by NMR and mass spectrometry and by single crystal X-ray diffraction analysis, Figure 1.38. The basic cluster structure was that of a twelve-vertex slightly distorted dodecahedron with the platinum and phosphorus atoms occupying adjacent sites. The metal to cluster bonding was rotationally fluxional with $\Delta G^{\ddagger}$ *ca.* 58 kJ mol^{-1}.

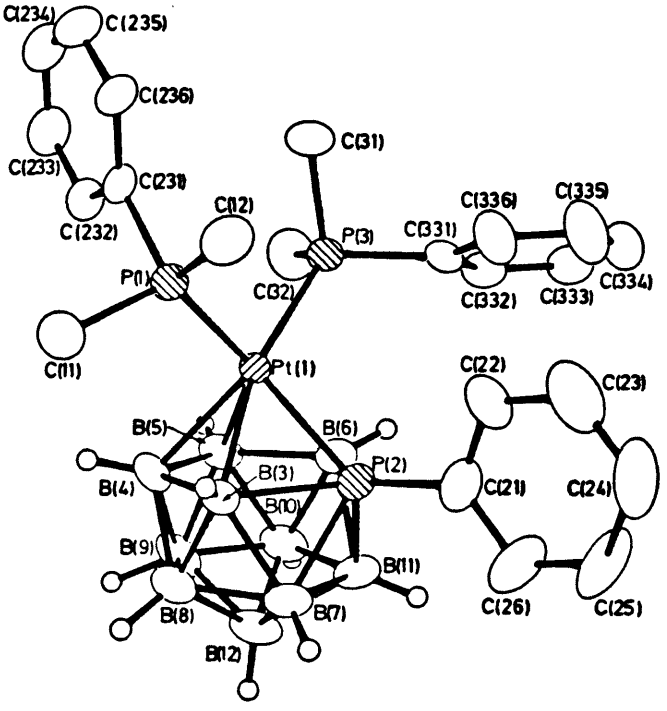

Figure 1.38 Molecular structure of *closo*-[1,1-$(PMe_2Ph)_2$-2-Ph-1,2-$PtPB_{10}H_{10}$] (124).[75]

In view of the successful preparation of (124), the *nido*-$[7\text{-}(PPh)B_{10}H_{11}]^-$ anion was reacted with a variety of other metal halide complexes, specifically, $[Rh(CO)(PPh_3)_2Cl_2]$, $[Rh(PMe_2Ph)_3Cl_3]$, $[\{Rh(\eta^5\text{-}Cp^*)Cl_2\}_2]$, $[Ir(PMe_2Ph)_3Cl_3]$ and $[\{Ru(\eta^6\text{-}C_6Me_6)Cl_2\}_2]$. Of these only $[\{Rh(\eta^5\text{-}Cp^*)Cl_2\}_2]$ gave viable quantities of metallaborane products, the others appeared not to react with Et_4N[*nido*-7-$(PPh)B_{10}H_{11}$], in CH_2Cl_2 solution. Reaction of $[\{Rh(\eta^5\text{-}Cp^*)Cl_2\}_2]$ with Et_4N[*nido*-7-$(PPh)B_{10}H_{11}$] following a procedure analogous to that described for (124) afforded two products. The first was identified from NMR spectroscopy as *nido*-[6-$(\eta^5\text{-}Cp^*)$-6-RhB_9H_{13}], a known species of straightforward *nido* configuration.[75] The second, an orange crystalline solid, was identified by its ^1H NMR and ^{11}B NMR spectra as *closo*-[7-Cl-2,3-$(\eta^5\text{-}Cp^*)$-1-Ph-2,3,1-$Rh_2PB_9H_8$] (125).[75]

1.5.2 Phosphacarboranes and their metal derivatives

In this section compounds based on the $CPB_{10}H_{11}$ cage are discussed initially. These are followed by phosphorus derivatives of *nido*-$[R_2C_2B_4H_4]^{2-}$.

The first compound of this type to be prepared was 1,2-$CPB_{10}H_{11}$ (77).[12,62] Slow addition of phosphorus trichloride in petroleum ether to a slurry of $Na_3[CB_{10}H_{11}]\cdot(thf)_2$ in petroleum ether gave 1,2-$CPB_{10}H_{11}$ in 40-50% yield.[12] Thermal isomerisation of 1,2-$CPB_{10}H_{11}$ in a sealed tube at 500 °C for 10h produced 1,7-$CPB_{10}H_{11}$ (126) in *ca.* 55% yield.[12,62] Pyrolysis of 1,2-$CPB_{10}H_{11}$ at 650 °C for 19h produced a 50:50 mixture of 1,7-$CPB_{10}H_{11}$ (126) and the more volatile 1,12-$CPB_{10}H_{11}$ (127).[12] The structures of the 1,2-, 1,7-, and 1,12-phosphacarboranes were tentatively assigned on the basis of ^{11}B NMR data, Figure 1.39.[76]

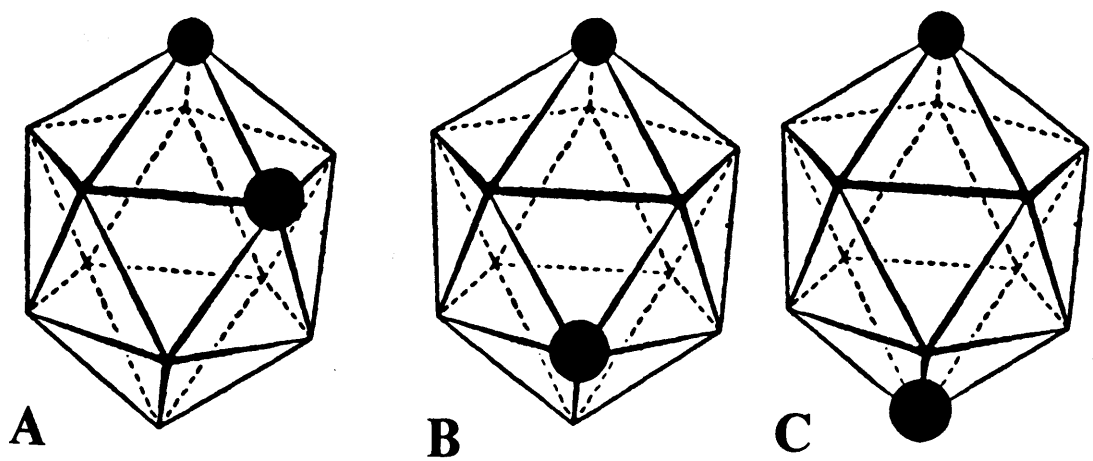

Figure 1.39 Proposed structures of (a) 1,2-$CPB_{10}H_{11}$ (77), (b) 1,7-$CPB_{10}H_{11}$ (126) and (c) 1,12-$CPB_{10}H_{11}$ (127).[12]

Todd *et al.* reported that deprotonation of 1,7-$CPB_{10}H_{11}$ (126) with butyllithium followed by reaction with methyl iodide produced 1,7-$CPB_{10}H_{11}Me$ (128).[62] Zakharkin and coworkers found that treatment of 1,2-$CPB_{10}H_{11}$ (77) with butyllithium in ether-benzene rapidly formed $Li_3[CB_{10}H_{11}]$ and *n*-Bu_3P.[77] Both the 1,7- and 1,12-phosphacarboranes reacted similarly on metallation of the C-H bond to give 1,7-C(Li)$PB_{10}H_{10}$ (129) and 1,12-C(Li)$PB_{10}H_{10}$ (130) respectively. These derivatives were used to prepare several C-substituted compounds.[78,79] For example, reaction with CO_2 gave 1,7-C(CO_2H)$PB_{10}H_{10}$ (131) and 1,12-C(CO_2H)$PB_{10}H_{10}$ (132) respectively and reaction of 1,7-C(Li)$PB_{10}H_{10}$ (129) with MeHgBr formed 1,7-C(HgMe)$PB_{10}H_{10}$ (133).

Zakharkin *et al.* subjected the isomers (77), (126) and (127) to electrophilic and photochemical halogenation (Cl, Br and I) and halogen exchange reactions.[80] The electrophilic substitutions and exchange reactions of (77) occurred mainly at the 8-, 9-, 10- and 12- positions, while (126) reacted mainly at the 9- and 10- positions and (127) at the 7-, 8-, 9-, 10- and 11- positions. The ease of electrophilic halogenation of the isomers declines in the order 1,2 > 1,7 > 1,12. In the photochlorination of compounds (77), (126) and (127), all possible isomeric halogen derivatives were formed.

Aluminium chloride-catalysed halogenations of the phosphacarboranes (77), (126) and (127) have been extensively investigated.[12,80] Reaction of 1,2-$CPB_{10}H_{11}$ (77) with bromine/aluminium trichloride in refluxing carbon disulphide gave 1,2-$CPB_{10}H_9Br_2$ (134).[12] The use of excess bromine ultimately afforded 1,2-$CPB_{10}H_8Br_3$ (135).[12,62] Bromination of 1,7-$CPB_{10}H_{11}$ (126) under similar conditions gave only the mono- and di-substituted derivatives, 1,7-$CPB_{10}H_{10}Br$ (136) and 1,7-$CPB_{10}H_9Br_2$ (137). The position of substitution in compounds (134)-(137) was not determined.

Studies of the thermal rearrangement of six 1,7-$CPB_{10}H_{10}Cl$ and two 1,12-$CPB_{10}H_{10}Cl$ isomers were reported.[81] Rearrangement at 450 °C of 12-Cl-1,2-$CPB_{10}H_{10}$ (138) gave almost exclusively 9,10-Cl_2-1,7-$CPB_{10}H_9$ (139), Figure 1.40.[81] The distorted icosahedron molecular structure of (139) is shown in Figure 1.40. The chlorine atoms are bound to the chemically equivalent B(9) and B(10) atoms.

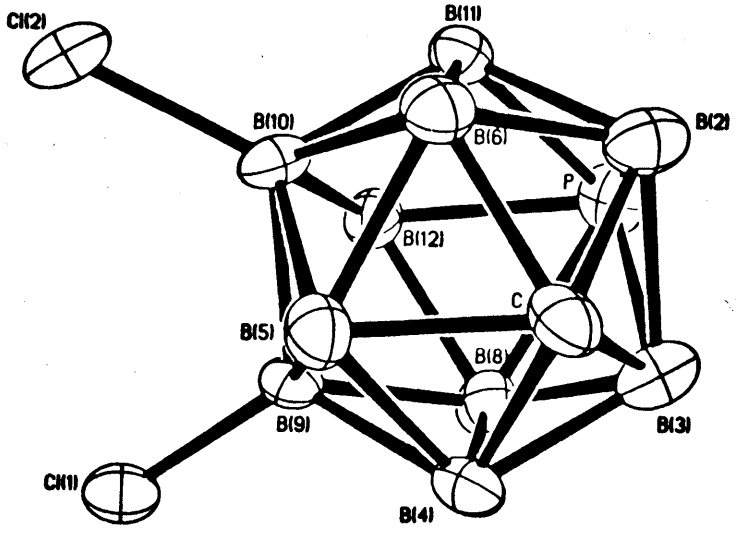

Figure 1.40 Molecular structure of 9,10-Cl_2-1,7-$CPB_{10}H_9$ (139).[81]

Reaction of 1,2-$CPB_{10}H_{11}$ (77), or 1,7-$CPB_{10}H_{11}$ (126) with piperidine at reflux resulted in boron abstraction to give [7,8-CPB_9H_{11}]$^-$ (140), and [7,9-CPB_9H_{11}]$^-$ (141) in 80% and 90% yields respectively.[12] The degradation of (77) was faster than (126). Treatment of 1,2-$CPB_{10}H_{11}$ with sodium ethoxide in ethanol at reflux resulted in abstraction of the heteroatom to give [$CB_{10}H_{13}$]$^-$.[12] In the case of 1,7-$CPB_{10}H_{11}$ (126), KOH caused abstraction of either the heteroatom or a boron atom, resulting in a mixture of products, [$CB_{10}H_{13}$]$^-$ and [7,9-CPB_9H_{11}]$^-$ (141).[77] Attempts to degrade 1,12-$CPB_{10}H_{11}$ (127) with methoxide ion or piperidine at 150 °C for a week were unsuccessful.[12] However, compound (127) was reduced by sodium in naphthalene to [$CPB_{10}H_{11}$]$^{2-}$ (142). Oxidation of (142) with [$CuCl_2$] formed 1,7-$CPB_{10}H_{11}$ (126).

Attempts to involve the lone pair electrons of 1,2-$CPB_{10}H_{11}$ (77) or 1,7-$CPB_{10}H_{11}$ (126) in chemical bonding (*e.g.* quaternisation with methyl iodide) were unsuccessful.[12] However, treatment of the tetramethylammonium salts of [7,8-CPB_9H_{11}]$^-$ (140) and [7,9-CPB_9H_{11}]$^-$ (141) with methyl iodide in thf gave 7,8-CPB_9H_{11}Me (143) and 7,9-CPB_9H_{11}Me (144) in 40% and 94% yields respectively.[12] When [7,9-CPB_9H_{11}]$^-$ (141) was passed through an acid ion-exchange column 7,9-CPB_9H_{12} (145) was produced in 91% yield.[12] Treatment of [7,8-CPB_9H_{11}]$^-$ (140) or [7,9-CPB_9H_{11}]$^-$ (141) with NaH removes the bridging hydrogen to form the corresponding 7,8- or [7,9-CPB_9H_{10}]$^{2-}$. These dianions were not isolated. However,

they are capable of bonding a transition metal atom to the open face of the phosphacarborane cage to complete the icosahedral structure and manganese, iron, cobalt and nickel complexes of 7,8- and $[7,9\text{-}CPB_9H_{10}]^{2-}$ have been characterised.[82,83] The iron complex $[Fe(7,9\text{-}CPB_9H_{10})_2]^{2-}$ reacted with methyl iodide to form $[Fe(1,7\text{-}CPB_9H_{10}Me)_2]$ (146).[82] The single crystal X-ray structure of (146) was reported, Figure 1.41.[82] The ^{11}B NMR data of the 7,8- and 7,9- compounds (140)-(144) were not sufficient for complete structural characterisation,[82] but the X-ray study of $[Fe(1,7\text{-}CPB_9H_{10}Me)_2]$ (146) was taken to confirm the 7,9- assignment for compounds (141) and (144).

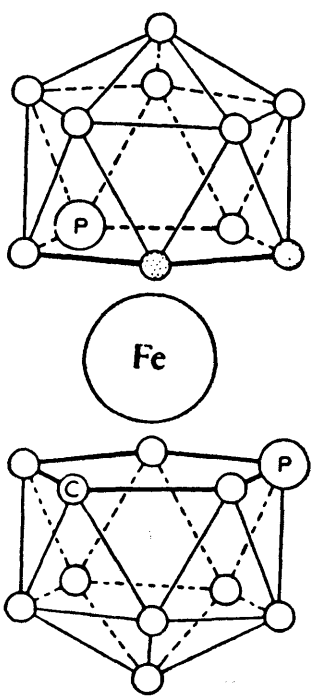

Figure 1.41 Idealised view of the molecular structure of $[Fe(1,7\text{-}CPB_9H_{10}Me)_2]$ (146).[82]

Other *nido* twelve-atom carbaphospha- derivatives which are isoelectronic with $[CPB_{10}H_{11}]^{2-}$ (142) have been reported.[84] Reaction of $B_{10}H_{12}CNMe_3$ with triethylamine initially and then $RPCl_2$ (R = Me, Et, Ph) in thf gave *nido*-$Me_3NCPRB_{10}H_{10}$ {R= Me(147), Et (148), Ph (149)} in *ca.* 85% yield. The molecular structure of *nido*-$Me_3NC(PPh)B_{10}H_{10}$ (149) was determined by low temperature single-crystal X-ray analysis and is shown in Figure 1.42. The PPh unit bridges boron atoms B(9) and B(10) on the open face of the $B_{10}H_{10}CNMe_3$ fragment. Heating *nido*-$Me_3NC(PPh)B_{10}H_{10}$ in a sealed tube at 475 °C afforded a compound which the authors suggested was *closo*-$Me_3NCPB_{10}H_{10}$ (150). However compound (150) was not fully characterised.

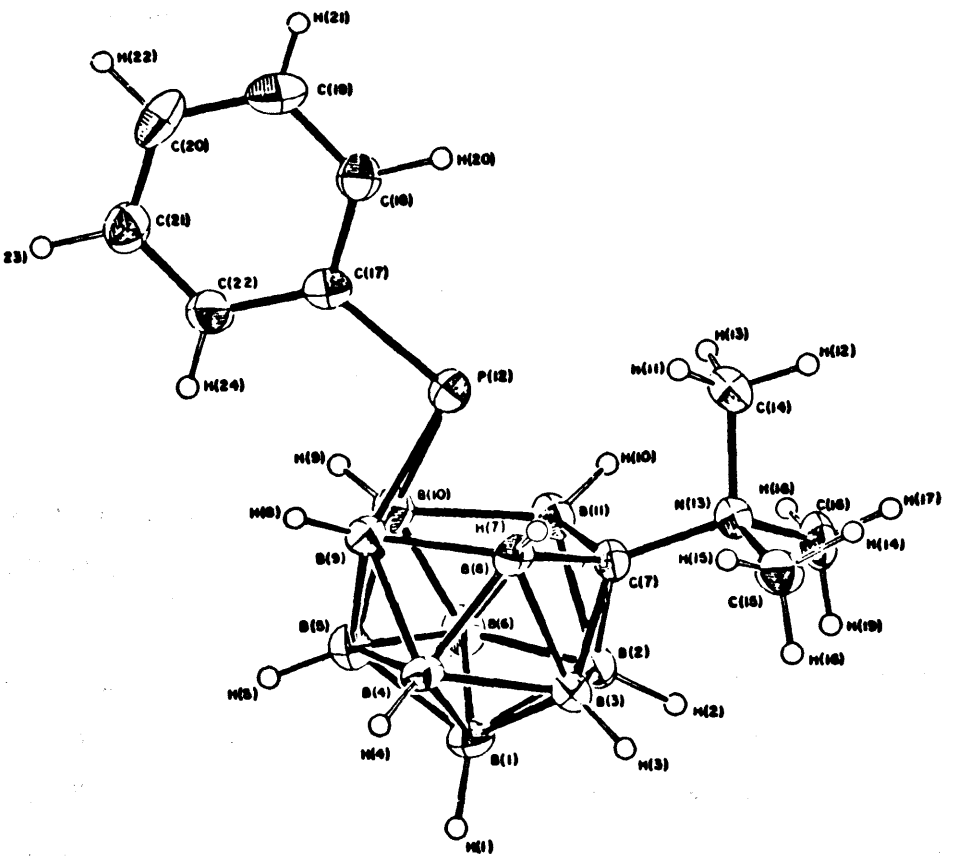

Figure 1.42 ORTEP drawing of *nido*-$Me_3NC(PPh)B_{10}H_{10}$ (149).[84]

It has been reported that treatment of the disodium salts of 7,8- and [7,9-$CPB_9H_{10}]^{2-}$ with germanium diiodide in refluxing benzene results in the formation of 1,2,3-$GeCPB_9H_{10}$ (151) and 1,2,7-$GeCPB_9H_{10}$ (152).[40] Compounds (151) and (152) were characterised by elemental analyses, IR and NMR spectroscopy and mass spectrometry. These were the first examples of polyhedral boranes with three different main group heteroatoms in the cage. The analogous arsenagermacarboranes have also been prepared (as discussed in section 1.2.3.2).

The reaction between the $[Na^+(thf)Li^+][2,3\text{-}(SiMe_3)_2C_2B_4H_4]^{2-}$ double salt and 2,4,6-$(Bu^t)_3C_6H_2PCl_2$ in a molar ratio of 1:1 in dry thf produced the previously unknown *closo*-phosphacarborane complex, 1-[2,4,6-$(Bu^t)_3C_6H_2$]-1-P-2,3-$(SiMe_3)_2$-2,3-$C_2B_4H_4$ (153) as an air-sensitive white crystalline solid in 38% yield.[85] The complex (153) was characterised by ^1H, ^{11}B, ^{13}C and ^{31}P NMR, IR and mass spectroscopy. These spectroscopic data are consistent with the proposed pentagonal bipyramidal structure, Figure 1.43.

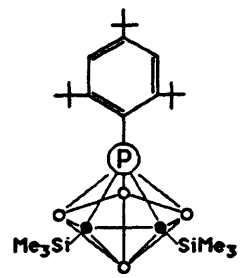

Figure 1.43 Proposed structure for *closo*-1-[2,4,6-$(Bu^t)_3C_6H_2$]-1-P-2,3-$(SiMe_3)_2$-2,3-$C_2B_4H_4$ (153).[85]

Reactions between $Na^+Li^+[nido\text{-}R_2C_2B_4H_4]^{2-}$ (R = Et or Bz) and $R'PCl_2$ (R' = Ph, Bu^t or Me) have yielded new phosphacarboranes of the general formula $R'R_2P_2B_4H_4$.[86] Their spectroscopic data and the results of an *ab initio*/IGLO/NMR study indicate that these compounds have open-cage 7-vertex *nido*-6-R'-3,4-R_2-6,3,4-$PC_2B_4H_4$ geometries based on a dodecahedron missing one five-connected vertex and the carbon and phosphorus atoms occupying positions on the open face, Figure 1.44, with the carbon atoms adjacent.

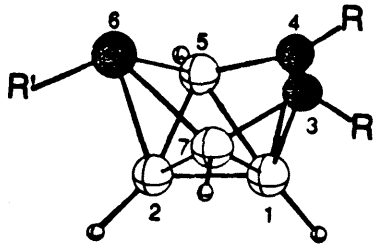

Figure 1.44 Proposed cage structure for *nido*-6-R'-3,4-R_2-6,3,4-$PC_2B_4H_4$ (R = Et or Bz; R' = Ph, Bu^t or Me).[86]

The reaction of *nido*-6-Ph-3,4-Et_2-6,3,4-$PC_2B_4H_4$ (154) with lithium metal or sodium naphthalenide in thf gives quantitative reduction of the phosphacarborane to form *arachno*-$[PhEt_2PC_2B_4H_4]^{2-}$ (155).[86] Subsequent reaction of (155) with $PhPCl_2$ afforded a product that NMR and mass spectral evidence suggested was the diphosphacarborane *arachno*-$Ph_2Et_2P_2C_2B_4H_4$ (156). Comparison of the spectral data obtained for *arachno*-$[PhEt_2PC_2B_4H_4]^{2-}$ (155) and *arachno*-$Ph_2Et_2P_2C_2B_4H_4$ (156) with the results of *ab initio*/IGLO/NMR calculations suggested 7-vertex and 8-vertex *arachno* geometries respectively for these cage systems.[86]

1.6 SUMMARY AND CONCLUSION

This chapter reviewed group V/15 (excluding nitrogen) containing boranes, carboranes and their metal derivatives. All the arsena- stiba- and bisma- boranes reported to date are eleven or twelve atom systems with either a *nido* or *closo* structure. The reported phosphaboranes are mainly eleven or twelve atom compounds although some smaller species are known. *Closo*, *nido* and *arachno* phosphacarboranes have been reported. In general, in the solid state group V/15 heteroboranes are all quite stable and many crystallographically determined structures have been reported.

Group V/15 heteroboranes are capable of forming metal complexes (although no metallabismaborane compounds have yet been reported). The most common group V/15 metal derivatives are *closo* 12-atom species. Six metalladiarsenaborane structures have been published which are of direct importance to the present work. These are *closo*-[8-{OPr^i(Et)}-3-PPh_3-3,1,2-$CuAs_2B_9H_8$] (71),[58] *closo*-[3-Cl-3,8-$(PPh_3)_2$-3,1,2-$PdAs_2B_9H_8$](67),[53] *closo*-[1,1-$(PMe_2Ph)_2$-1,2,3-$PdAs_2B_9H_9$](65),[44] *closo*-[3,4-Cl_2-3,8-$(PMe_2Ph)_2$-3,1,2-$PdAs_2B_9H_7$](68),[44] *closo*-[3,3-$(PPh_3)_2$-3,1,2-$PtAs_2B_9H_9$] (69),[53] and *closo*-[3,3-$(PMe_2Ph)_2$-3,1,2-$PtAs_2B_9H_9$] (70).[53]

It is notable that the reaction chemistry of 12-atom metallaarsenaboranes has not been studied in detail. Chapters 5 and 6 of this thesis will discuss the synthesis and reactions of derivatives of 12-atom metallaarsenaboranes.

Another emergent feature of this review is that although there are theoretical studies of cluster bonding in carboranes, phosphaboranes and thiaboranes, no comparative study on these heteroboranes has been completed. The following chapter presents novel work in this area for compounds which form the basis of the experimental work of this thesis.

CHAPTER TWO

THEORETICAL INVESTIGATION OF THE ELECTRONIC STRUCTURE AND BONDING OF ELEVEN-VERTEX *NIDO*-HETEROBORANE DIANIONS $[7,8\text{-}C_2B_9H_{11}]^{2-}$, $[7,9\text{-}C_2B_9H_{11}]^{2-}$, $[1,7\text{-}C_2B_9H_{11}]^{2-}$, $[4,7\text{-}C^2B_9H_{11}]^{2-}$, $[7,8\text{-}P_2B_9H_9]^{2-}$, $[7,9\text{-}P_2B_9H_9]^{2-}$ AND $[7\text{-}SB_{10}H_{10}]^{2-}$

2.1 INTRODUCTION

The electronic structure and bonding of boranes has attracted an enormous amount of attention since the basic set of geometric types became known. The interest stemmed initially from a general appreciation that the molecules presented a problem which was solvable using the mo (molecular orbital) approach and whose solution involved "nonclassical" bonding ideas. The problem became even more interesting when equivalent structural types of molecules were identified in heteroborane, metallaborane and all-metal clusters.

Approaches to the problem of bonding in these compounds have ranged in sophistication from the "simple" Lipscomb's *styx* rules[87] and Wades rules,[88] to the tensor surface harmonics theory developed by Stone and full *ab initio* mo calculations on individual molecules.[89,90] In the following sections a group of eleven-atom *nido* compounds are discussed and for this purpose MNDO (Modified Neglect of Differential Overlap) calculations were used.[91]

Studies of the structural and electronic properties of seven *nido* heteroboranes were carried out in the present work. The compounds investigated were [7,8-$C_2B_9H_{11}]^{2-}$, [7,9-$C_2B_9H_{11}]^{2-}$, [1,7-$C_2B_9H_{11}]^{2-}$, [4,7-$C_2B_9H_{11}]^{2-}$, [7,8-$P_2B_9H_9]^{2-}$, [7,9-$P_2B_9H_9]^{2-}$ and [7-$SB_{10}H_{10}]^{2-}$, Figure 2.1. These compounds were studied because subsequent work described in this thesis deals with metal complexes of these dianions. (Note, MNDO calculations cannot be performed on As or Te containing systems but the bonding in P and S containing systems should be similar).

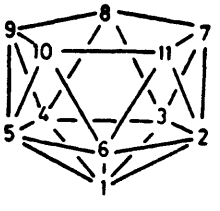

Figure 2.1 Numbering scheme for eleven atom *nido* compounds.

All these anions can be reacted with $[Pt(PR_3)_2Cl_2]$ or $[Rh(PR_3)_3Cl]$ to form $Pt(PR_3)_2$- and $Rh(PR_3)_2H$- containing twelve atom *closo* complexes and a substantial amount of the synthetic work described in this thesis concerns such compounds *vide infra.* Results from extended Hückel molecular orbital calculations suggest that the lumo (lowest unoccupied molecular orbital) of the metal containing $[RhL_2H]^{2+}$ and $[PtP_2]^{2+}$ units are of the form shown in Figure 2.2.[92,93] The molecular orbitals of the heteroborane anions which interact most strongly with the lumo of the metal cation are those which are localised predominantly on the open face of the structure (atoms 7-11) and point away from this face *i.e.* orbitals with a large p_x contribution where the x direction is perpendicular to the plane containing atoms 7-11. The homo (highest occupied molecular orbital) and shomo (second highest occupied molecular orbital) of the anions have these properties. The other filled molecular orbitals of similar energy (within 5 eV of the homo) do not have these properties and for the purpose of the present analysis only the homo and shomo of the *nido* anions will be discussed. For each of the following eleven atom *nido* dianions the homo and shomo are illustrated in section 2.2.3.

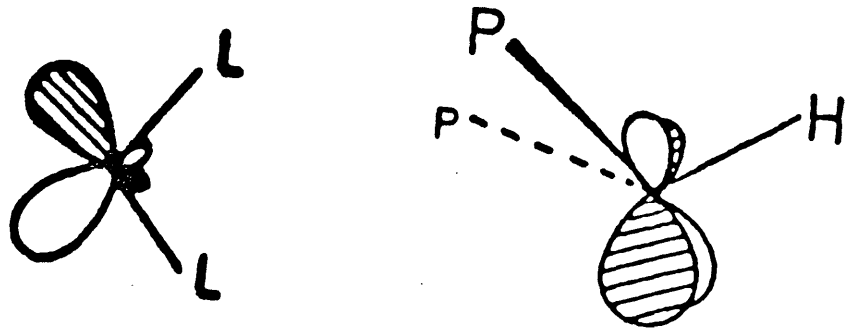

A B

Figure 2.2 Lumo of (a) $[PtP_2]^{2+}$ and (b) $[RhL_2H]^{2+}$ which are capable of interacting with the homo of the *nido* anions.

The MNDO program was used for all calculations as supplied by Quantum Chemistry Program Exchange (QCPE) in the AMPAC suite of programs.[94] The geometries were optimised with no restriction on the (3N-6) degrees of freedom of the molecules.[91] The validity of applying MNDO calculations to the analysis of boranes containing heteroatoms C, P and S has been established in many studies.[73,95-100]

The calculated heats of formation for the seven *nido* anions are given in Table 2.1. Those of $[7,8\text{-}C_2B_9H_{11}]^{2-}$ and $[7,9\text{-}C_2B_9H_{11}]^{2-}$ (-27.8 and -47.7 kJ mol^{-1}) are very similar to the values previously reported by Dewar and McKee (-28.0 and -46.3 kJ mol^{-1}).[94] It is found in the present work and previously[94] that the 7,9 heteroborane systems are always more stable than the corresponding 7,8 systems. The systems with the heteroatoms in the open face of the molecule are more stable than compounds with one or more heteroatom in the body of the molecule, Table 2.1. For the carborane dianions the thermodynamic stability sequence is 7,9 > 7,8 > 4,7 > 1,7.

Table 2.1 Calculated heats of formation for seven *nido* heteroborane dianions in decreasing order of stability.

Compound	ΔH/ kJ mol^{-1}
$[7,9\text{-}P_2B_9H_9]^{2-}$	-108.0
$[7,8\text{-}P_2B_9H_9]^{2-}$	-96.9
$[7\text{-}SB_{10}H_{10}]^{2-}$	-74.8
$[7,9\text{-}C_2B_9H_{11}]^{2-}$	-47.7
$[7,8\text{-}C_2B_9H_{11}]^{2-}$	-27.8
$[4,7\text{-}C_2B_9H_{11}]^{2-}$	-18.6
$[1,7\text{-}C_2B_9H_{11}]^{2-}$	-13.1

2.2 MOLECULAR AND ELECTRONIC STRUCTURE OF *NIDO* HETEROBORANE ANIONS

The cluster compounds studied were all closely related having the same basic eleven atom *nido* structure *i.e.* an icosahedron with one vertex missing as illustrated in Figure 2.1 and the same number of valence electrons. As expected all the 11 atom *nido* systems have 24 occupied molecular orbitals consisting of 11 non-cluster and 13 cluster bonding molecular orbitals. The calculated structures for all seven *nido* anions agree with the generalised structure illustrated in Figure 2.1.

In all the *nido* systems studied in the present work the interatomic distances were in good agreement with experimentally obtained data and previously reported calculated structures. For the four carborane anions the presently calculated C-B bond distances range from 1.600 to 1.822 Å and the B-B distances range from 1.681 to 1.922 Å. The latter are within the usual range of B-B bond distances for carboranes.[94] Similar values are observed in the following X-ray diffraction studies. In *nido*-[7,8-$C_2B_9H_{12}$]$^-$ the C-B distances are in the range 1.606(3)-1.726(3) Å and the B-B distances range from 1.754(3)-1.849(3) Å.[13] Similar ranges are observed in metallacarboranes. In *nido*-[8,8-$(PMe_2Ph)_2$-8,7-$PtCB_9H_{11}$] the B-B distances range from 1.702(11)-1.933(11) Å and the C-B range was from 1.570(11)-1.680(10) Å.[101] In the *arachno* compound [9,9-$(PPh_3)_2$-9,5,6-$PtC_2B_7H_{11}$] the C-B distances range from 1.599(12)-1.810(16) Å.[102] For [7,8-$C_2B_9H_{11}$]$^{2-}$ and [7,9-$C_2B_9H_{11}$]$^{2-}$ the interatomic distances, heats of formation (as discussed above) and charges on the atoms are very similar to those reported by Dewar and McKee.[94]

The phosphaborane anions had B-B bond distances ranging from 1.661-1.895 Å which are within the usual range of B-B bond distances for heteroboranes.[103] The P-B bond distances from the open face to the lower face of the phosphaborane anions were in the range 2.008-2.031 Å. In *nido*-7-$MePB_{10}H_{12}$ (90) the P-B bond distances were 1.996(5) and 2.001(6) Å and the B-B distances were in the range 1.740(7)-1.905(7) Å.[63] In *closo*-2-Me_3N-1-$PB_{11}H_{10}$ (108) the P-B distances range from 2.0287(20)-2.0488(21) Å and the B-B distances were in the range 1.776(4)-1.849(4) Å.[66] The S-B distances in [7-$SB_{10}H_{10}$]$^{2-}$ were in the range 1.868-2.086 Å. In the *nido* compound [8,8-$(PPh_3)_2$-μ-8;9-(S_2CH)-8,7-$RhSB_9H_9$] the S-B distances were in the

range 1.920(3)-2.072(3) Å.[104] In *nido*-[8,8,8-$(PMe_2Ph)_2$-8,7-$RhSB_9H_{10}$] the S-B distances were in the range 1.914(3)-2.061(2) Å.[2] These observations strongly support the suggestion that the MNDO calculations give good descriptions of the molecular structures and hence, imply good electronic structures.

2.2.1 Localised Molecular Orbital structure of dicarborane anions $[7,8\text{-}C_2B_9H_{11}]^{2-}$, $[7,9\text{-}C_2B_9H_{11}]^{2-}$, $[1,7\text{-}C_2B_9H_{11}]^{2-}$ and $[4,7\text{-}C_2B_9H_{11}]^{2-}$, the phosphaborane anions $[7,8\text{-}P_2B_9H_9]^{2-}$ and $[7,9\text{-}P_2B_9H_9]^{2-}$ and the thiaborane anion $[7\text{-}SB_{10}H_{10}]^{2-}$

A localised orbital calculation gives a readily interpreted description of the molecule. These will be given in detail for each of the following seven structures in Table 2.2. For all four $[C_2B_9H_{11}]^{2-}$ structures the MNDO localised calculation produces eleven non-cluster two-centre bonding molecular orbitals consisting of nine B-H and two C-H interactions. There are also thirteen cluster bonding orbitals as expected for an eleven atom *nido* system. These comprise five two-centre bonding orbitals and either eight three-centre orbitals {$[7,8\text{-}C_2B_9H_{11}]^{2-}$ and $[4,7\text{-}C_2B_9H_{11}]^{2-}$} or seven three-centre and one four-centre orbitals {$[7,9\text{-}C_2B_9H_{11}]^{2-}$ and $[1,7\text{-}C_2B_9H_{11}]^{2-}$}, Table 2.2. The five two-centre cluster bonding orbitals for all the $[C_2B_9H_{11}]^{2-}$ compounds except the 4,7- isomer are located on the top open face of the *nido* dianions, Table 2.2. For $[4,7\text{-}C_2B_9H_{11}]^{2-}$ one of the two-centre cluster bonding orbitals is located between atoms B(3)-C(4). It is clear that the overall pictures of localised bonding for the carborane isomers are remarkably similar.

For both $[P_2B_9H_9]^{2-}$ structures there are eleven non-cluster molecular orbitals consisting of nine B-H two-centre orbitals and two orbitals containing "lone pairs" of electrons in two sp orbitals, one on each of the phosphorus atoms. There are thirteen cluster bonding localised orbitals as expected for an eleven atom *nido* system. For each isomer these comprise of five two-centre bonding orbitals all in the upper face and eight other orbitals of three centres for $[7,8\text{-}P_2B_9H_9]^{2-}$ or seven three- and one four-centre orbitals for $[7,9\text{-}P_2B_9H_9]^{2-}$ as listed in Table 2.2.

Table 2.2 Localised description of the cluster bonding orbitals in $[7,8\text{-}C_2B_9H_{11}]^{2-}$ $[7,9\text{-}C_2B_9H_{11}]^{2-}$, $[1,7\text{-}C_2B_9H_{11}]^{2-}$ and $[4,7\text{-}C_2B_9H_{11}]^{2-}$, $[7,8\text{-}P_2B_9H_9]^{2-}$, $[7,9\text{-}P_2B_9H_9]^{2-}$ and $[7\text{-}SB_{10}H_{10}]^{2-}$.

Centres	$[7,8\text{-}C_2B_9H_{11}]^{2-}$	$[7,9\text{-}C_2B_9H_{11}]^{2-}$	$[1,7\text{-}C_2B_9H_{11}]^{2-}$	$[4,7\text{-}C_2B_9H_{11}]^{2-}$	$[7,8\text{-}P_2B_9H_9]^{2-}$	$[7,9\text{-}P_2B_9H_9]^{2-}$	$[7\text{-}SB_{10}H_{10}]^{2-}$
2	C7-C8	C7-B8	C7-B8	C7-B8	P7-P8	P7-B8	S7-B8
2	C7-B11	C7-B11	C7-B11	C7-B11	P7-B11	P7-B11	S7-B11
2	C8-B9	B8-C9	B8-B9	B8-B9	P8-B9	B8-P9	B8-B9
2	B9-B10	C9-B10	B9-B10		B9-B10	P9-B10	B9-B10
2	B10-B11	B10-B11	B10-B11	B10-B11	B10-B11	B10-B11	B10-B11
2				B3-C4			
3	B1-B2-B3	B1-B2-B3		B1-B2-B3	B1-B2-B3	B1-B2-B3	B1-B2-B3
3			C1-B2-B6				
3	B1-B3-B4		C1-B3-B4		B1-B3-B4		B1-B3-B4
3		B1-B4-B5		B1-C4-B5		B1-B4-B5	

Centres	$[7,8\text{-}C_2B_9H_{11}]^{2-}$	$[7,9\text{-}C_2B_9H_{11}]^{2-}$	$[1,7\text{-}C_2B_9H_{11}]^{2-}$	$[4,7\text{-}C_2B_9H_{11}]^{2-}$	$[7,8\text{-}P_2B_9H_9]^{2-}$	$[7,9\text{-}P_2B_9H_9]^{2-}$	$[7\text{-}SB_{10}H_{10}]^{2-}$
3	B1-B5-B6			B1-B5-B6	B1-B5-B6		B1-B5-B6
3	B2-B3-C7	B2-B3-C7	B2-B3-C7	B2-B3-C7	B2-B3-P7	B2-B3-P7	B2-B3-S7
3	B2-B6-B11	B2-B6-B11	B2-B6-B11	B2-B6-B11	B2-B6-B11	B2-B6-B11	B2-B6-B11
3	B3-B4-C8	B3-B4-B8	B3-B4-B8		B3-B4-P8	B3-B4-B8	B3-B4-B8
3	B4-B5-B9	B4-B5-C9	B4-B5-B9	C4-B5-B9	B4-B5-B9	B4-B5-P9	B4-B5-B9
3	B5-B6-B10	B5-B6-B10	B5-B6-B10	B5-B6-B10	B5-B6-B10	B5-B6-B10	B5-B6-B10
3				B5-B9-B10			
4		B1-B2-B5-B6				B1-B2-B5-B6	
4			C1-B4-B5-B6				

A localised orbital calculation of $[7\text{-}SB_{10}H_{10}]^{2-}$ shows eleven non-cluster orbitals consisting of ten B-H two-centre bonding orbitals and one sulphur sp "lone pair" orbital. There are also thirteen cluster bonding localised orbitals, described in Table 2.2. These comprise seven three-centre boron localised (B-B-B) orbitals located in the body of the dianion, three two-centre boron localised orbitals (B-B), three sulphur boron localised orbitals of which one is three-centre (B-B-S) and the other two are two-centre (S-B). As with the phosphaboranes all two-centre localised orbitals are located on the open face of the dianion.

2.2.2 Charge distribution in the *nido* anions $[7,8\text{-}C_2B_9H_{11}]^{2-}$, $[7,9\text{-}C_2B_9H_{11}]^{2-}$, $[1,7\text{-}C_2B_9H_{11}]^{2-}$, $[4,7\text{-}C_2B_9H_{11}]^{2-}$, $[7,8\text{-}P_2B_9H_9]^{2-}$, $[7,9\text{-}P_2B_9H_9]^{2-}$ and $[7\text{-}SB_{10}H_{10}]^{2-}$

For the seven *nido* anions the charges on the atoms are given in Table 2.3. Using arguments based on the calculated charge distribution and molecular orbital composition, one can make predictions about the reactivity of the seven *nido* anions towards electrophiles such as $[ML_n]^{2+}$. On the basis of the charge distribution, all seven *nido* anions would be expected to react at the open face with electrophiles since there is a gross negative electron density in the open face. If the charges on the hydrogen atoms are also included then the charges based on atoms 7-11 range from -0.73 for $[7,9\text{-}C_2B_9H_{11}]^{2-}$, -0.76 for $[7\text{-}SB_{10}H_{10}]^{2-}$, -0.78 for $[7,8\text{-}C_2B_9H_{11}]^{2-}$, -0.84 for $[7,9\text{-}P_2B_9H_9]^{2-}$, -0.85 for $[7,8\text{-}P_2B_9H_9]^{2-}$, -0.88 for $[1,7\text{-}C_2B_9H_{11}]^{2-}$, to -0.94 for $[1,7\text{-}C_2B_9H_{11}]^{2-}$. Moreover this reactivity at the open face is reinforced because of the steric factors involved. The strongest interaction between the dianion and an incoming electrophile would be expected to be with the two highest occupied molecular orbitals *i.e.* the homo and shomo since these are largely located on the same face and directed away from that face, see section 2.2.3 below. The details of their interaction and their consequence for determining the final conformation of a PtP_2 or RhP_2H unit above the heteroborane face are discussed in the next section. (Note $[7,9\text{-}P_2B_9H_{11}]^{2-}$ is unknown and there are no reported complexes of it).

Table 2.3 MNDO calculated ground state charge distribution of $[7,8\text{-}C_2B_9H_{11}]^{2-}$, $[7,9\text{-}C_2B_9H_{11}]^{2-}$, $[1,7\text{-}C_2B_9H_{11}]^{2-}$, $[4,7\text{-}C_2B_9H_{11}]^{2-}$, $[7,8\text{-}P_2B_9H_{11}]^{2-}$, $[7,9\text{-}P_2B_9H_{11}]^{2-}$ and $[7\text{-}SB_{10}H_{10}]^{2-}$.

Atom No.	$[7,8\text{-}C_2B_9H_{11}]^{2-}$ X H	$[7,9\text{-}C_2B_9H_{11}]^{2-}$ X H	$[1,7\text{-}C_2B_9H_{11}]^{2-}$ X H	$[4,7\text{-}C_2B_9H_{11}]^{2-}$ X H	$[7,8\text{-}P_2B_9H_9]^{2-}$ X H	$[7,9\text{-}P_2B_9H_9]^{2-}$ X H	$[7\text{-}SB_{10}H_{10}]^{2-}$ X H
1	-0.16 (-0.02)	-0.17 (-0.02)	-0.03 (+0.01)	-0.21 (-0.02)	-0.15 (-0.01)	-0.15 (-0.01)	-0.16 (-0.02)
2	-0.19 (-0.05)	-0.16 (-0.04)	-0.21 (-0.04)	-0.13 (-0.04)	-0.20 (-0.02)	-0.18 (-0.03)	-0.28 (-0.03)
3	-0.20 (-0.05)	-0.21 (-0.04)	-0.21 (-0.04)	-0.27 (-0.04)	-0.22 (-0.01)	-0.19 (-0.02)	-0.23 (-0.03)
4	-0.18 (-0.05)	-0.21 (-0.04)	-0.14 (-0.06)	-0.01 (-0.01)	-0.20 (-0.02)	-0.19 (-0.02)	-0.10 (-0.04)
5	-0.12 (-0.04)	-0.15 (-0.04)	-0.14 (-0.06)	-0.09 (-0.05)	-0.12 (-0.04)	-0.18 (-0.03)	-0.11 (-0.06)
6	-0.12 (-0.04)	-0.15 (-0.04)	-0.14 (-0.06)	-0.15 (-0.04)	-0.12 (-0.04)	-0.13 (-0.03)	-0.13 (-0.05)
7	+0.01 (-0.08)	+0.07 (-0.03)	+0.03 (-0.03)	+0.02 (-0.03)	-0.04	+0.06	+0.34
8	+0.01 (-0.08)	-0.20 (-0.07)	-0.11 (-0.11)	-0.02 (-0.14)	-0.04	-0.34 (-0.04)	-0.26 (-0.07)
9	-0.17 (-0.02)	+0.07 (-0.03)	-0.13 (-0.09)	-0.21 (-0.09)	-0.21 (-0.06)	+0.06	-0.14 (-0.08)
10	-0.17 (-0.09)	-0.19 (-0.08)	-0.13 (-0.09)	-0.15 (-0.08)	-0.15 (-0.08)	-0.23 (-0.06)	-0.14 (-0.08)
11	-0.17 (-0.02)	-0.19 (-0.08)	-0.11 (-0.11)	-0.14 (-0.10)	-0.21 (-0.06)	-0.23 (-0.06)	-0.26 (-0.07)

Generally the charges on the boron atoms are significantly more negative than those on the hetero atoms. In the open face of the carborane anions the carbon atoms are positively charged while in the body of the cage they are negatively charged. The phosphorus atoms in phosphaborane anions are essentially neutral. The sulphur atom in $[7\text{-}SB_{10}H_{10}]^{2-}$ has a large (+0.34) positive charge. All the hydrogen atoms with the exception of the hydrogen attached to C(1) in $[1,7\text{-}C_2B_9H_{11}]^{2-}$ are negatively charged. The greatest charge is on the hydrogen atoms attached to atoms 7-11 in the open face. The overall consequence of these observations is that there is a concentration of the negative charge on the B-H units in the open faces of the dianions.

2.2.3 Possible interactions of *nido* anions with metal units $[Pt(PR_3)_2]^{2+}$ and $[Rh(PR_3)_2H]^{2+}$

The homo.s and shomo.s for the four carborane anions, the two phosphaborane anions and the thiaborane anion all have considerable p_x character and are capable of bonding with the lumo of $[Pt(PR_3)_2]^{2+}$ or $[Rh(PR_3)_2H]^{2+}$. The homo.s and shomo.s for the seven *nido* dianions are illustrated in Figures 2.3-2.9. The difference in energy between the homo and shomo for each anion is given in the legends. In the following diagrams for the homo.s and shomo.s, the circles represent the relative percentage of p_x character, *i.e.* drawn proportional to the orbital coefficient squared and pointing away from the open face viewed along the x axis. The shaded circles have the opposite sign to the non-shaded circles. While it is possible for the metal unit lumo to interact with either homo or shomo, the extent of interaction will be determined by the compatibility of the energies of the lumo and homo or shomo and the % of these orbitals located on the open face. Since, in general, in any particular dianion the homo and shomo have similar percentages of orbitals located on the open face, the compatibility in energies between the metal-unit lumo and the homo or shomo is the dominating factor and the lumo-homo interaction is more significant. This determines the conformation of the metal unit above the face of the heteroborane ligand. However, if the difference between the energy levels for the homo and shomo is small it is possible that the lumo of the metal could interact strongly with both the homo and shomo and no clear conformational preference can be predicted.

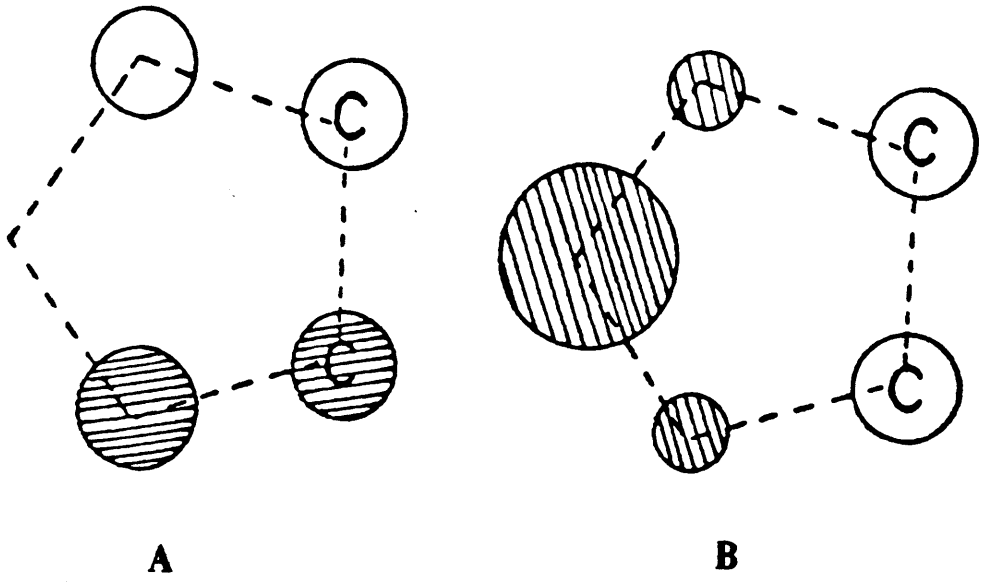

Figure 2.3 (a) homo, (b) shomo, of $[7,8\text{-}C_2B_9H_{11}]^{2-}$ (ΔE=0.25 eV).

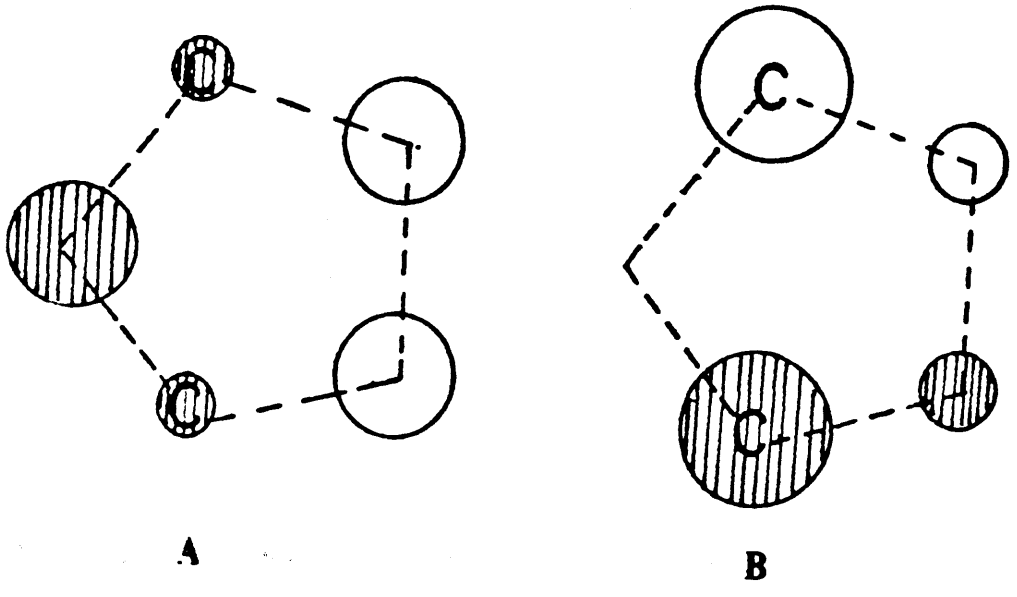

Figure 2.4 (a) homo, (b) shomo, of $[7,9\text{-}C_2B_9H_{11}]^{2-}$ (ΔE=1.15 eV).

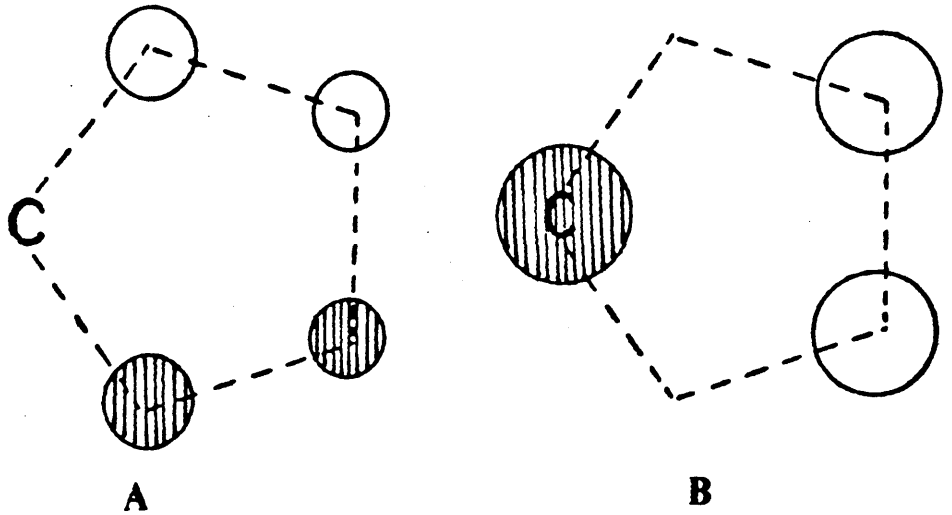

Figure 2.5 (a) homo, (b) shomo of $[1,7\text{-}C_2B_9H_{11}]^{2-}$ (ΔE=0.66 eV).

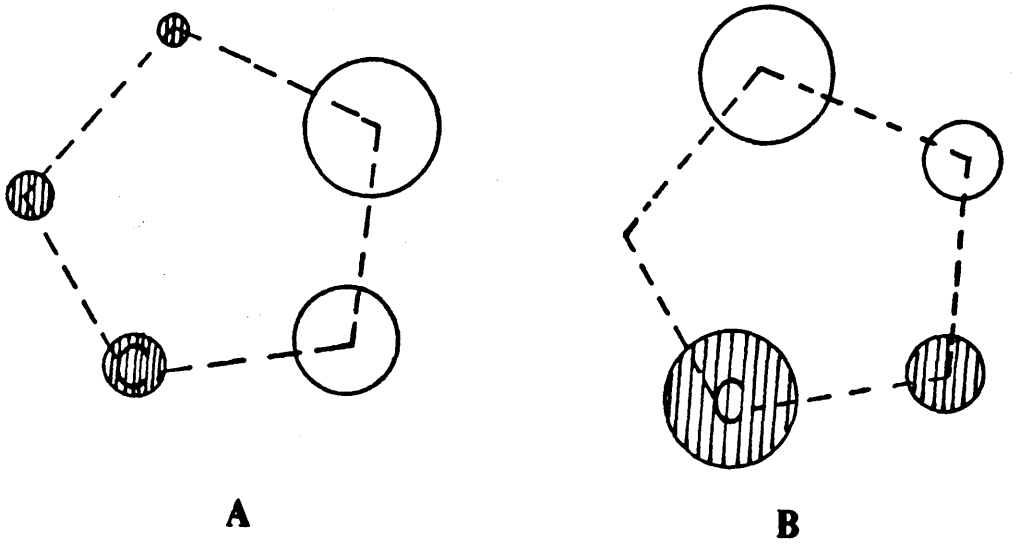

A B

Figure 2.6 (a) homo, (b) shomo of $[4,7\text{-}C_2B_9H_{11}]^{2-}$ (ΔE=0.77 eV).

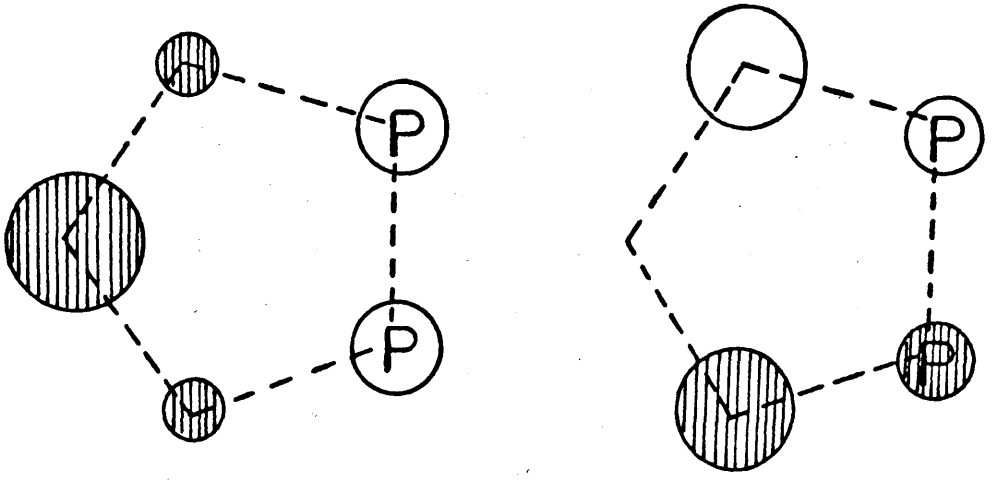

A B

Figure 2.7 (a) homo, (b) shomo, of $[7,8\text{-}P_2B_9H_9]^{2-}$ (ΔE=0.15 eV).

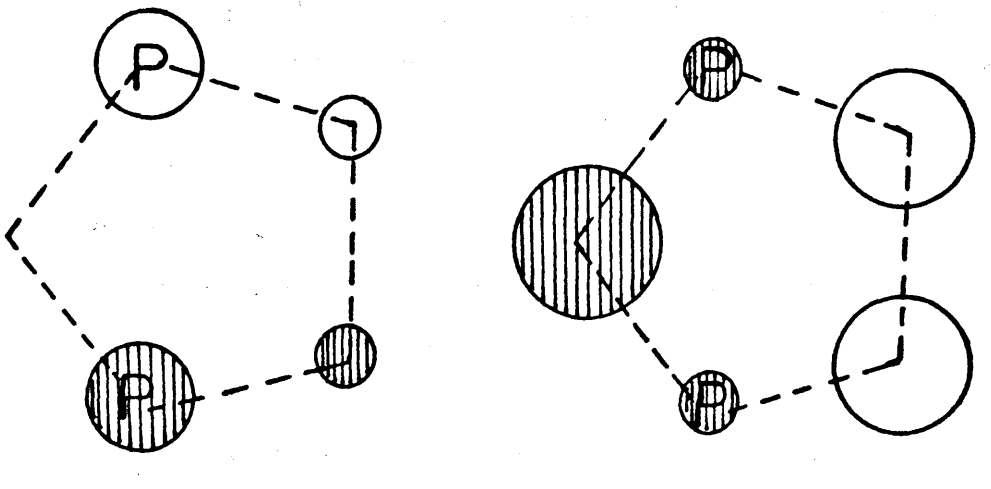

A B

Figure 2.8 (a) homo, (b) shomo, of $[7,9\text{-}P_2B_9H_9]^{2-}$ (ΔE=0.08 eV).

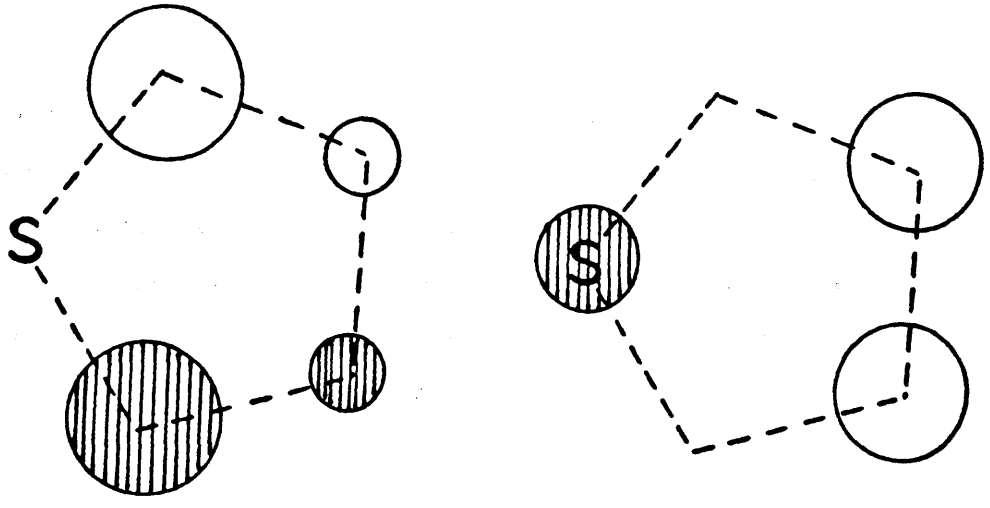

A B

Figure 2.9 (a) homo, (b) shomo, of $[7\text{-}SB_{10}H_{10}]^{2-}$ (ΔE=0.23 eV).

From data presented later in this thesis concerning solution phase studies, it is clear that in general, anions with relative energy differences of < 30 kJ mol^{-1} (0.3 eV) between the homo and shomo form molecules *e.g.* $[Pt(PR_3)_2C_2B_9H_{11}]$ or $[M(PR_3)\text{-}As_2B_9H_9]$ (M = Pt or Pd)[53] (As atoms may be considered similar to P atoms) which show low barriers to rotation of the ML_2 unit above the top face of the heteroborane cluster {see discussion on $[3,3\text{-}(PMe_2Ph)_2\text{-}3,1,2\text{-}PtC_2B_9H_{11}]$ in chapter 4}. For molecules with energy gaps > 0.3 eV, rotation barriers are higher *e.g.* $[2,2\text{-}(PMe_2Ph)_2\text{-}2,1,8\text{-}C_2B_9H_{11}]$ (as discussed in chapter 4). An exception to the above generalisation is seen in complexes of the $[7\text{-}SB_{10}H_{10}]^{2-}$ anion (Se and Te atoms may be considered similar to S). From the calculations one would expect low barriers to rotation for $[Pt(PR_3)_2XB_{10}H_{10}]$ (X = Se or Te) molecules however the Se and Te complexes show the barrier to rotation is high and it is unclear as to why this should be the case. It should be recalled however that free energy of rotation, $\Delta G^{\ddagger}$ is measured in solution whereas the mo calculations are based on independent molecules in the gas phase.

X-ray crystal structure results support the previous discussion of the relative importance of lumo-homo interactions *e.g.* for $[4,7\text{-}C_2B_9H_{11}]^{2-}$ the energy difference between the homo and shomo is 0.77 eV which would suggest that the lumo only of $[Pt(PR_3)_2]^{2+}$ would bond mainly with the homo and thus result in only one conformer. In chapter 4 the crystal structure of $[2,2\text{-}(PMe_2Ph)_2\text{-}2,1,8\text{-}PtC_2B_9H_{11}]$ contains just one conformer with the expected orientation, Figure 2.10 (a). For the $[7,8\text{-}C_2B_9H_{11}]^{2-}$

isomer, the energy difference between the homo and shomo is only 0.25 eV which would suggest that the lumo of $[Pt(PR_3)_2]^{2+}$ could bond with either the homo or the shomo and thus result in two possible conformations of the PtL_2 unit above the C_2B_3 face. In chapter 4 the crystal structure of $[3,3\text{-}(PMe_2Ph)_2\text{-}3,1,2\text{-}C_2B_9H_{11}]$ is shown to contain two different conformers in the unit cell consistent with the small difference in energy between the homo and shomo.

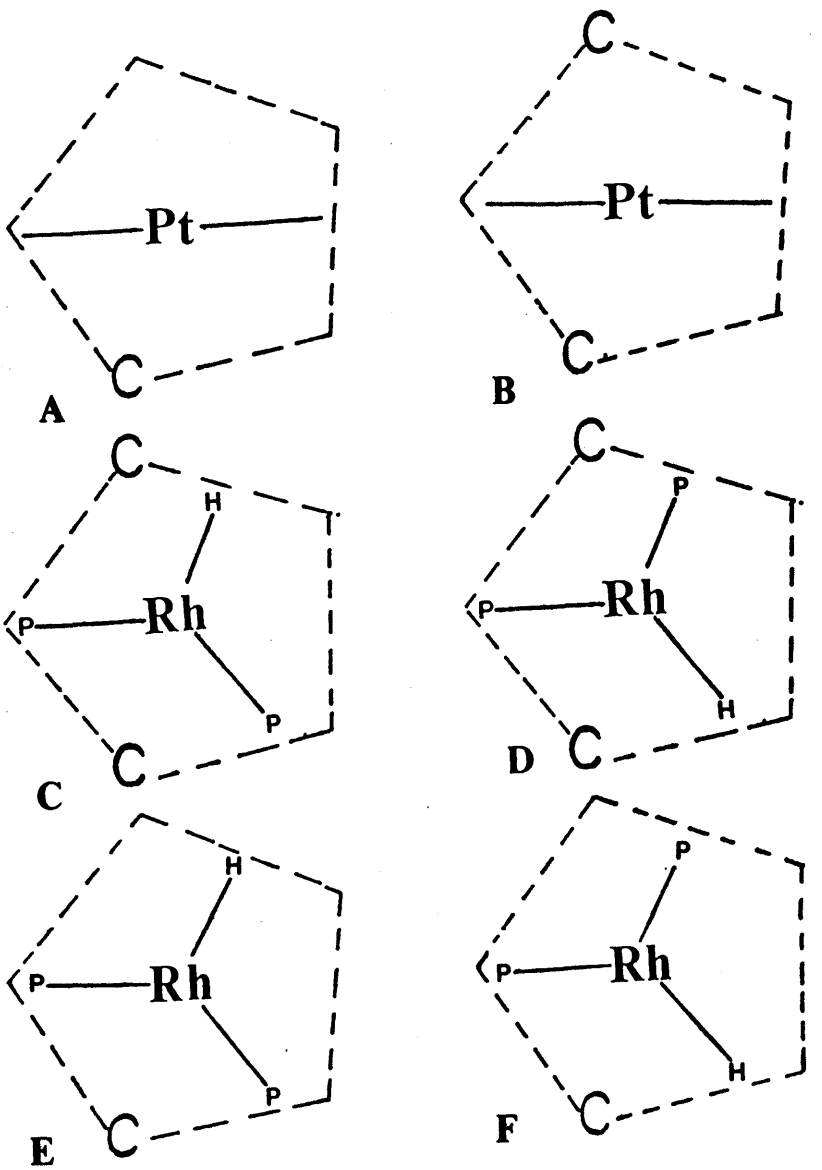

Figure 2.10 (a) proposed conformation for $[2,2\text{-}(PR_3)_2\text{-}2,1,8\text{-}PtC_2B_9H_{11}]$ (b) proposed conformation for $[2,2\text{-}(PR_3)_2\text{-}2,1,7\text{-}PtC_2B_9H_{11}]$ (c) possible conformation for $[2,2\text{-}(L)_2\text{-}2\text{-}H\text{-}2,1,7\text{-}RhC_2B_9H_{11}]$ (d) one alternative conformation for $[2,2\text{-}(L)_2\text{-}2\text{-}H\text{-}2,1,7\text{-}RhC_2B_9H_{11}]$ (e) possible conformation for $[2,2\text{-}(PR_3)_2\text{-}2\text{-}H\text{-}2,1,8\text{-}RhC_2B_9H_{11}]$ (f) one alternative conformation for $[2,2\text{-}(PR_3)_2\text{-}2\text{-}H\text{-}2,1,8\text{-}RhC_2B_9H_{11}]$.

Figure 2.10 (b), (c) and (d) show some other examples of the possible conformations of metal groups ML_n above the face of the $[7,9\text{-}C_2B_9H_{11}]^{2-}$ carborane ligand as in *closo*-$[2,2\text{-}(PR_3)_2\text{-}2,1,7\text{-}PtC_2B_9H_{11}]$ and *closo*-$[2,2\text{-}(L)_2\text{-}2\text{-}H\text{-}2,1,7\text{-}RhC_2B_9H_{11}]$. Figure 2.10 (a), (e) and (f) are examples of the possible conformations of metal groups ML_n above the face of the $[4,7\text{-}C_2B_9H_{11}]^{2-}$ carborane ligand as in *closo*-$[2,2\text{-}(PR_3)_2\text{-}2,1,8\text{-}PtC_2B_9H_{11}]$ and *closo*-$[2,2\text{-}(PR_3)_2\text{-}2,1,8\text{-}RhC_2B_9H_{11}]$. The energy difference between the homo and shomo is 1.15 eV for the 7,9 anion and 0.77 eV for the 4,7 anion which would suggest that the metals would only bond significantly with the homo. For the $[Pt(PR_3)_2]$ complex only one conformation is expected (and found) which is illustrated in Figure 2.10 (a) for $[2,2\text{-}(PR_3)_2\text{-}2,1,8\text{-}PtC_2B_9H_{11}]$ and Figure 2.10 (b) for $[2,2\text{-}(PR_3)_2\text{-}2,1,7\text{-}PtC_2B_9H_{11}]$. For the $[Rh(PR_3)_2H]$ complex there are several possible conformers, *e.g.* Figure 2.10 (c), (d) for $[2,2\text{-}(L)_2\text{-}2\text{-}H\text{-}2,1,7\text{-}RhC_2B_9H_{11}]$ and (e) and (f) for $[2,2\text{-}(PR_3)_2\text{-}2\text{-}H\text{-}2,1,8\text{-}RhC_2B_9H_{11}]$.

2.3 SUMMARY AND CONCLUSION

Analysis of the structures and bonding in the *nido* heteroborane anions $[7,8\text{-}C_2B_9H_{11}]^{2-}$, $[7,9\text{-}C_2B_9H_{11}]^{2-}$, $[1,7\text{-}C_2B_9H_{11}]^{2-}$, $[4,7\text{-}C_2B_9H_{11}]^{2-}$, $[7,8\text{-}P_2B_9H_9]^{2-}$, $[7,9\text{-}P_2B_9H_9]^{2-}$ and $[7\text{-}SB_{10}H_{10}]^{2-}$ was undertaken with MNDO calculations. (MNDO calculations cannot be performed on As or Te containing systems but the bonding in P and S containing systems should be similar). In all the *nido* systems studied in the present work the calculated bond lengths were in good agreement with the related data obtained experimentally. This observation strongly supports the suggestion that the calculations give good descriptions of the molecular structures and hence the electronic structures.

The calculated heats of formation for the seven *nido* anions were determined, Table 2.1. The 7,9-heteroborane systems were always more stable than the related 7,8 systems and those with the heteroatoms in the open face of the molecule were always more stable than compounds with the heteroatom in the body of the molecule.

The MNDO calculations showed that, as expected, there were thirteen *i.e.* n+2, cluster molecular orbitals in each anion. These consisted of five two-centre

orbitals and either eight three-centre orbitals, as in the $[7,8\text{-}C_2B_9H_{11}]^{2-}$, $[7,8\text{-}P_2B_9H_9]^{2-}$ and $[7\text{-}SB_{10}H_{10}]^{2-}$ anions, or seven three-centre orbitals and one four-centre orbital which was the case for the $[7,9\text{-}C_2B_9H_{11}]^{2-}$ and $[7,9\text{-}P_2B_9H_9]^{2-}$ anions.

On the basis of the charge distribution, all seven *nido* anions would be expected to react at the open face with $[ML_n]^{2+}$ electrophiles since there is a gross negative electron density in the open face and it is not sterically congested.

The nature of the homo or shomo and the energy difference between them have significance in determining the configurations of metal units such as $Pt(PR_3)_2$ and $Rh(PR_3)_2H$ above the heteroatom faces to which they are attached in twelve atom *closo* complexes. The orientation of the $Pt(PR_3)_2$ or $Rh(PR_3)_2H$ metal unit above the top face of the molecule may be predicted for all seven anions similar to the example of $[7,9\text{-}C_2B_9H_{11}]^{2-}$ illustrated in Figure 2.10. In the following chapters $Pt(PMe_2Ph)_2$- and RhL_3- complexes of $[C_2B_9H_{11}]^{2-}$, $[As_2B_9H_9]^{2-}$ and $[TeB_{10}H_{10}]^{2-}$ are discussed. The MNDO calculations discussed here may be used to compare the predicted conformations with actual conformations from crystal structure analysis.

CHAPTER THREE

MICROWAVE HEATING EFFECTS AND THEIR APPLICATION TO SYNTHETIC METALLABORANE CHEMISTRY

3.1 THE INTERACTION OF MICROWAVES WITH MATTER

The microwave region of the electromagnetic spectrum (see Figure 3.1) lies between infra-red and radio frequencies and corresponds to frequencies of 30 GHz to 300 MHz (wavelengths of 1 cm to 1 m respectively). The frequencies between 30 GHz and 1.2 GHz are extensively used for RADAR transmissions and the remaining frequencies are used for telecommunications. In order not to interfere with these uses, domestic and industrial microwave heaters are required to operate at either 2.45 GHz (12.2 cm) or 900 MHz (33.3 cm) (unless the apparatus is shielded in such a way that no radiation losses occur). Domestic microwave ovens generally operate at 2.45 GHz.

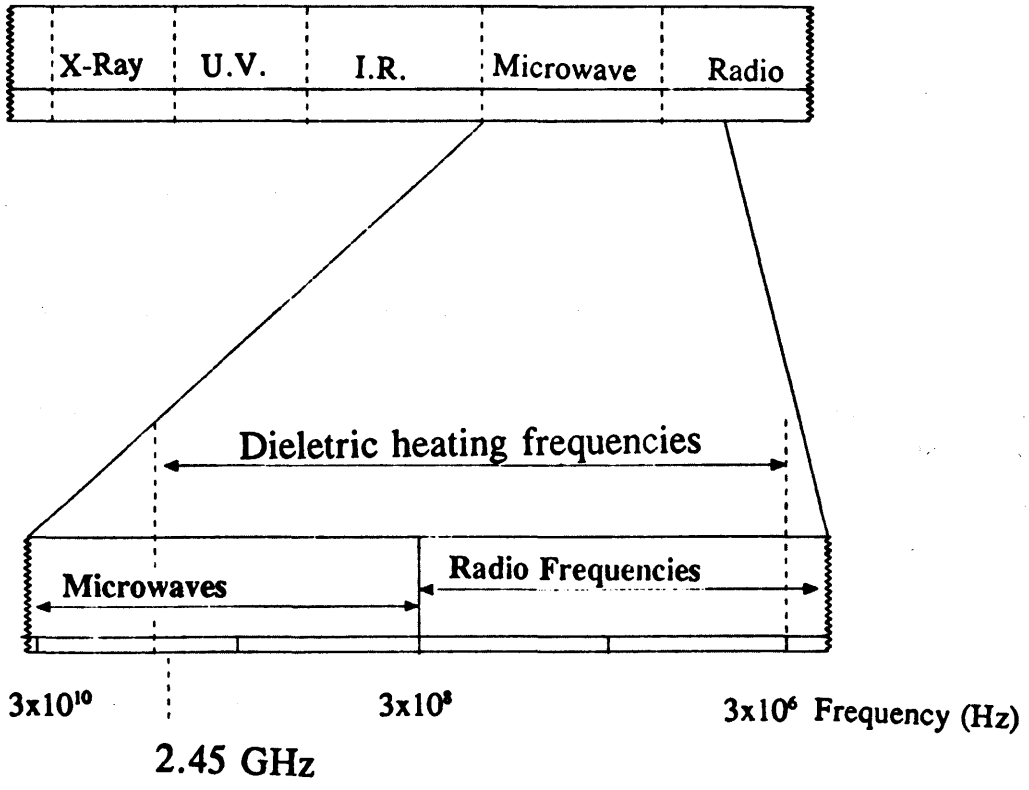

Figure 3.1 The electromagnetic spectrum indicating the microwave frequencies and the frequencies which are used for dielectric heating.

A material can be heated by applying energy to it in the form of high frequency electromagnetic waves. The origin of the heating effect produced by the high frequency electromagnetic waves arises from the ability of an electric field to exert a force on charged particles. The microwave heating effect depends on the

frequency as well as the power applied. The theory of microwave heating has been developed by many people and has been summarised recently by Mingos and Baghurst.[105]

3.1.1 Dielectric properties

Two parameters define the dielectric properties of materials. The first ϵ', the dielectric constant describes the ability of the molecule to be polarised by the electric field. The second ϵ'', the dielectric loss measures the efficiency with which the energy of the electromagnetic radiation can be converted into heat. The ratio of the dielectric loss and the dielectric constant define the (dielectric) loss tangent $= \epsilon'/\epsilon'' = \tan \delta$, which is the ability of a material to convert electromagnetic energy into heat energy at a given frequency and temperature. The dielectric properties of some common solvents are given in Table 3.1. The high dielectric losses of the alcohols are particularly noteworthy.

Table 3.1 Dielectric properties of common solvents.

	Operating Frequency $3x10^8$ Hz		Operating Frequency $3x10^9$ Hz	
Solvent	ϵ'	ϵ''	ϵ'	ϵ''
Water	77.5	1.2	76.7	12.0
Heptane*	1.97	---*	1.97	$2x10^{-4}$
Methanol	30.9	2.5	23.9	15.3
Ethanol	22.3	6.0	6.5	1.6
n-Propanol	16.0	6.7	3.7	2.5
n-Butanol	11.5	6.3	3.5	1.6

* At an operating frequency of $3X10^{10}$ Hz $\epsilon'' = 3X10^{-3}$

3.2 MICROWAVE HEATING OF LIQUIDS

The rate of rise in temperature of a liquid or solid due to the application of an electric field of microwave radiation is determined by the dielectric loss, specific heat capacity and emissivity of the sample as well as the strength of the applied field. These physical properties of the liquid or solid are all temperature dependent, making the complete theoretical analysis of dielectric heating mathematically very complex.[106]

The dielectric constant and dielectric loss values have been established for a number of materials at room temperature. The largest collection of data is due to von Hippel although much of this data applies to foodstuffs and is of limited use to the chemist.[107,108]

Several workers have reported the temperatures reached by liquids and solids when placed in conventional microwave ovens for a given time. Some of the available data for liquids (1 minute / 560 W/ 2.45 GHz) are given in Table 3.2.[105]

Table 3.2 The temperature of several solvents after heating from room temperature for one minute at 560 W, 2.45 GHz.

SOLVENT	T/°C (after 1 minute)	b.p. °C
Water	81	100
Methanol	65	65
Ethanol	78	78
Dichloromethane	40	40
Chloroform	49	61
D.M.F.	131	153
Ether	32	35
CCl_4	28	77
Hexane	25	68

3.3 APPLICATIONS OF MICROWAVE DIELECTRIC HEATING EFFECTS IN CHEMICAL SYNTHESES UTILISING THE DIELECTRIC LOSS PROPERTIES OF SOLVENTS

In general any organic or inorganic solvent with a low molecular weight and a high dipole moment will couple effectively with microwaves at 2.45 GHz. The solvents that have been most commonly used for synthetic reactions are water, ethanol and methanol. Other solvents such as dichloromethane, acetonitrile and dimethylformamide couple effectively to microwaves but have been less commonly used. Non-polar solvents such as benzene, petroleum ethers and carbon tetrachloride have negligible dielectric loss and therefore do not couple efficiently with microwaves.

3.3.1 Low pressure conditions

Microwave heating provides an alternative to conventional oil bath and heating mantle techniques. Several authors have used microwaves in organic synthesis.[109-111] By substituting a high boiling solvent for a low boiling one it has been possible to speed up several syntheses.[112] The reactions are usually performed in Erlenmeyer flasks inside a microwave oven and the microwave power is adjusted so that the solvent does not boil.[113] Hence, no precautions are necessary to contain organic vapours. An example of the use of this technique is given below. On substituting chlorobenzene (b.p. 131°C) for benzene the following reaction was held at 110°C for 5 minutes (65 - 70% yield). Previously the reaction took several hours.

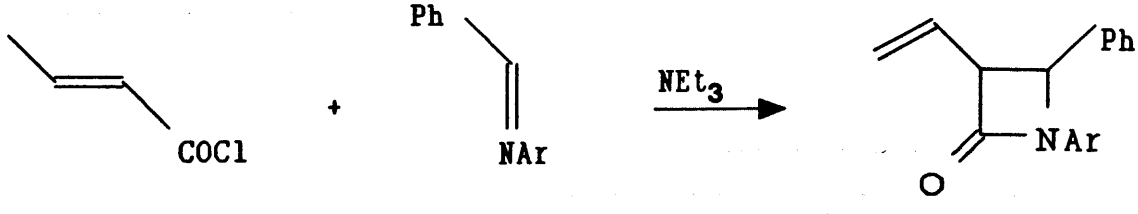

3.3.2 A Microwave Heated Reflux Apparatus

Recently, the modification of a microwave heating system was described which enables a chemist to heat solutions using microwave dielectric loss heating effects safely at reflux.[114] This procedure involves modifying a conventional microwave oven as illustrated in Figure 3.2. The conventional chemical reflux system cannot be introduced into a microwave cavity because the circulating water would absorb microwaves very strongly and heat up rapidly. An air condenser would not be effective in returning the flammable solvents safely to the flask. One solution would be to use a coolant which does not absorb microwaves strongly *e.g.* a non-polar organic or inorganic solvent with a low dielectric loss. An alternative strategy is to locate the water cooled reflux condenser outside the microwave cavity. The condenser is connected to the reaction vessel by means of a port which ensures that microwave losses are kept to a safe limit and the volatile solvents do not pose a hazard.

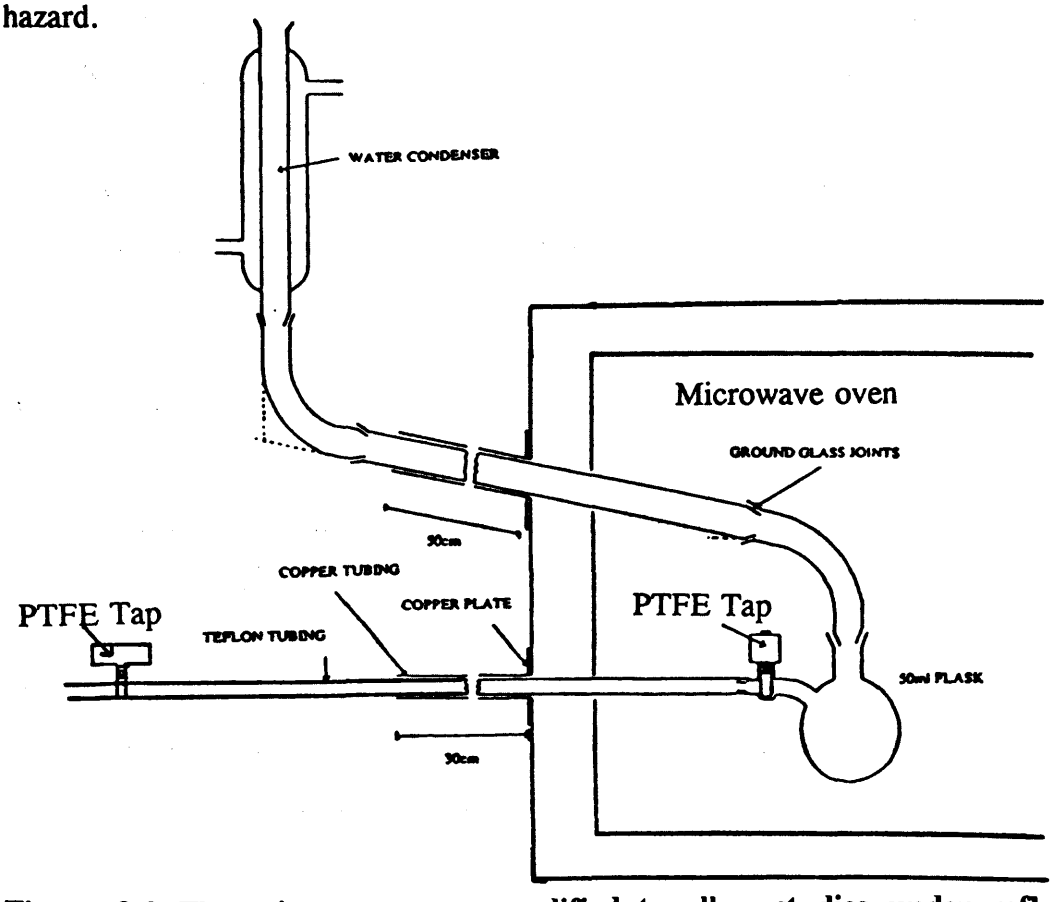

Figure 3.2 The microwave oven modified to allow studies under refluxing conditions.[114]

In the modification illustrated in Figure 3.2, the solution is contained within a round bottom flask which is connected via a length of glass tubing passing through a copper tube (a "choke") bolted to the side of a conventional microwave oven. To prevent leakage the choke should have a diameter equal to one half a wavelength *i.e.* 6 cm, and should be at least one wavelength long. The apparatus can be confirmed safe by using a hand-held microwave leakage detector capable of measuring power levels greater than 1 $mWcm^{-2}$.[115] The end of the glass tube is connected to a water-cooled condenser located completely outside the oven. This allows the solutions to heat up when the microwave source is switched on and to reflux safely without a build up of pressure or release of volatile solvents into the atmosphere. The atmosphere in the round bottom flask can be controlled by means of a Teflon tube inlet passing through a choke in the side of the microwave cavity. This tube is connected on the outside to an inert gas supply and on the inside to the round bottom flask.

The reflux apparatus is most effective when used for pure solvents or mixtures of solvents with high dielectric loss factors, *i.e.* generally solvents with a high dielectric constant. The two main advantages of the reflux technique over the high pressure technique described later are, firstly there are no high pressures involved so it is safer, and secondly it provides "gentler" reaction conditions leading to less decomposition.

3.3.3 Solid CO_2-cooled Apparatus

Due to the lack of a dipole moment in carbon dioxide, solid CO_2 is transparent to microwaves. It has been observed that little or no sublimation of solid CO_2 occurs after 4 min in a microwave oven at the highest setting.[116] As a result of this an extremely simple apparatus has been developed, consisting of a 250 ml beaker (as the reaction vessel) and a 150 ml beaker with a 2 cm flanged lip placed as a cover over the large beaker to act as a "cold finger". Over 100 reactions were conducted on a 2-4 gram scale on iron sandwich complexes [Fe(η-Cp)(η-Arene)] using this apparatus, with no problems of solvent escape even when using volatile solvents such as benzene.[116]

3.4 HIGH PRESSURE CONDITIONS

The effective coupling between microwaves and polar inorganic and organic solvents can be used to accelerate the rate of reaction with reactants in a suitable closed vessel *i.e.* one which is transparent to microwaves and can sustain the high pressures produced. The temperatures and pressures generated in such a vessel depend on the level of the input microwave power, time of microwave irradiation, the dielectric loss of the reacting solution, the volatility of the solvent, the volume of the container occupied by the solvent and whether gases are generated in the reaction. The presence of ions in solution which is often the case when studying reactions of transition metal salts, can have a profound effect on the pressure generated inside the reaction vessel. However while the presence of ions leads to greater coupling when at relatively low concentrations, high concentrations of ions reduce the heating rate as the solution then reflects a large proportion of the available microwave energy. Recent studies show that initial concentrations kept to around 0.1 M provide the most effective heating rate.[117] A detailed description of the microwave high pressure reaction vessel is given below.

3.4.1 A High Pressure Reaction Vessel

A thick-walled pyrex reaction vessel can be admitted into a microwave cavity through a suitably designed port. Pressure measurement and control is performed by external circuitry. The glass vessel allows visual examination of the reaction mixture.

The design of the pyrex reaction system is illustrated in Figure 3.3. A port in the form of a copper "choke" as described in section 3.3.2 has been attached to the roof of the microwave oven, Figure 3.4.[118] The pyrex vessel used in the studies described in this thesis had a 34 mm outer diameter and a wall thickness of 3.5 mm and was 25 cm long.[119] The pyrex tube was covered in a protective sheath made from transparent polyolefin heat-shrink.[120] In the event of the vessel failing the sheath would prevent fragmentation of the glass tube. The glass vessel is attached to a series of Swagelock[121] fittings *via* a "Viton"[122] sealed stainless-steel insert 27mm in diameter.[123]

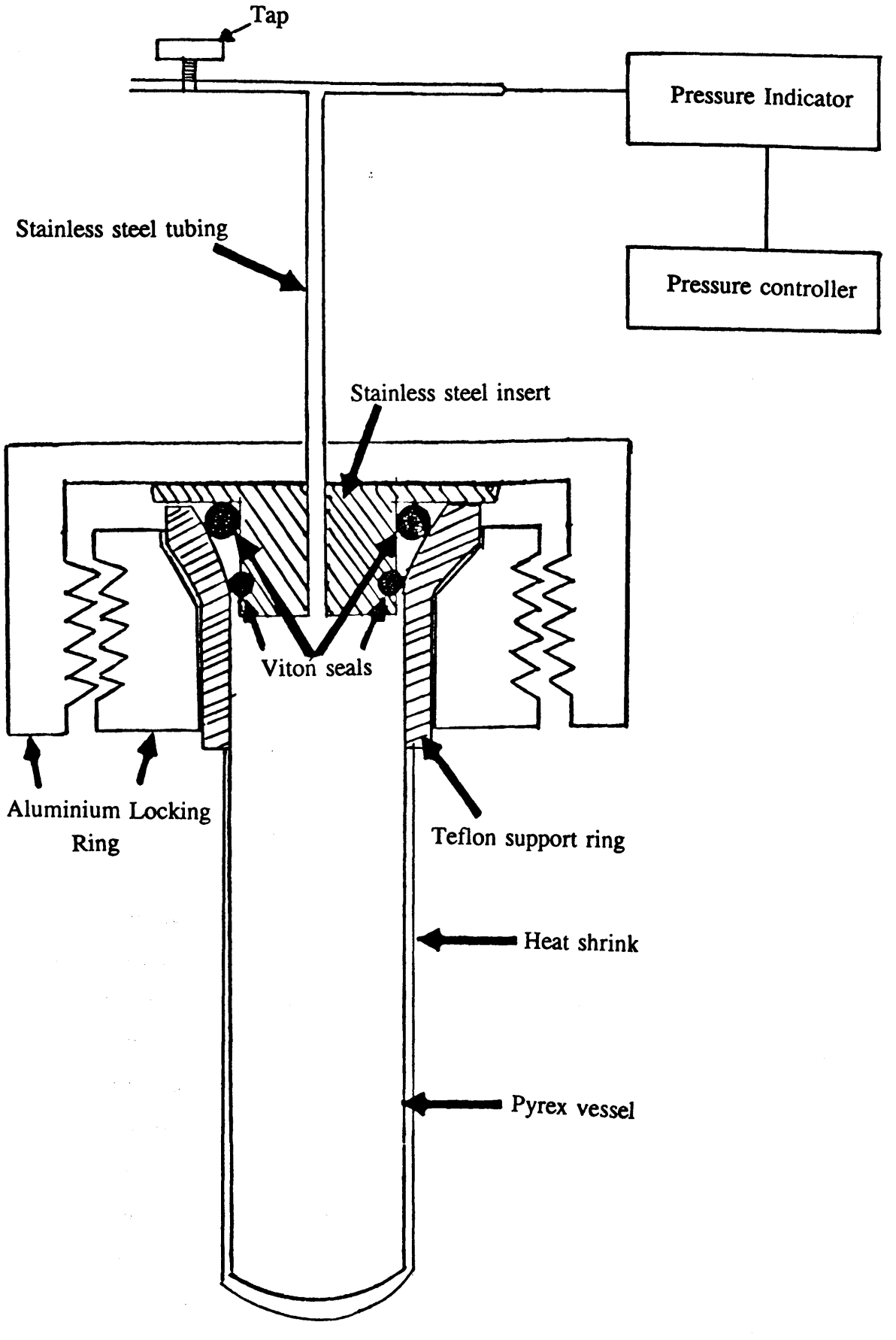

Figure 3.3 Schematic diagram of the high pressure reaction vessel.

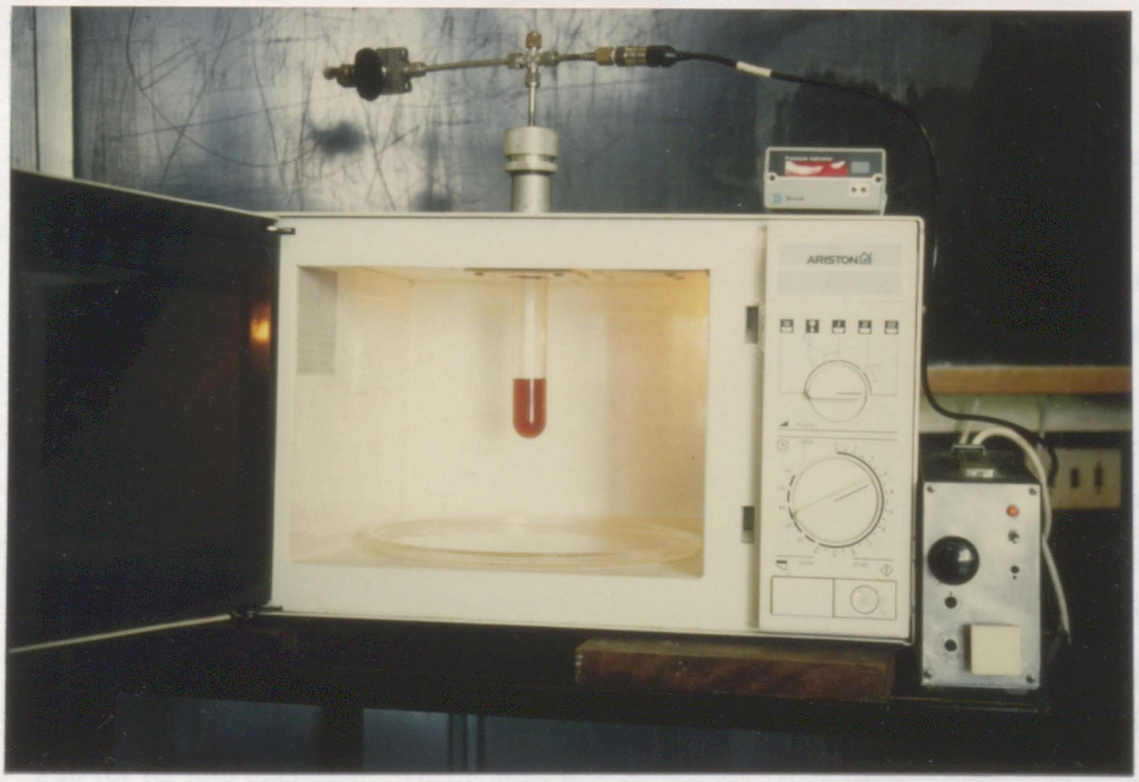

Figure 3.4 The microwave oven with the reaction vessel inserted.

In Figure 3.3 the positions of the pressure transducer and two-way tap are shown. Some care has to be taken to calibrate and maintain the pressure transducer. A photograph of the reaction vessel and the manner in which it is inserted into the microwave cavity is given in Figure 3.4.

The output from the pressure transducer was fed directly into a pressure monitor which was calibrated in pounds per square inch, psi (15 psi $\approx$ 1 Atm). From the pressure monitor a linear (0-2 V) voltage output was fed into a comparator circuit which compare the output with the predetermined reaction hold-pressure.[124] When the pressure was below the set pressure the magnetron was turned on at full power of 650 W. On reaching the set pressure the comparator which controls a relay incorporated in series with the magnetron turns the supply off. The circuit diagram was similar to the one recently described by Baghurst and Mingos.[117] It is noteworthy that the hysteresis in the circuit can be controlled. On/off switching needs to be fast enough to ensure microwave power is removed before dangerous pressures were achieved but not so fast that the magnetron is damaged. The hysteresis is adjustable between 10-30 psi. Measurement of approximate reaction temperatures has been

achieved by using a hand-held infra-red pyrometer which is directed at the sample reaction.[125]

The effect of solvent volume on pressure build up has been investigated.[117] It appears that the optimum volume for efficient heating is between 20 and 30 cm^3. Thus when the volume is smaller only a small fraction of the available microwave energy is absorbed by the sample. For larger volumes there is insufficient microwave energy available to heat the large volume of solvent.

The microwave heating method described above has considerable advantages in terms of convenience, speed of heating and reaction visibility. The pressure of the reaction vessel can be monitored and controlled and the reaction time can be varied to optimise the yield of the reaction. With the glass vessel, the reaction can be viewed to ascertain when it has reached completion. The pressure limitations associated with the glass reaction vessel set an upper limit of approximately 10 - 12 atm for its safe operation. This results in superheating of the reaction solution by at least 40° and a reaction time decrease by a factor of *ca* 10^2.

In summary, the apparatus provides a convenient and inexpensive way of using microwave dielectric heating effects to accelerate a wide range of inorganic and organometallic synthetic reactions which commonly require days of refluxing to achieve reasonable yields.[117] This technique is particularly suitable for synthesising compounds which are thermodynamically robust but are the end products of kinetically slow reactions.

3.4.2 Applications

(i) Sample Preparation for Chemical Analysis

The use of microwave energy and closed vessel containers in sample preparation prior to chemical analysis has many advantages over classical techniques. It was one of the earliest (1974) reported uses of microwave heating techniques.[126] Firstly, the sample preparation time is reduced in a typical example from 2 hours to 10 minutes.[127] Secondly, the use of closed vessels reduces the extent of sample

contamination due to contact with the atmosphere and prevents losses of volatile elements such as mercury.[128] Finally, fully automated multi-sample preparation systems are available which require only the minimum of supervision by the operator.[129]

Microwave closed vessel techniques have been successfully applied to a wide range of elemental determinations in mineralogical[130,131] and biological samples.[132-134]

(ii) Organic syntheses

Early work in this area (1986-88) was performed by Gedye[109,135,136] and Giguere,[110,137] and reviewed by Abramovitch.[111] Organic reaction rates were accelerated by up to 10^2 times when the syntheses were performed in sealed vessels. Both groups suggested that the rate of heating of the solvent depended qualitatively upon the room temperature dielectric constant, ϵ', whereas Mingos and Baghurst have suggested that the dielectric loss, ϵ'', is the more reliable parameter.[105] Gedye has also shown that the rate of acceleration relative to conventional syntheses depends upon container volume, the ratio of reaction volume to container volume and the solvent boiling point.[135] Lower boiling point solvents give reactions where the greatest rates of acceleration were observed. An example of an esterification reaction is given in Table 3.3.[135]

Table 3.3 Esterification of benzoic acid with a selection of alcohols.[135]

Alcohol	b.p.	ϵ'	Microwave/yield	Thermal/yield	Rate Ratio
n-Butanol	118°	17.8	7.5min/79%	1h/82%	8
Propanol	97°	20.1	18min/86%	7.5h/89%	25
Methanol	65°	32.6	5min/76%	8h/74%	96

(iii) Organometallic and Inorganic Syntheses

The rhodium and iridium dimers $[M_2Cl_2(diolefin)_2]$ (M = Rh or Ir) are widely used as starting materials for organometallic syntheses and are conventionally synthesised from $[MCl_3.xH_2O]$ and the olefin in aqueous alcohol.[138-140] Good yields are obtained after many hours of refluxing (4-36 hours). Using microwave radiation of 2.45 GHz and a power level of 500 W, these dimers can be conveniently synthesised from the same reagents in good yields in less than one minute.[141] Some of the compounds that can be synthesised in this manner, their yields, reaction mixtures and reaction times are summarised in Table 3.4.

A wide range of inorganic co-ordination compounds have been rapidly and conveniently synthesised using microwave dielectric loss heating effects.[142] For example using microwave radiation of 2.45 GHz and a power level of 500 - 600 W, the 2,2′,2′′-terpyridine complexes of Pt and Au (Table 3.4) have been successfully prepared in reaction times of 1 minute.

Table 3.4 Inorganic and organometallic compounds synthesised by microwave techniques.

Product	Solvent	Microwave/ yield	Thermal/ yield	Rate
$[Rh(C_8H_{12})Cl]_2$	$EtOH/H_2O$	50sec/91%	18h/94%	1296
$[Ir(C_8H_{12})Cl]_2$	$EtOH/H_2O$	45sec/72%	24h/72%	1920
$[AuCl(tpy)]Cl.3H_2O$	H_2O	60sec/37%	24h/37%	1440
$[PtCl(tpy)]Cl.3H_2O$	H_2O	60sec/47%	24h/47%	1440

Recently it was described how the high dielectric loss tangents of metal powders have been used to facilitate the syntheses of a wide range of compounds by direct combination of metals and gases.[143] The reactions of metal powders, which are volumetrically heated by microwave radiation, with gases has led to the convenient

and rapid syntheses of a wide range of metal chlorides, oxochlorides, bromides and nitrides of transition metals.[143]

3.5 SUPERHEATING OF SOLVENTS

When reactions are performed in closed vessels there will be an increase in pressure which may lead to superheating of solvents. Those solvents which have high dielectric loss tangents and low boiling points are heated most rapidly and generate high pressures most quickly.[117] High boiling alcohols and low polarity solvents only generate high pressures on prolonged heating if at all. It has been suggested that the use of high boiling alcohols and low polarity solvents may lead to overheating of the magnetron and a reduction in its operating lifetime.[129]

In Table 3.5 the temperature reached for a range of common solvents, following microwave heating for 10 minutes at a constant pressure of 10 atm is shown along with their boiling points. In general, these superheating conditions will result in an increase in temperatures of between 40-70 °C above the normal boiling point of the solvents. This can be expected to lead directly to an acceleration in the reaction times compared with conventional reflux conditions.

It has been noted that large accelerations in reaction rates (up to 10^3 times) need not necessarily be due to any specific molecular microwave absorption effect.[142,144] Rather they may be due to the macroscopic dielectric loss heating effects taking place in a sealed container. Efficient microwave heating leads to a "pressure cooker" effect in the sealed container due to the volatility of the solvents. As the pressure increases inside the vessel the boiling temperature of the solvent increases. As microwave exposure continues, both the pressure and temperature inside the vessel increase very rapidly. The relative importance of microwave induced superheating, and superheating due to the increase in reaction pressure has not been established.[145]

Table 3.5 Temperature reached after 10 min of microwave heating to ≈ 10 atm.[117]

Solvent	T/°C	b.p. °C
Methanol	106	65
Ethanol	117	78
Acetonitrile	142	82
DMF	205	153
CH_2Cl_2	110	40

3.6 CONCLUSION

Microwave dielectric loss heating techniques may be routinely employed for the synthesis of inorganic and organometallic compounds.[114] Provided suitable modifications (as described in sections 3.4 and 3.4.1) are made to commercial microwave ovens the technique is safe. Some microwave heated (low-pressure) reactions carried out at reflux and atmospheric pressure can be accelerated by 6 - 40 times their conventional reflux reaction rates.[129] These observations have been accounted for by a specific model of microwave superheating.[145]

In sealed vessel reactions which generally occur at high pressure, microwave dielectric heating techniques have the ability to reduce the reaction time by a factor of up to 10^3. Thus a reaction occurring by conventional 24 hour reflux can now be achieved in less than a minute provided that the reaction mixture couples effectively with microwaves and that the reactants, intermediates and products are all stable to the high temperatures and pressures developed within the sealed vessel.[141,142]

Both low and high pressure reaction techniques are of interest to the research chemist. However, as noted by Gedye, large scale reactions using sealed vessels in

a microwave oven are not feasible because of problems associated with the generation of the large amount of microwave power needed to process larger volumes.[135] Instead, techniques are being devised which involve pumping the reactants from a reservoir through a reaction coil inside a microwave oven through to a collection vessel.[146]

This chapter initially reviewed the relatively new area of the application of microwave heating effects to synthetic chemistry. Subsequently the modifications required to enable the adaptation of a conventional microwave oven for chemical reactions were described in detail. In the following three chapters the microwave apparatus described in section 3.4.1 will be used in the syntheses of metallaheteroborane complexes.

CHAPTER FOUR

SYNTHESIS AND CHARACTERISATION OF SOME PLATINUM DERIVATIVES OF $C_2B_9H_{11}$, $As_2B_9H_9$ AND $TeB_{10}H_{10}$

4.1 RESULTS AND DISCUSSION

The work described below is concerned with the synthesis of platinum derivatives of $C_2B_9H_{11}$, $As_2B_9H_9$ and $TeB_{10}H_{10}$ ligands. Reactions were carried out under normal (thermal) conditions and in the high-pressure microwave apparatus (as described in section 3.4.1). The products synthesised were three new platina-carboranes, *closo*-[3,3-$(PMe_2Ph)_2$-3,1,2-$PtC_2B_9H_{11}$] (157), *closo*-[2,2-$(PMe_2Ph)_2$-2,1,8-$PtC_2B_9H_{11}$] (158) and *closo*-[8-Ph-2,2-$(PMe_2Ph)_2$-2,1,8-$PtC_2B_9H_{10}$] (159), and the previously known compounds, the platinaarsenaborane, *closo*-[3,3-$(PMe_2Ph)_2$-3,1,2-$PtAs_2B_9H_9$] (70) and the platinatelluraborane, *closo*-[2,2-$(PMe_2Ph)_2$-2,1-$PtTeB_{10}H_{10}$] (160).

All reactions were carried out using 1:1 molar ratio of heteroborane to metal complex in the presence of a ten fold excess of triethylamine. In each case the major reaction products were purified by preparative tlc followed by crystallisation from CH_2Cl_2-hexane solutions.

All these compounds were fully characterised by spectroscopic methods and the structures of (157) and (158) were established by X-ray crystallographic analyses. This chapter also describes the first reported rearrangement of a non-carbon-substituted metallacarborane at relatively low temperatures ($\leq$ 130°C).

4.1.1 Syntheses

Reaction between *nido*-$[7,8\text{-}C_2B_9H_{12}]^-$ and *cis*-$[Pt(PMe_2Ph)_2Cl_2]$ in a refluxing ethanol solution in the presence of excess triethylamine produced *closo*-[3,3-$(PMe_2Ph)_2$-3,1,2-$PtC_2B_9H_{11}$] (157) and *closo*-[2,2-$(PMe_2Ph)_2$-2,1,8-$PtC_2B_9H_{11}$] (158) in 26 and 4% yields respectively, (see Table 4.1). When the reaction was subjected to microwave irradiation the yields of products changed dramatically with (158) being the major product and (157) the minor one, the yields were 19 and 4% respectively. Although there were other products formed in the reaction (*vide* tlc) these were not isolated since they were formed in too small quantities (*ca.* 1-2mg) for a complete characterisation. These products may be different isomers of MC_2B_9 as discussed in

section 4.1.5. No rearrangement occurred on subjecting an ethanolic solution of the anion *nido*-[7,8-$C_2B_9H_{12}$]$^-$ and excess triethylamine to microwave irradiation. On subjecting *closo*-[3,3-$(PMe_2Ph)_2$-3,1,2-$PtC_2B_9H_{11}$] (157) in ethanol to microwave irradiation for 10 minutes it rearranged to (158) (90% yield). Taken with the results discussed above this suggests that the formation of (158) is *via* the rearrangement of (157) which happens readily under the conditions of microwave irradiation.

Reaction between Cs[7-Ph-*nido*-7,8-$C_2B_9H_{11}$] and *cis*-[$Pt(PMe_2Ph)_2Cl_2$] in ethanol solution at reflux for six days in the presence of excess triethylamine produced *closo*-[8-Ph-2,2-$(PMe_2Ph)_2$-2,1,8-$PtC_2B_9H_{10}$] (159) in 65% yield. (This compound was subsequently prepared in Oxford by microwave heating and characterised by spectroscopic and crystallographic techniques.[129,147]) No yield was reported in data from Oxford. Section 4.3.7 describes the synthesis of (159) by microwave induced heating (procedure 2) to enable comparisons to be made between microwave induced and thermal (procedure 1) heating, Table 4.1. It is interesting, that as well as the 2,1,8 isomer the 3,1,11 isomer was also isolated and characterised but none of the 3,1,2 isomer was isolated from either procedure described in section 4.3.7. The anion [7-Ph-*nido*-7,8-$C_2B_9H_{11}$]$^-$ like *nido*-[7,8-$C_2B_9H_{12}$]$^-$ does not undergo any rearrangement when subjected to microwave irradiation in ethanol solution in the presence of excess triethylamine.

The compounds *closo*-[3,3-$(PMe_2Ph)_2$-3,1,2-$PtAs_2B_9H_9$] (70) and *closo*-[2,2-$(PMe_2Ph)_2$-2,1-$PtTeB_{10}H_{10}$] (160) had been previously synthesised in moderate yields, 45 and 49% respectively, in refluxing thf solution. To compare the reactivity of anions used in this study, both [$As_2B_9H_{10}$]$^-$ and [7-$TeB_{10}H_{11}$]$^-$ were separately reacted with *cis*-[$Pt(PMe_2Ph)_2Cl_2$] in ethanol solution in the presence of excess triethylamine under both conventional and microwave conditions, Table 4.1. The effect of changing the solvent from thf to ethanol was very significant and led to an improvement in the yields of both (70) and (160). In the case of the microwave preparation of (70) it appeared {from tlc evidence and overall yield of (70)} that some decomposition occurred.

Table 4.1 Comparison of yields from microwave and thermally heated reactions for the syntheses of platinaheteroboranes in ethanol solution.

Compound/isomer	Thermal % Yield	Microwave[a] % Yield	$\Delta G^{\ddagger}$/kJ mol^{-1}
(157) 3,1,2-$PtC_2B_9H_{11}$	26.4[b]	4.4	≤ 30
(158) 2,1,8-$PtC_2B_9H_{11}$	3.5[b]	19.4	57.8 ± 1.2
(159) 8-Ph-2,1,8-$PtC_2B_9H_{10}$	64.7[b]	82.3	---[c]
(70) 3,1,2-$PtAs_2B_9H_9$	85.2[d,e]	74.6	≤ 30
(160) 2,1-$PtTeB_{10}H_{10}$	34.0[d,f]	84.9	62

[a] 650W for 30 minutes. [b] Six days at reflux. [c] Data not available.[129] [d] Stir at ambient temperature for 18 hours. [e] Original yield was 44.6% in thf.[22] [f] Original yield was 49.0% in thf.[4]

4.1.2 Infrared Spectra

An important feature of the IR spectra of the compounds (70) and (157)-(160) was the presence of strong absorptions due to terminal B-H stretching bands in the region 2600-2400 cm^{-1}, Table 4.2. Other important features were bands due to phosphine ligands arising from C-H stretching in the region 3100-2800 cm^{-1}, P-C stretching in the region 795-650 cm^{-1}, P-Ph stretching in the regions 1600-1425 and 1110-960 cm^{-1}, and P-Me stretching in the region 960-835 cm^{-1}.

Table 4.2 B-H stretching frequencies for compounds (70), (157), (158), (159) and (160).

Compound	ν(B-H)/cm^{-1}
(70) 3,1,2-$PtAs_2B_9H_9$	2530(vs), 2505(vs,sh), 2495(vs,sh)
(157) 3,1,2-$PtC_2B_9H_{11}$	2565(s), 2530(vs,sh), 2518(vs), 2490(s,sh), 2460(m,sh)
(158) 2,1,8-$PtC_2B_9H_{11}$	2555(vs), 2518(vs), 2497(s,sh), 2458(s)
(159) 8-Ph-2,1,8-$PtC_2B_9H_{10}$	2550(vs), 2535(vs), 2518(vs), 2500(vs), 2480(s,sh)
(160) 2,1-$PtTeB_{10}H_{10}$	2540(vw), 2525(vs), 2495(vs), 2475(vw)

4.1.3 NMR Spectroscopy

4.1.3.1 Fluxionality in Platinacarboranes *closo*-[3,3-$(PMe_2Ph)_2$-3,1,2-$PtC_2B_9H_{11}$] (157) and *closo*-[2,2-$(PMe_2Ph)_2$-2,1,8-$PtC_2B_9H_{11}$] (158)

Dynamic behaviour is frequently observed in polyhedral boron compounds and often results in simpler NMR spectra than those required by static structures.[4] For example, the ^{1}H NMR spectrum of the free $[B_3H_8]^-$ ion at room temperature, consists of a symmetrical ten lined pattern at *ca.* +0.3 ppm with $J(^{11}B\text{-}^1H)$ = 33Hz.[39] The corresponding ^{11}B spectrum has a symmetrical nonet at *ca.* -30.0 ppm. These data indicate that all hydrogens and all boron atoms of the $[B_3H_8]^-$ ion are equivalent. This is possible only if a rapid internal exchange is taking place. Other examples of such dynamic behaviour include the scrambling of all boron positions with retention of individual *exo* B-H bonds *e.g.* in $[B_{11}H_{11}]^{2-}$,[148] exchange of external phosphine ligands *e.g.* in $[(PPh_3)_2CuB_3H_8]$,[149] and exchange of internal groups *e.g.* in $[Me_2AlB_3H_8]$,[150] as well as exchange among bridging protons only *e.g.* in B_6H_{10}.[151]

In metal derivatives of boranes, carboranes and other heteroboranes additional varieties of fluxional processes associated with metal-to-borane bonding and/or metal bound *exo*polyhedral ligands have been observed.[4] A non-dissociative (mutual) rotation of the borane cage and metal unit about an axis passing through the metal coordination plane was observed in the two platinacarboranes (157) and (158) (see section 4.1.3.2). This kind of rotation effect was reported for the twelve vertex *closo* compound [2,2-$(PMe_2Ph)_2$-2,1-$PtTeB_{10}H_{10}$] (160).[4,152] It was observed that the two P-methyl ^1H NMR resonances first broaden with increasing temperature and then coalesce and finally merge into a single centred peak when a $CD_3C_6D_5$ solution of the complex is heated from 305 to 355K, Figure 4.1. Site exchange *via* phosphine ligand or borane ligand dissociation was precluded because the P-methyl coupling $^3J(^{195}Pt\text{-}^1H)$ and borane couplings $^2J(^{195}Pt\text{-}^1H)$ and $^3J(^{195}Pt\text{-}^1H)$ were all retained at all temperatures.

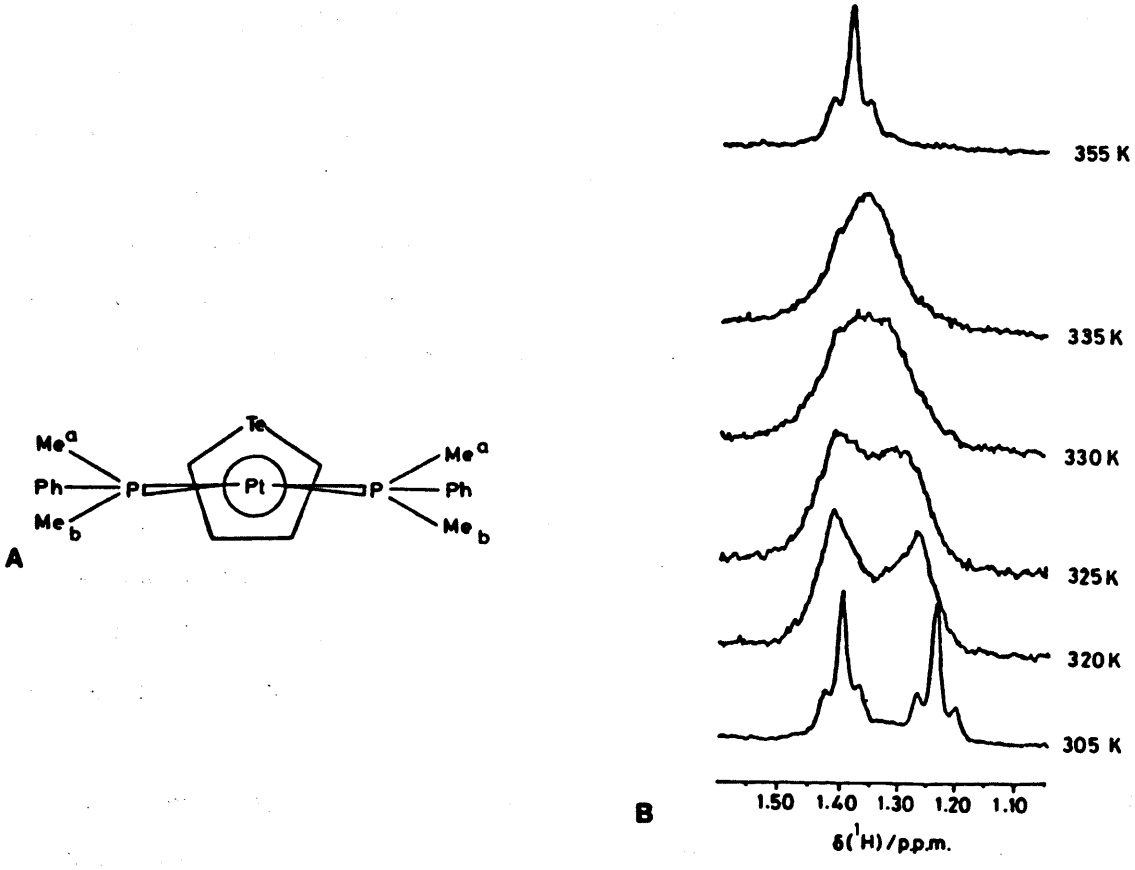

Figure 4.1 (A) An illustration of one possible conformation of the ligands about Pt in a static structure of [2,2-$(PMe_2Ph)_2$-2,1-$PtTeB_{10}H_{10}$] (160) showing two Me group environments. (B) 400-MHz ^1H NMR spectra in the Me_2PhP region of (160) in $CD_3C_6D_5$ solution at temperatures from 305 to 355 K.[152]

Dynamic NMR can be used to determine the free energy of activation $\Delta G^{\ddagger}$ from the fluxional exchange process provided the value of $\Delta G^{\ddagger}$ is between 21 - 105 kJ $mole^{-1}$.[153] The value of $\Delta G^{\ddagger}$ can be calculated from the Eyring equation (1) provided the value of the rate constant "K_c" is known.

$$K_c = \frac{K_b T . e^{-\Delta G^{\ddagger}/RT}}{h} \qquad (1)$$

K_b = Boltzmann's Constant, h = Planck's Constant, R = Gas Constant,
T = Absolute Temperature
Whence,

$$\Delta G^{\ddagger} = 4.57\ T\ (10.32 + \log T/K_c) \qquad (2)$$

The value of K_c can be determined by variable temperature NMR experiments. Two methods *i.e.* an analysis of the coalescence phenomenon or total line shape analysis are commonly used for this purpose.[154,155] The simplest and the more rapid procedure is that of the coalescence analysis which under optimum conditions yields substantially the same value of $\Delta G^{\ddagger}$ as does the more laborious complete line shape analysis.[156] It basically involves the calculation of the rate of exchange/rotation "K_c" at the coalescence temperature T_c, using either of the approximate equations (3) or (4).[157]

$K_c = \pi\Delta\nu/(2)^{1/2}$ (for uncoupled AB case) (3)

$K_c = \pi(\Delta\nu^2+6J^2)^{1/2}/(2)^{1/2}$ (for the coupled AB system) (4)

$\Delta\nu$ = line separation or change in chemical shift (in units of Hz) between signal A and B without exchange.

J = coupling constant between nuclei A and B.

Graphical methods are available which are particularly suitable for the evaluation of certain spectral parameters,[158] since the intrinsic widths of the lines and the temperature dependence of the splitting without chemical exchange are taken into account more satisfactorily.[155,159]

It is important to note that $\Delta G^{\ddagger}$ contains the temperature dependent entropy term $T\Delta S$ and is, therefore, not a good term for comparison. The best quantities to

use for comparison are the Arrhenius activation energy "E_a" or ΔH ($\Delta H = E_a - RT$) which do not have the temperature dependent term $T\Delta S$. However, the E_a values are mostly indeterminable and at best uncertain. For instance, the reported E_a values, calculated by NMR spectroscopy, for dimethylformamide range from 7 - 28 kcal mole^{-1} while the values found for $\Delta G^{\ddagger}$ by the peak coalescence method differ by less than 1 kcal mole^{-1} from the average of 21.5 kcal mole^{-1}.[153] Thus, if accurate measurements are not available, it is better to use the $\Delta G^{\ddagger}$ values rather than the physically accurate but numerically doubtful E_a or ΔH values with the temperature dependence of $\Delta G^{\ddagger}$ ignored.[159] This procedure is not problematic in the comparison of similar types of compounds like (157) and (158).

4.1.3.2 NMR Spectroscopy of *closo*-[3,3-$(PMe_2Ph)_2$-3,1,2-$PtC_2B_9H_{11}$] (157)

All the NMR spectra discussed in this section were kindly recorded by Dr. J. D. Kennedy, University of Leeds, England. Multinuclear ^{11}B, $^{11}B\{^1H\}$, ^{31}P, ^{135}Pt and ^1H NMR spectroscopy was used to characterise *closo*-[3,3-$(PMe_2Ph)_2$-3,1,2-$PtC_2B_9H_{11}$] (157), Table 4.3. There were six signals with an intensity pattern 1:1:2:2:1:2 in the $^{11}B\{^1H\}$ spectrum of (157). The shielding patterns (^{11}B) can be traced to those of *closo*-$C_2B_{10}H_{12}$ (161), Figure 4.2, demonstrating the approximation to true *closo* nature, and there are also similarities with $[C_2B_9H_{12}]^-$ (162) (albeit with massive downfield shifts for B8 {adjacent} and B10 {antipodal} to platinum).[160] There is also a close relationship to [3-Cp*-3,1,2,-$IrC_2B_9H_{11}$] (163) showing a general *closo* {3,1,2-$MC_2B_9H_{11}$} bonding pattern.[161] The greatest differences from both the $C_2B_{10}H_{12}$ and the 3,1,2-$IrC_2B_9H_{11}$ compounds are in the 8 and 4,7 positions, adjacent to the metal. The ^1H NMR shielding (Figure 4.3), when plotted against the ^{11}B shielding, falls into established *closo* patterns with a gradient of 11:1. The somewhat higher shielding of $^1H(4,7)$ and somewhat lower shielding of ^1H (6), as compared to the general trend, are also found for {ArM}$C_2B_{10}H_{12}$ where {ArM} = CpRh, CpIr and Cp*Ru. The much lower shielding of $^1H(10)$, antipodal to the 3rd row transition element Pt, has precedent in the previously examined MAs_2B_{10} *closo* systems.[53]

Table 4.3 ^{1}H and ^{11}B NMR data for *closo*-[3,3-$(PMe_2Ph)_2$-3,1,2-$PtC_2B_9H_{11}$] (157) $CDCl_3$ solution at 294-297 K unless otherwise indicated.

Assignment	$\delta(^{11}B)$/ppm	$^{1}J(^{195}Pt-^{11}B)$	$\delta(^{1}H)$/ppm	$^{n}J(^{195}Pt-^{1}H)$
8	+5.7	260	+3.66	+39 (^{2}J)
10	-9.2	---	+4.15	-28 (^{4}J)
9,12	-9.9	---	+2.28	-38 (^{3}J)
5,11	-14.5	---	+1.91	(-)≤20 (^{2}J)
6	-20.8	---	+2.05	---
4,7	-20.8	170	+0.88	+60
1,2	(CH)	---	+2.98	---
3	(Pt)	---	+1.72 (PMe's)[a]	+32.6 (^{3}J)

[a] $N(^{31}P-^{1}H)$ = 10.5Hz

Additional Data:

$\delta(^{195}Pt)$ -371 (Goodfellow scale)

$\delta(^{31}P)$ -13.1 $^{1}J(^{195}Pt-^{31}P)$ 3445Hz at -54°C $CDCl_3$ and -12.6 $^{1}J(^{195}Pt-^{31}P)$ 3450Hz at -90°C CD_2Cl_2

Low temperature spectra of P-methyl groups		$\delta(^{1}H)$/ppm	Width at half height
CD_2Cl_2 solution	-70°C	δ +1.63	$W_{½}$ 6.6Hz
	-90°C	δ +1.62	$W_{½}$ 8.0Hz
	-110°C	δ +1.62	$W_{½}$ 13.0Hz
$CD_3C_6D_5$ solution	-82°C	δ +1.28	$W_{½}$ 7.5Hz
	-94°C	δ +1.30	$W_{½}$ 8.5Hz

If broadening is due to incipient peak separation at -110°C, there is an upper limit to $\Delta G^{\ddagger}$ of *ca.* 30 kJ mol^{-1}

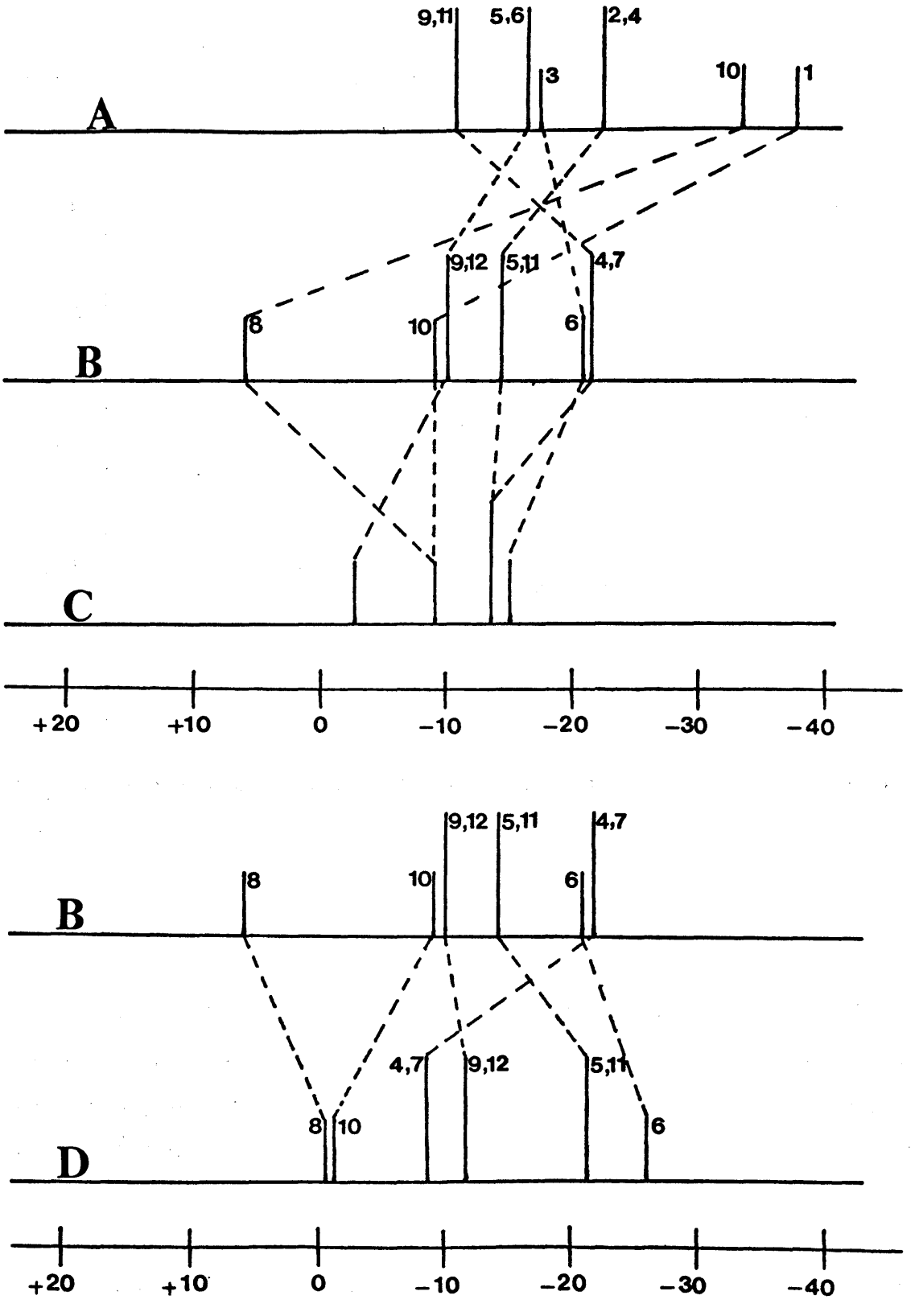

Figure 4.2 "Stick" diagrams of the chemical shifts and relative intensities of the ^{11}B NMR spectra of (A) $C_2B_9H_{12}^-$ (162), (B) *closo*-[3,3-$(PMe_2Ph)_2$-3,1,2-$PtC_2B_9H_{11}$] (157), (C) *closo*-$C_2B_{10}H_{12}$ (161) and (D) *closo*-[3-Cp^*-3,1,2,-$IrC_2B_9H_{11}$] (163).[161]

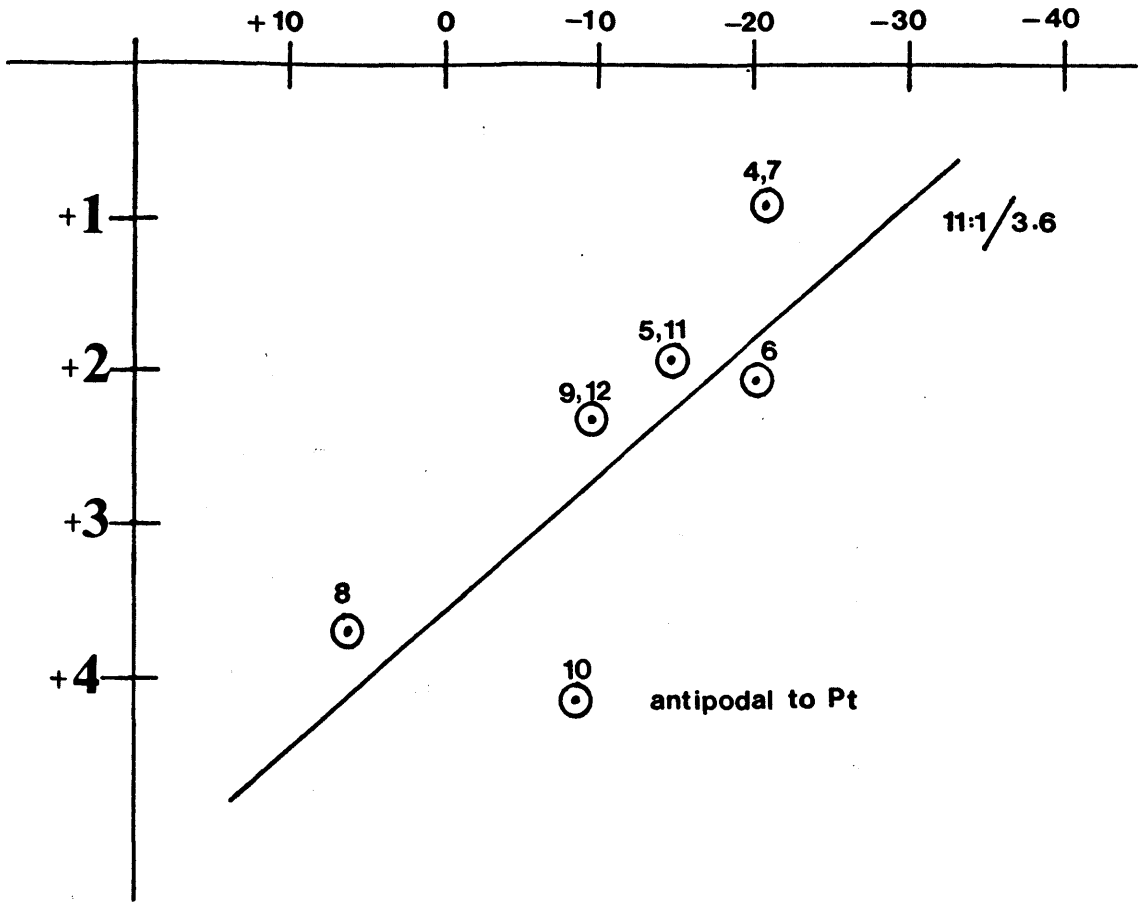

Figure 4.3 Plot of $\delta(^1B)$ versus $\delta(^1H)$ for *closo*-[3,3-$(PMe_2Ph)_2$-3,1,2-$PtC_2B_9H_{11}$] (157).

Molecular Fluxionality

From the X-ray determined crystal structure of *closo*-[3,3-$(PMe_2Ph)_2$-3,1,2-$PtC_2B_9H_{11}$] (157) (section 4.1.4.1) there are two molecules, A and B present in the unit cell, Figure 4.4 (*vide infra*) which have significantly different conformations of the $Pt(PMe_2Ph)_2$- unit above the C_2B_3 face. Clearly the static form A (Figure 4.4) is excluded both on the basis of ^{31}P NMR (*i.e.* there is only one ^{31}P resonance down to -90°C) and on the basis of ^1H NMR (there is only one ^1H resonance down to -110°C). Furthermore the observation of only one PMe resonance also precludes the static form B. Although this could in principle arise because of accidental coincidence of ^1H chemical shifts, it is unlikely, particularly as both CD_2Cl_2 and the highly anisotropic solvent $CD_3C_6D_5$ each only show one P-methyl resonance.

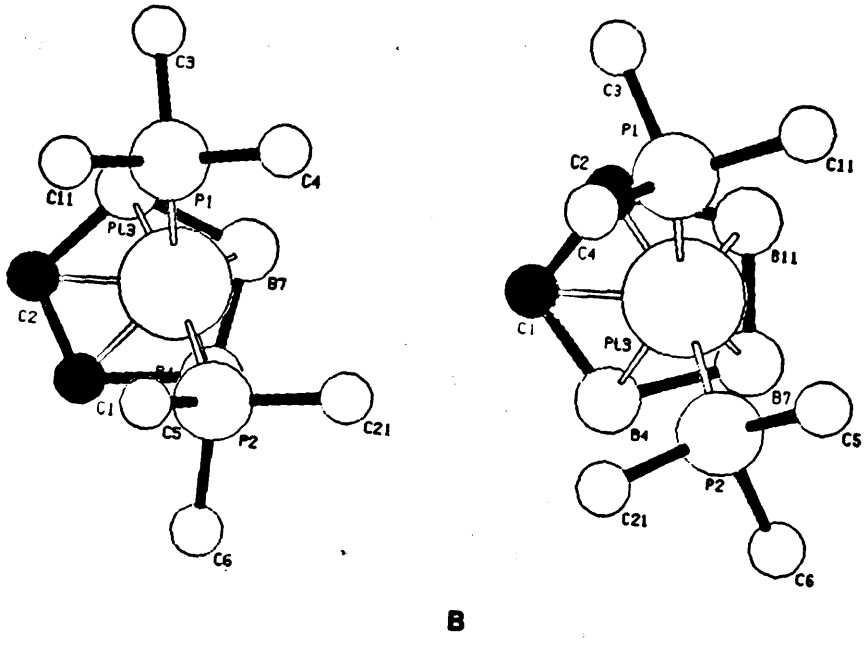

Figure 4.4 A view of the $Pt(PMe_2Ph)_2$ unit above the C_2B_3 face for molecules A and B of *closo*-[3,3-$(PMe_2Ph)_2$-3,1,2-$PtC_2B_9H_{11}$] (157)

The upper limit on $\Delta G^{\ddagger}$ for the rotational process is estimated at $<$ *ca.* 30 kJ mol^{-1}, and is possibly somewhat less than this if the broadening at -110°C (supercooled CD_2Cl_2 solution) arises from solution effects rather than any incipient fluxionality. This means that the energy difference between A and B or *any* other rotamer is 30 kJ mol^{-1} at a maximum. This is very small and of the same order of magnitude as crystal packing forces. It is therefore possible for the solid state structure to show any rotamer, as in this case of molecules A and B (Figure 4.4) *i.e.* they are two snapshots of the rotation process.

4.1.3.3 NMR Spectra of *closo*-[2,2-$(PMe_2Ph)_2$-2,1,8-$PtC_2B_9H_{11}$] (158)

The NMR parameters (for ^{11}B, ^{31}P and ^{1}H nuclei) for *closo*-[2,2-$(PMe_2Ph)_2$-2,1,8-$PtC_2B_9H_{11}$] (158) are given in Table 4.4. The $^{11}B\{^{1}H\}$ spectrum of (158) consisted of nine different resonances in the region δ/ppm -7.6 to -24.2 with unit intensity ratio Figure 4.5. The measured NMR features were entirely consistent with the X-ray structure of (158) described in section 4.1.4.2.

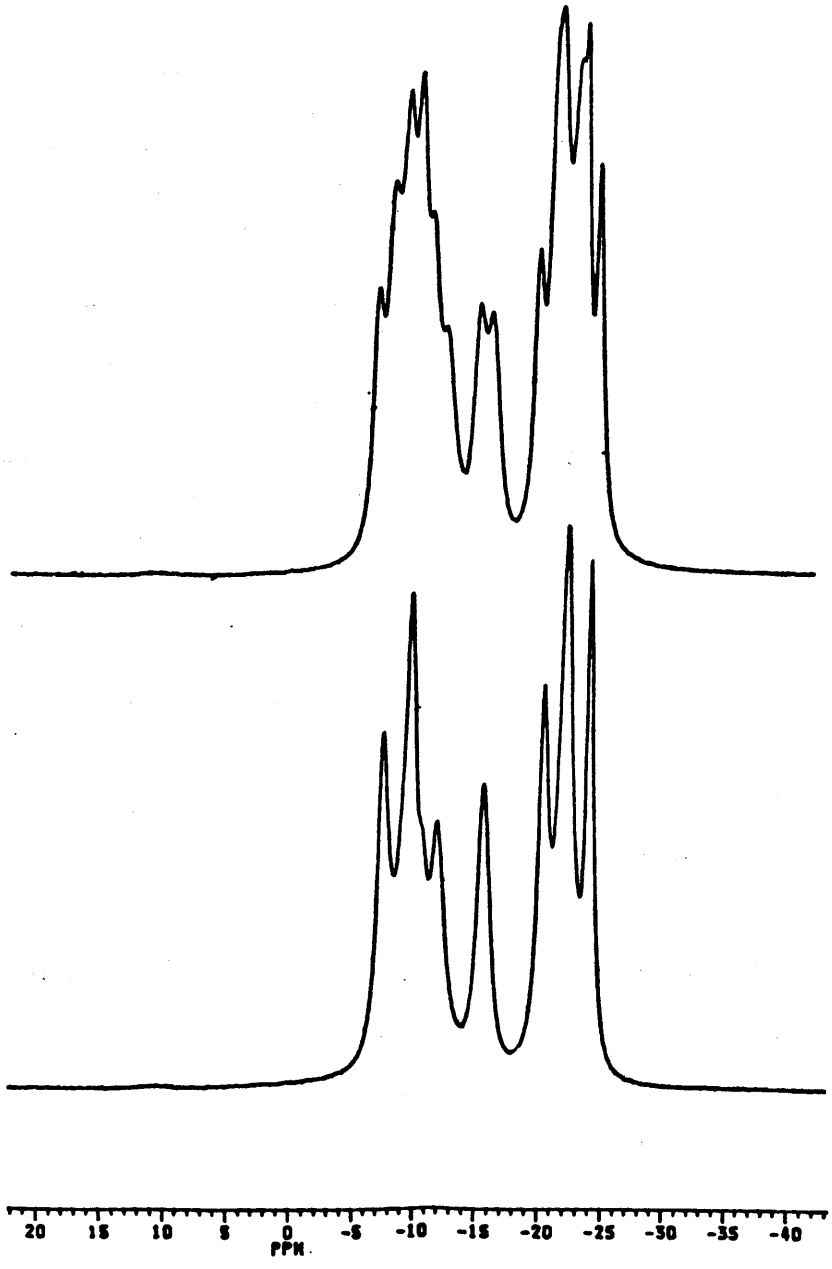

Figure 4.5 ^{11}B(top trace) and $^{11}B\{^{1}H\}$(lower trace) NMR spectra of *closo*-[2,2-$(PMe_2Ph)_2$-2,1,8-$PtC_2B_9H_{11}$] (158).

Table 4.4 ^{1}H and ^{11}B NMR data for *closo*-[2,2-$(PMe_2Ph)_2$-2,1,8-$PtC_2B_9H_{11}$] (158) $CDCl_3$ solution at 294-297 K unless otherwise indicated.

Relative Intensity	$\delta(^{11}B)$/ppm	$\delta(^{1}H)$/ppm
1	-7.6	+2.53
1	-9.4	+1.73
1	-9.9[a]	+2.24
1	-12.1	+4.11
1	-15.7	+1.38
1	-20.5	+1.87
1	-21.8	+2.24
1	-22.8	+1.41
1	-24.2	+1.58

$\Delta G^{\ddagger}$ = 57.8±1.2 kJ mol^{-1} at 272K

-52°C $\delta(^{31}P)$ ($CDCl_3$) -16.3 $^{1}J(^{195}Pt\text{-}^{31}P)$ 3299±5 Hz $^{1}J(^{31}P\text{-}^{31}P)$ 36Hz

-16.5 $^{1}J(^{195}Pt\text{-}^{31}P)$ 3284±5 Hz $^{1}J(^{31}P\text{-}^{31}P)$ 36Hz

-53°C $\delta(^{1}H)$ (PMe) 1.72 *N* 9.1 $J(^{195}Pt\text{-}^{1}H)$ 22.4Hz[b]

1.53 *N* 9.9 $J(^{195}Pt\text{-}^{1}H)$ 33.2Hz[b]

1.69 *N* 9.6 $J(^{195}Pt\text{-}^{1}H)$ 23.5Hz[c]

1.47 *N* 9.9 $J(^{195}Pt\text{-}^{1}H)$ 23.5Hz[c]

[a] $^{1}J(^{195}Pt\text{-}^{11}B)$ 260 Hz

[b] signals coalesce at 21°C with δ=1.66

[c] signals coalesce at 21°C with δ=1.63

4.1.4 Crystal and Molecular Structures

4.1.4.1 Crystal and Molecular Structure of *closo*-[3,3-$(PMe_2Ph)_2$-3,1,2-$PtC_2B_9H_{11}$] (157)

In order to elucidate the structural features of the platinacarborane (157), it was decided to undertake a single crystal X-ray analysis of the compound. Crystals suitable for study were grown by the so-called layering technique by which hexane slowly diffused into a CH_2Cl_2 solution of the platinacarborane. The collection of the data and the structure solution were carried out by Professor George Ferguson, University of Guelph, Canada, as stated in the experimental section 4.3.1. Crystal data and relevant structure solution data are given in experimental section 4.3.5.

The successful solution and refinement of the molecular structure showed that compound (157) had a *closo* twelve vertex PtC_2B_9 geometry based on a distorted dodecahedron with platinum and both carbon atoms adjacent to one another, Figures 4.6 and 4.7. There were two independent molecules in the asymmetric unit cell which differed primarily in the platinum-carborane cage bond lengths and in the orientation of the platinum phosphine unit over the C_2B_3 face to which it was bonded, Figure 4.8. Important bond distances and angles are given in Tables 4.5 and 4.6 respectively. To compare the many platinacarborane compounds that have been characterised crystallographically a selection of twelve atom *closo* platinacarborane bond distances are given in Tables 4.7 and 4.8.

The Pt-C bond distances in *closo*-[3,3-$(PMe_2Ph)_2$-3,1,2-$PtC_2B_9H_{11}$] (157) differ (by 0.213 Å) in molecule A, whereas in molecule B these distances are slightly (0.045 Å) but not significantly different. Previously reported Pt-C bond distances for 12 atom *closo* structures vary from 2.326(10) Å in *closo*-[1-Ph-3,3-$(PMe_2Ph)_2$-3,1,2-$PtC_2B_9H_{10}$] (164) to 2.622(8) Å in *closo*-[1-Ph-3,3-$(PMe_2Ph)_2$-3,1,11-$PtC_2B_9H_{10}$] (165), with many intermediate values some of which are given in Table 4.7.[147] Molecule A has similar Pt-C bond distances to *closo*-[1-Ph-3,3-$(PMe_2Ph)_2$-3,1,2-$PtC_2B_9H_{10}$] (164), and molecule B has similar Pt-C bond distances to those in *closo*-[3,3-$(Et_3P)_2$-3,1,2-$PtC_2B_9H_{11}$] (166).[162] In terms of the metal-to-cluster interaction, the two Pt-C interactions in molecule B {2.529(6) and 2.574(6)} and one in molecule A {2.515(6)} may be described as weakly bonding, whereas the second Pt-C interaction in A is much stronger {2.302(7)}.[160]

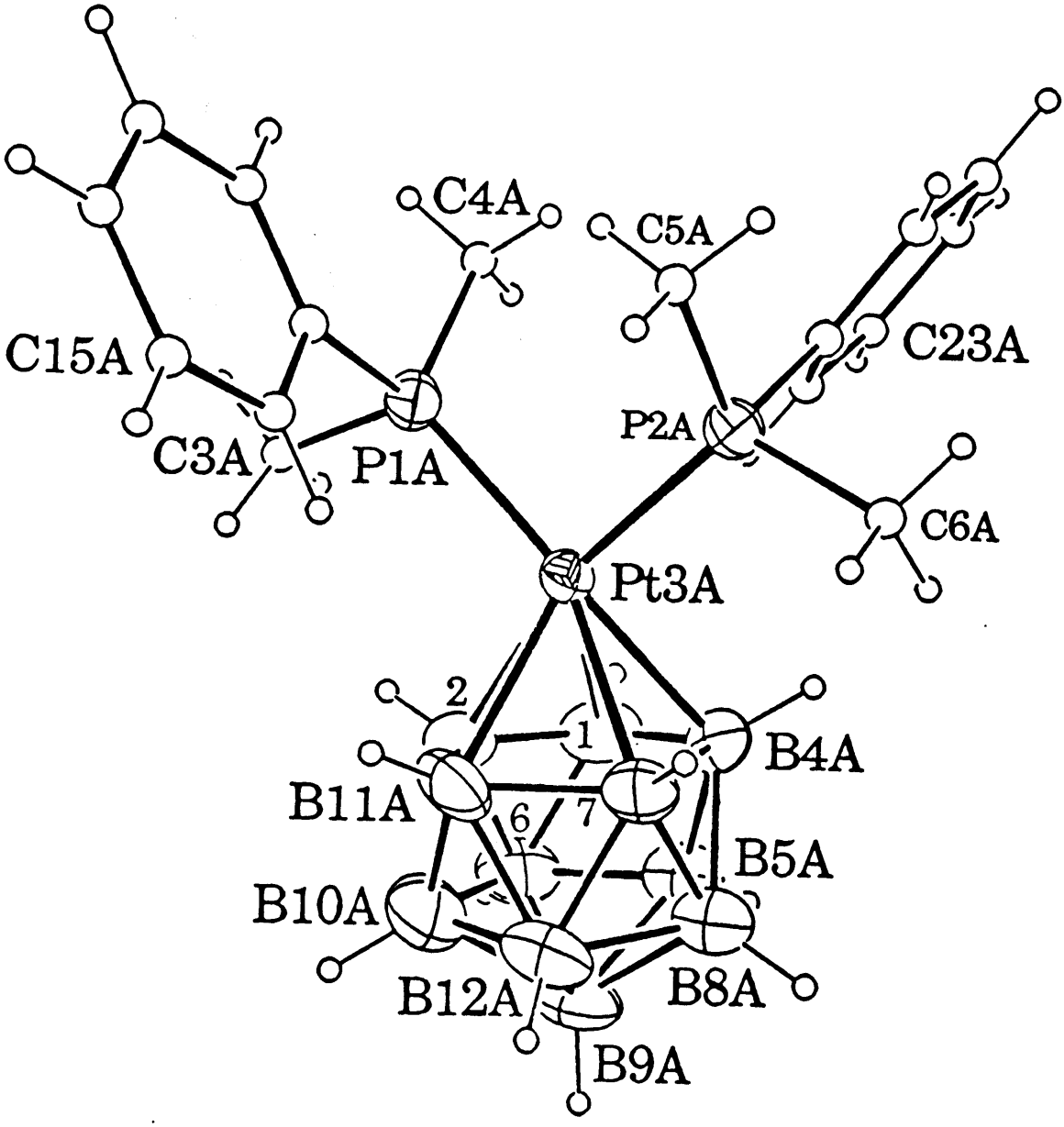

Figure 4.6 An ORTEP view of *closo*-[3,3-$(PMe_2Ph)_2$-3,1,2-$PtC_2B_9H_{11}$] (157) molecule A, with atom numbering scheme.

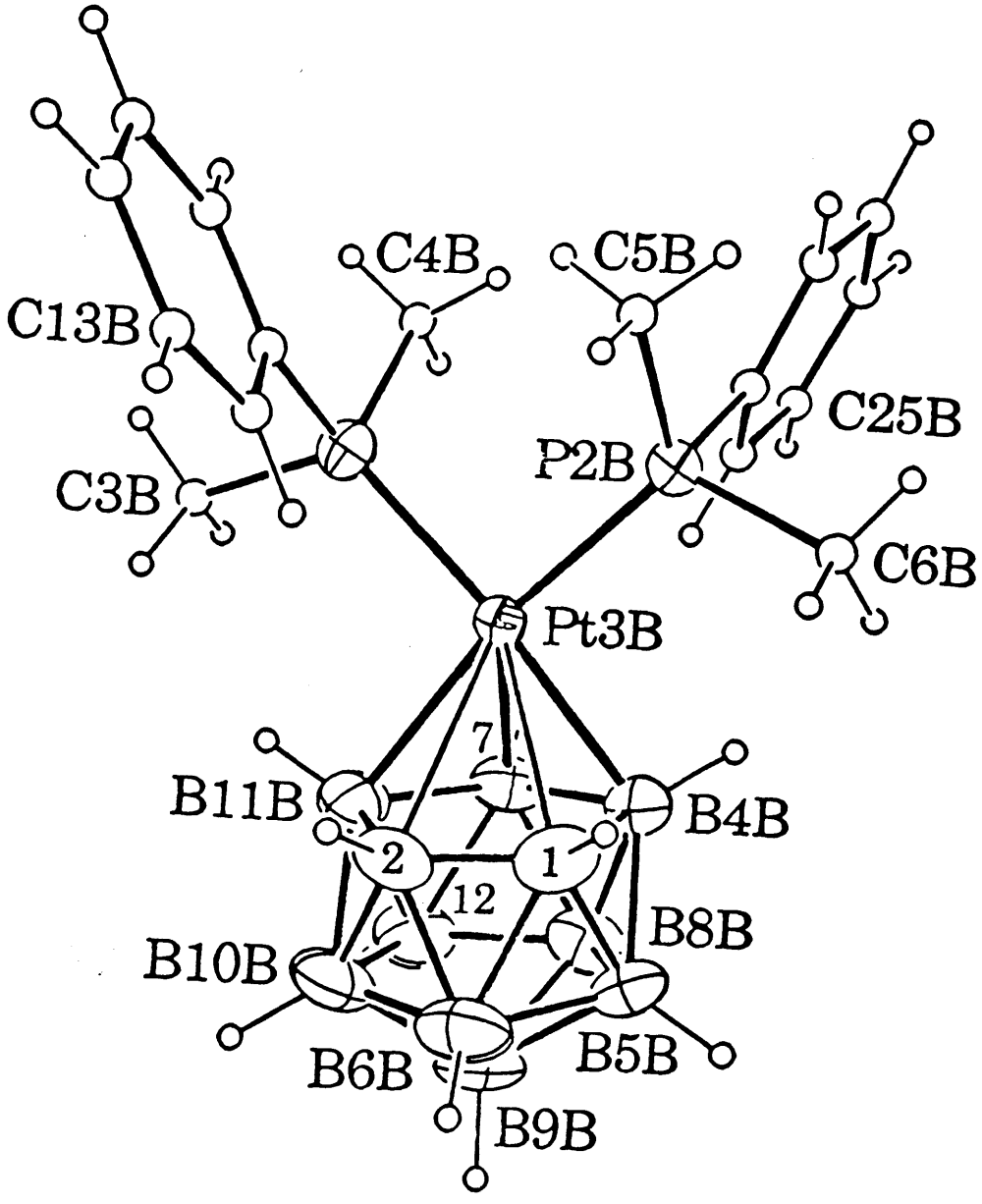

Figure 4.7 An ORTEP view of *closo*-[3,3-$(PMe_2Ph)_2$-3,1,2-$PtC_2B_9H_{11}$] (157) molecule B, with atom numbering scheme.

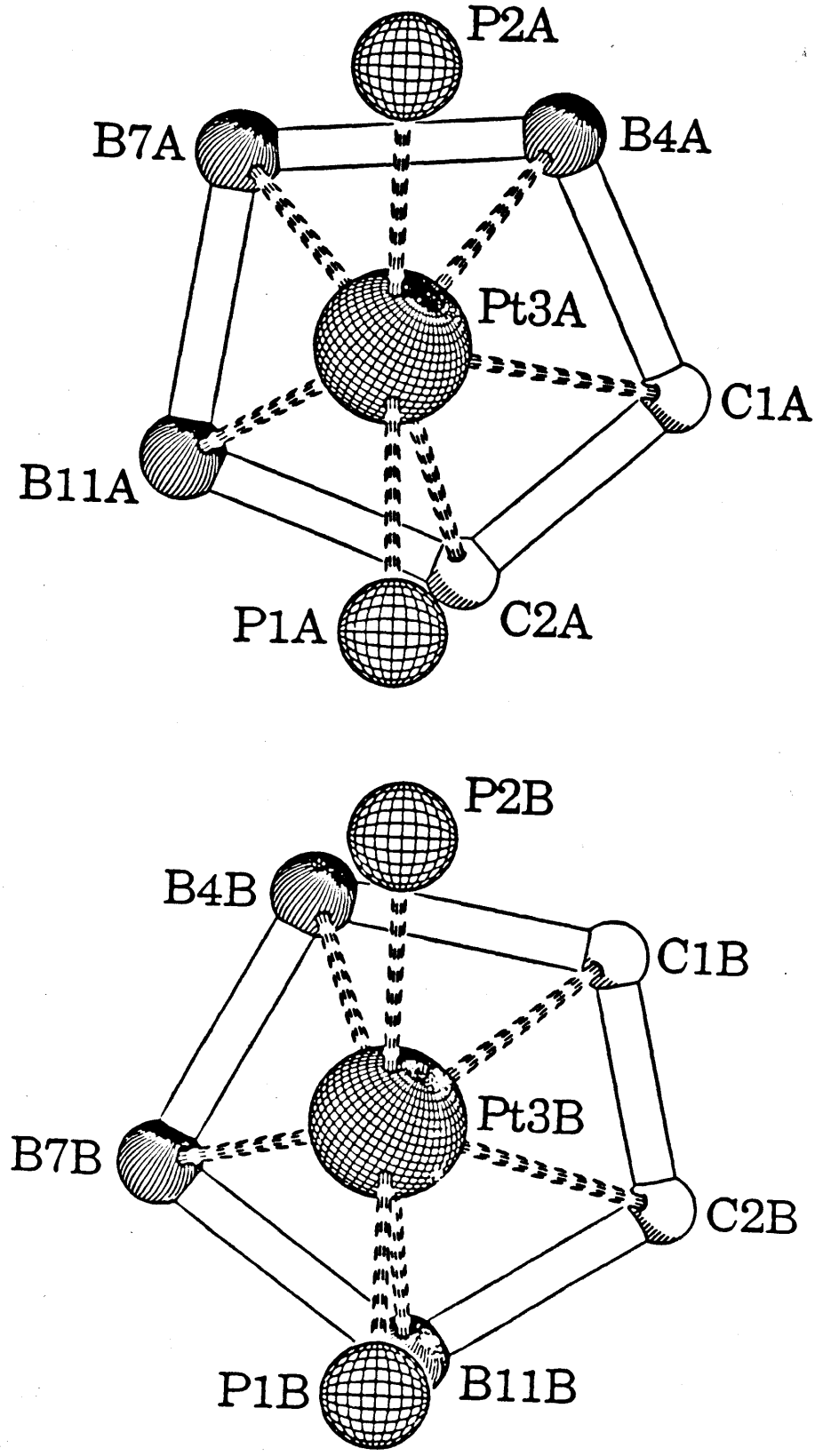

Figure 4.8 A view of the orientation of the $Pt(PMe_2Ph)_2$ unit above the C_2B_3 face of *closo*-[3,3-$(PMe_2Ph)_2$-3,1,2-$PtC_2B_9H_{11}$] (157) for both molecules A and B.

Table 4.5 Important bond distances (Å) for *closo*-[3,3-$(PMe_2Ph)_2$-3,1,2-$PtC_2B_9H_{11}$] (157).

Pt(3A)-P(1A)	2.2875(16)	Pt(3B)-P(1B)	2.2599(16)
Pt(3A)-P(2A)	2.2353(16)	Pt(3B)-P(2B)	2.2705(15)
Pt(3A)-C(1A)	2.515(6)	Pt(3B)-C(1B)	2.529(6)
Pt(3A)-C(2A)	2.302(7)	Pt(3B)-C(2B)	2.574(6)
Pt(3A)-B(4A)	2.307(7)	Pt(3B)-B(4B)	2.264(7)
Pt(3A)-B(7A)	2.265(7)	Pt(3B)-B(7B)	2.260(7)
Pt(3A)-B(11A)	2.284(8)	Pt(3B)-B(11B)	2.266(7)
C(1A)-C(2A)	1.571(11)	C(1B)-C(2B)	1.496(10)
C(1A)-B(4A)	1.667(9)	C(1B)-B(4B)	1.748(10)
C(1A)-B(5A)	1.683(11)	C(1B)-B(5B)	1.662(10)
C(1A)-B(6A)	1.687(11)	C(1B)-B(6B)	1.728(11)
C(2A)-B(6A)	1.781(11)	C(2B)-B(6B)	1.688(11)
C(2A)-B(10A)	1.731(12)	C(2B)-B(10B)	1.637(11)
C(2A)-B(11A)	1.737(12)	C(2B)-B(11B)	1.712(10)
B(4A)-B(5A)	1.826(11)	B(4B)-B(5B)	1.795(10)
B(4A)-B(7A)	1.826(10)	B(4B)-B(7B)	1.783(10)
B(4A)-B(8A)	1.765(11)	B(4B)-B(8B)	1.785(10)
B(5A)-B(6A)	1.733(14)	B(5B)-B(6B)	1.773(13)
B(5A)-B(8A)	1.752(12)	B(5B)-B(8B)	1.768(11)
B(5A)-B(9A)	1.758(12)	B(5B)-B(9B)	1.790(11)
B(6A)-B(9A)	1.747(13)	B(6B)-B(9B)	1.729(13)
B(6A)-B(10A)	1.795(15)	B(6B)-B(10B)	1.716(14)
B(7A)-B(8A)	1.762(12)	B(7B)-B(8B)	1.767(11)
B(7A)-B(11A)	1.789(11)	B(7B)-B(11B)	1.804(12)
B(7A)-B(12A)	1.758(11)	B(7B)-B(12B)	1.747(11)
B(8A)-B(9A)	1.805(12)	B(8B)-B(9B)	1.769(12)
B(8A)-B(12A)	1.755(13)	B(8B)-B(12B)	1.753(13)
B(9A)-B(10A)	1.750(14)	B(9B)-B(10B)	1.748(14)
B(9A)-B(12A)	1.742(13)	B(9B)-B(12B)	1.756(11)

B(10A)-B(11A)	1.738(12)	B(10B)-B(11B)	1.781(12)
B(10A)-B(12A)	1.737(15)	B(10B)-B(12B)	1.793(15)
B(11A)-B(12A)	1.753(13)	B(11B)-B(12B)	1.809(12)

Table 4.6 Important bond angles (°) for *closo*-[3,3-$(PMe_2Ph)_2$-3,1,2-$PtC_2B_9H_{11}$] (157).

P(1A)-Pt(3A)-P(2A)	93.11(6)	P(1B)-Pt(3B)-P(2B)	92.33(6)
P(1A)-Pt(3A)-C(2A)	98.47(16)	P(1B)-Pt(3B)-C(2B)	115.21(16)
P(1A)-Pt(3A)-B(4A)	153.24(18)	P(1B)-Pt(3B)-B(4B)	164.70(19)
P(1A)-Pt(3A)-B(11A)	111.28(22)	P(1B)-Pt(3B)-B(11B)	97.21(19)
P(2A)-Pt(3A)-C(2A)	163.01(20)	P(2B)-Pt(3B)-C(2B)	130.48(16)
P(2A)-Pt(3A)-B(4A)	95.56(19)	P(2B)-Pt(3B)-B(4B)	96.50(19)
P(2A)-Pt(3A)-B(11A)	140.44(23)	P(2B)-Pt(3B)-B(11B)	169.62(19)
C(1A)-Pt(3A)-C(2A)	37.7(3)	C(1B)-Pt(3B)-C(2B)	34.09(22)
C(1A)-Pt(3A)-B(4A)	40.16(23)	C(1B)-Pt(3B)-B(4B)	42.33(24)
C(2A)-Pt(3A)-B(11A)	44.5(3)	C(2B)-Pt(3B)-B(11B)	40.8(3)
B(4A)-Pt(3A)-B(7A)	47.1(3)	B(4B)-Pt(3B)-B(7B)	46.4(3)
B(7A)-Pt(3A)-B(11A)	46.3(3)	B(7B)-Pt(3B)-B(11B)	47.0(3)
Pt(3A)-C(1A)-C(2A)	63.8(3)	Pt(3B)-C(1B)-C(2B)	74.6(3)
Pt(3A)-C(1A)-B(4A)	63.2(3)	Pt(3B)-C(1B)-B(4B)	60.7(3)
C(2A)-C(1A)-B(4A)	106.9(5)	C(2B)-C(1B)-B(4B)	112.7(5)
C(2A)-C(1A)-B(6A)	66.2(5)	C(2B)-C(1B)-B(6B)	62.7(5)
B(4A)-C(1A)-B(5A)	66.0(5)	B(4B)-C(1B)-B(5B)	63.5(4)
B(5A)-C(1A)-B(6A)	61.9(5)	B(5B)-C(1B)-B(6B)	63.0(5)
Pt(3A)-C(2A)-C(1A)	78.5(4)	Pt(3B)-C(2B)-C(1B)	71.3(3)
Pt(3A)-C(2A)-B(11A)	67.2(3)	Pt(3B)-C(2B)-B(11B)	59.9(3)
C(1A)-C(2A)-B(6A)	60.1(5)	C(1B)-C(2B)-B(6B)	65.4(5)
C(1A)-C(2A)-B(11A)	116.8(5)	C(1B)-C(2B)-B(11B)	110.2(5)
B(6A)-C(2A)-B(10A)	61.5(5)	B(6B)-C(2B)-B(10B)	62.1(5)

B(10A)-C(2A)-B(11A)	60.2(5)	B(10B)-C(2B)-B(11B)	64.2(5)
Pt(3A)-B(4A)-C(1A)	76.7(3)	Pt(3B)-B(4B)-C(1B)	77.0(3)
Pt(3A)-B(4A)-B(7A)	65.3(3)	Pt(3B)-B(4B)-B(7B)	66.7(3)
C(1A)-B(4A)-B(5A)	57.4(4)	C(1B)-B(4B)-B(5B)	55.9(4)
C(1A)-B(4A)-B(7A)	109.2(5)	C(1B)-B(4B)-B(7B)	106.7(5)
B(5A)-B(4A)-B(8A)	58.4(4)	B(5B)-B(4B)-B(8B)	59.2(4)
B(7A)-B(4A)-B(8A)	58.7(4)	B(7B)-B(4B)-B(8B)	59.4(4)
C(1A)-B(5A)-B(4A)	56.6(4)	C(1B)-B(5B)-B(4B)	60.6(4)
C(1A)-B(5A)-B(6A)	59.2(5)	C(1B)-B(5B)-B(6B)	60.3(5)
B(6A)-B(5A)-B(9A)	60.1(5)	B(6B)-B(5B)-B(9B)	58.1(5)
B(8A)-B(5A)-B(9A)	61.9(5)	B(8B)-B(5B)-B(9B)	59.6(5)
C(1A)-B(6A)-C(2A)	53.8(4)	C(1B)-B(6B)-C(2B)	51.9(4)
C(1A)-B(6A)-B(5A)	58.9(5)	C(1B)-B(6B)-B(5B)	56.7(4)
C(2A)-B(6A)-B(10A)	57.9(5)	C(2B)-B(6B)-B(10B)	57.5(5)
B(5A)-B(6A)-B(9A)	60.7(5)	B(5B)-B(6B)-B(9B)	61.5(5)
B(9A)-B(6A)-B(10A)	59.2(5)	B(9B)-B(6B)-B(10B)	61.0(6)
Pt(3A)-B(7A)-B(4A)	67.7(3)	Pt(3B)-B(7B)-B(4B)	66.9(3)
Pt(3A)-B(7A)-B(11A)	67.4(4)	Pt(3B)-B(7B)-B(11B)	66.7(3)
B(4A)-B(7A)-B(8A)	58.9(4)	B(4B)-B(7B)-B(8B)	60.4(4)
B(4A)-B(7A)-B(11A)	104.0(5)	B(4B)-B(7B)-B(11B)	100.7(5)
B(8A)-B(7A)-B(12A)	59.8(5)	B(8B)-B(7B)-B(12B)	59.8(5)
B(11A)-B(7A)-B(12A)	59.2(5)	B(11B)-B(7B)-B(12B)	61.2(5)
B(4A)-B(8A)-B(5A)	62.6(4)	B(4B)-B(8B)-B(5B)	60.7(4)
B(4A)-B(8A)-B(7A)	62.4(4)	B(4B)-B(8B)-B(7B)	60.2(4)
B(5A)-B(8A)-B(9A)	59.2(5)	B(5B)-B(8B)-B(9B)	60.8(5)
B(7A)-B(8A)-B(12A)	60.0(5)	B(7B)-B(8B)-B(12B)	59.5(5)
B(9A)-B(8A)-B(12A)	58.6(5)	B(9B)-B(8B)-B(12B)	59.8(5)
B(5A)-B(9A)-B(6A)	59.2(5)	B(5B)-B(9B)-B(6B)	60.5(5)
B(5A)-B(9A)-B(8A)	58.9(5)	B(5B)-B(9B)-B(8B)	59.6(4)
B(6A)-B(9A)-B(10A)	61.8(6)	B(6B)-B(9B)-B(10B)	59.1(6)
B(8A)-B(9A)-B(12A)	59.3(5)	B(8B)-B(9B)-B(12B)	59.7(5)
B(10A)-B(9A)-B(12A)	59.7(6)	B(10B)-B(9B)-B(12B)	61.6(6)

C(2A)-B(10A)-B(6A)	60.6(5)	C(2B)-B(10B)-B(6B)	60.4(5)
C(2A)-B(10A)-B(11A)	60.1(5)	C(2B)-B(10B)-B(11B)	59.9(4)
B(6A)-B(10A)-B(9A)	59.0(5)	B(6B)-B(10B)-B(9B)	59.9(5)
B(9A)-B(10A)-B(12A)	59.9(6)	B(9B)-B(10B)-B(12B)	59.5(5)
B(11A)-B(10A)-B(12A)	60.6(5)	B(11B)-B(10B)-B(12B)	60.8(5)
Pt(3A)-B(11A)-C(2A)	68.3(3)	Pt(3B)-B(11B)-C(2B)	79.3(3)
Pt(3A)-B(11A)-B(7A)	66.3(3)	Pt(3B)-B(11B)-B(7B)	66.3(3)
C(2A)-B(11A)-B(7A)	102.3(5)	C(2B)-B(11B)-B(7B)	108.8(5)
C(2A)-B(11A)-B(10A)	59.7(5)	C(2B)-B(11B)-B(10B)	55.9(4)
B(7A)-B(11A)-B(12A)	59.5(5)	B(7B)-B(11B)-B(12B)	57.9(5)
B(10A)-B(11A)-B(12A)	59.7(5)	B(10B)-B(11B)-B(12B)	59.9(5)
B(7A)-B(12A)-B(8A)	60.2(5)	B(7B)-B(12B)-B(8B)	60.6(5)
B(7A)-B(12A)-B(11A)	61.3(5)	B(7B)-B(12B)-B(11B)	60.9(5)
B(8A)-B(12A)-B(9A)	62.2(5)	B(8B)-B(12B)-B(9B)	60.5(5)
B(9A)-B(12A)-B(10A)	60.4(6)	B(9B)-B(12B)-B(10B)	59.0(5)
B(10A)-B(12A)-B(11A)	59.7(5)	B(10B)-B(12B)-B(11B)	59.3(5)

Reported Pt-P bond distances in 12 atom *closo* platinacarboranes range from 2.249(2) Å in [1,1-$(PMe_2Ph)_2$-2,4-Me_2-1,2,4-$PtC_2B_9H_9$] (167)[163] to 2.3035(9) Å in [8-Ph-2,2-$(PMe_2Ph)_2$-2,1,8-$PtC_2B_9H_{10}$] (168),[129,147] Table 4.7. The Pt-P distance of 2.2353(16) Å in molecule A of (157) is the shortest Pt-P distance reported for a 12 atom *closo* carborane, Table 4.7. There are significant differences in the Pt-P distances in molecule A (0.0522 Å) and molecule B (0.0106 Å). In both molecules the Pt-P vector which is "*trans*" to a PtCB face is longer than the Pt-P vector "*trans*" to a PtB_2 face, but this is not unusual since in the majority of compounds containing the PtP_2 unit the platinum-phosphorus bonds are not equal.[164]

In molecule A the Pt-B distances vary from 2.265(7)-2.307(7) Å and in molecule B the Pt-B bond distances are within the range 2.260(7)-2.266(7) Å. While the Pt-B(7) and Pt-B(11) distances are similar in molecules A and B the Pt-B(4) distances differ significantly being 2.307(7) and 2.264(7) Å respectively. All the Pt-B values for both molecules A and B can be considered typical for Pt-B interactions and fall within the wide range reported for numerous platinaboranes,[103] and are similar to

Table 4.7 Bond distances for a selection of 12 atom *closo* platinacarboranes.

No.	Compound structure	Pt-C/Å	Pt-P/Å	Pt-B/Å
157	[3,3-$(PMe_2Ph)_2$-3,1,2-$PtC_2B_9H_{11}$]	(A) 2.515(6), 2.302(7) --- (B) 2.529(6), 2.574(6)	2.2353(16), 2.2875(16) --- 2.2599(16), 2.2705(15)	2.265(7)-2.307(7) --- 2.260(7)-2.266(7)
158	[2,2-$(PMe_2Ph)_2$-2,1,8-$PtC_2B_9H_{11}$]	2.570(3)	2.2891(6), 2.2972(6)	2.215(3)-2.2273(3)
164	[1-Ph-3,3-$(PMe_2Ph)_2$-3,1,2-$PtC_2B_9H_{10}$][147]	2.596(10), 2.326(10)	2.288(3), 2.250(3)	2.239(12)-2.313(12)
165	[1-Ph-3,3-$(PMe_2Ph)_2$-3,1,11-$PtC_2B_9H_{10}$][129,147]	2.622(8)	2.296(2), 2.299(2)	2.211(9)-2.275(8)
166	[3,3-$(Et_3P)_2$-3,1,2-$PtC_2B_9H_{11}$][162]	2.530(7), 2.613(7)	2.2750(18), 2.2843(18)	2.264(8)-2.283(8)
167	[1,1-$(PMe_2Ph)_2$-2,4-Me_2-1,2,4-$PtC_2B_9H_9$][163]	2.452(8), 2.442(7)	2.249(2), 2.303(2)	2.255(9)-2.270(9)
168	[8-Ph-2,2-$(PMe_2Ph)_2$-2,1,8-$PtC_2B_9H_{10}$][129,147]	2.581[a]	2.290(1), 2.3035(9)	2.211(4)-2.281(4)
169	[3,3-$(PMe_2Ph)_2$-1,11-Ph_2-3,1,11-$PtC_2B_9H_9$][147]	2.610(5)	2.2864(14), 2.2909(14)	2.219(6)-2.293(6)
171	[3-(dppe)-3,1,2-$PtC_2B_9H_{11}$][166] dppe=[1,2-bis(diphenylphosphino)ethane]	2.502(3), 2.505(3)	2.266(3), 2.259(3)	2.251(3)-2.279(3)

[a]No standard deviation given

Table 4.8 Bond distances for a selection of 12 atom *closo* platinacarboranes

No.	Compound structure	B-B/Å	B-C/Å	C-C/Å
157	[3,3-$(PMe_2Ph)_2$-3,1,2-$PtC_2B_9H_{11}$]	(A) 1.733(14)-1.826(11) --- (B) 1.716(14)-1.809(12)	1.667(9)-1.781(11) --- 1.637(11)-1.748(10)	1.571(11) --- 1.496(10)
158	[2,2-$(PMe_2Ph)_2$-2,1,8-$PtC_2B_9H_{11}$]	1.726(5)-1.881(5)	1.644(4)-1.746(4)	[a]
164	[1-Ph-3,3-$(PMe_2Ph)_2$-3,1,2-$PtC_2B_9H_{10}$][147]	[b]	[b]	1.594(14)
165	[1-Ph-3,3-$(PMe_2Ph)_2$-3,1,11-$PtC_2B_9H_{10}$][129,147]	1.76(1)-1.88(1)	1.67(1)-1.74(1)	[a]
166	[3,3-$(Et_3P)_2$-3,1,2-$PtC_2B_9H_{11}$][162]	1.751(11)-1.826(12)	1.659(11)-1.757(11)	1.529(10)
167	[1,1-$(PMe_2Ph)_2$-2,4-Me_2-1,2,4-$PtC_2B_9H_9$][163]	1.72(2)-1.89(1)	1.64(1)-1.71(1)	[a]
168	[8-Ph-2,2-$(PMe_2Ph)_2$-2,1,8-$PtC_2B_9H_{10}$][129,147]	1.742(6)-1.878(6)	1.645(6)-1.755(5)	[a]
169	[3,3-$(PMe_2Ph)_2$-1,11-Ph_2-3,1,11-$PtC_2B_9H_9$][147]	[b]	[b]	[b]
171	[3-(dppe)-3,1,2-$PtC_2B_9H_{11}$][166] dppe=[1,2-bis(diphenylphosphino)ethane]	1.74(3)-1.85(3)	1.63(3)-1.79(3)	1.53(3)

[a] Not applicable, [b] Data not available

other 12 atom *closo* carborane Pt-B distances which range from 2.211(4) Å in [8-Ph-2,2-$(PMe_2Ph)_2$-2,1,8-$PtC_2B_9H_{10}$] (168) to 2.293(6) Å in [3,3-$(PMe_2Ph)_2$-1,11-Ph_2-3,1,11-$PtC_2B_9H_9$] (169), Table 4.7.[147]

The B-B distances for molecule A range from 1.733(14)-1.826(11) Å and from 1.716(14)-1.809(12) Å for molecule B which are not unusually large for metallaheteroboranes, Table 4.8, *e.g.* the B-B distances in [8-Ph-2,2-$(PMe_2Ph)_2$-2,1,8-$PtC_2B_9H_{10}$] (168) range from 1.742(6)-1.878(6) Å.

The C-C bond distances of 1.571(11) and 1.496(10) Å for molecules A and B respectively are similar to the distance of 1.542(3) Å in the carborane anion [7,8-$C_2B_9H_{11}$]$^-$ (170),[13] and the other platinacarborane compounds in Table 4.8, which have been reported to range from 1.529(10) Å in [3,3-$(Et_3P)_2$-3,1,2-$PtC_2B_9H_{11}$] (166) to 1.594(14) Å in [1-Ph-3,3-$(PMe_2Ph)_2$-3,1,2-$PtC_2B_9H_{10}$] (164). In molecule B the C-C distance of 1.496(10) Å is shorter than an sp^3-sp^3 single bond that is commonly held to be ≈ 1.54 Å.[165]

The C-B bond distances range from 1.667(9)-1.781(11) Å in molecule A and from 1.637(11)-1.748(10) Å in molecule B. These bond distances are similar to those in [3-(dppe)-3-Pt-1,2-$C_2B_9H_{11}$] (171) {dppe = 1,2-bis(diphenylphosphino)ethane} which range from 1.63(3)-1.79(3) Å.[166]

4.1.4.2 Crystal and Molecular Structure of *closo*-[2,2-$(PMe_2Ph)_2$-2,1,8-$PtC_2B_9H_{11}$] (158)

For complete structural characterisation of the platinacarborane (158), it was decided to undertake a single crystal X-ray analysis of the compound. Crystals suitable for study were grown by slow diffusion of a layer of hexane into a CH_2Cl_2 solution of the platinacarborane. The collection of the data and the structure solution were carried out by Professor George Ferguson and Dr. John Gallagher, University of Guelph, Canada, as stated in the experimental section 4.3.1. Crystal data and relevant structure solution data are given in experimental section 4.3.6.

The analysis showed that compound (158) had a *closo* twelve vertex PtC_2B_9 geometry based on a distorted dodecahedron with platinum and one of the carbon

atoms adjacent to one another, Figure 4.9. It should be noted that because the X-ray data was of such good quality (R=0.018, R_w=0.023) the boron and carbon atoms could be easily distinguished within the cage and therefore the structure was solved unambiguously as the 2,1,8 isomer. Unlike *closo*-[3,3-$(PMe_2Ph)_2$-3,1,2-$PtC_2B_9H_{11}$] (157) there was only one molecule in the unit cell. The structure is an isomer of (157) in which a carbon and a boron atom are interchanged. Possible mechanisms of this interchange will be discussed in section 4.1.5. Important bond distances and angles are given in Table 4.9 and 4.10 respectively. Tables 4.7 and 4.8 in the previous section 4.1.4.1 contain a selection of 12 atom *closo* platinacarboranes and should be consulted in conjunction with the following discussion. It is noteworthy that the value of $\Delta G^{\ddagger}$ was found to be 57.8$\pm$1.2 kJ mol^{-1} which is greater than the crystal packing forces of $\approx$30 kJ mol^{-1} hence only the most stable conformer *i.e.* Figure 4.10 would be expected to be present from a frontier mo analysis as discussed in chapter 2.[162,167,168]

The Pt-C bond distance of 2.570(3) Å in (158) is similar to 2.581(4) Å in [8-Ph-2,2-$(PMe_2Ph)_2$-2,1,8-$PtC_2B_9H_{10}$] (159) and is at the higher end of the range {2.302(7)-2.622(8) Å} of Pt-C bond distances, Table 4.7.[129]

The Pt-P distances of 2.2891(6) and 2.2972(6) Å are significantly different but are similar to the Pt-P distances of 2.2864(14) and 2.2909(14) Å in [3,3-$(PMe_2Ph)_2$-1,11-Ph_2-3,1,11-$PtC_2B_9H_9$] (169), Table 4.7.[147]

The Pt-B distances of 2.215(3), 2.223(3), 2.233(3) and 2.273(3) Å for boron atoms (7), (11), (3) and (6) respectively are very similar to the corresponding distances in [8-Ph-2,2-$(PMe_2Ph)_2$-2,1,8-$PtC_2B_9H_{10}$] (159) of 2.211(9), 2.212(7), 2.237(8) and 2.275(8) Å, Table 4.7.[129]

The B-B bond distances range from 1.726(5)-1.881(5) Å which is quite usual for metallaheteroboranes, Table 4.8.[108]

The C-B bond distances are in the range 1.644(4)-1.746(4) Å which are very similar to those in [8-Ph-2,2-$(PMe_2Ph)_2$-2,1,8-$PtC_2B_9H_{10}$] (168) which range from 1.645(6)-1.755(5) Å, Table 4.8.[147]

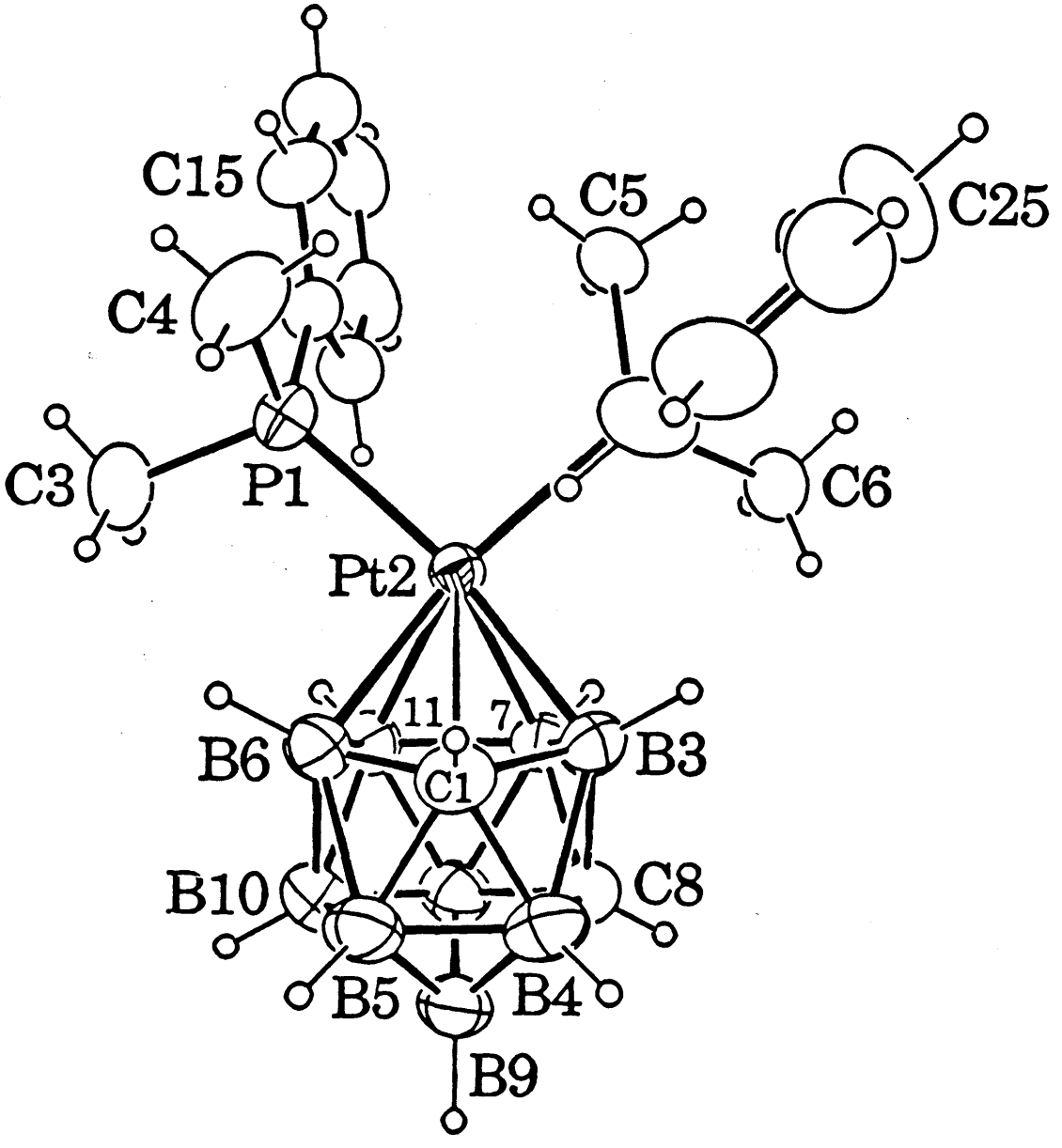

Figure 4.9 An ORTEP view of *closo*-[2,2-$(PMe_2Ph)_2$-2,1,8-$PtC_2B_9H_{11}$] (158) with atom numbering scheme.

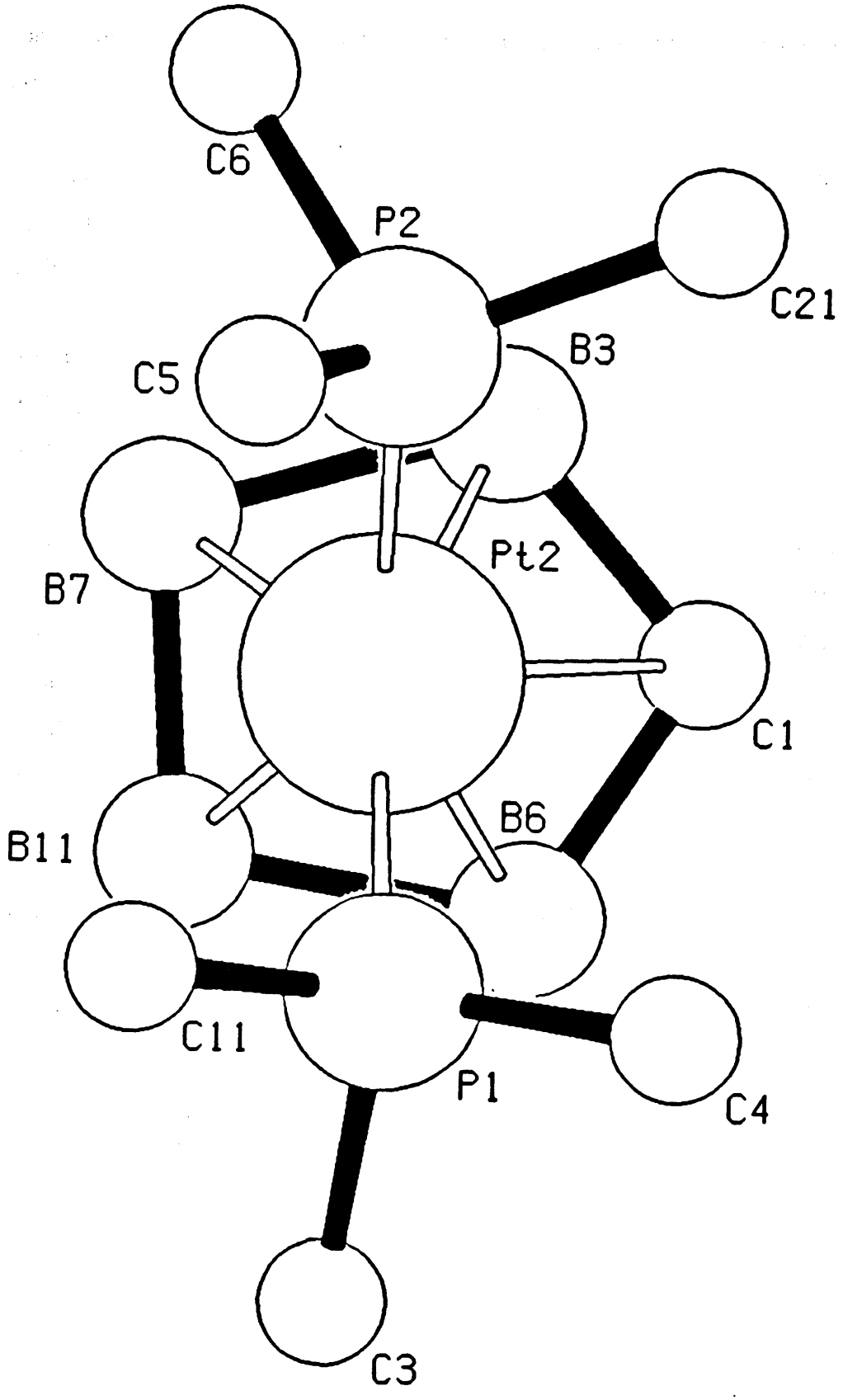

Figure 4.10 A view of the orientation of the $Pt(PMe_2Ph)_2$ unit above the C_2B_3 face of *closo*-[2,2-$(PMe_2Ph)_2$-2,1,8-$PtC_2B_9H_{11}$] (158).

Table 4.9 Important bond distances (Å) for *closo*-[2,2-$(PMe_2Ph)_2$-2,1,8-$PtC_2B_9H_{11}$] (158).

Pt(2)-P(1)	2.2891(6)	Pt(2)-P(2)	2.2972(6)
Pt(2)-C(1)	2.570(3)	Pt(2)-B(3)	2.233(3)
Pt(2)-B(6)	2.273(3)	Pt(2)-B(7)	2.215(3)
Pt(2)-B(11)	2.223(3)	P(1)-C(3)	1.817(3)
P(1)-C(4)	1.807(3)	P(1)-C(11)	1.819(3)
P(2)-C(5)	1.821(3)	P(2)-C(6)	1.814(3)
P(2)-C(21)	1.822(2)	C(1)-B(3)	1.674(4)
C(1)-B(4)	1.644(4)	C(1)-B(5)	1.662(4)
C(1)-B(6)	1.678(5)	B(3)-B(4)	1.840(4)
B(3)-B(7)	1.873(4)	B(3)-C(8)	1.746(4)
B(4)-B(5)	1.726(5)	B(4)-C(8)	1.722(4)
B(4)-B(9)	1.755(5)	B(5)-B(6)	1.820(5)
B(5)-B(9)	1.749(5)	B(5)-B(10)	1.770(6)
B(6)-B(10)	1.781(5)	B(6)-B(11)	1.881(5)
B(7)-C(8)	1.707(4)	B(7)-B(11)	1.796(4)
B(7)-B(12)	1.766(4)	C(8)-B(9)	1.725(4)
C(8)-B(12)	1.702(4)	B(9)-B(10)	1.774(5)
B(9)-B(12)	1.759(5)	B(10)-B(11)	1.755(5)
B(10)-B(12)	1.749(5)	B(11)-B(12)	1.758(4)

Table 4.10 Important bond angles (°) for *closo*-[2,2-$(PMe_2Ph)_2$-2,1,8-$PtC_2B_9H_{11}$] (158).

P(1)-Pt(2)-P(2)	97.426(23)	P(1)-Pt(2)-C(1)	121.07(6)
P(1)-Pt(2)-B(3)	160.51(8)	P(1)-Pt(2)-B(6)	93.60(8)
P(1)-Pt(2)-B(7)	142.74(8)	P(1)-Pt(2)-B(11)	101.05(8)
P(2)-Pt(2)-C(1)	116.59(7)	P(2)-Pt(2)-B(3)	91.04(8)
P(2)-Pt(2)-B(6)	155.50(9)	P(2)-Pt(2)-B(7)	103.27(7)
P(2)-Pt(2)-B(11)	147.03(8)	C(1)-Pt(2)-B(3)	40.02(10)
C(1)-Pt(2)-B(6)	39.95(11)	C(1)-Pt(2)-B(7)	76.05(9)
B(3)-Pt(2)-B(7)	49.81(10)	B(6)-Pt(2)-B(11)	49.46(12)
B(7)-Pt(2)-B(11)	47.73(11)	Pt(2)-P(1)-C(3)	115.60(12)
Pt(2)-P(1)-C(4)	116.82(12)	Pt(2)-P(1)-C(11)	113.29(8)
C(3)-P(1)-C(4)	102.44(18)	C(3)-P(1)-C(11)	100.90(14)
C(4)-P(1)-C(11)	105.97(16)	Pt(2)-P(2)-C(5)	120.20(9)
Pt(2)-P(2)-C(6)	112.72(9)	Pt(2)-P(2)-C(21)	115.36(8)
C(5)-P(2)-C(6)	100.33(13)	C(5)-P(2)-C(21)	102.40(12)
C(6)-P(2)-C(21)	103.55(12)	P(2)-C(1)-B(3)	59.06(12)
Pt(2)-C(1)-B(6)	60.42(12)	B(3)-C(1)-B(4)	67.38(18)
B(3)-C(1)-B(6)	105.08(19)	B(4)-C(1)-B(5)	62.97(20)
B(5)-C(1)-B(6)	66.04(20)	Pt(2)-B(3)-C(1)	80.93(14)
Pt(2)-B(3)-B(7)	64.60(12)	C(1)-B(3)-B(4)	55.54(16)
C(1)-B(3)-B(7)	113.08(20)	B(7)-B(3)-C(8)	56.14(15)
C(1)-B(4)-B(3)	57.09(16)	C(1)-B(4)-B(5)	59.02(19)
B(3)-B(4)-C(8)	58.59(16)	B(5)-B(4)-C(8)	105.10(24)
B(5)-B(4)-B(9)	60.32(21)	C(8)-B(4)-B(9)	59.46(18)
C(1)-B(5)-B(4)	58.01(19)	C(1)-B(5)-B(6)	57.41(17)
B(4)-B(5)-B(9)	60.65(20)	B(4)-B(5)-B(10)	107.69(23)
B(6)-B(5)-B(10)	59.48(20)	B(9)-B(5)-B(10)	60.52(21)
Pt(2)-B(6)-C(1)	79.62(15)	Pt(2)-B(6)-B(11)	63.90(12)
C(1)-B(6)-B(5)	56.54(19)	C(1)-B(6)-B(11)	112.57(20)
B(5)-B(6)-B(10)	58.86(20)	B(10)-B(6)-B(11)	57.19(18)

Pt(2)-B(7)-B(3)	65.59(12)	Pt(2)-B(7)-B(11)	66.38(13)
B(3)-B(7)-C(8)	58.17(15)	B(3)-B(7)-B(11)	103.21(19)
C(8)-B(7)-B(12)	58.69(17)	B(11)-B(7)-B(12)	59.14(17)
B(3)-C(8)-B(4)	64.09(17)	B(3)-C(8)-B(7)	65.69(16)
B(4)-C(8)-B(9)	61.22(19)	B(4)-C(8)-B(12)	113.68(22)
B(7)-C(8)-B(12)	62.39(17)	B(9)-C(8)-B(12)	61.75(19)
B(4)-B(9)-B(5)	59.03(21)	B(4)-B(9)-C(8)	59.32(18)
B(5)-B(9)-B(10)	60.31(21)	C(8)-B(9)-B(12)	58.50(18)
B(10)-B(9)-B(12)	59.36(20)	B(5)-B(10)-B(6)	61.66(19)
B(5)-B(10)-B(9)	59.16(20)	B(5)-B(10)-B(12)	108.98(24)
B(6)-B(10)-B(11)	64.27(18)	B(9)-B(10)-B(12)	59.90(20)
B(11)-B(10)-B(12)	60.21(19)	Pt(2)-B(11)-B(6)	66.64(13)
Pt(2)-B(11)-B(7)	65.88(12)	B(6)-B(11)-B(7)	103.43(19)
B(6)-B(11)-B(10)	58.54(18)	B(7)-B(11)-B(12)	59.59(17)
B(10)-B(11)-B(12)	59.73(19)	B(7)-B(12)-C(8)	58.92(16)
B(7)-B(12)-B(11)	61.28(17)	C(8)-B(12)-B(9)	59.74(19)
C(8)-B(12)-B(10)	103.62(23)	B(9)-B(12)-B(10)	60.74(20)
B(10)-B(12)-B(11)	60.07(19)		

4.1.5 Rearrangements of Carboranes

Polyhedral isomerisation of dicarbacarboranes can be a thermodynamically favourable process. The 1,2 → 1,7 → 1,12 isomerisation of *closo*-$C_2B_{10}H_{12}$ (Figure 4.11), and its C-substituted analogues at elevated temperatures (*ca.* 470°C and 700°C respectively for the parent compounds) has been known for many years,[169] but the precise mechanism(s) by which such rearrangement processes occur continue to be the subject of speculation.[170-173] A recent study has claimed to present the first calculations of true transition states in the rearrangement pathways for $C_2B_{10}H_{12}$.[174] In the study the potential energy surfaces of $[B_{12}H_{12}]^{2-}$ and $C_2B_{10}H_{12}$ were investigated by *ab initio* calculations at the minimum basis set level, and numerous reaction pathways were characterised. In contrast to most previous discussions, but in accord with orbital symmetry considerations, all the transition states were found to have low symmetry; the three carborane isomers of icosahedral $[B_{12}H_{12}]^{2-}$ interconvert *via* a complex series of higher energy minima. The results illustrate how these systems adapt to the lack of low-energy orbital-symmetry-allowed pathways and show that the topology of the potential energy surface changes significantly from the borane to the carborane.[174]

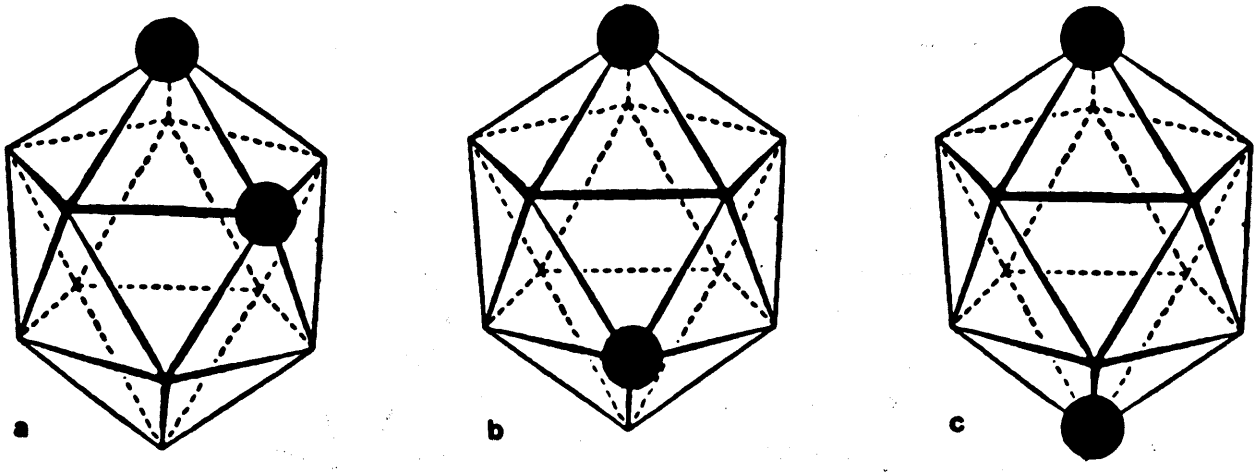

Figure 4.11 The 1,2(a) → 1,7(b) → 1,12(c) isomerisation of *closo*-$C_2B_{10}H_{12}$.[169]

Isomerisation has also been observed in metal derivatives of carboranes.[147,175,176] The formation of six isomeric cobaltacarboranes has been reported in thermal rearrangement of [3-Cp-1,2-Me_2-3,1,2-$CoC_2B_9H_9$] (172) between

400 and 600°C.[177,178] An added complication in these reactions is the presence of C-substituents.[176] Indeed, Lewis and Welch recently claimed that severe molecular deformation in essentially icosahedral rhodacarboranes could be induced by the presence of "bulky" (phenyl) substituents on the carbon atoms, and suggested that transition metal derivatives of phenylcarboranes might undergo relatively facile rearrangement processes.[179] The present work describes the first non-substituted carbon-containing metallacarborane *closo*-[3,3-$(PMe_2Ph)_2$-3,1,2-$PtC_2B_9H_{11}$] (157) to undergo rearrangement at a relatively low temperature ($\leq 130°C$).

4.1.5.1 Cage Numbering Schemes

The cage numbering system used for *closo*-[2,2-$(PMe_2Ph)_2$-2,1,8-$PtC_2B_9H_{11}$] (158) is consistent with the numbering system favoured by IUPAC, Figure 4.12 (A).[180] The recommended numbering system for 3,1,2 MC_2B_9 compounds is illustrated in Figure 4.12(B).[180] However in a series of papers on rearrangements of MC_2B_9 isomers, the numbering system used was based on 1,2-dicarba-3-metalladodeca-boranes *i.e.* 3,1,2 MC_2B_9 isomers as in Figure 4.12 (B), but with the isomers labelled with the metal atom retained in position 3, Figure 4.13.[147,177,178]

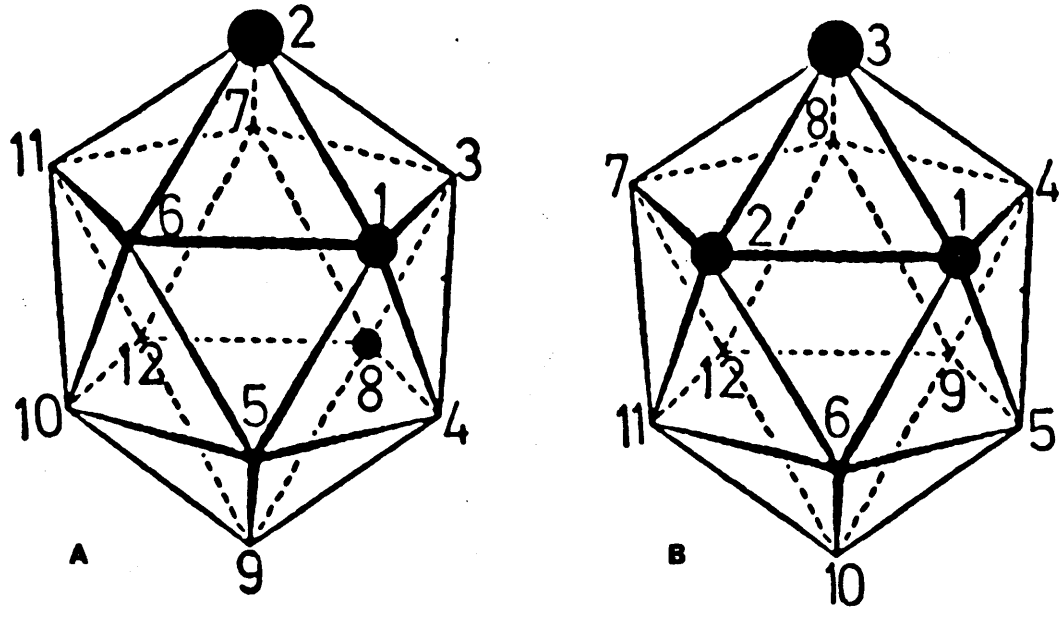

Figure 4.12 (A), Numbering system for *closo*-[2,2-$(PMe_2Ph)_2$-2,1,8-$PtC_2B_9H_{11}$] (158), (B) Numbering system for 1,2-dicarba-3-metalladodecaborane.[180]

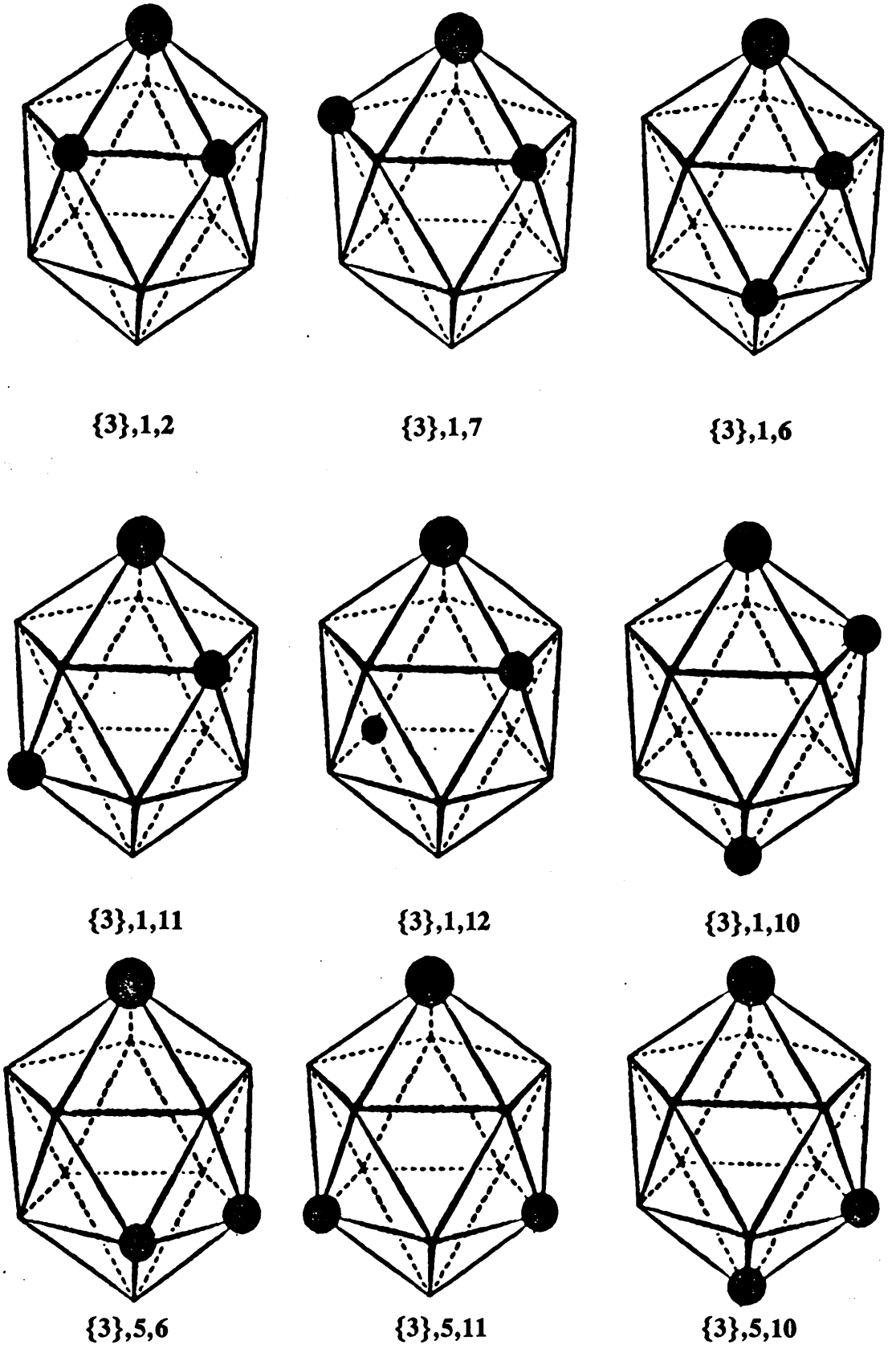

Figure 4.13 The numbering system of 9 possible isomers of MC_2B_9 based on Figure 4.12 (B), *i.e.* with M in position 3.

Since a lot of work has been published on these rearrangements using this "old" numbering system, it will be used for the remainder of this section. If one considers the MC_2B_9 cage there are 11 possible isomers of which 9 are shown in Figure 4.13. The other two isomers are the {3},1,9 and {3},1,5 which are mirror images of the {3},1,11 and {3},1,6 isomers respectively. According to the "old" numbering system the {3},1,9 isomer is equivalent to the 2,1,8 platinacarborane (158) isomer.

4.1.5.2 Rearrangement Mechanisms

Five different mechanisms have been advanced to explain the observed cage rearrangements.[181] The original and most generally accepted one is Lipscomb's diamond-square-diamond (DSD) process.[182] In this mechanism (Figure 4.14), the edge common to two triangular faces which are being rearranged breaks, and a new edge is formed perpendicular to it. Note that the transition state in this mechanism is commonly drawn to involve the breakage of six edges of the thirty originally present. DSD rearrangements, single and multiple, concerted and stepwise have been proposed to rationalise the fluxionality of boranes, carboranes and metallaboranes.[103,174]

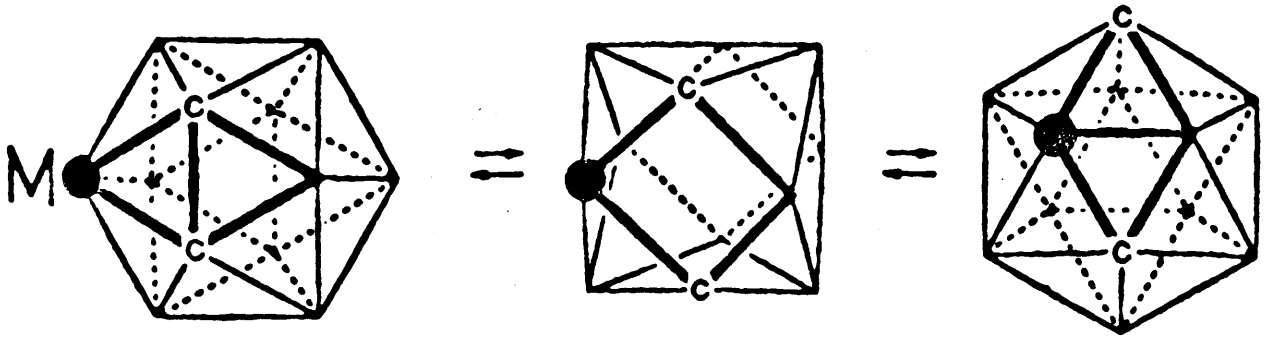

Figure 4.14 The diamond-square-diamond (DSD) process illustrating the rearrangement of the {3},1,2 to {3},1,7 isomer.[182]

Scheme 1 Using the single step DSD mechanism, the following interconversions are possible for MC_2B_9.[177]

Class	
I	1,2 ⇌ 1,6 ⇌ 5,6 ⇅ ⇅ 1,7 ⇌ 1,11 ⇌ 5,11
II	1,10 ⇌ 5,10
III	1,12

Note, according to the single DSD mechanism the 9 isomers drawn in Figure 4.13 can be grouped into three classes, scheme 1. No interclass crossing is possible between the six members of the first class, the two members of the second class, and the only member of the third. The DSD mechanism alone is inadequate in explaining the thermal rearrangement of 1,2-carborane to 1,12-carborane. Furthermore, the mechanism cannot be used to explain the results of the cobalt carborane studies of [3-Cp-1,2-Me_2-3,1,2-$CoC_2B_9H_9$] (172),[177] and no single step using the DSD mechanism can convert *closo*-[3,3-$(PMe_2Ph)_2$-3,1,2-$PtC_2B_9H_{11}$] (157) to *closo*-[2,2-$(PMe_2Ph)_2$-2,1,8-$PtC_2B_9H_{11}$] (158). This restriction applies only to the single DSD rearrangement.

A second mechanism based on a cuboctahedral intermediate but modified by the assumption that the triangular faces of this intermediate can rotate is shown in Figure 4.15. According to this mechanism, six edges are broken in forming the intermediate and a further six edges are broken in rotating the triangle. This "modified DSD" mechanism can explain the formation of 1,12-carborane from 1,7-carborane and was originally proposed by Lipscomb and co-workers to account for the composition of the isomer mixture formed in the rearrangement of boron-halogenated 1,2-carboranes.[183] However, this mechanism cannot convert (157) to (158) in a single step.

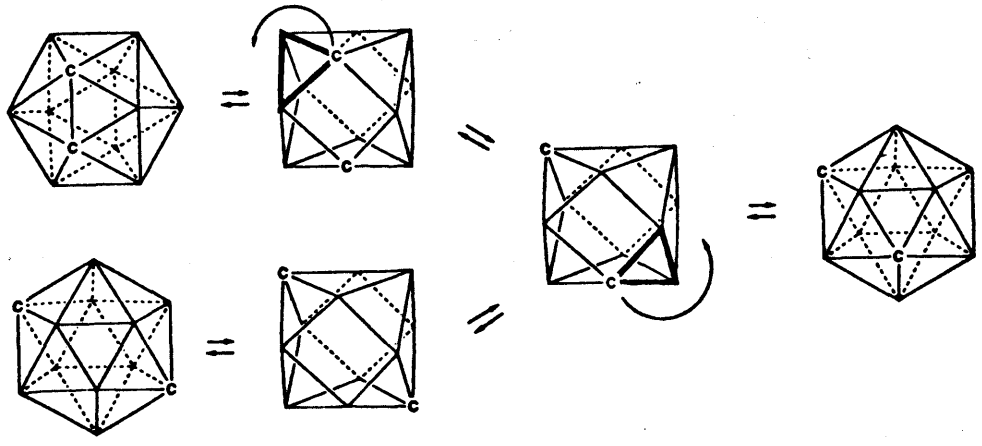

Figure 4.15 Two 120° counterclockwise rotations of the triangles (drawn with heavy lines) in the cuboctahedral intermediates, leads 1,2-carborane to 1,12-carborane, probably through 1,7-carborane as an intermediate.[183]

A third mechanism has been suggested by Grafstein and Dvorak[184] and also by Zakharkin and Kalinin.[185] This involves a pentagonal pyramidal rotation whereby two icosahedral halves rotate in opposite directions as in Figure 4.16. In performing this rotation ten edges of the icosahedron have to be broken.

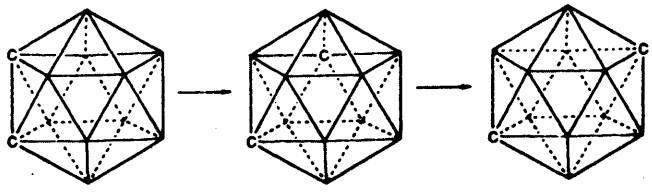

Figure 4.16 The most simple way to generate 1,7-carborane from 1,2-carborane is to rotate the upper pentagon clockwise. A second clockwise rotation gives 1,12-carborane.

This "pentagonal rotation" would allow the following interconversions of MC_2B_9, scheme 2.

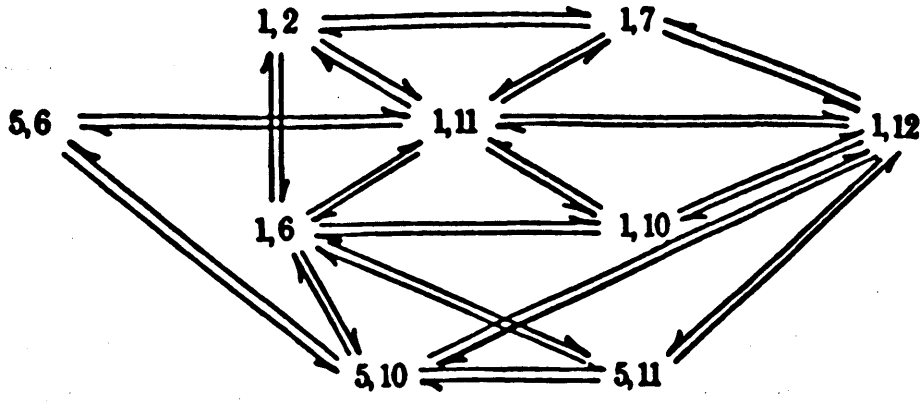

Scheme 2 Interconversions allowed by the "pentagonal rotation" mechanism.

In contrast to the DSD scheme, this scheme allows interconversions between all eleven isomers. In the present work (157) could rearrange to (158) through a two stage mechanism as shown in Figure 4.17.

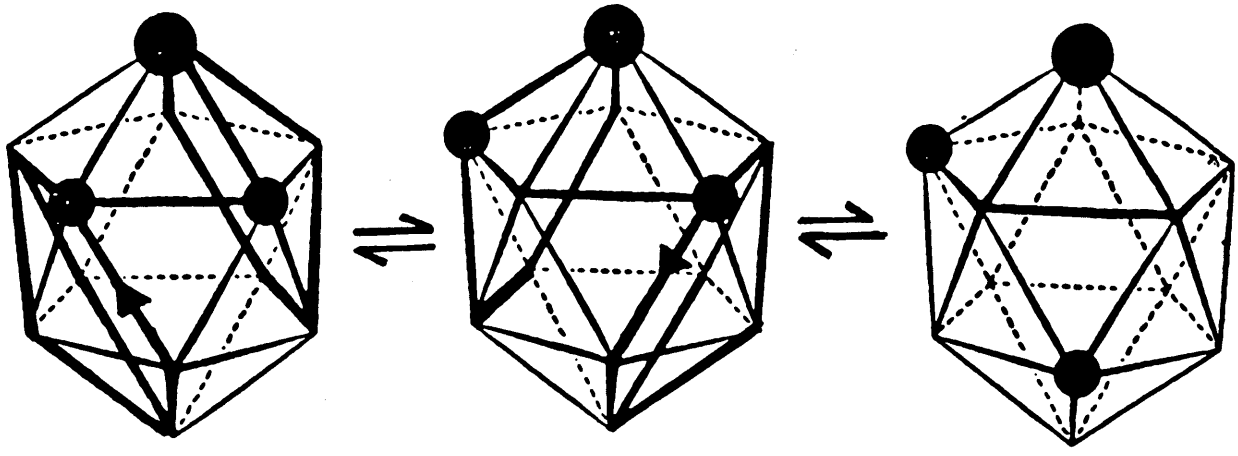

Figure 4.17 The formation of (158) from (157) through two pentagonal rotations.

The fourth mechanism involves the rotation of triangular faces in the icosahedron in which nine edges are broken as shown in Figure 4.18.

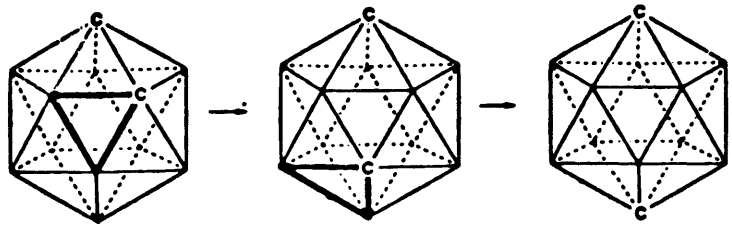

Figure 4.18 Clockwise rotation of the bold face triangle 120° gives 1,7-carborane, which can undergo a second 120° clockwise rotation to give the 1,12-carborane.

This mechanism was proposed by Zakharkin and Kalinin[185] as well as Muetterties and Knoth.[186] Gimarc *et al* in a study of isomerisation mechanisms of $C_2B_{10}H_{12}$ found support for triangular face rotation as the mechanism that can best account for the observed isomerisations of 1,2-, 1,7- and 1,12-$C_2B_{10}H_{12}$.[171] Wu and Jones, in their experiments on 1,2-carborane suggest that triangular face rotation is the major contributor in the mechanism for rearrangements.[181] The triangular face rotation mechanism is capable of providing routes for all eleven MC_2B_9 isomers, scheme 3.

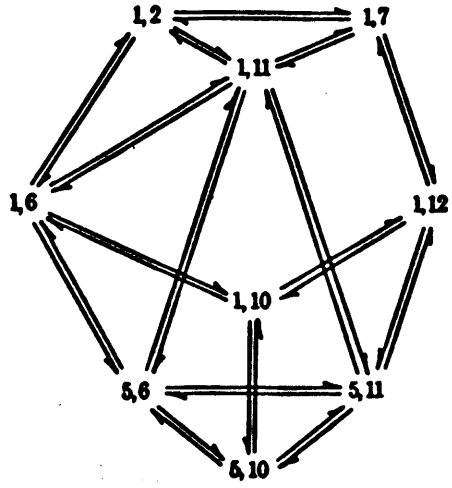

Scheme 3 Interconversions allowed by the "triangular face rotation" mechanism.

In the present work (157) could rearrange to (158) as shown in Figure 4.19.

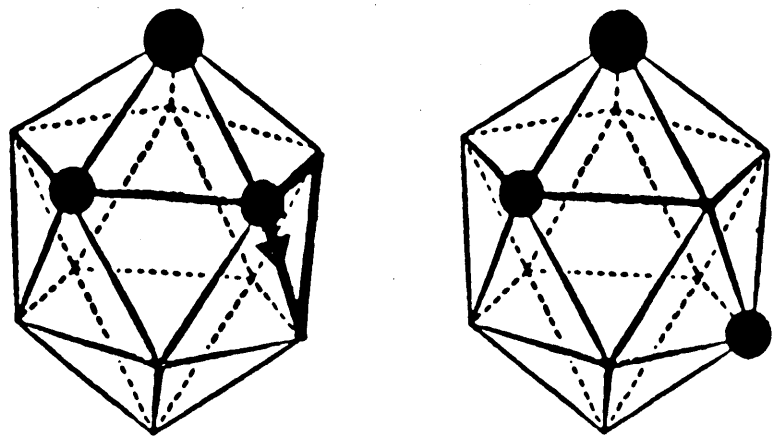

Figure 4.19 Rotation of the bold-face triangle in (157) generates (158).

The fifth mechanism for rearrangement of icosahedral molecules differs fundamentally from the others. It was proposed by Wong and Lipscomb and involves the breaking of five edges {(4,8), (4,9), (4,5), (1,3) and (1,2)} in the opening of the icosahedral *closo* cage to give a *nido* structure which is a fragment of a 13 vertex polyhedron.[81] This process breaks three edges. The closure of the polyhedron in other directions leads to the formation of different isomeric products as illustrated in Figure 4.20.

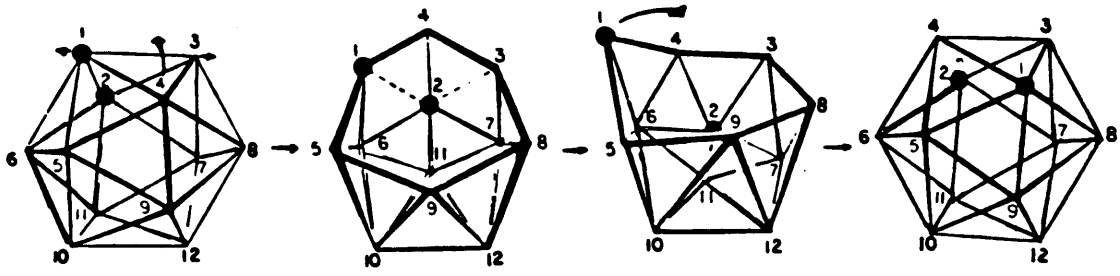

Figure 4.20 Rearrangement through the *pseudo* 13 atom *nido* intermediate.[81]

Edvenson and Gaines have studied the movement of ^{10}B labelled sites in 1,2-$C_2B_{10}H_{12}$ at 350°C and have compared the results to the movement predicted by various isomerisation mechanisms.[172] The mechanism that appears to give the closest agreement involves a 12-vertex *nido* intermediate. According to Edvenson and Gaines a number of previously considered mechanisms, including simple exchange between two boron sites, triangular face rotation in an icosahedron, diamond-square-diamond twist and rotation of pentagonal pyramids can all be considered as extensions of the *nido* (distorted) intermediate mechanism. Thus, particular aspects of each of the previous mechanisms may become the rate controlling steps in the "true" mechanism of the process *e.g.* shown in Figure 4.17.

It is not too surprising that the precise mechanism by which 1,2-carborane, or *closo*-[3-Cp-1,2-Me_2-3,1,2-$CoC_2B_9H_9$] (172), or *closo*-[3,3-$(PMe_2Ph)_2$-3,1,2-$PtC_2B_9H_{11}$] (157) may rearrange cannot be completely resolved on the basis of the present evidence. Indeed it is possible that different mechanisms may dominate

different rearrangements depending on the isomer involved. A variety of combined processes, major and minor, may also exist for any single isomerisation step.

In the case of the conversion of *closo*-[3,3-$(PMe_2Ph)_2$-3,1,2-$PtC_2B_9H_{11}$] (157) to *closo*-[2,2-$(PMe_2Ph)_2$-2,1,8-$PtC_2B_9H_{11}$] (158) it is clear that no single step DSD mechanism can convert *closo*-[3,3-$(PMe_2Ph)_2$-3,1,2-$PtC_2B_9H_{11}$] (157) to *closo*-[2,2-$(PMe_2Ph)_2$-2,1,8-$PtC_2B_9H_{11}$](158) and the "modified DSD" mechanism cannot convert (157) to (158) in a single step. However, using the pentagonal pyramidal rotation (157) could rearrange to (158) through a two stage mechanism as shown in Figure 4.17 and it is also plausible to suggest that the mechanism for the conversion of (157) to (158) could be the triangular face rotation as described in Figure 4.19. Either or both of these could be operative through a distorted *nido* intermediate of the type suggested by Edvenson and Gaines.[172]

4.2 SUMMARY AND CONCLUSION

Where previously the direct reaction between simple starting materials has been kinetically slow *eg.* in the present case six days for the reaction of *nido*-[7,8-$C_2B_9H_{12}$]$^-$ and *cis*-[$Pt(PMe_2Ph)_2Cl_2$], the microwave technique (as described in chapter 3) speeds up the process to 30 minutes. This leads not only to a considerable saving in time but also to a marked improvement in the overall reaction yield in certain reactions, Table 4.1.

In the present study isomeric products *closo*-[3,3-$(PMe_2Ph)_2$-3,1,2-$PtC_2B_9H_{11}$] (157) and *closo*-[2,2-$(PMe_2Ph)_2$-2,1,8-$PtC_2B_9H_{11}$] (158) from *nido*-[7,8-$C_2B_9H_{12}$]$^-$ and *cis*-[$Pt(PMe_2Ph)_2Cl_2$] and the rearrangement product *closo*-[8-Ph-2,2-$(PMe_2Ph)_2$-2,1,8-$PtC_2B_9H_{10}$] (159), from *nido*-[7-Ph-7,8-$C_2B_9H_{11}$]$^-$ and *cis*-[$Pt(PMe_2Ph)_2Cl_2$] were formed from reactions performed under microwave irradiation. Experiments carried out on the parent carborane starting materials (sections 4.3.10 and 4.3.11) show that these materials do not isomerise under the conditions used for the microwave syntheses. As a result it is likely that the 2,1,8 isomers are formed by isomerisation of the 3,1,2 isomers under the vigorous conditions of the microwave experiments. This was confirmed by subjecting *closo*-[3,3-$(PMe_2Ph)_2$-3,1,2-$PtC_2B_9H_{11}$] (157) in

ethanol to microwave irradiation for 10 minutes by which time it rearranged to (158) in 90% yield. Since the temperature in the ethanol solution at 10 atm did not exceeded 130°C, these rearrangements occurred at a much lower temperature than those reported for corresponding cobalt compounds [3-Cp-3,1,2-$CoC_2B_9H_{11}$], [3-Cp-1,2-Me_2-3,1,2-$CoC_2B_9H_9$] and [3-Cp-μ-1,2-$(CH_2)_3$-3,1,2-$CoC_2B_9H_9$].[177,178]

Three new platinacarboranes, *closo*-[3,3-$(PMe_2Ph)_2$-3,1,2-$PtC_2B_9H_{11}$] (157), *closo*-[2,2-$(PMe_2Ph)_2$-2,1,8-$PtC_2B_9H_{11}$] (158) and *closo*-[8-Ph-2,2-$(PMe_2Ph)_2$-2,1,8-$PtC_2B_9H_{10}$] (159), and the previously known platinaarsenaborane, *closo*-[3,3-$(PMe_2Ph)_2$-3,1,2-$PtAs_2B_9H_9$] (70) and platinatelluraborane, *closo*-[2,2-$(PMe_2Ph)_2$-2,1-$PtTeB_{10}H_{10}$] (160) were prepared by heating in ethanol *cis*-[$Pt(PMe_2Ph)_2Cl_2$] and the appropriate heteroborane anion in the presence of triethylamine by both conventional reflux and by microwave irradiation. The results are summarised in Table 4.1. Compounds (70), (157), (158), (159) and (160) were characterised by IR and NMR spectroscopy and compounds (157) and (158) were studied by X-ray diffraction methods.

IR spectra of the compounds (70), (157), (158), (159) and (160) contained characteristic bands due to B-H stretching bonds and bands due to phosphine ligands. No M-H band or B-H-B or M-H-B bridging bands were observed in any case.

An important feature of the NMR spectra of both (157) and (158) were that both compounds were fluxional. The value of $\Delta G^{\ddagger}$ for the fluxional process involving the rotation of the $Pt(PMe_2Ph)_2$ unit for (157) was found to be < 30 kJ mol^{-1}. The value of $\Delta G^{\ddagger}$ for the fluxional process involving the $Pt(PMe_2Ph)_2$ unit for (158) was found to be 57.8 ± 1.2 kJ mol^{-1}.

Single crystal X-ray analyses of (157) and (158) showed that both compounds had a *closo* twelve vertex PtC_2B_9 geometry based on a distorted dodecahedron. From the X-ray determined crystal structure of (157) (section 4.1.4.1) there were two molecules present in the unit cell which differed primarily in the platinum-carborane cage bond lengths and in the orientation of the platinum phosphine unit above the C_2B_3 faces. The small $\Delta G^{\ddagger}$ for the rotational process in (157) is of the same order of magnitude as crystal packing forces. With this low barrier any rotamer could in principle be observed in the solid state. The compound *closo*-[2,2-$(PMe_2Ph)_2$-2,1,8-$PtC_2B_9H_{11}$] (158) is only the third platina-carborane with non-directly bonded carbons

in adjacent rings to be fully characterised. Compounds (157) and (158) provide a useful insight into the mechanism of the thermal rearrangement of icosahedral metallacarboranes and a detailed discussion of possible mechanisms based on data for rearrangements of carboranes is presented.

4.3 EXPERIMENTAL

4.3.1 General Methodology

All reactions were carried out under an inert atmosphere but products were isolated and manipulated in air. All solvents were distilled and dried prior to use by standard procedures according to Perrin *et al.*[187] Thin layer chromatography (tlc) and preparative thin layer chromatography (plc) were carried out using commercially prepared Merck silica gel 60 (Art. 5553) on aluminium foil (tlc) and Merck silica gel PF_{254} on glass plates (plc) prepared in U.C.C.

Elemental analyses were performed at the Microanalytical Laboratory, University College, Cork. Infrared spectra were recorded as KBr discs in the range 4000-625 cm^{-1} on a Perkin Elmer 682 spectrometer. Relative intensities are designated as vs, very strong; s, strong; m, medium; w, weak; vw, very weak; sh, shoulder; br, broad. Most NMR spectra were recorded by Mr. D. O'Leary, University College, Cork at 6.3 Tesla using a JEOL FT GSX-270 series NMR spectrometer. Additional ^{11}B, ^{31}P and ^{1}H NMR spectra were recorded by Dr. J. D. Kennedy, University of Leeds on a BRUKER AM 400 instrument. Some ^{31}P NMR were recorded on a BRUKER AM 250 instrument at Oxford University, England by Mr. D. Baghurst. Chemical shifts (δ) are expressed in parts per million (ppm) and are relative to internal $SiMe_4$ {(^{1}H) and (^{13}C)}, H_3PO_4 (external) (^{31}P) and $BF_3.OEt_2$ (external) (^{11}B); positive values represent shifts to high frequency ("low field") of the standards.

Single crystal X-ray analyses were performed by Professor George Ferguson and Dr. John Gallagher, University of Guelph, Canada, using an Enraf-Nonius CAD-4 diffractometer. Accurate cell dimensions and crystal orientation matrices were

determined by a least squares procedure using graphite monochromatised (Mo-K_α) radiation (λ = 0.7093 Å) following a procedure described elsewhere in detail.[188] The structures were solved *via* standard heavy atom procedures and refined with full matrix least squares analysis using either the SHELX-76[189] program system or the NRCVAX[190] suite of programs, initially with isotropic and later with anisotropic thermal parameters for all non-hydrogen atoms.

All the microwave initiated reactions were performed in a modified (as described in section 3.4.1) Ariston model MW 950 TW domestic microwave oven which has a maximum power setting of 650W. The pressure measuring system was based on a Druck Ltd., PDCR 810-0799 0-35 bar pressure transducer.[117] This and the associated pressure indicator were purchased from RS components.[191]

4.3.2 General

The anions $[7,8\text{-}As_2B_9H_{10}]^-$,[5] $[7\text{-}TeB_{10}H_{11}]^-$,[35] $[7,8\text{-}C_2B_9H_{12}]^-$,[192] and $[7\text{-Ph-}7,8\text{-}C_2B_9H_{11}]^-$,[192] were prepared according to literature methods. The compounds $C_2B_{10}H_{12}$ and 1-Ph-1,2-$C_2B_{10}H_{11}$ were gifts from Dr. B. Štíbr, Academy of Sciences of the Czech Republic, Řež near Prague, The Czech Republic. *Cis*-$[Pt(PMe_2Ph)_2Cl_2]$ was prepared as described in the literature.[193] Triethylamine was used as supplied by Aldrich Chemical Company Ltd., England.

4.3.3 Reaction between *cis*-$[Pt(PMe_2Ph)_2Cl_2]$ and $Et_4N[7,8\text{-}As_2B_9H_{10}]$ (67)

Procedure 1 (Microwave Irradiation)

Samples of $Et_4N[7,8\text{-}As_2B_9H_{10}]$ (67) (0.10 g, 0.258 mmol), ethanol (20ml), triethylamine (0.26g, 2.58mmol) and *cis*-$[Pt(PMe_2Ph)_2Cl_2]$ (0.14g, 0.258mmol) were introduced into the glass microwave (as described in section 3.4.1) reaction vessel.[117] The pressure-control line was attached to the vessel which was then located in the microwave oven, Figure 3.4. A hold pressure of 10 atm with a 0.5 atm hysteresis

was set on the controller. The solution was subjected to microwave irradiation (650W) for 30 minutes.

The ethanol was removed under reduced pressure (rotatory film evaporator, 35°C). The reaction mixture was dissolved in CH_2Cl_2 and was subjected to preparative tlc using CH_2Cl_2 - hexane (3:2) eluting solvent. The single major band was extracted into CH_2Cl_2 and recrystallised from CH_2Cl_2 - hexane (3:2) as red crystals of *closo*-[3,3-$(PMe_2Ph)_2$-3,1,2-$PtAs_2B_9H_9$] (70) (0.14g, 74.6%). (Found: C, 26.3; H, 4.7. $C_{16}H_{31}As_2B_9P_2Pt$ requires C, 26.4; H, 4.3%). IR and NMR data were as stated in the literature.[22]

Procedure 2

Triethylamine (0.26g, 2.58mmol) was added to a solution of Et_4N[7,8-$As_2B_9H_{10}$] (67) (0.10g, 0.258mmol) in ethanol (10ml). The solution was stirred at room temperature for *ca.* 10 minutes. A suspension of *cis*-[$Pt(PMe_2Ph)_2Cl_2$] (0.14g, 0.258mmol) in ethanol (10ml) was added. The mixture was stirred for 18h at ambient temperature. The ethanol was removed under reduced pressure (rotatory film evaporator, 35°C) and the reaction mixture was dissolved in CH_2Cl_2 and subjected to preparative tlc {CH_2Cl_2 - hexane (3:2)}. The single major band was extracted into CH_2Cl_2 and recrystallised from CH_2Cl_2 - hexane (3:2) as red crystals of *closo*-[3,3-$(PMe_2Ph)_2$-3,1,2-$PtAs_2B_9H_9$] (70) (0.16g, 85.2%). IR and NMR data were identical to those reported in procedure 1.

4.3.4 Reaction between *cis*-[$Pt(PMe_2Ph)_2Cl_2$] and Cs[7,8-$C_2B_9H_{12}$]

Procedure 1 (Microwave Irradiation)

The reactants Cs[7,8-$C_2B_9H_{12}$] (0.10g, 0.376mmol), ethanol (20ml), triethylamine (0.38g, 3.76mmol) and *cis*-[$Pt(PMe_2Ph)_2Cl_2$] (0.204g, 0.376mmol) were introduced into the glass reaction vessel as described in section 4.3.3. The solution was subjected to microwave irradiation (650W) for 30 minutes. The dark yellow solution was filtered and the ethanol was removed under reduced pressure (rotatory

film evaporator, 35°C). The reaction mixture was dissolved in CH_2Cl_2 and was subjected to preparative tlc {CH_2Cl_2 - hexane (3:2)}, affording two major products: (a) a very pale yellow band (R_f = 0.65) and (b) a dark yellow band (R_f = 0.3).

(a) The pale yellow band was extracted into CH_2Cl_2 and recrystallised from CH_2Cl_2 - hexane (3:2) as colourless crystals of *closo*-[2,2-$(PMe_2Ph)_2$-2,1,8-$PtC_2B_9H_{11}$] (158) (0.044g, 19.4%). (Found: C, 36.2; H, 5.9. $C_{18}H_{33}B_9P_2Pt$ requires C, 35.8; H 5.5%). IR: ν_{max}(KBr) 3030(w), 2960(vw), 2900(vw), 2555(vs) (BH), 2518(vs) (BH), 2497(s,sh) (BH), 2458(s) (BH), 1476(m), 1426(s), 1410(vs), 1397(m,sh), 1318(vw), 1300(w), 1291(w), 1279(s), 1175(w), 1152(w), 1138(w), 1110(w,sh), 1099(s), 1069(s), 1040(m), 1018(s), 996(vw), 973(s), 942(vs), 900(vs), 898(vs,sh), 865(vw), 839(m), 760(m), 740(vs), 732(vs,sh), 710(s), 688(vs), 638(w) cm^{-1}. NMR data $^{11}B\{^1H\}$ ($CDCl_3$, 298K) {ordered as: δ ppm (multiplicity, intensity, $^1J(^{11}B\text{-}^1H)$)} -7.6 (s,1B, 154 ± 5 Hz), -9.4 (s,1B, 129 ± 5 Hz), -9.9 (s,1B, 129 ± 5 Hz), -12.1(s,1B, 158 ± 5 Hz), -15.7 (s,1B, 138 ± 5 Hz), -20.5 (s,1B, 167 ± 5 Hz), -21.8 (s,1B, 172 ± 5 Hz), -22.8 (s,1B, 173 ± 5 Hz), -24.2 (s,1B, 143 ± 5 Hz). ^{31}P ($CDCl_3$ 221K) {ordered as: δ ppm (multiplicity, intensity, $^1J(^{195}Pt\text{-}^{31}P)$)} -16.3 (s,1P, 3299 ± 5 Hz) -16.5 (s,1P, 3284 ± 5 Hz). $\Delta G^{\ddagger}$=57.8±1.2 kJ mol^{-1}

(b) The dark yellow band was extracted into CH_2Cl_2 and recrystallised from CH_2Cl_2 - hexane (3:2) as orange crystals of *closo*-[3,3-$(PMe_2Ph)_2$-3,1,2-$PtC_2B_9H_{11}$] (157) (0.01g, 4.4%). (Found: C, 35.9; H, 5.8. $C_{18}H_{33}B_9P_2Pt$ requires C, 35.8; H 5.5%). IR: ν_{max}(KBr) 3055(vw), 3020(w), 2930(vw,sh), 2900(m), 2835(w), 2565(s) (BH), 2530(vs,sh) (BH), 2518(vs) (BH), 2490(s,sh) (BH), 2460(m,sh) (BH), 1465(w), 1458(w), 1424(s), 1408(m), 1300(w), 1289(w), 1278(m), 1098(s), 1062(m), 1020(m), 992(w), 973(m), 940(s), 903(vs), 835(m), 745(s), 732(s), 711(m), 691(m), 680(w,sh) cm^{-1}. NMR data $^{11}B\{^1H\}$ ($CDCl_3$, 298K) {ordered as: δ ppm (multiplicity, intensity)} -20.8(s,3B), -14.5(s,2B), -9.9(s,2B), -9.2(s,1B), +5.7(s,1B). ^{31}P ($CDCl_3$) {ordered as: δ ppm (multiplicity, intensity, $^1J(^{195}Pt\text{-}^{31}P)$)} -13.1 (s,2P, 3445 ± 5 Hz) at 219K, -12.6 (s,2P, 3450 ± 5 Hz) at 183K. $\Delta G^{\ddagger} \leq$ 30 kJ mol^{-1}

Procedure 2

To a solution of $Cs[7,8\text{-}C_2B_9H_{12}]$ (0.10g, 0.376mmol) in ethanol (20ml) was added triethylamine (0.38g, 3.76mmol) and *cis*-$[Pt(PMe_2Ph)_2Cl_2]$ (0.204g, 0.376mmol). The mixture was heated at reflux for 6 days. The dark yellow solution was filtered and the ethanol was removed under reduced pressure (rotatory film evaporator, 35°C). The reaction mixture was dissolved in CH_2Cl_2 and was subjected to preparative tlc {CH_2Cl_2 - hexane (3:2)} affording two major products: (a) a very pale yellow band (R_f = 0.65) and (b) a dark yellow band (R_f = 0.3).

(a) The pale yellow band was extracted into CH_2Cl_2 and recrystallised from CH_2Cl_2 - hexane (3:2) as colourless crystals of *closo*-$[2,2\text{-}(PMe_2Ph)_2\text{-}2,1,8\text{-}PtC_2B_9H_{11}]$ (158) (0.008g, 3.5%). IR and NMR data were identical to those reported in procedure 1.

(b) The dark yellow band was extracted into CH_2Cl_2 and recrystallised from CH_2Cl_2 - hexane (3:2) as orange crystals of *closo*-$[3,3\text{-}(PMe_2Ph)_2\text{-}3,1,2\text{-}PtC_2B_9H_{11}]$ (157) (0.06g, 26.4%). IR and NMR data were identical to those reported in procedure 1.

4.3.5 X-ray analysis of *closo*-$[3,3\text{-}(PMe_2Ph)_2\text{-}3,1,2\text{-}PtC_2B_9H_{11}]$ (157)

Crystal Data: $C_{18}H_{33}B_9P_2Pt$, M = 1207.56, monoclinic, $P2_1/c$, a = 12.7387(5), b = 21.7062(12), c = 17.9793(11) Å, β = 99.105(4)°, U = 4908.8(4) Å^3, Z = 8, D_c = 1.634 g cm^{-3}, λ(Mo-K$_\alpha$) = 0.7093 Å, μ(Mo-K$_\alpha$) = 5.91 mm^{-1}, F(000) = 2352, T = 294 K, R = 0.030, R_w = 0.029 for 6762 observed reflections. There are two molecules in the asymmetric unit which differ primarily in the platinum-carborane cage bond lengths.

4.3.6 X-ray analysis of *closo*-$[2,2\text{-}(PMe_2Ph)_2\text{-}2,1,8\text{-}PtC_2B_9H_{11}]$ (158)

Crystal Data: $C_{18}H_{33}B_9P_2Pt$, M = 603.78, triclinic, $P\bar{1}$, a = 9.3892(5), b = 10.0918(5), c = 14.1517(6) Å, α = 81.045(4), β = 72.233(4), γ = 76.766(4)°, U = 1237.7(1) Å^3, Z = 2, D_c = 1.62 g cm^{-3}, λ(Mo-K$_\alpha$) = 0.7093 Å, μ(Mo-K$_\alpha$) = 5.9 mm^{-1}, F(000) = 584, T = 294 K, R = 0.018, R_w = 0.023 for 6431 observed reflections.

4.3.7 Reaction between *cis*-[$Pt(PMe_2Ph)_2Cl_2$] and Cs[7-Ph-7,8-$C_2B_9H_{11}$]

Procedure 1 (Microwave Irradiation)

The reactants Cs[7-Ph-7,8-$C_2B_9H_{11}$] (0.06g, 0.175mmol), ethanol (20ml), triethylamine (0.177g, 1.75mmol) and *cis*-[$Pt(PMe_2Ph)_2Cl_2$] (0.095g, 0.175mmol) were introduced into the glass microwave reaction vessel as described in section 4.3.3. The solution was subjected to microwave irradiation (650W) for 30 minutes. The dark yellow solution was filtered and the ethanol was removed under reduced pressure (rotatory film evaporator, 35°C). The reaction mixture was dissolved in CH_2Cl_2 and was subjected to preparative tlc {CH_2Cl_2 - hexane (3:2)} affording one major product. The product was extracted into CH_2Cl_2 and recrystallised from CH_2Cl_2 - hexane (3:2) as yellow crystals of *closo*-[8-Ph-2,2-$(PMe_2Ph)_2$-2,1,8-$PtC_2B_9H_{10}$] (159) (0.098g, 82.3%). IR and NMR data were as stated in the literature.[129]

Procedure 2

To a solution of *cis*-[$Pt(PMe_2Ph)_2Cl_2$] (0.095g, 0.175mmol) in ethanol was added Cs[7-Ph-7,8-$C_2B_9H_{11}$] (0.06g, 0.175mmol) and triethylamine (0.177g, 1.75mmol). The solution was heated at reflux for 6 days. The solution was cooled and filtered. The ethanol was removed under reduced pressure (rotatory film evaporator, 35°C). The mixture was dissolved in CH_2Cl_2 and was subjected to preparative tlc {CH_2Cl_2 - hexane (3:2)} affording one major product. The product was extracted into CH_2Cl_2 and recrystallised from CH_2Cl_2 - hexane (3:2) as yellow crystals of *closo*-[8-Ph-2,2-$(PMe_2Ph)_2$-2,1,8-$PtC_2B_9H_{10}$] (159) (0.077g, 64.7%). IR and NMR data analyses were as stated in the literature.[129]

4.3.8 Reaction between *cis*-[$Pt(PMe_2Ph)_2Cl_2$] and $Cs[7,8\text{-}TeB_{10}H_{11}]$

Procedure 1

A sample of $Cs[7\text{-}TeB_{10}H_{11}]$ (0.127g, 0.34mmol), ethanol (20ml), triethylamine (0.474g, 3.4mmol) and *cis*-[$Pt(PMe_2Ph)_2Cl_2$] (0.182g, 0.34mmol) were introduced into the glass microwave reaction vessel as described in section 4.3.3. The solution was subjected to microwave irradiation (650W) for 30 minutes. The ethanol was removed under reduced pressure (rotatory film evaporator, 35°C). The reaction mixture was dissolved in CH_2Cl_2 and was subjected to preparative tlc {CH_2Cl_2 - hexane (3:2)} affording one major product. The product was extracted into CH_2Cl_2 and recrystallised from CH_2Cl_2 - hexane (3:2) as red crystals of *closo*-[2,2-$(PMe_2Ph)_2$-2,1-$PtTeB_{10}H_{10}$] (160) (0.207g, 84.9%). IR and NMR data were as stated in the literature.[4]

Procedure 2

To a solution of *cis*-[$Pt(PMe_2Ph)_2Cl_2$] (0.182g, 0.34mmol) in ethanol was added $Cs[7\text{-}TeB_{10}H_{11}]$ (0.127g, 0.34mmol) and triethylamine (0.474g, 3.4mmol). The solution was stirred for 18h at ambient temperature. The ethanol was removed under reduced pressure (rotatory film evaporator, 35°C). The mixture was dissolved in CH_2Cl_2 and subjected to preparative tlc {CH_2Cl_2 - hexane (3:2)}. The single major band was extracted into CH_2Cl_2 and recrystallised from CH_2Cl_2 - hexane (3:2) as red crystals of *closo*-[2,2-$(PMe_2Ph)_2$-2,1-$PtTeB_{10}H_{10}$] (160) (0.083g, 34.0%). IR and NMR data were as stated in the literature.[4]

4.3.9 Microwave Irradiation of $[7,8\text{-}C_2B_9H_{12}]^-$

The compound $Cs[7,8\text{-}C_2B_9H_{12}]$ (0.10g, 0.376mmol), ethanol (20ml) and triethylamine (0.38g, 3.76mmol) were introduced into the glass microwave reaction vessel as described in section 4.3.3. The solution was subjected to microwave

irradiation (650W) for 30 minutes. The ethanol and triethylamine was removed under reduced pressure (rotatory film evaporator, 35°C). No rearrangement reaction occurred with $Cs[7,8\text{-}C_2B_9H_{12}]$. IR and NMR data were as stated in the literature for $[7,8\text{-}C_2B_9H_{12}]^-$.[192]

4.3.10 Microwave Irradiation of $[7\text{-Ph-}7,8\text{-}C_2B_9H_{11}]^-$

The compound $Cs[7\text{-Ph-}7,8\text{-}C_2B_9H_{11}]$ (0.06g, 0.175mmol), ethanol (20ml) and triethylamine (0.177g, 1.75mmol) were introduced into the glass reaction vessel as described in section 4.3.3. The solution was subjected to microwave irradiation (650W) for 30 minutes. The ethanol and triethylamine was removed under reduced pressure (rotatory film evaporator, 35°C). The product which was recovered had not reacted as confirmed by IR and ^{11}B spectroscopic analyses.

4.3.11 Microwave Irradiation of *closo*-$[3,3\text{-}(PMe_2Ph)_2\text{-}3,1,2\text{-}PtC_2B_9H_{11}]$ (157)

A sample of *closo*-$[3,3\text{-}(PMe_2Ph)_2\text{-}3,1,2\text{-}PtC_2B_9H_{11}]$ (0.02g, 0.033mmol) was introduced into the glass reaction vessel as described in section 4.3.3. The solution was subjected to microwave irradiation (650W) for 10 minutes. The ethanol was removed under reduced pressure (rotatory film evaporator, 35°C). The reaction mixture was dissolved in CH_2Cl_2 and was subjected to preparative tlc {CH_2Cl_2 - hexane (3:2)}, affording one major product. The pale yellow band was extracted into CH_2Cl_2 and recrystallised from CH_2Cl_2 - hexane (3:2) as colourless crystals of *closo*-$[2,2\text{-}(PMe_2Ph)_2\text{-}2,1,8\text{-}PtC_2B_9H_{11}]$ (158) (0.018g, 90.0%). IR data and R_f position were identical to those reported in section 4.3.4

4.3.12 Iodination of $As_2B_{10}H_{10}$

To a solution of 1,2-$As_2B_{10}H_{10}$ (1.00g, 3.73mmol) in CH_2Cl_2 (15ml) was added $AlCl_3$ (0.40g, 3.00mmol) and iodine (1.20g, 4.73mmol). The solution was stirred for 16h at ambient temperature. The initial purple colour of the solution gradually changed to orange and a cream solid precipitated. The mixture was filtered and the cream solid was recrystallised from thf/di-n-butylether (5:1) to yield colourless crystals of $As_2B_{10}H_8I_2$ (0.50g, 25.7%). IR: ν_{max}(KBr) 2560(s) (BH), 1255(w), 1095(w), 890(m), 830(m), 805(m), 795(s) (BI), 755(w), 745(w), 735(w) and 705(m) cm^{-1}. The ^{11}B NMR data consisted of three badly resolved peaks in a 2:3:5 intensity ratio. The low resolution mass spectrum showed a cut-off at m/z 522 corresponding to the $^{11}B_{10}{}^{75}As_2{}^{1}H_8{}^{127}I_2{}^{+}$ parent ion.

4.3.13 X-ray analysis of *closo*-$As_2B_{10}H_8I_2$

Crystal Data: $As_2B_{10}H_8I_2$, M = 519.8, monoclinic, *I2/a*, a = 14.262(3), b = 8.128(2), c = 21.575(4) Å, β = 92.65(2), U = 2498 Å^3, Z = 8, D_c = 2.76 g cm^{-3}, λ(Mo-K$_\alpha$) = 0.71073 Å, μ(Mo-K$_\alpha$) = 101.8 cm^{-1}, F(000) = 1840, T = 294 K, R = 0.036 for 2066 observed reflections.

CHAPTER FIVE

SYNTHESIS AND CHARACTERISATION OF METAL-HALIDE COMPLEXES OF $C_2B_9H_{11}$ AND $As_2B_9H_9$ AND THEIR REACTIONS WITH $Ag[BF_4]$

5.1 INTRODUCTION

This chapter is concerned with the synthesis and characterisation of metal-halide complexes of $C_2B_9H_{11}$ and $As_2B_9H_9$ and their reactions with $Ag[BF_4]$. The topic of metal-halide containing metallaheteroboranes was reviewed recently.[3] The present work concerns the synthesis and characterisation of *closo*-[3-PPh_3-3-I-4-SMe_2-3,1,2-$PdC_2B_9H_{10}$] (173) and *closo*-[3,3-$(PMePh_2)_2$-3-Cl-3,1,2-$RhC_2B_9H_{11}$] (174) and their further reaction with $Ag[BF_4]$ leading to the formation of cationic metalla-carboranes. A brief introduction to related reactions in the literature is necessary and accordingly section 5.1.1 reports known cationic metallaboranes and metallaheteroboranes and section 5.1.2 discusses the reaction of $Ag[BF_4]$ with metal-halide complexes.

5.1.1 Cationic Metallaboranes and Metallaheteroboranes

Virtually all the metallaboranes and metallaheteroboranes which have been described in the literature are either neutral or anionic.[25,39,103,194-196] Until 1993 very few cationic compounds were known. Typical of previously reported compounds were *nido*-$[Fe(CO)_3B_5H_9]^+$ (175)[197] and *closo*-[1-(η^5-Cp)-7-C_5H_5N-1,2,4-$CoC_2B_8H_9$]$^+$ (176)[198] which were rather unstable. The former was unstable above -30°C and the latter decomposed in polar solvents in a few hours at room temperature. The preparation of compounds (175) and (176) involved either the protonation of the borane cage or the removal of a hydride ion from a μ-B-H-M fragment.[198] An alternative approach to cationic compounds was reported with the electrochemical oxidation of *commo*-[3,3′-Fe{3,1,2-$FeC_2B_9H_{10}(SEt_2)$}$_2$].[199] However, the Fe(III) complex cation, isolated as the perchlorate salt, defied all attempts at purification and work on this complex ceased. Recently, Hawthorne *et al.* reported the synthesis of *commo*-[3,3′-Co{4-(4-$(C_5H_4N)CO_2Me$)-3,1,2-$CoC_2B_9H_{10}$}$_2$][Cl] from the reaction between $CoCl_2$ and *nido*-[9-(4-$(C_5H_4N)CO_2Me$)-7,8-$C_2B_9H_{11}$]$^-$ in thf.[200] Since the chloride complex was relatively unstable, another salt was prepared with the *nido*-[7,8-$C_2B_9H_{12}$]$^-$ anion. Both compounds were characterised by spectroscopic methods

but no crystallographic studies were reported. One of the conclusions of the study was that the "instability of the cobaltacarborane cation was due to the presence of the positive charge".[200]

More recently a series of fifteen cationic palladatelluraboranes have been synthesised.[3,197] These were *closo*-[2-(L)-2-(PPh_3)-2,1-$PdTeB_{10}H_9(PPh_3)$][BF_4] {L = CO (177), Bu^{t}NC (178), *cyclo*hexylNC (179), R-(+)-1-phenylethylamine (180), C_4H_8S (181), $C_6H_{10}S$ (182), CH_3CN (183), C_4H_8O (184), PhNCS (185), PhNHC(OMe)S (186)}, *closo*-[2,2-(PMe_2Ph)$_2$-2,1-$PdTeB_{10}H_9(PPh_3)$][BF_4] (187), [2,2′-μ-N_3-{2-(PPh_3)-2,1-$PdTeB_{10}H_9(PPh_3)$}$_2$][BF_4](188), *closo*-[2-(H_2O)-(PPh_3)-2,1-$PdTeB_{10}H_9$][Z] {where Z = BF_4^- (189) and SbF_6^- (190)} and *closo*-[2,2-(PMe_3)$_2$-2,1-$PdTeB_{10}H_9(PPh_3)$][I] (191). All the compounds were characterised by spectroscopic methods and the structures of (177).toluene, (188), (189).0.89CH_2Cl_2 and (191) were established by X-ray crystallographic analysis.[3]

The first stable cationic metallacarborane that has been structurally characterised is *closo*-[3-(η^2,η^2-1,5-C_8H_{12})-4-SMe_2-3,1,2-$PdC_2B_9H_{10}$][BF_4] (192).[201] A crystallographic study of (192) revealed a molecular conformation substantially influenced by H...F inter-ion contacts. Comparative EHMO calculations on *closo*-[3-(η^2,η^2-C_8H_{12})-4-SMe_2-3,1,2-$RhC_2B_9H_{10}$] (193) and (192) imply that the majority of the additional positive charge in (192) is not localised on the pendant sulphur atom but rather is delocalised over the twelve cluster vertices and the atoms directly bonded to them.

5.1.2 Reaction of metal-halide bonds with silver tetrafluoroborate

The importance of the reaction of Ag[BF_4] with M-X (M=Pd, X=I and M=Rh, X=Cl) lies in the potential to produce cationic metallaheteroboranes by removing the X^- ligand as Ag[X]. Specifically, it was hoped to produce cationic pallada- and rhoda-carboranes from the reaction between Ag[BF_4] and the neutral species *closo*-[3-PPh_3-3-I-4-SMe_2-3,1,2-$PdC_2B_9H_{10}$] (173) and *closo*-[3,3-($PMePh_2$)$_2$-3-Cl-3,1,2-$RhC_2B_9H_{11}$] (174).

5.2 RESULTS AND DISCUSSION

This chapter is concerned with the syntheses and characterisation of three new metal-halide complexes namely, *closo*-[3-PPh_3-3-I-4-SMe_2-3,1,2-$PdC_2B_9H_{10}$] (173), *closo*-[3,3-$(PMePh_2)_2$-3-Cl-3,1,2-$RhC_2B_9H_{11}$] (174) and *closo*-[3,3-$(PMePh_2)_2$-3-Cl-3,1,2-$RhAs_2B_9H_9$] (194) and the preparation of two new cationic complexes formed from the reaction of (173) and (174) with $Ag[BF_4]$ in the presence of a slight excess of Bu^{t}NC *i.e.* *closo*-[3-PPh_3-3-Bu^{t}NC-4-SMe_2-3,1,2-$PdC_2B_9H_{10}$][BF_4] (195) and *closo*-[3,3-$(PMePh_2)_2$-3-Bu^{t}NC-3,1,2-$RhC_2B_9H_{11}$][BF_4] (196). All the compounds were characterised by spectroscopic methods. Single crystal X-ray diffraction analyses of (173) and (174) were carried out to confirm the exact nature of the cluster and *exo*cluster ligand bonding.

5.2.1 Syntheses

(a) Synthesis of *closo*-[3-PPh_3-3-I-4-SMe_2-3,1,2-$PdC_2B_9H_{10}$] (173)

The reaction between Tl[9-SMe_2-7,8-$C_2B_9H_{10}$] and [$Pd(PPh_3)_2I_2$] in CH_2Cl_2 solution heated at reflux for 2.5h afforded the green complex *closo*-[3-PPh_3-3-I-4-SMe_2-3,1,2-$PdC_2B_9H_{10}$] (173) in 81% yield. If the reaction time was allowed to exceed 2.5h, the yield of (173) was reduced due to decomposition. The decomposition products could be clearly seen on the baseline of the plc plate.

(b) Syntheses of *closo*-[3,3-$(PMePh_2)_2$-3-Cl-3,1,2-$RhC_2B_9H_{11}$] (174) and *closo*-[3,3-$(PMePh_2)_2$-3-Cl-3,1,2-$RhAs_2B_9H_9$] (194)

These compounds were prepared in a similar manner. The rhodacarborane (174) was synthesised from the reaction between excess $PMePh_2$ with *closo*-[3-{η^2-SC(H)NPh}-3-PPh_3-3,1,2-$RhC_2B_9H_{11}$] (197) {see chapter 6 section 6.4.7 for synthesis of (197)} in refluxing CH_2Cl_2 solution for 48h. The product was purified by plc and recrystallised from CH_2Cl_2/hexane to give orange crystals of (174) in 80% yield. The isolation of (174) was unexpected. It had been anticipated that a compound such as *closo*-[{η^2-SC(H)NPh}-3-$PMePh_2$-3,1,2-$RhC_2B_9H_{11}$] would have been the product. However, the complete SC(H)NPh ligand had been replaced by $PMePh_2$ and Cl

ligands. The formation of the Rh-Cl bond (from CH_2Cl_2) suggested that the reaction may be photolytically initiated. To test this hypothesis it was decided to repeat the reaction in the presence of extra light (60 Watt light bulb 8 cm from the reaction flask), and in the dark (by covering the reaction flask with aluminium foil). The addition of chlorine to metals from CH_2Cl_2 may be photoinduced and has been known for many years. However this type of reaction can occur even in the dark.[202,203] The results are tabulated in Table 5.1.

Table 5.1 Comparison of yields from the synthesis of *closo*-[3,3-$(PMePh_2)_2$-3-Cl-3,1,2-$RhC_2B_9H_{11}$] (174) in the presence and absence of light.

Reaction conditions	Yield
Normal reaction conditions	79.6%
60 Watt light source present for duration of experiment	96.2%
Reaction flask covered in aluminium foil	67.9%

Clearly, when the reaction was performed in the presence of light there was a marked increase in the yield of (174), and when the reaction was carried out in the dark there was a decrease in the yield. This suggests that the photolytic reaction is significant in the synthesis of (174).

The rhodaarsenaborane *closo*-[3,3-$(PMePh_2)_2$-3-Cl-3,1,2-$RhAs_2B_9H_9$] (194) was synthesised by the reaction of an excess of $PMePh_2$ with *closo*-[3-{η^2-SC(H)N-Ph}-3-PPh_3-3,1,2-$RhAs_2B_9H_9$] (198) in refluxing CH_2Cl_2 in the presence of light similar to the synthesis of (174). The yield of the orange compound (194) was 62.9%.

(c) Syntheses of *closo*-[3-PPh_3-3-Bu^{t}NC-4-SMe_2-3,1,2-$PdC_2B_9H_{10}$][BF_4] (195) and *closo*-[3,3-$(PMePh_2)_2$-3-Bu^{t}NC-3,1,2-$RhC_2B_9H_{11}$][BF_4] (196)

The two cationic metallacarboranes (195) and (196) were synthesised from the reaction between either (173) or (174) in toluene and one equivalent of Ag[BF_4] at

ambient temperature for 5 min. A slight excess of BuᵗNC was added. The products were filtered from the mixture and purified by recrystallisation from CH_2Cl_2/hexane. The pink compound (195) was isolated in 72% yield and the yellow compound (196) was isolated in 46% yield, these compounds were not stable in solution for more than 8 hours. This tendency to decompose made purification of (195) and (196) rather difficult.

5.2.2 Infrared Spectra

An important feature of the infrared spectra of all the compounds (173), (174), (194), (195) and (196) was the presence of terminal B-H stretching bands in the range 2580-2480 cm^{-1}. No B-H-B, M-H-B or M-H (M=Rh or M=Pd) bands were observed. The two cationic metallacarboranes (195) and (196) had strong, broad absorption bands associated with the $[BF_4]^-$ anion at between 1082-1040 cm^{-1} for both (195) and (196).[14] The isocyanide (NC) absorptions in compounds (195) and (196) appeared at ν_{max} 2182(s) and 2178(s) cm^{-1} respectively. These are typical of terminal metal-isocyanide absorptions which have been interpreted to contain a strong σ-element and weak π-element in the M-C bond.[3] Rhodium-chloride stretching vibrations were expected in the range 240-310 cm^{-1}.[204] However in the present work infrared spectra could only be obtained in the region 625-4000 cm^{-1} and therefore it was not possible to determine the Rh-Cl stretching frequency for compounds (174) and (194). Other important features were bands due to phosphine ligands arising from C-H stretching in the region 3100-2800 cm^{-1}, P-C stretching in the region 795-650 cm^{-1}, P-Ph stretching in the regions 1600-1425 and 1110-960 cm^{-1}, and P-Me stretching in the region 960-835 cm^{-1}.

5.2.3 NMR Spectroscopy

All the NMR spectra discussed in this section were kindly recorded by Dr. J. D. Kennedy, University of Leeds, England. Multinuclear ^{11}B, $^{11}B\{^1H\}$, ^{31}P and ^1H NMR spectroscopy was used to characterise the compounds (173), (174), (195) and (196).

5.2.3.1 NMR Spectroscopy of *closo*-[3-PPh_3-3-I-4-SMe_2-3,1,2-$PdC_2B_9H_{10}$] (173)

The measured NMR parameters for the palladacarborane (173) are given in Table 5.2. The ^{11}B and $^{11}B\{^1H\}$ NMR spectra of (173) are illustrated in Figure 5.1. The $^{11}B\{^1H\}$ NMR spectrum displayed eight resonances of relative intensity 1:1:1:1:1:1:2:1, consistent with a fully asymmetric carbametallaborane cage (with one coincidence). On retention of proton coupling, all resonances in the ^{11}B spectrum appear as doublets ($^1J_{BH}$ 135-144±5 Hz), except for one singlet signal at *ca.* 11.0 ppm which may be assigned to B(4), the sulphur bearing boron atom. In the ^1H NMR spectrum the methyl protons give rise to two singlets (2.47 and 2.91 ppm). This confirms the magnetic inequivalence of the two methyl groups of the SMe_2 function at ambient temperature. No bridging hydrogen resonances were observed in the ^1H NMR spectra of (173) which was consistent with the *closo* nature of the compound.

Table 5.2 ^1H and ^{11}B data for *closo*-[3-PPh_3-3-I-4-SMe_2-3,1,2-$PdC_2B_9H_{10}$] (173).

Intensity	$\delta(^{11}B)$/ppm	$\delta(^1H)$/ppm
1	+2.3	+3.61
1	-2.8	+2.65
1	-10.8	+1.79
1 B(4)	*ca* -11.0	SMe_2 +2.47, +2.91
1	-11.5	+2.73
1	-14.8	+1.20
1	-21.1	+2.06
1	-21.1	+1.03
1	-23.1	+1.02
	CH	+3.07, +3.60

$\delta(^{31}P)$ +41.7 at 219K

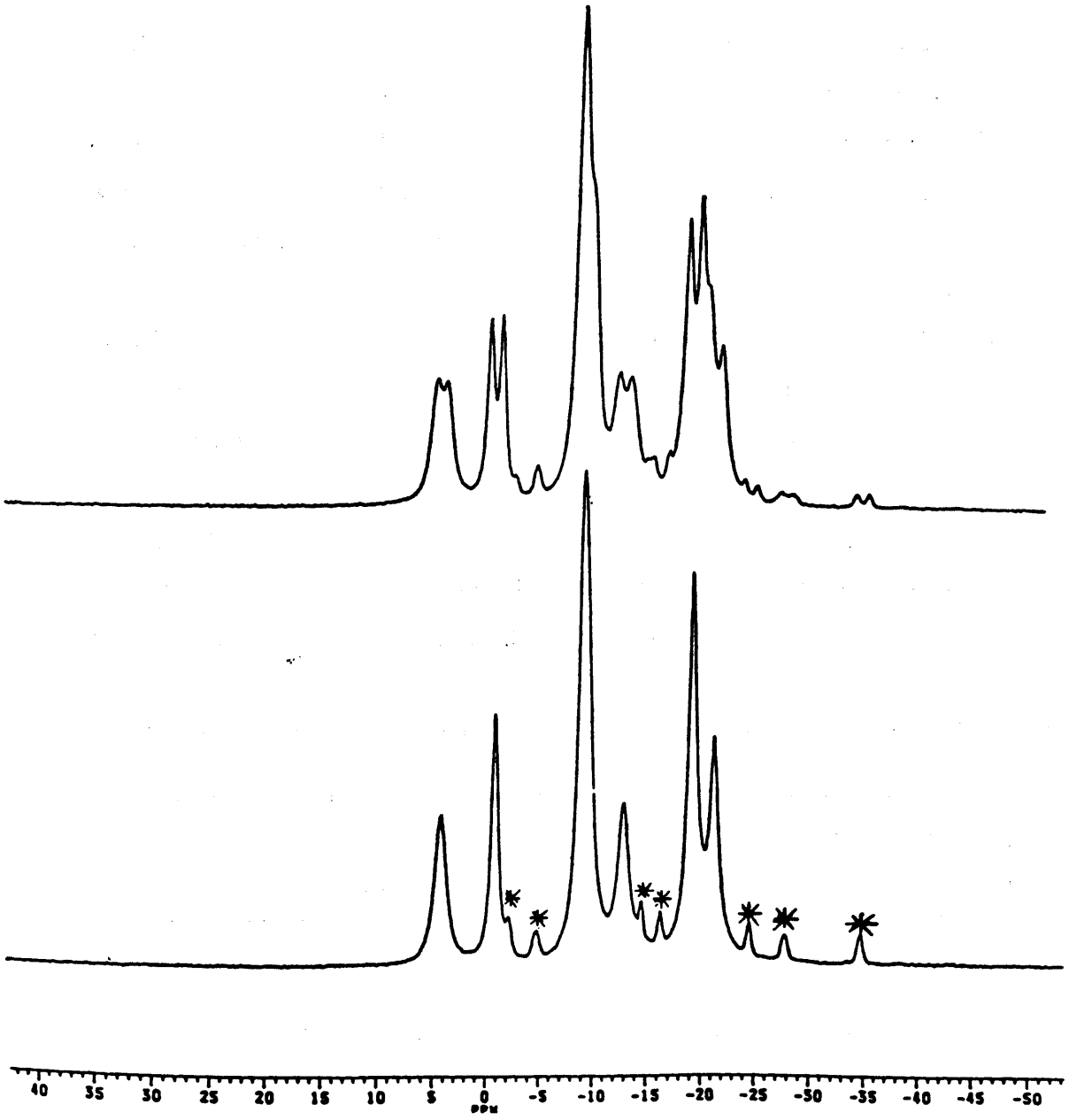

Figure 5.1 ^{11}B(top trace) and $^{11}B\{^1H\}$(lower trace) NMR spectra of *closo*-[3-PPh_3-3-I-4-SMe_2-3,1,2-$PdC_2B_9H_{10}$] (173).

---

*Impurities present in the sample.

5.2.3.2 NMR Spectroscopy of *closo*-[3,3-$(PMePh_2)_2$-3-Cl-3,1,2-$RhC_2B_9H_{11}$] (174)

The measured NMR parameters for the rhodadicarborane (174) are given in Table 5.3. The ^{11}B and $^{11}B\{^1H\}$ NMR spectra of (174) are illustrated in Figure 5.3. In general the ^{11}B shielding pattern for (174) shows some similarities with *closo*-[3,3-$(PPh_3)_2$-3-H-3,1,2-$RhC_2B_9H_{11}$] (59),[205] but data for (174) are even more similar to *closo*-[3-(η^5-Cp*)-3,1,2-$RhC_2B_9H_{11}$] (199),[161] and *precloso*-[2-PPh_3-2-Cl-2,1,7-$RhC_2B_9H_{11}$] (200).[48] In Figure 5.2 the chemical shifts and relative intensities in the ^{11}B NMR spectra of (59), (199), (200) and (174) are illustrated in stick diagram form. The assignment of the boron resonances to the corresponding boron atom positions in (174) was made by comparison with the previously assigned ^{11}B NMR resonances of (199).[161] All boron atom positions had *exo*-terminal hydrogen atoms bound to them and the borane ^1H resonances were assigned to their directly bound boron atoms by ^1H-{^{11}B(selective)} spectroscopy. The peaks at δ +3.64 were assigned to the two C*H* units and the peak at δ +1.62 was assigned to the methyl hydrogens. No bridging hydrogen resonances were observed in the ^1H NMR spectra of (174) which was consistent with the *closo* nature of the compound.

Table 5.3 ^1H and ^{11}B data for *closo*-[3,3-$(PMePh_2)_2$-3-Cl-3,1,2-$RhC_2B_9H_{11}$] (174).

Intensity	$\delta(^{11}B)$/ppm	$\delta(^1H)$/ppm	Tentative Assignment
1	+8.8	+3.74	B(8)
1	-0.4	+1.84	B(10)
2	-2.6	+2.83	B(4/7)
2	-4.9	+2.17	B(9/12)
2	-17.2	+1.49	B(5/11)
1	-17.7	+2.05	B(6)
	CH	+3.64	
	PMe	+1.62[a]	

[a] N=10.5Hz at 219K $\delta(^{31}P)$ +19.1 $^1J(^{103}Rh\text{-}^{31}P)$ 129Hz

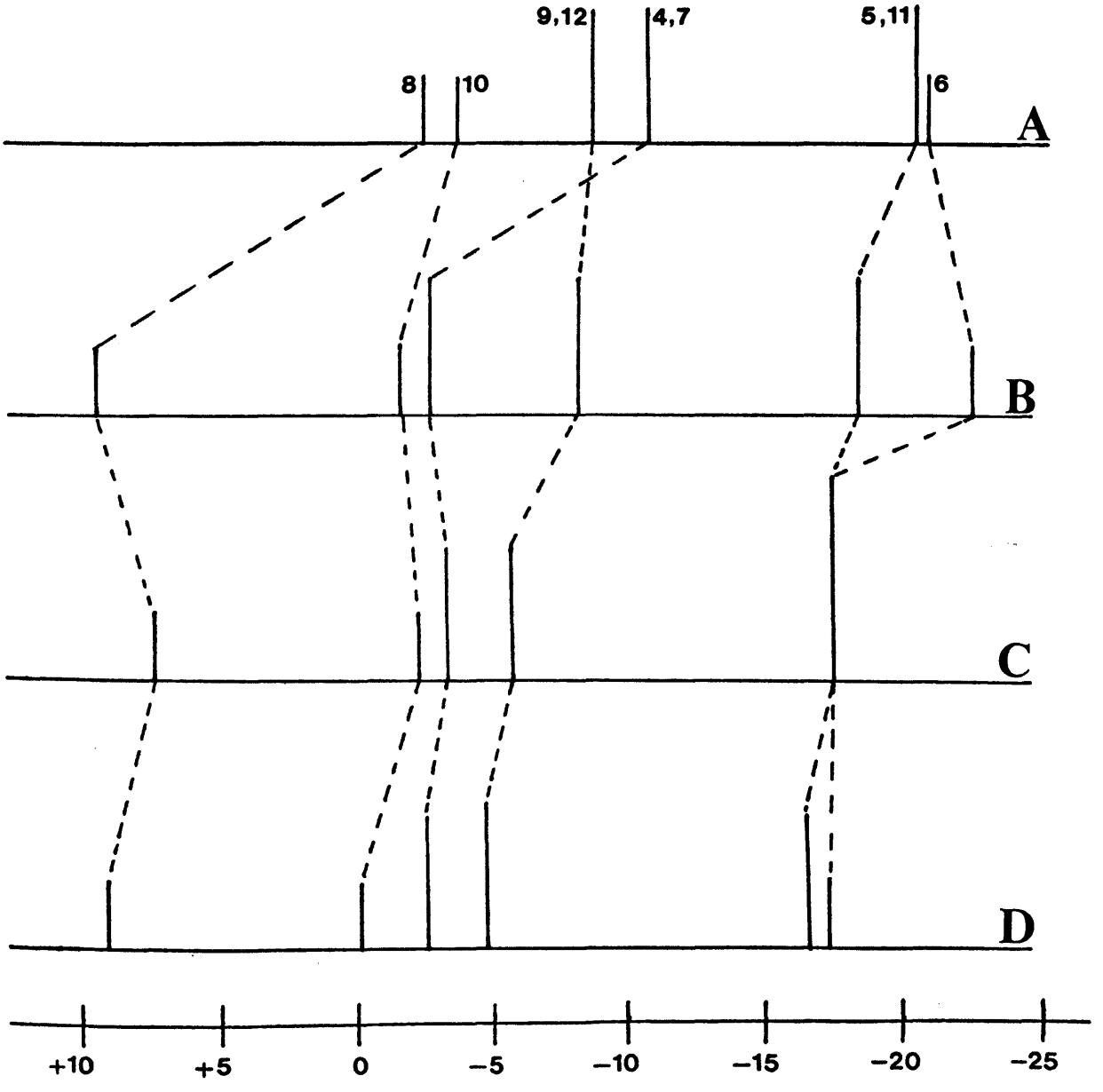

Figure 5.2 Stick diagrams of the chemical shifts and relative intensities in the ^{11}B NMR spectra of (A) *closo*-[3,3-$(PPh_3)_2$-3-H-3,1,2-$RhC_2B_9H_{11}$] (59), (B) *closo*-[3-(η^5-Cp^*)-3,1,2-$RhC_2B_9H_{11}$] (199), (C) *precloso*-[2-PPh_3-2-Cl-2,1,7-$RhC_2B_9H_{11}$] (200) and (D) *closo*-[3,3-$(PMePh_2)_2$-3-Cl-3,1,2-$RhC_2B_9H_{11}$] (174).

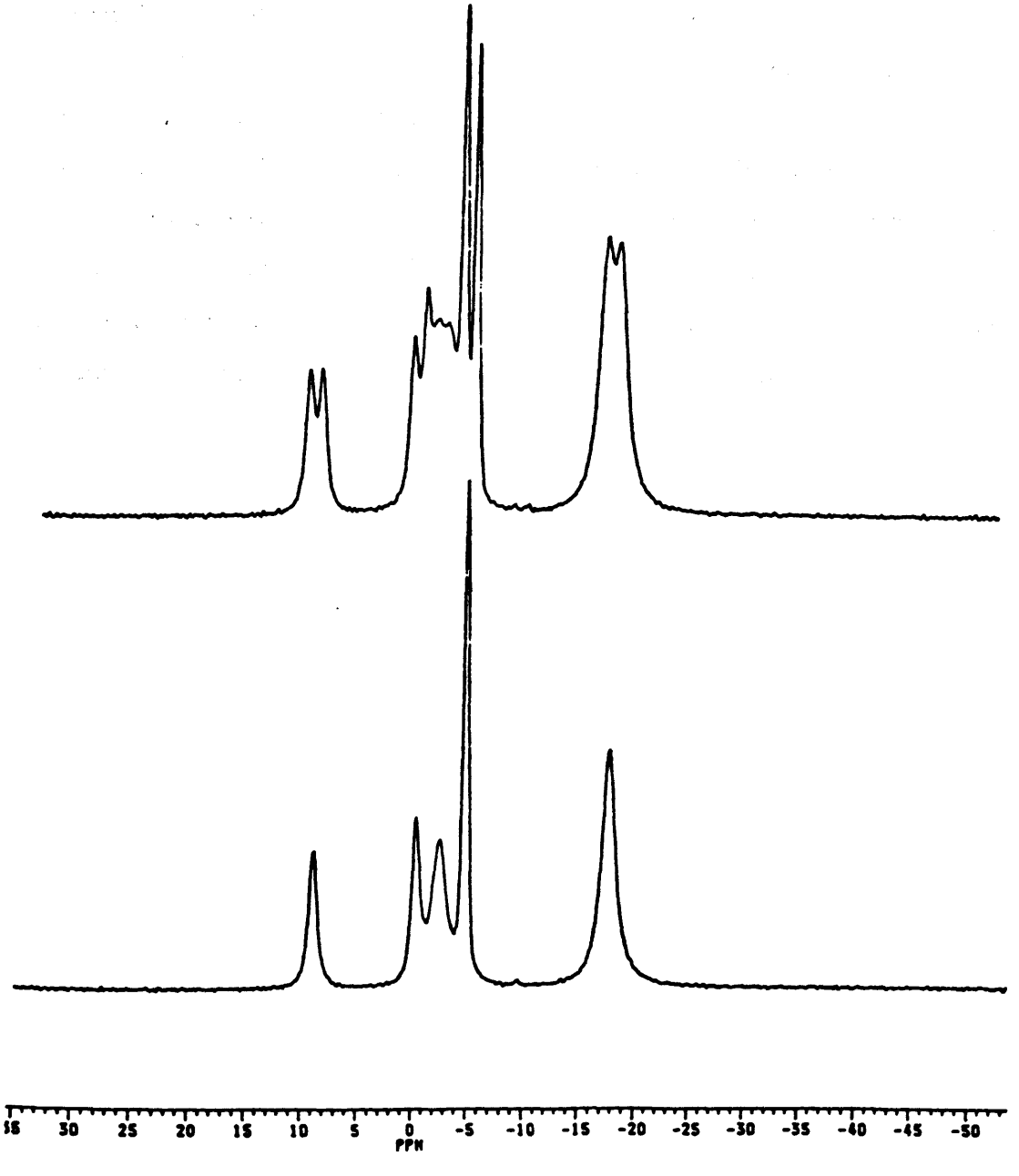

Figure 5.3 ^{11}B**(top trace) and** $^{11}B\{^1H\}$**(lower trace) NMR spectra of *closo*-[3,3-(PMePh$_2$)$_2$-3-Cl-3,1,2-RhC$_2$B$_9$H$_{11}$] (174).**

5.2.3.3 ^{11}B NMR Spectroscopy of *closo*-[3-PPh_3-3-Bu^{t}NC-4-SMe_2-3,1,2-$PdC_2B_9H_{10}$][BF_4] (195) and *closo*-[3,3-$(PMePh_2)_2$-3-Bu^{t}NC-3,1,2-$RhC_2B_9H_{11}$][BF_4] (196)

The measured ^{11}B and $^{11}B\{^1H\}$ NMR spectra of (195) showed eight peaks in an intensity pattern of 1:1:1:2:2:1:1:1. The signal of intensity 1B at δ +0.1 ppm was sharper than the others and was assigned to the $[BF_4]^-$ anion. The measured ^{11}B and $^{11}B\{^1H\}$ NMR spectrum of (196) showed seven peaks in an intensity pattern of 1:1:1:4:1:1:1 (though not all peaks were fully resolved even at 128 MHz), Figure 5.4. The signal of intensity 1B at δ -0.7 ppm was notably much sharper than the others and was assigned to the $[BF_4]^-$ anion. In general even though the ^{11}B spectra are not very informative they have similar intensity patterns and both spectra are consistent with a RhC_2B_9 *closo* cation and a $[BF_4]^-$ anion and both spectra have a general appearance very like the ^{11}B spectra of the reported palladatelluraboranes.[3]

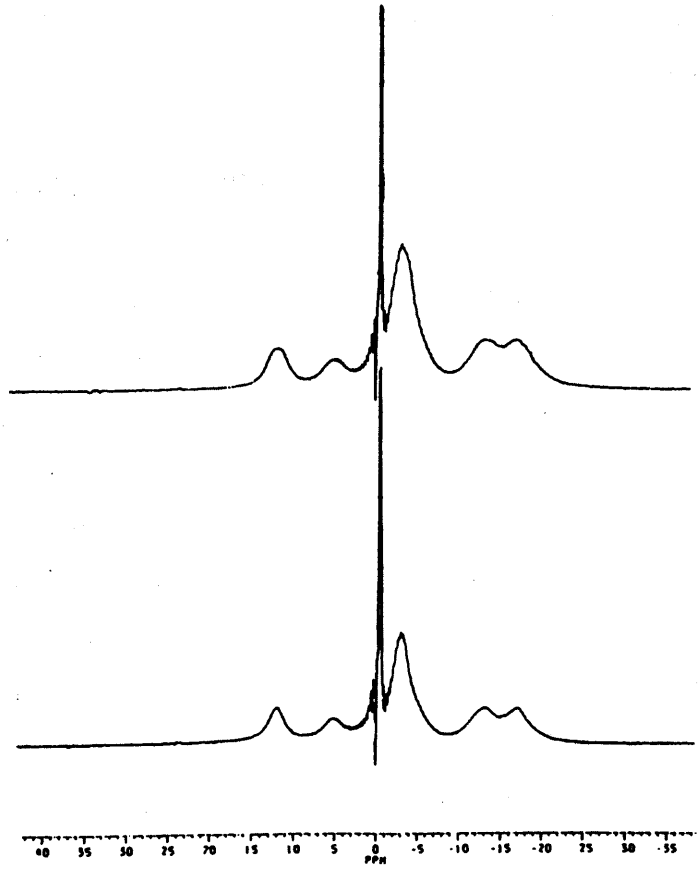

Figure 5.4 ^{11}B(top trace) and $^{11}B\{^1H\}$(lower trace) NMR spectra of *closo*-[3,3-$(PMePh_2)_2$-3-Bu^{t}NC-3,1,2-$RhC_2B_9H_{11}$][BF_4] (196).

5.2.4 Crystal and Molecular Structures

5.2.4.1 Crystal and Molecular Structure of *closo*-[3-PPh_3-3-I-4-SMe_2-3,1,2-$PdC_2B_9H_{10}$] (173)

In order to fully elucidate the structural features of the palladacarborane (173), it was decided to undertake a single crystal X-ray analysis of the compound. Crystals suitable for study were grown by the so-called layering technique by which hexane slowly diffused into a CH_2Cl_2 solution of the palladacarborane. Collection of the data and the structure solution were carried out by Professor George Ferguson, University of Guelph, Canada, as stated in the experimental section 4.3.1. Crystal data and relevant structure solution data are given in experimental section 5.4.3.

The successful solution and refinement of the molecular structure showed that compound (173) had a *closo* twelve vertex PdC_2B_9 geometry based on a distorted dodecahedron with the palladium and carbon atoms adjacent to one another, Figure 5.5. Important bond distances and angles are given in Tables 5.4 and 5.5 respectively.

The orientation of the $Pd(PPh_3)(I)$ unit above the C_2B_3 face is shown in Figure 5.6, and it would seem to be affected by the SMe_2 on B(4). Based on molecular orbital calculations the expected conformation of the $Pd(PPh_3)I$ unit above the C_2B_3 face would be "parallel" to the two carbon atoms.[162] Due to the SMe_2 group on B(4) the $Pd(PPh_3)(I)$ unit is twisted away from B(4) and towards C(1), Figure 5.6. The conformation has become more like the "perpendicular" conformation that is expected for a 7,9-C_2B_9 ligand (see chapter 2).

The Pd-I distance of 2.6734(5) in (173) is longer than most of the previously reported values.[206] The average Pd-I distances in typical Pd(II) non-cluster *trans* compounds are, 2.6029(5) Å in $[Pd(PPh_3)_2I_2].CHCl_3$,[207] 2.599(6) Å in $[Pd(Bu^tNC)_2I_2]$[208] and 2.63(1) Å in $[Pd(PMe_2Ph)_2I_2]$.[209] The value in (173) is longer than these but shorter than 2.7151(9) Å in *closo*-[2-I-2-(Bu^tNC)-6-(Bu^tNHCH)-2,1-$PdTeB_{10}H_9$] (201).[3]

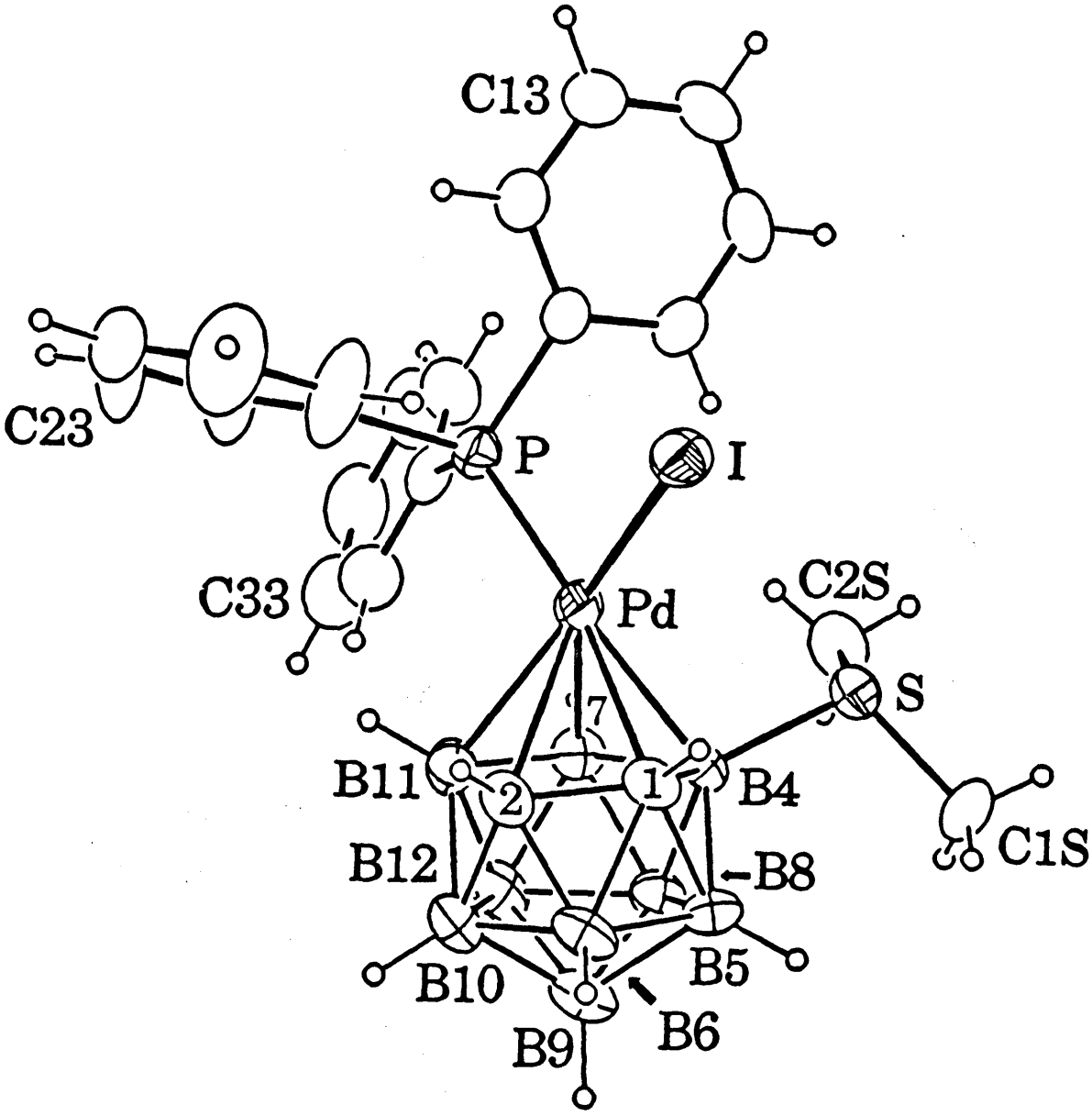

Figure 5.5 An ORTEP view of *closo*-[3-PPh_3-3-I-4-SMe_2-3,1,2-$PdC_2B_9H_{10}$] (173) with atom numbering scheme.

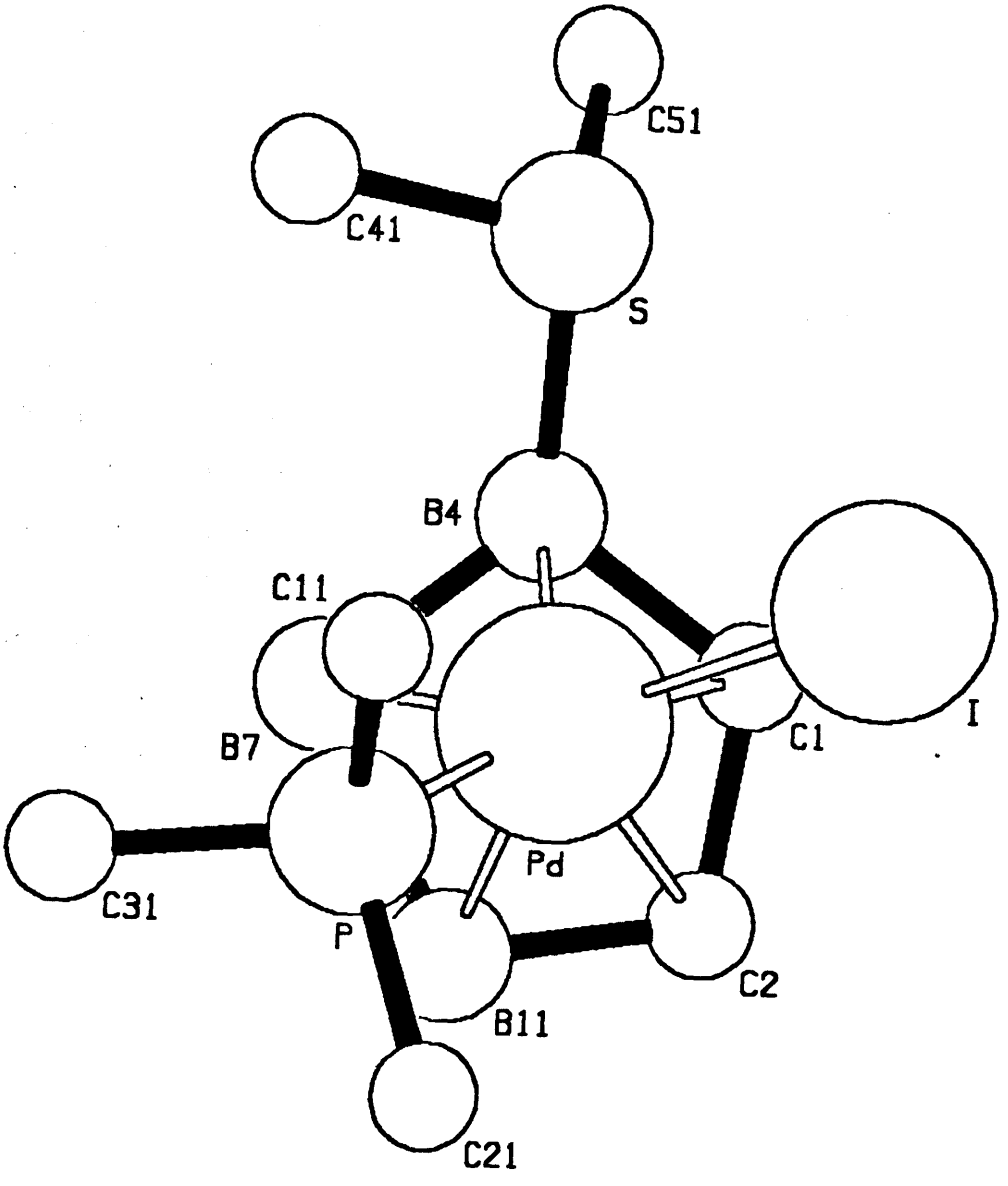

Figure 5.6 A view of the orientation of the $Pd(PPh_3)(I)$ unit above the C_2B_3 face of *closo*-[3-PPh_3-3-I-4-SMe_2-3,1,2-$PdC_2B_9H_{10}$] (173).

Table 5.4 Important bond distances (Å) for *closo*-[3-PPh_3-3-I-4-SMe_2-3,1,2-$PdC_2B_9H_{10}$] (173).

Pd-I	2.6734(5)	Pd-P	2.2512(15)
Pd-C(1)	2.286(5)	Pd-C(2)	2.470(5)
Pd-B(4)	2.306(6)	Pd-B(7)	2.253(6)
Pd-B(11)	2.260(7)	S-C(1S)	1.784(6)
S-C(2S)	1.794(6)	S-B(4)	1.899(6)
P-C(11)	1.826(6)	P-C(21)	1.838(5)
P-C(31)	1.830(6)	C(1)-C(2)	1.590(8)
C(1)-B(4)	1.683(7)	C(1)-B(5)	1.737(8)
C(1)-B(6)	1.775(8)	C(2)-B(6)	1.674(9)
C(2)-B(10)	1.670(9)	C(2)-B(11)	1.653(9)
B(4)-B(5)	1.749(8)	B(4)-B(7)	1.767(9)
B(4)-B(8)	1.742(8)	B(5)-B(6)	1.772(9)
B(5)-B(8)	1.765(9)	B(5)-B(9)	1.768(9)
B(6)-B(9)	1.766(10)	B(6)-B(10)	1.741(10)
B(7)-B(8)	1.807(9)	B(7)-B(11)	1.893(9)
B(7)-B(12)	1.770(9)	B(8)-B(9)	1.751(9)
B(8)-B(12)	1.777(10)	B(9)-B(10)	1.743(11)
B(9)-B(12)	1.805(10)	B(10)-B(11)	1.814(10)
B(10)-B(12)	1.781(10)	B(11)-B(12)	1.797(10)

Table 5.5 Important bond angles (°) for *closo*-[3-PPh_3-3-I-4-SMe_2-3,1,2-$PdC_2B_9H_{10}$] (173).

I-Pd-P	95.03(4)	I-Pd-C(1)	90.77(13)
I-Pd-C(2)	106.03(13)	I-Pd-B(4)	110.40(14)
I-Pd-B(7)	155.19(17)	I-Pd-B(11)	143.38(17)
P-Pd-C(1)	169.42(14)	I-Pd-C(2)	130.67(14)
P-Pd-B(4)	140.85(14)	P-Pd-B(7)	102.99(16)
P-Pd-B(11)	100.16(17)	C(1)-Pd-C(2)	38.84(19)
C(1)-Pd-B(4)	43.01(19)	C(1)-Pd-B(7)	74.35(20)
C(1)-Pd-B(11)	70.18(21)	C(2)-Pd-B(4)	71.13(19)
C(2)-Pd-B(7)	74.80(20)	C(2)-Pd-B(11)	40.62(22)
B(4)-Pd-B(7)	45.60(21)	B(4)-Pd-B(11)	77.08(21)
B(7)-Pd-B(11)	49.60(23)	C(1S)-S-C(2S)	100.0(3)
C(1S)-S-B(4)	101.1(3)	C(2S)-S-B(4)	108.3(3)
Pd-P-C(11)	110.99(17)	Pd-P-C(21)	112.31(18)
Pd-P-C(31)	119.07(20)	C(11)-P-C(21)	106.8(3)
C(11)-P-C(31)	102.7(3)	C(21)-P-C(31)	103.8(3)
P-C(11)-C(12)	122.6(4)	P-C(11)-C(16)	118.0(4)
P-C(21)-C(22)	122.7(5)	P-C(21)-C(26)	119.7(5)
P-C(31)-C(32)	120.8(5)	P-C(31)-C(36)	121.8(5)
Pd-C(1)-C(2)	76.8(3)	Pd-C(1)-B(4)	69.1(3)
C(2)-C(1)-B(4)	116.3(4)	C(2)-C(1)-B(5)	109.6(4)
C(2)-C(1)-B(6)	59.3(4)	B(4)-C(1)-B(5)	61.5(3)
B(5)-C(1)-B(6)	60.6(4)	Pd-C(2)-C(1)	64.3(3)
Pd-C(2)-B(11)	62.9(3)	C(1)-C(2)-B(6)	65.8(4)
C(1)-C(2)-B(11)	107.3(4)	B(6)-C(2)-B(10)	62.7(4)
B(10)-C(2)-B(11)	66.2(4)	Pd-B(4)-S	104.6(3)
Pd-B(4)-C(1)	67.9(3)	Pd-B(4)-B(7)	65.6(3)
S-B(4)-C(1)	119.4(4)	S-B(4)-B(5)	114.7(4)
S-B(4)-B(7)	126.7(4)	S-B(4)-B(8)	123.6(4)
C(1)-B(4)-B(5)	60.8(3)	C(1)-B(4)-B(7)	105.3(4)

B(5)-B(4)-B(8)	60.7(3)	B(7)-B(4)-B(8)	60.0(4)
C(1)-B(5)-B(4)	57.7(3)	C(1)-B(5)-B(6)	60.8(3)
B(4)-B(5)-B(8)	59.4(3)	B(6)-B(5)-B(9)	59.9(4)
B(8)-B(5)-B(9)	59.4(4)	C(1)-B(6)-C(2)	54.8(3)
C(2)-B(6)-B(10)	58.5(4)	B(5)-B(6)-B(9)	60.0(4)
B(9)-B(6)-B(10)	59.6(4)	Pd-B(7)-B(4)	68.8(3)
Pd-B(7)-B(11)	65.4(3)	B(4)-B(7)-B(8)	58.3(3)
B(4)-B(7)-B(11)	102.0(4)	B(8)-B(7)-B(12)	59.6(4)
B(11)-B(7)-B(12)	58.6(4)	B(4)-B(8)-B(5)	59.8(3)
B(4)-B(8)-B(7)	59.7(3)	B(5)-B(8)-B(9)	60.4(4)
B(7)-B(8)-B(12)	59.2(4)	B(9)-B(8)-B(12)	61.6(4)
B(5)-B(9)-B(6)	60.2(4)	B(5)-B(9)-B(8)	60.2(3)
B(6)-B(9)-B(10)	59.5(4)	B(8)-B(9)-B(12)	59.9(4)
B(10)-B(9)-B(12)	60.2(4)	C(2)-B(10)-B(6)	58.7(4)
C(2)-B(10)-B(11)	56.5(4)	B(6)-B(10)-B(9)	60.9(4)
B(9)-B(10)-B(12)	61.6(4)	B(11)-B(10)-B(12)	60.0(4)
Pd-B(11)-C(2)	76.5(3)	Pd-B(11)-B(7)	65.0(3)
C(2)-B(11)-B(7)	108.1(4)	C(2)-B(11)-B(10)	57.4(4)
B(7)-B(11)-B(12)	57.3(3)	B(10)-B(11)-B(12)	59.1(4)
B(7)-B(12)-B(8)	61.3(4)	B(7)-B(12)-B(11)	64.1(4)
B(8)-B(12)-B(9)	58.5(4)	B(9)-B(12)-B(10)	58.2(4)

The Pd-P distance of 2.2512(15) Å is much shorter than the value predicted from the sum of the covalent radii for Pd and P *i.e.* 2.383 Å.[165] The Pd-P distances in typical Pd(II) non-cluster *trans* compounds are 2.343(2) Å in $[Pd(PPh_3)_2I_2]$,[207] and 2.326(7) Å in $[Pd(PMe_2Ph)_2I_2]$.[209] Indeed most Pd-P bond distances in heteroborane cluster compounds are greater than 2.3 Å[3,53,197,210] with 75% of all reported Pd-P distances greater than 2.281 Å.[206] The value in (173) is close to the Pd-P bond distance of 2.252(1) Å in the thirteen vertex [4-(dppe)-4-1,6-$PdC_2B_{10}H_{12}$] (202) {dppe = 1,2-bis(diphenylphosphino)ethane}.[166] The compound *closo*-[3-PMe_2Ph-3-Cl-4-SMe_2-3,1,2-$PdC_2B_9H_{10}$] (203) has a Pd-P distance of 2.2275(5) Å which is even shorter than that in (173).[211]

The Pd-C bond distances of 2.286(5) and 2.470(5) Å are significantly different with Pd-C(1) being considerably shorter than Pd-C(2). The Pd-C distances are similar to those in *closo*-[3-PMe_2Ph-3-Cl-4-SMe_2-3,1,2-$PdC_2B_9H_{10}$] (203) of 2.302(2) and 2.479(2) Å, and in *closo*-[3-(η^2,η^2-C_8H_{12})-4-SMe_2-3,1,2-$PdC_2B_9H_{10}$][BF_4] (204) {2.371(4) and 2.434(4) Å}.[201] The values in (173) are within the reported range of Pd-C bond distances in palladacarboranes, which vary from 2.187(5) Å in (202)[166] to 2.600(6) Å in [1,1-($Bu^tNC)_2$-2-NMe_3-1,2-$PdCB_{10}H_{10}$] (205).[212]

The Pd-B distances of 2.306(6), 2.253(6) and 2.260(7) Å for B(4), B(7) and B(11) respectively, are within the range of Pd-B distances reported in a recent study of palladaboranes, {2.192(6)-2.309(5) Å}.[3] However they are slightly longer than those in the equivalent chloropalladacarbaborane *closo*-[3-PMe_2Ph-3-Cl-4-SMe_2-3,1,2-$PdC_2B_9H_{10}$] (203) which are 2.277(2), 2.229(2) and 2.210(2) Å, for B(4), B(7) and B(11) respectively.[211]

The S-B(4) distance of 1.899(6) Å is very similar to 1.895(2) Å found in the palladacarborane (203),[211] and corresponds very closely (within experimental error), to values quoted in the literature for the compounds *nido*-[10,11-μ-{(PPh_3)Au}-9-SMe_2-7,8-$C_2B_9H_{10}$] (206) {1.896(6)} Å,[213] *closo*-[3,3-$(CO)_2$-4-SMe_2-3,1,2-$RhC_2B_9H_{10}$] (207) {1.897(3)} Å,[201] *closo*-[3-(η^2,η^2-C_8H_{12})-4-SMe_2-3,1,2-$RhC_2B_9H_{10}$] (193) {1.899(3)} Å,[201] *nido*-[9-C_6H_{11}-5-SMe_2-$B_{10}H_{11}$] (208) {1.892(6)} Å,[214] and [RuH_2-($N_2B_{10}H_8SMe_2$)($PPh_3)_2$] {1.89(1)} Å (209),[215] Table 5.6.

For the selected SMe_2 compounds in Table 5.6 the S-C_{Me} distances range from 1.782(4) Å in *closo*-[3,3-$(CO)_2$-4-SMe_2-3,1,2-$RhC_2B_9H_{10}$] (207)[201] to 1.800(6) Å in *closo*-[3-PPh_3-4-SMe_2-3,1,2-$CuC_2B_9H_{10}$] (210).[216] The S-C_{Me} distances of 1.784(6) and 1.794(6) Å correspond exactly, within experimental error, to those in *nido*-[8-SMe_2-7,9-$C_2B_9H_{11}$] (211) of 1.786(6) and 1.794(6) Å,[217] in *closo*-[3-(η^2,η^2-C_8H_{12})-4-SMe_2-3,1,2-$PdC_2B_9H_{10}$][BF_4] (204) of 1.789(7) and 1.795(4) Å,[201] in *closo*-[3,3-$(CO)_2$-4-SMe_2-3,1,2-$RhC_2B_9H_{10}$] (207) of 1.782(4) and 1.799(4) Å and *closo*-[3-PPh_3-4-SMe_2-3,1,2-$CuC_2B_9H_{10}$] (210) of 1.784(5) and 1.800(6) Å,[216] Table 5.6. The S-C_{Me} distances also correspond to those in (203) of 1.785(2) and 1.796(2) Å.[211] The S-C_{Me} distance are also similar to 1.790(7) and 1.769(9) Å in the cation $[SMe_2]^+[C_9H_4O_2]^-$ (2-Dimethylsulphuranylidene-1,3-indanedione).[218-220]

Table 5.6 Bond Distances for Carboranes containing a SMe_2 group bonded to a Boron Atom.

No.	Compound	S-B/Å	S-C_{Me}/Å
173	*closo*-[3-PPh_3-3-I-4-SMe_2-3,1,2-$PdC_2B_9H_{10}$]	1.899(6)	1.784(6) 1.794(6)
193[201]	*closo*-[3-(η^2,η^2-C_8H_{12})-4-SMe_2-3,1,2-$RhC_2B_9H_{10}$]	1.899(3)	1.793(3) 1.794(4)
203[211]	*closo*-[3-PMe_2Ph-3-Cl-4-SMe_2-3,1,2-$PdC_2B_9H_{10}$]	1.895(2)	1.785(2) 1.796(2)
204[201]	*closo*-[3-(η^2,η^2-C_8H_{12})-4-SMe_2-3,1,2-$PdC_2B_9H_{10}$][BF_4]	1.913(4)	1.795(4) 1.784(4)
206[213]	*nido*-[10,11-μ-{(PPh_3)Au}-9-SMe_2-7,8-$C_2B_9H_{10}$]	1.896(6)	1.796(8) 1.798(7)
207[201]	*closo*-[3,3-$(CO)_2$-4-SMe_2-3,1,2-$RhC_2B_9H_{10}$]	1.897(3)	1.782(4) 1.799(4)
208[214]	*nido*-[9-C_6H_{11}-5-SMe_2-$B_{10}H_{11}$]	1.892(6)	1.791(7) 1.797(8)
210[216]	*closo*-[3-PPh_3-4-SMe_2-3,1,2-$CuC_2B_9H_{10}$]	1.911(4)	1.784(5) 1.800(6)
211[217]	*nido*-[8-SMe_2-7,9-$C_2B_9H_{11}$]	1.886(4)	1.786(6) 1.794(6)

The C-C bond distance in the carborane cage {1.590(8) Å} is very similar to 1.596(4) Å in (207) but longer than 1.515(5) Å in (204), 1.555(5) Å in (210),[216] 1.558(8) Å in (206),[213] or 1.560(2) Å in (203).[211] It is shorter than the value of 1.628(4) Å in (193) also 1.618(5) Å in *closo*-[3,3-$(PMePh_2)_2$-3-Cl-3,1,2-$RhC_2B_9H_{11}$] (174) (see section 5.2.4.2).

The C-B distances range from 1.653(9) to 1.775(8) Å and cover a wider range than in (203) {1.678(3)-1.779(3) Å},[211] but are not as wide ranging as those in [3-(η^2,η^2-C_8H_{12})-3,1,2-$PdC_2B_9H_{10}$] (212) {1.637(5)-1.785(5) Å},[221] or [3-(tmed)-3,1,2-$PdC_2B_9H_{11}$] (213) {tmed = 1,2-$(NMe_2)_2C_2H_4$} {1.643(7)-1.778(7) Å}.[222]

The B-B bond distances range from 1.741(10)-1.893(9) Å, a similar range to that observed in (203) {1.742(3)-1.890(3) Å},[211] and typical of the ranges of B-B bond distances published in a recent study of palladatelluraboranes {1.729(8)-1.978(7) Å}.[3] The longest B-B distance is between B(7) and B(11) which are bonded to B(4) (attached to the SMe_2 group) and C(2) respectively and both B(7) and B(11) are bonded to the palladium atom.

5.2.4.2 Crystal and Molecular Structure of *closo*-[3,3-$(PMePh_2)_2$-3-Cl-3,1,2-$RhC_2B_9H_{11}$] (174)

For complete structural characterisation of the rhodacarborane (174), it was decided to undertake a single crystal X-ray analysis of the compound. Crystals suitable for study were grown by slow diffusion of a layer of hexane into a CH_2Cl_2 solution of the rhodacarborane. The collection of the data and the structure solution were carried out by Professor George Ferguson and Dr. John Gallagher, University of Guelph, Canada, as stated in the experimental section 4.3.1. Crystal data and relevant structure solution data are given in experimental section 5.4.5.

Analysis showed that compound (174) had a *closo* twelve vertex RhC_2B_9 geometry based on a distorted dodecahedron with the rhodium and carbon atoms adjacent to one another, Figure 5.7. Important bond distances and angles are given in Tables 5.7 and 5.8 respectively.

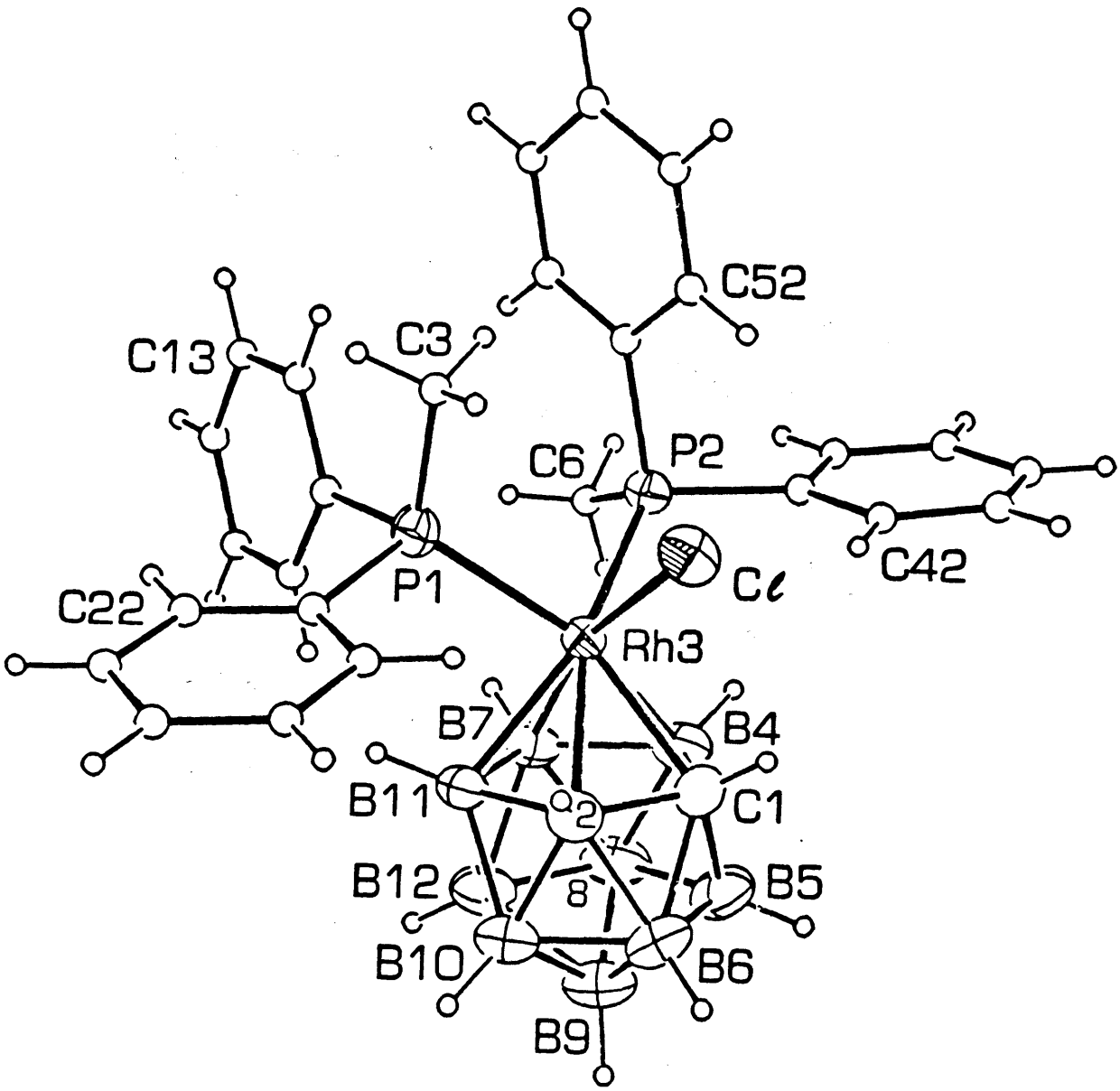

Figure 5.7 An ORTEP view of *closo*-[3,3-$(PMePh_2)_2$-3-Cl-3,1,2-$RhC_2B_9H_{11}$] (174) with numbering scheme.

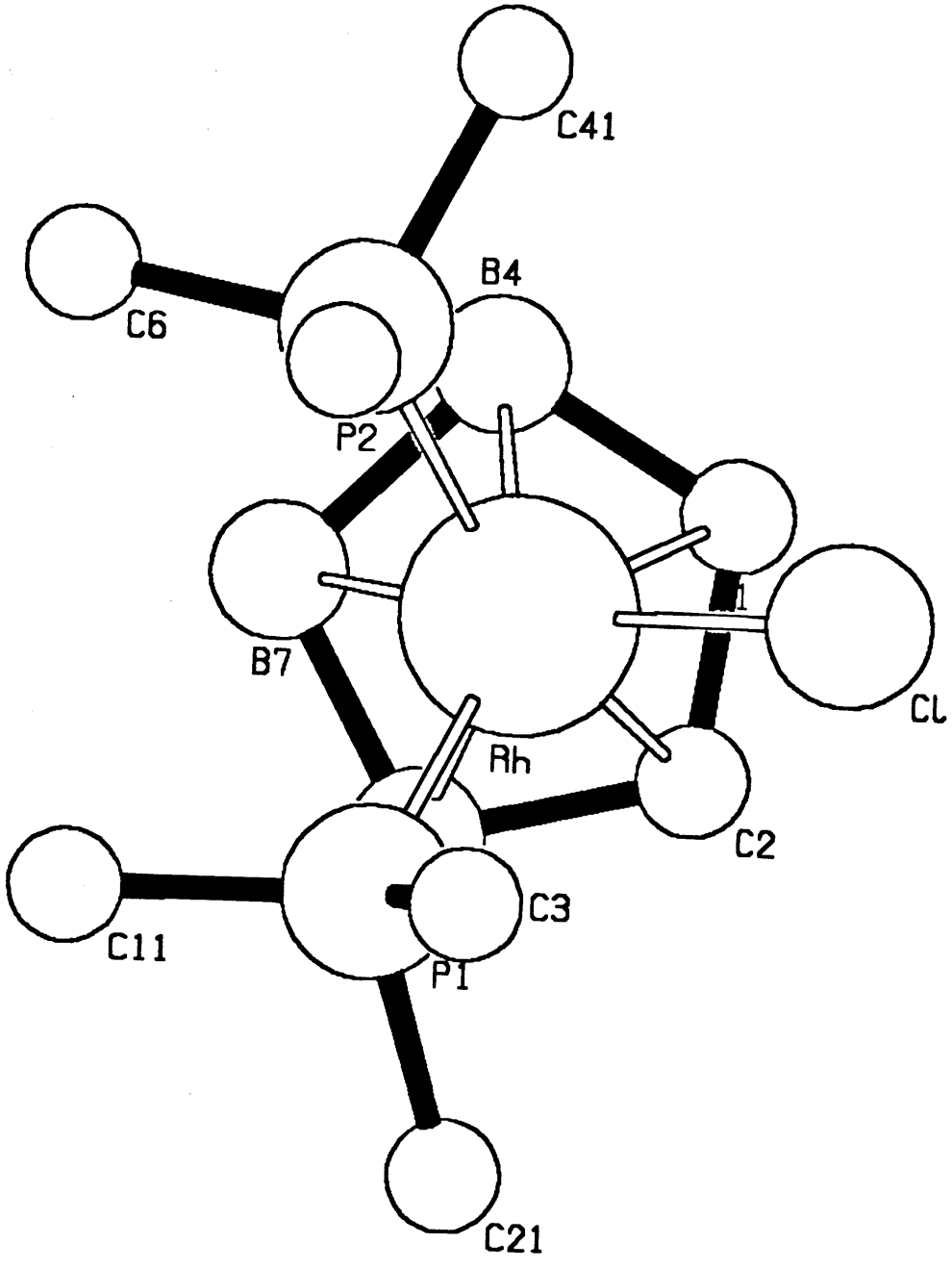

Figure 5.8 A view of the $Rh(PMePh_2)_2Cl$ unit above the C_2B_3 face of *closo*-[3,3-$(PMePh_2)_2$-3-Cl-3,1,2-$RhC_2B_9H_{11}$] (174).

Table 5.7 Important bond distances (Å) for *closo*-[3,3-$(PMePh_2)_2$-3-Cl-3,1,2-$RhC_2B_9H_{11}$] (174).

Rh(3)-Cl	2.4205(8)	Rh(3)-P(1)	2.3500(9)
Rh(3)-P(2)	2.3414(9)	Rh(3)-C(1)	2.208(3)
Rh(3)-C(2)	2.205(3)	Rh(3)-B(4)	2.254(4)
Rh(3)-B(7)	2.244(4)	Rh(3)-B(11)	2.223(4)
P(1)-C(11)	1.822(4)	P(1)-C(21)	1.838(4)
P(1)-C(3)	1.818(4)	P(2)-C(41)	1.836(4)
P(2)-C(51)	1.830(3)	P(2)-C(6)	1.809(4)
C(1)-C(2)	1.618(5)	C(1)-B(4)	1.698(6)
C(1)-B(5)	1.690(6)	C(1)-B(6)	1.733(6)
C(2)-B(6)	1.724(5)	C(2)-B(10)	1.694(5)
C(2)-B(11)	1.702(5)	B(4)-B(5)	1.790(6)
B(4)-B(7)	1.825(6)	B(4)-B(8)	1.749(6)
B(5)-B(6)	1.755(7)	B(5)-B(8)	1.754(7)
B(5)-B(9)	1.761(7)	B(6)-B(9)	1.763(7)
B(6)-B(10)	1.748(7)	B(7)-B(8)	1.793(6)
B(7)-B(11)	1.807(6)	B(7)-B(12)	1.796(6)
B(8)-B(9)	1.774(7)	B(8)-B(12)	1.779(7)
B(9)-B(10)	1.769(7)	B(9)-B(12)	1.770(7)
B(10)-B(11)	1.786(6)	B(10)-B(12)	1.765(7)
B(11)-B(12)	1.755(6)		

Table 5.8 Important bond angles (°) for *closo*-[3,3-$(PMePh_2)_2$-3-Cl-3,1,2-$RhC_2B_9H_{11}$] (174).

Cl-Rh(3)-P(1)	87.67(3)	Cl-Rh(3)-P(2)	92.00(3)
Cl-Rh(3)-C(1)	87.03(9)	Cl-Rh(3)-C(2)	91.90(9)
Cl-Rh(3)-B(4)	118.59(12)	Cl-Rh(3)-B(7)	164.49(11)
Cl-Rh(3)-B(11)	130.17(11)	P(1)-Rh(3)-P(2)	92.68(3)
P(1)-Rh(3)-C(1)	150.50(10)	P(1)-Rh(3)-C(2)	108.28(9)
P(1)-Rh(3)-B(4)	153.47(12)	P(1)-Rh(3)-B(7)	106.59(12)
P(1)-Rh(3)-B(11)	85.15(11)	P(2)-Rh(3)-C(1)	116.49(10)
P(2)-Rh(3)-C(2)	158.82(9)	P(2)-Rh(3)-B(4)	83.24(12)
P(2)-Rh(3)-B(7)	93.37(12)	P(2)-Rh(3)-B(11)	137.51(11)
C(1)-Rh(3)-C(2)	43.01(13)	C(1)-Rh(3)-B(4)	44.74(15)
C(2)-Rh(3)-B(11)	45.21(14)	B(4)-Rh(3)-B(7)	47.89(17)
B(7)-Rh(3)-B(11)	47.73(16)	Rh(3)-P(1)-C(11)	113.98(12)
Rh(3)-P(1)-C(21)	113.91(12)	Rh(3)-P(1)-C(3)	118.09(13)
C(11)-P(1)-C(21)	106.58(18)	C(11)-P(1)-C(3)	104.96(19)
C(21)-P(1)-C(3)	97.52(17)	Rh(3)-P(2)-C(41)	115.29(13)
Rh(3)-P(2)-C(51)	118.95(11)	Rh(3)-P(2)-C(6)	112.77(13)
C(41)-P(2)-C(51)	99.96(15)	C(41)-P(2)-C(6)	104.91(18)
C(51)-P(2)-C(6)	103.08(17)	Rh(3)-C(1)-C(2)	68.40(17)
Rh(3)-C(1)-B(4)	69.06(19)	C(2)-C(1)-B(4)	112.9(3)
C(2)-C(1)-B(6)	61.82(23)	B(4)-C(1)-B(5)	63.8(3)
B(5)-C(1)-B(6)	61.7(3)	Rh(3)-C(2)-C(1)	68.59(18)
Rh(3)-C(2)-B(11)	67.95(18)	C(1)-C(2)-B(6)	62.39(24)
C(1)-C(2)-B(11)	111.1(3)	B(6)-C(2)-B(10)	61.5(3)
B(10)-C(2)-B(11)	63.46(24)	Rh(3)-B(4)-C(1)	66.20(18)
Rh(3)-B(4)-B(7)	65.78(18)	C(1)-B(4)-B(5)	57.89(24)
C(1)-B(4)-B(7)	104.5(3)	B(5)-B(4)-B(8)	59.4(3)
B(7)-B(4)-B(8)	60.2(3)	C(1)-B(5)-B(4)	58.34(23)
C(1)-B(5)-B(6)	60.38(25)	B(4)-B(5)-B(8)	59.2(3)

B(6)-B(5)-B(9)	60.2(3)	B(8)-B(5)-B(9)	60.6(3)
C(1)-B(6)-C(2)	55.79(21)	C(1)-B(6)-B(5)	57.96(25)
C(2)-B(6)-B(10)	58.39(23)	B(5)-B(6)-B(9)	60.1(3)
B(9)-B(6)-B(10)	60.5(3)	Rh(3)-B(7)-B(4)	66.34(17)
Rh(3)-B(7)-B(11)	65.53(17)	B(4)-B(7)-B(8)	57.82(24)
B(4)-B(7)-B(11)	105.5(3)	B(8)-B(7)-B(12)	59.4(3)
B(11)-B(7)-B(12)	58.30(24)	B(4)-B(8)-B(5)	61.5(3)
B(4)-B(8)-B(7)	62.01(24)	B(5)-B(8)-B(9)	59.9(3)
B(7)-B(8)-B(12)	60.4(3)	B(9)-B(8)-B(12)	59.8(3)
B(5)-B(9)-B(6)	59.7(3)	B(5)-B(9)-B(8)	59.5(3)
B(6)-B(9)-B(10)	59.3(3)	B(8)-B(9)-B(12)	60.3(3)
B(10)-B(9)-B(12)	59.8(3)	C(2)-B(10)-B(6)	60.08(24)
C(2)-B(10)-B(11)	58.49(22)	B(6)-B(10)-B(9)	60.2(3)
B(9)-B(10)-B(12)	60.1(3)	B(11)-B(10)-B(12)	59.23(24)
Rh(3)-B(11)-C(2)	66.83(17)	Rh(3)-B(11)-B(7)	66.74(18)
C(2)-B(11)-B(7)	105.8(3)	C(2)-B(11)-B(10)	58.05(22)
B(7)-B(11)-B(12)	60.52(25)	B(10)-B(11)-B(12)	59.79(25)
B(7)-B(12)-B(8)	60.2(3)	B(7)-B(12)-B(11)	61.18(24)
B(8)-B(12)-B(9)	60.0(3)	B(9)-B(12)-B(10)	60.0(3)
B(10)-B(12)-B(11)	60.98(24)		

Coordination about the rhodium atom could be described as *pseudo*-octahedral for the $RhClP_2$ unit with bonds to P(1), P(2), Cl and multicentre bonds to C(1), C(2), B(7), B(4) and B(11). The *pseudo*-octahedral description is supported by some of the angles around the rhodium atom which are close to 90° *e.g.* Cl-Rh(3)-P(1) 87.67(3)° and Cl-Rh(3)-P(2) 92.00(3)°. The orientation of the $Rh(PMePh_2)_2Cl$ unit above the C_2B_3 face, Figure 5.8, is as expected from MNDO calculations and has been discussed in detail for the corresponding $RhHP_2$ unit, (see chapter 2).[162]

The Rh-Cl distance of 2.4205(8) Å in (174) is slightly longer than the average bond distance of 2.377 Å reported in the literature,[206] and longer than the terminal Rh-Cl distances observed in two recently characterised rhodathiaboranes *i.e.* 2.356(2) Å in *closo*-[2,3-$(PPh_3)_2$-3-Cl-μ-2,3-Cl-2-$(Ph_2PC_6H_4)$-2,3,1-$Rh_2SB_9H_8$][2] and 2.3710(10)

Å in [8,8,10-$(PPh_3)_3$-8-H-10-Cl-8,10,7,9-$Rh_2S_2B_7H_7$].[223] The *exo*-cage Rh-Cl bond distances in rhodacarboranes have been observed to vary from 2.299(1) Å in *closo*-[2-PPh_3-2-Cl-2,1,7-$RhC_2B_9H_{11}$] (214),[48] to 2.525(2) Å in [NMe_4][RhCl{7,8-μ-$S(CH_2CH_2)S$-$C_2B_9H_{10}$}{σ-7,8-μ-$S(CH_2CH_2)S$-$C_2B_9H_9$}] (215).[224] Examples of Rh-Cl bond distances reported in non-cluster compounds have been observed to vary from 2.3439(14) Å in [$RhCl_2(NO)(PPh_3)_2$][227] to 3.3967(11) Å in [(η^5-Cp^*)RhCl](μCl)$_2$.[228]

Table 5.9 Bond distances for compound (174) and four related 12 vertex rhodacarboranes [2-PPh_3-2-Cl-2,1,7-$RhC_2B_9H_{11}$] (214),[48] *closo*-[1-Me-2,2-$(PEt_3)_2$-2-H-8-Ph-2,1,8-$RhC_2B_9H_9$] (216),[225] *closo*-[3-PPh_3-3-(η^3-C_3H_5)-3,1,2-$RhC_2B_9H_{11}$] (217)[226] and *closo*-[3-{η^2-S_2CH}-3-PPh_3-3,1,2-$RhC_2B_9H_{11}$] (218).[2]

No.	Rh-P/Å	Rh-C/Å	Rh-B/Å	C-B/Å	B-B/Å
174	2.3500(9) 2.3414(9)	2.208(3) 2.205(3)	2.223(4)- 2.254(4)	1.690(6)- 1.733(6)	1.748(7)- 1.825(6)
214	2.329(1)	2.215(4)	2.106(5)- 2.151(5)	1.675(6)- 1.731(6)	1.749(7)- 1.887(7)
216	2.357(1) 2.346(1)	2.332(4)	2.159(5)- 2.221(5)	1.681(6)- 1.745(7)	1.736(8)- 1.839(7)
217	2.349(1)	2.212(4) 2.227(4)	2.180(5)- 2.277(5)	1.690(7)- 1.738(6)	1.753(8)- 1.807(7)
218	2.374(1)	2.195(3) 2.201(3)	2.204(3)- 2.205(3)	1.683(3)- 1.723(4)	1.746(4)- 1.822(4)

Compound (214), *precloso*-[2-PPh_3-2-Cl-2,1,7-$RhC_2B_9H_{11}$] is unusual in that it is a sixteen electron Rh complex. Skeletal electron counting[88] suggests that (214) contains 12 electron pairs for skeletal bonding and should exhibit *precloso* geometry.[48] It has been suggested that the effective atomic number of the metal centre must be considered in order to determine the geometry of the polyhedron and the formally 16-

electron Rh(III) might actually donate electron density to provide thirteen skeletal electron pairs for cage bonding and thus the complex exhibits a *closo* geometry.[48] Since the structure of (214) is unambiguously that of the 12-vertex polyhedron, it may be concluded that the electron deficiency of (214) is "metal centre" and the molecule suffers little polyhedral distortion.[48] It is also clear, however, that any alternative to the dodecahedron would be highly unlikely, for example the $B_{12}Cl_{12}$ and $[B_{12}Cl_{12}]^{2-}$ clusters both have dodecahedral geometries.[229]

The Rh-P distances in (174) differ slightly {2.3500(9) and 2.3414(9) Å} but are typical of Rh-P distances in 12 vertex rhodacarboranes, Table 5.9.

The Rh-C bond distances of 2.208(3) and 2.205(3) Å are similar to those in (214) of 2.215(4) and 2.165(4) Å and are within the range of Rh-C bond distances, of typical 12 vertex rhodacarboranes, Table 5.9.[206]

The Rh-B bond distances of 2.254(4), 2.244(4) and 2.223(4) Å are the largest range of Rh-B distances of the typical 12 vertex rhodacarboranes in Table 5.9, but are within the accepted range of rhodium boron bond distances.[206]

The C-C distance of 1.618(5) Å is similar to the C-C bond distance in *closo*-[3-PPh_3-3-(η^3-C_3H_5)-3,1,2-$RhC_2B_9H_{11}$ (217) of 1.601(6) Å.[226]

The C-B bond distances range from 1.690(6)-1.733(6) Å, which are within the range of C-B distances of the typical rhodacarboranes in Table 5.9. The distances are similar to those in *closo*-[3-{η^2-S_2CH}-3-PPh_3-3,1,2-$RhC_2B_9H_{11}$] (218) which range from 1.683(3)-1.723(4) Å.[2] The largest C-B distances observed in (174) are for C(1)-B(6) {1.733(6)Å} and C(2)-B(6) {1.724(5) Å} where B(6) is the unique boron atom bonded to both carbon atoms.

The B-B bond distances range from 1.748(7)-1.825(6) Å which is within the accepted range for metallaheteroboranes,[103] and are within the range of the B-B distances of the typical 12 vertex rhodacarboranes in Table 5.9.

5.3 SUMMARY AND CONCLUSIONS

Three metallaheteroborane complexes were prepared with *exo*cage metal halogen bonds. The two rhodium-chloride complexes *closo*-[3,3-$(PMePh_2)_2$-3-Cl-3,1,2-$RhC_2B_9H_{11}$] (174) and *closo*-[3,3-$(PMePh_2)_2$-3-Cl-3,1,2-$RhAs_2B_9H_9$] (194) were synthesised in 96.2 and 62.9% yields respectively from the reactions between $PMePh_2$, CH_2Cl_2 and *closo*-[3-{η^2-SC(H)NPh}-3-PPh_3-3,1,2-$RhC_2B_9H_{11}$] (197) or *closo*-[3-{η^2-SC(H)NPh}-3-PPh_3-3,1,2-$RhAs_2B_9H_9$](198). When the reaction of (197) was carried out with irradiation provided by a 60 Watt light there was a marked increase in the yield. This suggested that the reactions were at least partly photolytic in nature.

The reaction of Tl[9-SMe_2-7,8-$C_2B_9H_{10}$] and [$Pd(PPh_3)_2I_2$] in refluxing CH_2Cl_2 for 2.5h resulted in the formation of *closo*-[3-PPh_3-3-I-4-SMe_2-3,1,2-$PdC_2B_9H_{10}$] (173) in 81.3% yield.

Two cationic metallacarboranes, *closo*-[3-PPh_3-3-Bu^{t}NC-4-SMe_2-3,1,2-$PdC_2B_9H_{10}$][BF_4] (195) and *closo*-[3,3-$(PMePh_2)_2$-3-Bu^{t}NC-3,1,2-$RhC_2B_9H_{11}$][BF_4] (196), were synthesised from reactions of *closo*-[3-PPh_3-3-I-4-SMe_2-3,1,2-$PdC_2B_9H_{10}$] (173) and *closo*-[3,3-$(PMePh_2)_2$-3-Cl-3,1,2-$RhC_2B_9H_{11}$] (174). Both reactions were carried out in toluene with one equivalent of Ag[BF_4] at ambient temperature for 5 minutes. A slight excess of Bu^{t}NC was added immediately after precipitation of AgX to stabilise the cationic products. Neither of compounds (195) and (196) were stable in solution for more than 8 hours. The tendency to decompose made purification of (195) and (196) difficult.

All the above compounds were isolated as the sole major products of the reactions and were characterised by spectroscopic methods and elemental analysis. Single crystal X-ray analyses of (173) and (174) were carried out to confirm the exact nature of the cluster and *exo*cluster ligand bonding.

The single crystal X-ray analyses of *closo*-[3-PPh_3-3-I-4-SMe_2-3,1,2-$PdC_2B_9H_{10}$] (173) and *closo*-[3,3-$(PMePh_2)_2$-3-Cl-3,1,2-$RhC_2B_9H_{11}$] (174) confirmed that the structures had *closo* cage geometries based on a twelve vertex distorted dodecahedron with the metal and carbon atoms in adjacent positions.

Infrared spectra of (173), (174), (194), (195) and (196) contained characteristic B-H bands and bands due to phosphine ligands. Additionally, compounds (195) and (196) contained characteristic bands associated with Bu^{t}NC and $[BF_4]^-$. No B-H-B, M-H-B or M-H bands were observed.

The ^{11}B spectra of *closo*-[3-PPh_3-3-I-4-SMe_2-3,1,2-$PdC_2B_9H_{10}$] (173) showed peaks in an intensity of 1:1:1:1:1:1:2:1. In the case of *closo*-[3,3-$(PMePh_2)_2$-3-Cl-3,1,2-$RhC_2B_9H_{11}$] (174) the ^{11}B resonances were tentatively assigned by comparison with the similar previously reported rhodacarboranes, *closo*-[3,3-$(PPh_3)_2$-3-H-3,1,2-$RhC_2B_9H_{11}$] (59), *closo*-[3-(η^5-Cp*)-3,1,2-$RhC_2B_9H_{11}$] (199) and *precloso*-[2-PPh_3-2-Cl-2,1,7-$RhC_2B_9H_{11}$] (200). The ^{11}B NMR spectra of *closo*-[3-PPh_3-3-Bu^{t}NC-4-SMe_2-3,1,2-$PdC_2B_9H_{10}$][BF_4] (195) showed eight peaks in an intensity pattern of 1:1:1:2:2:1:1:1. The signal of intensity 1B at δ +0.1 ppm was sharper than the others and was assigned to the $[BF_4]^-$ anion. The ^{11}B NMR spectra of *closo*-[3-PPh_3-3-Bu^{t}NC-3,1,2-$RhC_2B_9H_{11}$][BF_4] (196) showed seven peaks in an intensity pattern of 1:1:1:4:1:1:1. The signal of intensity 1B at δ -0.7 ppm was notably much sharper than the others and was assigned to the $[BF_4]^-$ anion. In general even though the ^{11}B spectra of (195) and (196) are not very informative they have similar intenstity patterns and both spectra are consistent with a RhC_2B_9 *closo* cation and a $[BF_4]^-$ anion and both spectra have a general appearence very like the ^{11}B spectra of the reported palladatelluraboranes.[3]

5.4 EXPERIMENTAL

5.4.1 General Methodology

All reactions were carried out under an inert atmosphere but products were isolated and manipulated in air. Thin layer chromatography (tlc), preparative thin layer chromatography (plc) and all spectroscopic and analytical analyses were carried out as stated in section 4.3.1.

Single crystal X-ray analyses were performed by Professor George Ferguson and Dr. John Gallagher, University of Guelph, Canada (see section 4.3.1 for details).

Dr. J.D. Kennedy, University of Leeds, recorded the ^{31}P, ^{11}B and ^{1}H NMR spectra on a BRUKER AM 400 instrument.

The compounds Tl[9-SMe_2-7,8-*nido*-$C_2B_9H_{10}$][216] and [$Pd(PPh_3)_2I_2$][209] were prepared according to literature methods. The compounds *closo*-[3-{η^2-SC(H)NPh}-3-(PPh_3)-3,1,2-$RhAs_2B_9H_9$] (198) and *closo*-[3-{η^2-SC(H)NPh}-3-(PPh_3)-3,1,2-$RhC_2B_9H_{11}$] (197) were prepared according to methods outlined elsewhere in this work (sections 6.4.2 and 6.4.6). Methyldiphenylphosphine and silver tetrafluoroborate were used as supplied by Aldrich Chemical Company Ltd.

5.4.2 Reaction between Tl[9-SMe_2-7,8-*nido*-$C_2B_9H_{10}$] and [$Pd(PPh_3)_2I_2$]

To a solution of Tl[9-SMe_2-7,8-*nido*-$C_2B_9H_{10}$] (0.02g, 0.05mmol) in CH_2Cl_2 (10ml) was added a solution of [$Pd(PPh_3)_2I_2$] (0.044g, 0.05mmol) in CH_2Cl_2 (10ml). The mixture was heated at reflux for 2.5h. The dark green solution was concentrated under reduced pressure (rotatory film evaporator, 25°C) and subjected to preparative tlc {CH_2Cl_2 - hexane (3:2)}. The single major band was extracted into CH_2Cl_2 and recrystallised from CH_2Cl_2 - hexane (3:2) as dark green block crystals of *closo*-[3-PPh_3-3-I-4-SMe_2-3,1,2-$PdC_2B_9H_{10}$] (173) (0.028g, 81.3%). (Found: C, 38.4; H, 5.0; I, 18.1, $C_{22}H_{31}B_9IPPdS$ requires C, 38.35; H, 4.5; I, 18.4%). IR: ν_{max}(KBr) 3020(w), 2890(vw), 2555(s) (BH), 2513(vs) (BH), 2499(vs,sh) (BH), 2480(s) (BH), 1465(m), 1420(vs), 1402(m), 1312(w), 1175(w), 1150(w), 1090(s,sh), 1082(s), 1068(m,sh), 1027(m), 1018(m,sh), 990(m), 953(w), 940(vw), 920(vw), 740(s), 698(m,sh), 689(vs) cm^{-1}. NMR data are given in Table 5.2.

5.4.3 X-ray analysis of *closo*-[3-PPh_3-3-I-4-SMe_2-3,1,2-$PdC_2B_9H_{10}$] (173)

Crystal Data: $C_{22}H_{31}B_9IPPdS$, M = 689.11, Orthorhombic, *Pbca*, a = 10.9576(5), b = 16.8316(10), c = 30.2015(17) Å, U = 5570.2(5) $Å^3$, Z = 8, D_c = 1.64 g cm^{-3}, λ(Mo-K_α) = 0.7093 Å, μ(Mo-K_α) = 19 cm^{-1}, F(000) = 2704, T = 294 K, R = 0.030, R_w = 0.039 for 3374 observed reflections.

5.4.4 Reaction between *closo*-[3-{η^2-SC(H)NPh}-3-(PPh_3)-3,1,2-$RhC_2B_9H_{11}$] (197) and $PMePh_2$

Procedure 1

To a solution of *closo*-[3-{η^2-SC(H)NPh}-3-(PPh_3)-3,1,2-$RhC_2B_9H_{11}$] (197) (0.05g, 0.079mmol) in CH_2Cl_2 (20ml) was added $PMePh_2$ (0.158g, 0.79mmol). The mixture was heated at reflux for 48h. The orange solution was concentrated under reduced pressure (rotatory film evaporator, 25°C) and subjected to preparative tlc {CH_2Cl_2 - hexane (3:2)}. The single major band was extracted into CH_2Cl_2 and recrystallised from CH_2Cl_2 - hexane (3:2) as orange block crystals of *closo*-[3,3-($PMePh_2$)$_2$-3-Cl-3,1,2-$RhC_2B_9H_{11}$] (174) (0.042g, 79.6%). (Found: C, 50.45; H, 5.6; Cl, 5.5, $C_{28}H_{37}B_9ClP_2Rh$ requires C, 50.1; H, 5.6; Cl, 5.3%). IR: ν_{max}(KBr) 3012(vw), 2925(w,sh), 2895(m), 2820(w), 2525(vs) (BH), 1565(vw), 1551(vw), 1490(vw), 1462(w), 1418(s), 1359(vw), 1320(w), 1298(vw), 1273(w), 1249(vw), 1180(w), 1147(vw), 1085(s), 1000(vw), 985(w,br), 880(vs), 736(s), 720(s,sh), 683(s) cm^{-1}. NMR data are given in Table 5.3.

Procedure 2

To a solution of *closo*-[3-{η^2-SC(H)NPh}-3-(PPh_3)-3,1,2-$RhC_2B_9H_{11}$] (197) (0.05g, 0.079mmol) in CH_2Cl_2 (20ml) was added $PMePh_2$ (0.158g, 0.79mmol). The mixture was heated at reflux for 48h in the presence of a 60 Watt light bulb 8 cm from the reaction flask. The orange solution was concentrated under reduced pressure (rotatory film evaporator, 25°C) and subjected to preparative tlc {CH_2Cl_2 - hexane (3:2)}. The single major band was extracted into CH_2Cl_2 and recrystallised from CH_2Cl_2 - hexane (3:2) as orange block crystals of *closo*-[3,3-($PMePh_2$)$_2$-3-Cl-3,1,2-$RhC_2B_9H_{11}$] (174) (0.051g, 96.2%). IR and NMR data were identical to those reported in procedure 1.

Procedure 3

To a solution of *closo*-[3-{η^2-SC(H)NPh}-3-(PPh_3)-3,1,2-$RhC_2B_9H_{11}$] (197) (0.05g, 0.079mmol) in CH_2Cl_2 (20ml) was added $PMePh_2$ (0.158g, 0.79mmol). The mixture was heated at reflux for 48h in an aluminium foil covered reaction flask.

The orange solution was concentrated under reduced pressure (rotatory film evaporator, 25°C) and subjected to preparative tlc {CH_2Cl_2 - hexane (3:2)}. The single major band was extracted into CH_2Cl_2 and recrystallised from CH_2Cl_2 - hexane (3:2) as orange block crystals of *closo*-[3,3-$(PMePh_2)_2$-3-Cl-3,1,2-$RhC_2B_9H_{11}$] (174) (0.036g, 67.9%). IR and NMR data were identical to those reported in procedure 1.

5.4.5 X-ray analysis of *closo*-[3,3-$(PMePh_2)_2$-3-Cl-3,1,2-$RhC_2B_9H_{11}$] (174)

Crystal Data: $C_{28}H_{37}B_9ClP_2Rh$, M = 671.19, monoclinic, $P2_1/n$, a = 10.6861(5), b = 16.1880(12), c = 18.8621(10) Å, β = 99.814°, U = 3215.1(3) Å^3, Z = 4, D_c = 1.39 g cm^{-3}, λ(Mo-K$_\alpha$) = 0.7093 Å, μ(Mo-K$_\alpha$) = 7.0 cm^{-1}, F(000) = 1368, T = 294 K, R = 0.031, R_w = 0.034 for 4450 observed reflections.

5.4.6 Reaction between *closo*-[3-{η^2-SC(H)NPh}-3-(PPh_3)-3,1,2-$RhAs_2B_9H_9$] (198) and $PMePh_2$

To a solution of *closo*-[3-{η^2-SC(H)NPh}-3-(PPh_3)-3,1,2-$RhAs_2B_9H_9$] (198) (0.05g, 0.066mmol) in CH_2Cl_2 (20ml) was added $PMePh_2$ (0.132g, 0.66mmol). The mixture was heated at reflux for 48h in the presence of a 60 Watt light source. The orange solution was concentrated under reduced pressure (rotatory film evaporator, 25°C) and subjected to preparative tlc {CH_2Cl_2 - hexane (3:2)}. The single major band was extracted into CH_2Cl_2 and recrystallised from CH_2Cl_2 - hexane (3:2) as orange block crystals of *closo*-[3,3-$(PMePh_2)_2$-3-Cl-3,1,2-$RhAs_2B_9H_9$] (194) (0.033g, 62.9%). (Found: C, 39.7; H, 4.7; Cl, 4.0. $C_{26}H_{35}As_2B_9ClP_2Rh$ requires C, 39.3; H, 4.4; Cl, 4.5%). IR: ν_{max}(KBr) 3003(w), 2885(m), 2818(vw), 2540(s,sh) (BH), 2520(vs) (BH), 2480(s) (BH), 1565(vw), 1550(vw), 1469(m), 1419(vs), 1300(vw), 1278(w), 1273(w), 1180(vw), 1147(w), 1082(s), 1062(m,sh), 998(s), 990(m,sh), 880(vs), 748(m), 738(s), 731(s,sh), 720(m), 689(s) cm^{-1}.

5.4.7 Reaction between *closo*-[3-PPh_3-3-I-4-SMe_2-3,1,2-$PdC_2B_9H_{10}$] (173) and $Ag[BF_4]$

A suspension of $Ag[BF_4]$ (0.028g, 0.145 mmol) in toluene (10ml) was added to a solution of *closo*-[3-PPh_3-3-I-4-SMe_2-3,1,2-$PdC_2B_9H_{10}$] (173) (0.10g, 0.145 mmol) in toluene (10ml). The green solution immediately lightened in colour and a precipitate of AgI was formed. After stirring at room temperature for 5 min an excess of *t*-butylisocyanide (0.0125g, 0.15mmol) was added and the solution immediately changed colour from green to red. The solution was allowed to stir at ambient temperature for 10 min. The solution was filtered under gas in order to remove the AgI precipitate. The precipitate was washed with CH_2Cl_2 and the washings added to the toluene solution. The toluene and CH_2Cl_2 were removed under reduced pressure (rotary film evaporator, 35 and 25°C respectively). Recrystallisation from CH_2Cl_2-hexane {3:2} afforded pink crystals of *closo*-[3-PPh_3-3-Bu^tNC-4-SMe_2-3,1,2-$PdC_2B_9H_{10}$][BF_4] (195) (0.076g, 71.7%) (Found: C, 44.2; H, 5.9; N,1.9, $C_{27}H_{40}B_{10}F_4NPPdS$ requires C, 44.3; H, 5.5; N, 1.9%) IR: ν_{max}(KBr) 3015(w), 2965(w), 2920(w), 2885(m), 2720(w), 2530(s,sh) (BH), 2518(s) (BH), 2500(s,sh) (BH), 2182(s) (N≡C), 1462(m), 1440(w), 1420(m,sh), 1418(s), 1410(m,sh), 1401(w,sh), 1315(vw), 1300(vw), 1268(vw), 1248(vw), 1220(vw), 1175(m), 1082(vs) (BF), 1048(vs) (BF), 1040(vs) (BF), 985(m), 905(w), 790(w), 739(m), 700(m), 685(s) cm^{-1}. NMR data: $^{11}B\{^1H\}$ (CH_2Cl_2, 298K) {ordered as: δ ppm (multiplicity, intensity)} +4.5(s,1B), +0.1(s,1B), -4.2(s,1B), -8.2(s,2B), -10.3(s,2B), -15.8(s,1B), -16.3(s,1B), -21.8(s,1B). ^{31}P ($CDCl_3$, 223K) δ ppm +31.5(s,1P).

5.4.8 Reaction between *closo*-[3,3-$(PMePh_2)_2$-3-Cl-3,1,2-$RhC_2B_9H_{11}$] (174) and $Ag[BF_4]$

A suspension of $Ag[BF_4]$ (0.029g, 0.149 mmol) in toluene (10ml) was added to a solution of *closo*-[3,3-$(PMePh_2)_2$-3-Cl-3,1,2-$RhC_2B_9H_{11}$] (174) (0.1g, 0.149 mmol) in toluene (10ml). The orange solution immediately lightened in colour and a precipitate of AgI was formed. After stirring at room temperature for 5 min an excess of *t*-butylisocyanide (0.0132g, 0.159mmol) was added. The solution was allowed to stir at ambient temperature for 10 min. The solution was filtered under gas in order to remove the AgI precipitate. The precipitate was washed with CH_2Cl_2 and the washings added to the toluene solution. The toluene and CH_2Cl_2 were removed under reduced pressure (rotary film evaporator, 35 and 25°C respectively). The yellow product was dried under vacuum to yield *closo*-[3-PPh_3-3-BuᵗNC-3,1,2-$RhC_2B_9H_{11}$][BF_4] (196) (0.046g, 46.18%). IR: ν_{max}(KBr) 3015(m), 2985(m), 2920(w), 2580(m,sh) (BH), 2542(s) (BH), 2533(s) (BH), 2520(s,sh) (BH), 2500(s,sh) (BH), 2178(s) (N≡C), 1468(m), 1442(w), 1418(s), 1410(w,sh), 1355(m), 1320(w), 1300(w), 1270(w), 1245(w), 1170(m), 1082(vs) (BF), 1052(vs) (BF), 1045(vs) (BF), 988(m), 875(s), 790(w), 735(s), 728(s), 685(s) cm^{-1}. Attempted recrystallisation from CH_2Cl_2-hexane resulted in decomposition. (This prevented the sample from being analysed by elemental analysis). NMR data: $^{11}B\{^1H\}$ (CH_2Cl_2, 298K) {ordered as: δ ppm (multiplicity, intensity)} +11.9(s,1B), +5.4(s,1B), -0.7(s,1B), -3.2(s,4B), -13.1(s,1B), -16.6(s,1B), -16.9(s,1B).

CHAPTER SIX

SYNTHESIS AND CHARACTERISATION OF SOME ISOTHIOCYANATE DERIVATIVES OF RHODAHETEROBORANES

6.1 INTRODUCTION

In recent years, much work has been reported on *closo*-twelve-vertex metallaheteroboranes and in particular rhodaheteroboranes.[2,4,22] Metallaheteroboranes provide a bridge between polyhedral borane chemistry and transition metal chemistry. They serve as models for structural, bonding, and reactivity studies in both organometallic and inorganic cluster chemistry.[39] Additionally, chemists interested in developing homogeneous catalysts for simple organic reactions are beginning to consider metallacarboranes due to their potential chirality, unusual electronic properties and the stability of the carborane cages.[230] More recently the discovery of catabolism-resistant high performance tumour imaging and radiotherapy agents based upon functionalised metallacarboranes has opened up a new field of study in biomedical research.[231,232]

The following introduction (section 6.1.1) initially considers the synthesis and reactivity of twelve-vertex rhodaheteroborane clusters. The majority of the compounds contain two phosphine ligands and one hydride ligand attached to rhodium. Subsequently (section 6.2) this chapter reports the reaction of rhodium hydride bonds with isothiocyanates (RNCS, R = Ph, *p*-tol and Bz) to generate ten new twelve-vertex rhodaheteroborane complexes. A brief introduction (section 6.1.2) to the reactions of transition metal complexes with RNCS is given with examples of complexes containing RNCS based ligands which are related directly and indirectly to the present work.

6.1.1 Twelve-vertex Rhodaheteroboranes

(i) Twelve-vertex Rhodacarboranes

Twelve-vertex rhodacarboranes are well known mainly due to the work of Hawthorne and his group. The first to be synthesised were the hydridorhoda-carboranes *closo*-[3,3-$(PPh_3)_2$-3-H-3,1,2-$RhC_2B_9H_{11}$] (59)[43] and the isomeric *closo*-2,1,7-RhC_2 (219) complex. Compounds (59) and (219) were prepared originally by the reaction of $[Rh(PPh_3)_3Cl]$ with *nido*-[7,8-$C_2B_9H_{12}$]$^-$ or *nido*-[7,9-$C_2B_9H_{12}$]$^-$

respectively, in refluxing MeOH and more recently from refluxing in EtOH.[43,48] Both were characterised spectroscopically and the solid state structure of (59) was established later by X-ray crystallography, Figure 6.1.[48,233] It was considered that the rhodium atom exhibited *pseudo*-octahedral coordination with the carborane cage occupying three coordination sites, and the two phosphine and one hydride ligand occupying the remaining sites. The bonding between the $Rh(PPh_3)_2H$ unit and the B_3C_2 face appeared to be highly symmetrical Rh-B{2.22(1)-2.28(1) Å} and Rh-C{2.22(1)-2.27(1) Å} but there was some C/B disorder in the structure. Apparently, no "slip" distortion of the kind observed in the icosahedral platinacarborane *closo*-$[3,3\text{-}(Et_3P)_2\text{-}3,1,2\text{-}PtC_2B_9H_{11}]$,[162] had occurred in (59). The $Rh(PPh_3)_2H$ unit can be considered as a two electron cluster unit and the *closo* structure is in agreement with the electron count as described by Wade's rules.[88] The source of the hydride ligand has been shown to be the bridging B-H-B of the incoming carborane anion (by D-labelling experiments).[48,205] The complexes (59) and (219) have been found to catalyse deuterium exchange in a variety of substrates including boranes, carboranes and metallacarboranes.

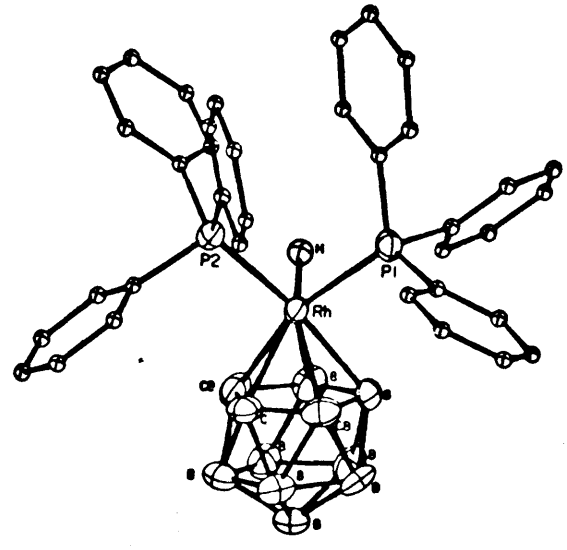

Figure 6.1 Molecular structure of *closo*-$[3,3\text{-}(PPh_3)_2\text{-}3\text{-}H\text{-}3,1,2\text{-}RhC_2B_9H_{11}]$ (59).[48]

The role of (59) and (219) and their derivatives in catalysing a wide variety of reactions of organic substrates has been explored by Hawthorne and his co-workers,[48,225,234] and their work has been summarised in a recent review.[235] A detailed review of RhC_2B_9 chemistry has also been published.[2]

(ii) Twelve-vertex Rhodatelluraboranes

Unlike the twelve-vertex rhodacarboranes discussed above, very little work has been published on twelve-vertex rhodatelluraboranes. There seems to be only three published X-ray structures. The first published structure was of the hydridorhoda-telluraborane *closo*-[2,2-$(PPh_3)_2$-2-H-2,1-$RhTeB_{10}H_{10}$] (220).[4,97] Compound (220) was prepared by the reaction of [$Rh(PPh_3)_3Cl$] with *nido*-[7-$TeB_{10}H_{11}$]$^-$ by stirring in EtOH for 1-3 days at room temperature. Reaction between *nido*-[7-$TeB_{10}H_{11}$]$^-$ and [{Rh(η^5-Cp^*)Cl_2}$_2$] in a 2:1 mole ratio in CH_2Cl_2 at ambient temperature for several days gave air-stable *closo*-[2-(η^5-Cp^*)-1,2-$RhTeB_{10}H_{10}$] (221) in moderate yield.[4,236] The structures of (220) and (221) were established by X-ray crystallography, Figures 6.2 and 6.3 respectively.

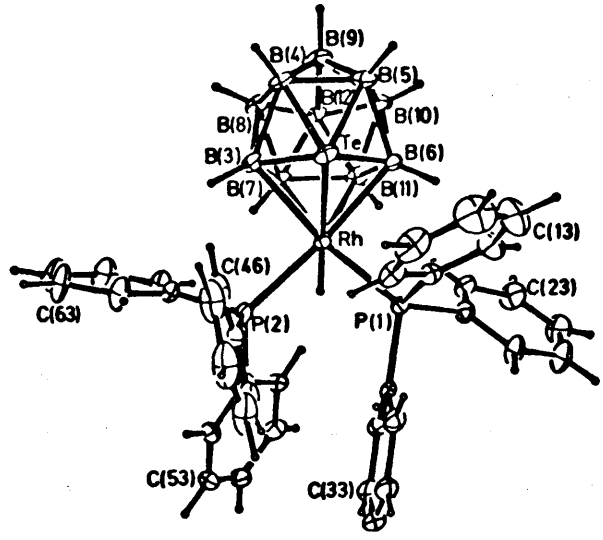

Figure 6.2 Molecular structure of *closo*-[2,2-$(PPh_3)_2$-2-H-2,1-$RhTeB_{10}H_{10}$] (220).[4,97]

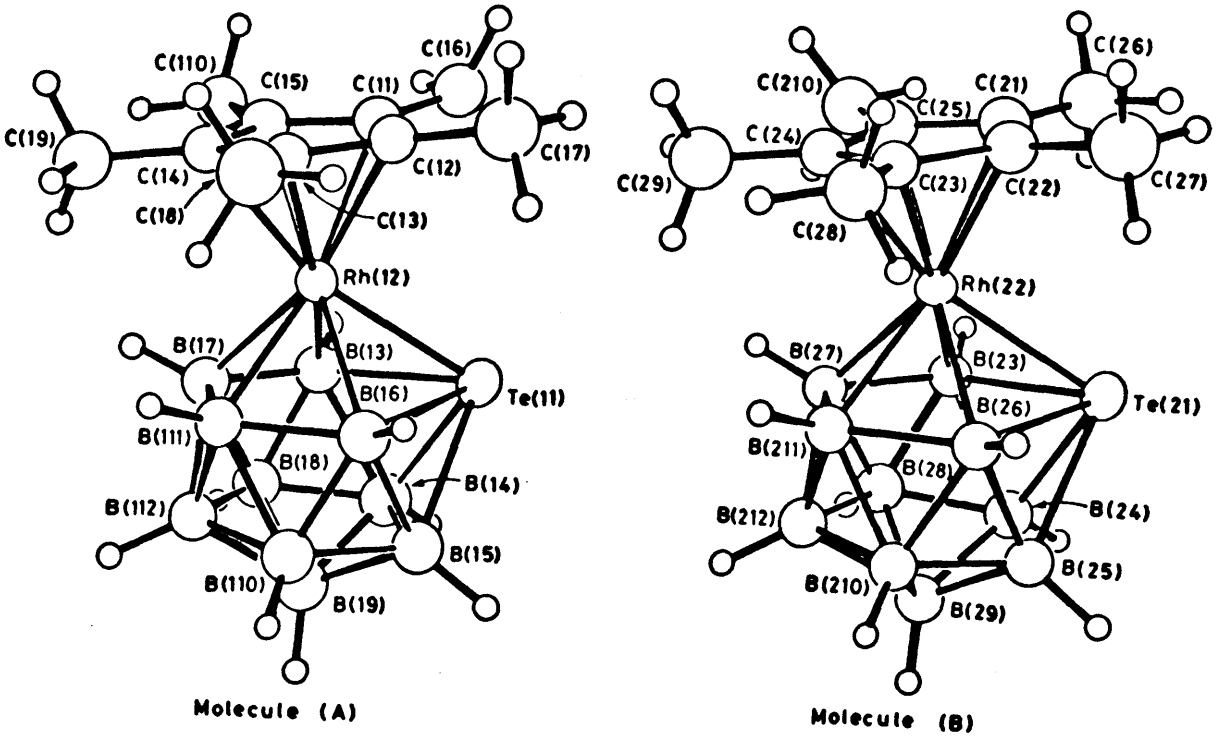

Figure 6.3 Molecular structure of *closo*-[2-(η^5-Cp*)-1,2-RhTe$B_{10}H_{10}$] (221).[4,236]

The reaction of (220) with diphenylacetylene in benzene at 323 K gave the *cyclo*boronated product *closo*-[2-(PPh_3)-2-H-2-($Ph_2PC_6H_4$)-1,2-Te$RhB_{10}H_9$] (222) in moderate yield.[4,237] The structure of (222) has been determined, Figure 6.4. The (P)(P')(H)-ligand conformation about the Rh atom is different from that in (220), Figure 6.2 where the Rh-H vector is *trans* to the Te atom and lies above the mid-point of the B2-B3 bond and the Rh-P1 and Rh-P2 bonds are located above the Te-B1 and Te-B4 bonds. In the cyclised product the position of the Rh-H bond corresponds to a 46° rotation of the Rh-H moiety away from an eclipsed orientation with Rh-Te. It is also worth noting that the cyclic Rh-P-C-C-B system is not quite planar; the Rh atom is 0.24 Å from the best mean P-C-C-B plane.

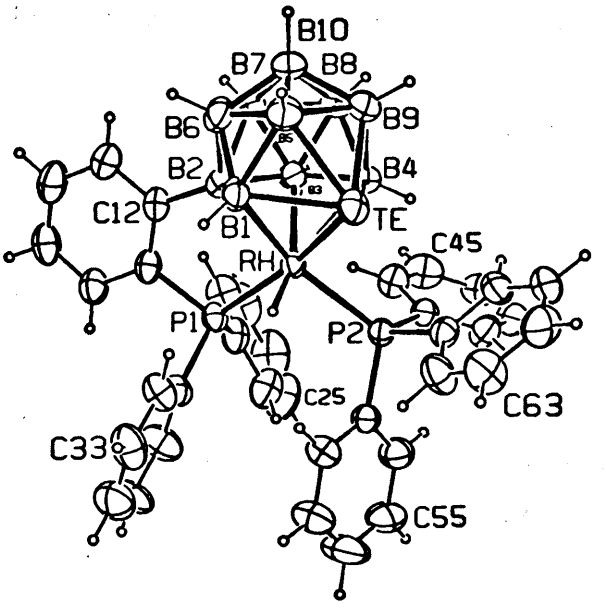

Figure 6.4 **Molecular structure of *closo*-[2-(PPh_3)-2-H-2-($Ph_2PC_6H_4$)-1,2-$TeRhB_{10}H_9$] (222).**[4,237]**

(iii) Twelve-vertex Rhodaarsenaboranes

To date there has been only two twelve-vertex rhodaarsenaboranes reported, *closo*-[3,3-(PPh_3)$_2$-3-H-3,1,2-$RhAs_2B_9H_9$] (58), and *closo*-[3-(η^5-Cp*)-3,1,2-$RhAs_2B_9H_9$] (60).[6,22] Reaction of *nido*-[7,8-$As_2B_9H_{10}$]$^-$ with [$Rh(PPh_3)_3Cl$] in a 1:1 molar ratio in absolute alcohol at room temperature for 24h gave a yellow precipitate of (58) in 98% yield. Reaction of *nido*-[7,8-$As_2B_9H_{10}$]$^-$ with [{$Rh(\eta^5$-Cp*$)Cl_2$}$_2$] in a 2:1 molar ratio in CH_2Cl_2 with ten times excess triethylamine present, at room temperature for 4d and then at reflux for 20 min, afforded (60) in 51% yield. Compounds (58) and (60) were characterised by IR and NMR spectroscopy.[6,22] There has been no reported X-ray crystal structure analysis of any twelve-vertex rhodaarsenaborane.

6.1.2 Reactivity of Transition Metals with Isothiocyanates

The reactivity of isocyanates with transition metal centres has been studied in some detail.[238] However reactions of organometallic complexes with the related isothiocyanates have received little attention.[239-242] The latter are, however, potentially useful reagents for introducing a number of ligands to a metal centre,[243] and isothiocyanates remain very important starting materials for the construction of heterocycles.[244] Because of the poor orbital overlap between carbon and sulphur in isothiocyanates the cleavage of this bond is expected to be facile resulting in the formation of sulfido and isocyanide moieties or more unusual ligands.[243] Recently the reaction of $[Cp_2Ru_2(CO)(\mu\text{-}CO)\{\mu\text{-}C(O)C(Ph)=C(Ph)\}]$ with PhNCS afforded $[Cp_2Ru_2(CO)(\mu\text{-}CO)\{\mu\text{-}SC(Ph)=C(Ph)C(=NPh)\}]$ as a result of alkyne insertion into the carbon-sulphur bond of the isothiocyanate, Figure 6.5.[243]

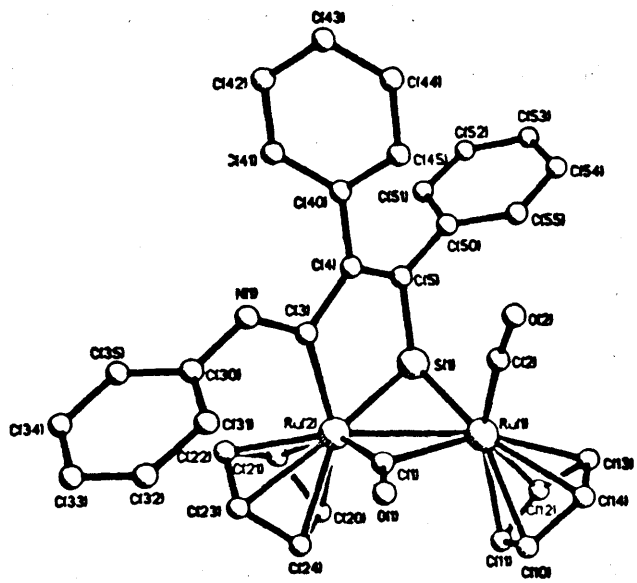

Figure 6.5 Molecular structure of $[Cp_2Ru_2(CO)(\mu\text{-}CO)\{\mu\text{-}SC(Ph)=C(Ph)C(=NPh)\}]$.[243]

The organic isothiocyanates (RNCS) have been shown to undergo many general types of reactions with metal complexes.[245] In the first example the molecule can bind to a metal *via* the carbon-sulphur double bond forming a three centred M-C-S metallacycle, Figure 6.6.[246,247] This coordination mode (termed η^2 and illustrated in Figure 6.6) although quite common for CS_2,[2] is somewhat rarer for isothiocyanate molecules.[245]

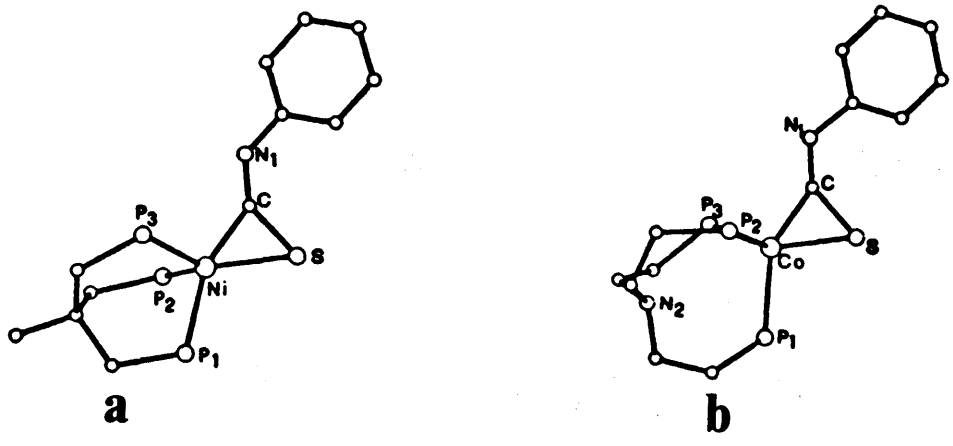

Figure 6.6 **(a) View of the skeleton of (triphos)Ni(η^2-SCNPh)[246,247] triphos=1,1,1-tris{(diphenylphosphino)methyl}ethane; (b) View of $(np)_3Co(\eta^2$-SCNPh) np_3=tris{2-(diphenylphosphino)ethyl}amine.[246]**

Isothiocyanates may also undergo condensation reactions in the presence of metal complexes yielding species in which two or three isothiocyanate molecules are fused and attached to the metal.[245,248] This often occurs with the extrusion of sulphur. The addition of phenylisothiocyanate to $[W(\eta^5\text{-}Cp)_2(CO)]$ forms $[W(\eta^5\text{-}Cp)_2\{C(S)N(Ph)C(NPh)\}]$ (223) in 30% yield, Figure 6.7(a).[249] The proposed mechanism for the formation of (223) first involved the addition of one molecule of PhNCS with the elimination of a molecule of COS to form $[W(\eta^5\text{-}Cp)_2(CNPh)]$, on addition of a second equivalent of PhNCS this could lead to the formation of (223).[249] This proposed mechanism was strongly supported by a GC study which indicated the generation of one mole of COS formed for each mole of $[W(\eta^5\text{-}Cp)_2(CO)]$ that reacted.[249] Multiple C=S bond cleavage takes place at ambient temperatures when PhNCS reacts with $[Co(\eta^5\text{-}Cp)_2(C_2H_4)_2]$ giving the five membered metallacyclic complex $[Co(\eta^5\text{-}Cp)_2\{C(NPh)NPhC(S)S\}(CNPh)]$, Figure 6.7(b).[248] The structure shows that three isothiocyanate ligands have combined and one sulphur atom extruded. The five-membered CoCNCS metallacyclic ring is planar.

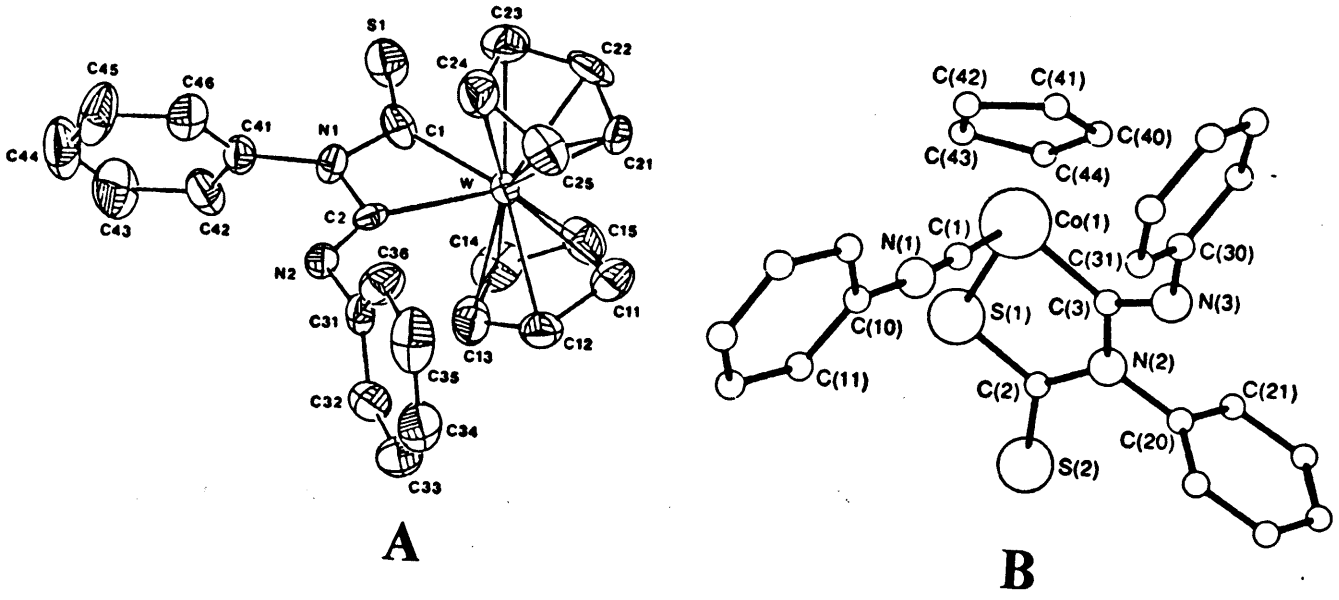

Figure 6.7 **(a) Molecular structure of $[W(\eta^5\text{-}Cp)_2\{C(S)N(Ph)C(NPh)\}]$ (223).[249] (b) Molecular structure of $[Co(\eta^5\text{-}Cp)_2\{C(NPh)NPhC(S)S\}(CN\text{-}Ph)]$.[248]**

Several disproportionation reactions can readily be envisaged as proceeding by C-S bond cleavage and may result in products in which the isocyanide and dithiocarbamato ligands remain coordinated to the same metal,[250-253] or products in which the sulphur atom and the isocyanide ligand are both coordinated to the metal,[254,255] Figure 6.8, or products in which only one remains coordinated to the metal,[250-252,256-259] Figures 6.9-6.11.

Reaction of equimolar quantities of $[Fe(CO)_5]$ and PhNCS under UV irradiation produced $[Fe_3(CO)_8(CNPh)(\mu_3\text{-}S)_2]$ (224) in 14% yield.[254] The crystal structure of (224) was determined with X-ray diffraction, Figure 6.8(a).

The slow addition of EtNCS to $[Co(\eta^5\text{-}Cp)(PPh_3)_2]$ in benzene at room temperature gave $[Co_3(\eta^5\text{-}Cp)_3(\mu_3\text{-}S)(\mu_3\text{-}CNEt)]$ in 60% yield. The molecular structure is based on a Co_3 triangle capped on one side by a μ_3-CNEt ligand and on the other by a μ_3-S with a η^5-Cp group coordinated to each cobalt, Figure 6.8(b).[255]

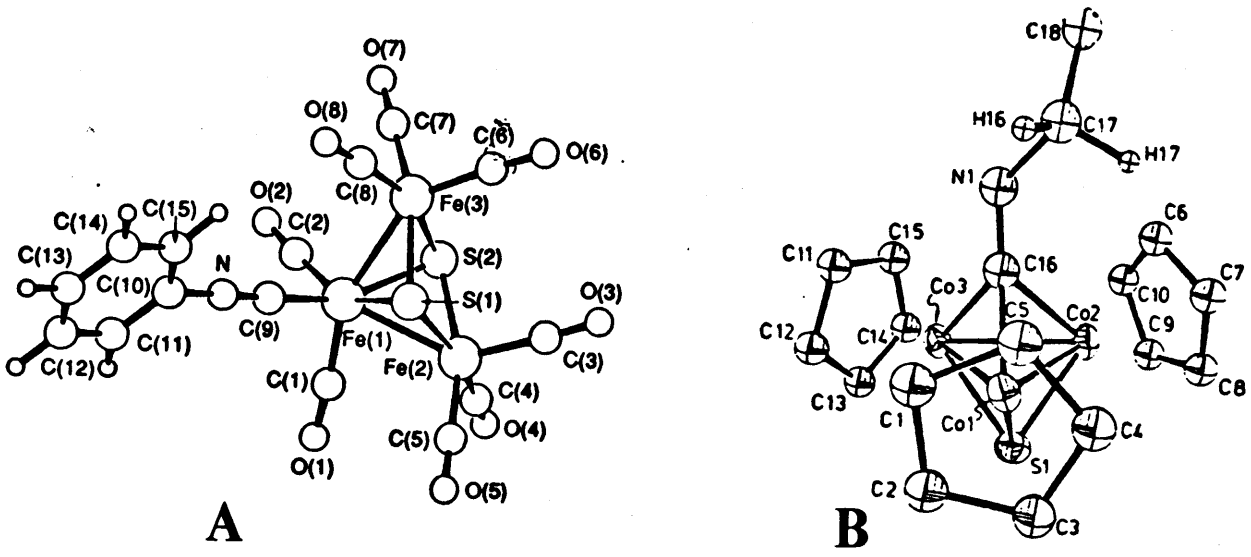

Figure 6.8 **(a) Molecular structure of $[Fe_3(CO)_8(CNPh)(\mu_3\text{-}S)_2]$ (224).[254]**
(b) Molecular structure of $[Co_3(\eta^5\text{-}Cp)_3(\mu_3\text{-}S)(\mu_3\text{-}CNEt)]$.[255]

Reaction of a 1:1 mole ratio of $[(\eta^5\text{-}Cp^*)(CO)_2Mo]_2$ and MeNCS in toluene at 100° for 15 h resulted in the formation of $[(\eta^5\text{-}Cp^*)_2(CO)_4Mo_2(\mu,\eta^2\text{-}C{\equiv}NMe)]$ in 25% yield, Figure 6.9.[258]

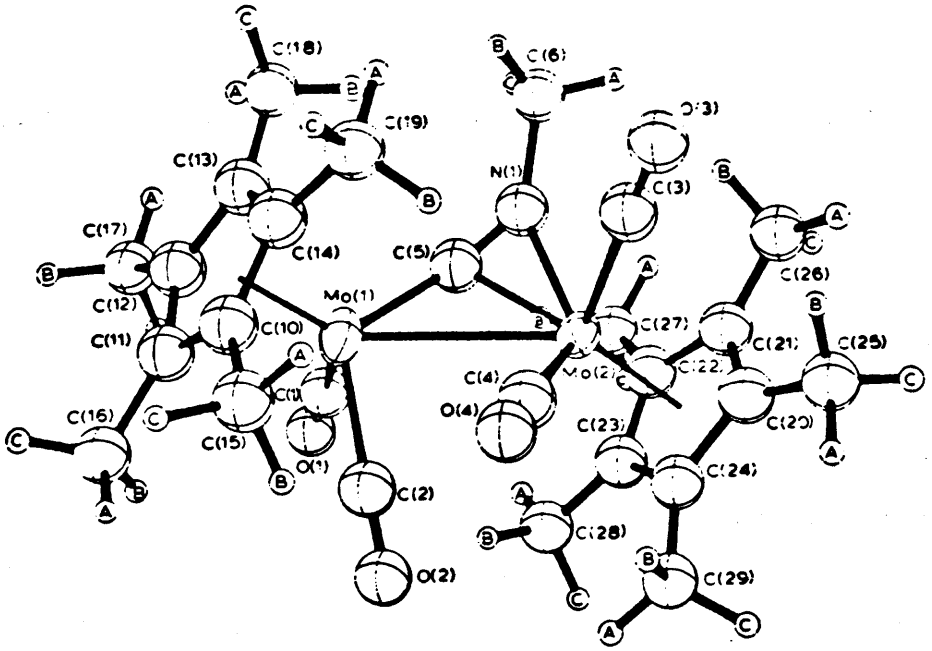

Figure 6.9 Molecular structure of $[(\eta^5\text{-}Cp^*)_2(CO)_4Mo_2(\mu,\eta^2\text{-}C{\equiv}NMe)]$.[258]

Another common reaction of isothiocyanates is a disproportionation reaction which yields isocyanide and sulphide groups which react further in the presence of excess isothiocyanate to afford dithiocarbamato groups. Reaction of a 3:1 molar ratio of PhNCS and $[(PPh_3)_2Cu(BH_4)]$ in CH_2Cl_2 for 2h resulted in the formation of yellow air-stable crystals of $[Cu(PPh_3)_2\{\eta^2\text{-}S_2CN(H)Ph\}]$ in 80% yield, Figure 6.10.[257]

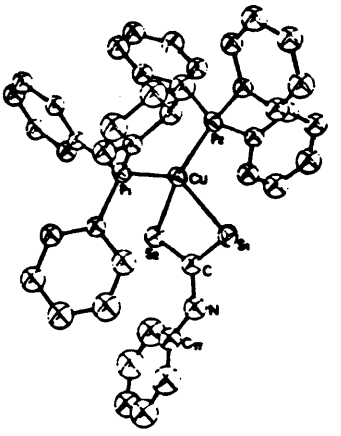

Figure 6.10 Molecular structure of $[Cu(PPh_3)_2\{\eta^2\text{-}S_2CN(H)Ph\}]$.[257]

The reaction of $[Re(CO)_2(PPh_3)_2(OCHNC_6H_4Me\text{-}p)]$ with a large excess of PhNCS in wet benzene resulted in the formation of the monothio- and dithiocarbamate complexes $[Re(CO)_2(PPh_3)_2\{O(S)C(NHPh)\}]$ (225) and $[Re(CO)_2(PPh_3)_2\text{-}\{S_2C(NHPh)\}]$ (226). The formation of complex (226) proceeds *via* the intermediate formation of (225). A mixture of complexes of (225) and (226) gives rise to a compound, which X-ray analysis formulated as $[Re(CO)_2(PPh_3)_2\{S_2C(NHPh)\}]\bullet[Re\text{-}(CO)_2(PPh_3)_2\{O(S)C(NHPh)\}]$ where discrete molecules of two isostructural rhenium complexes are co-crystallised in the monoclinic cell, Figure 6.11.[256]

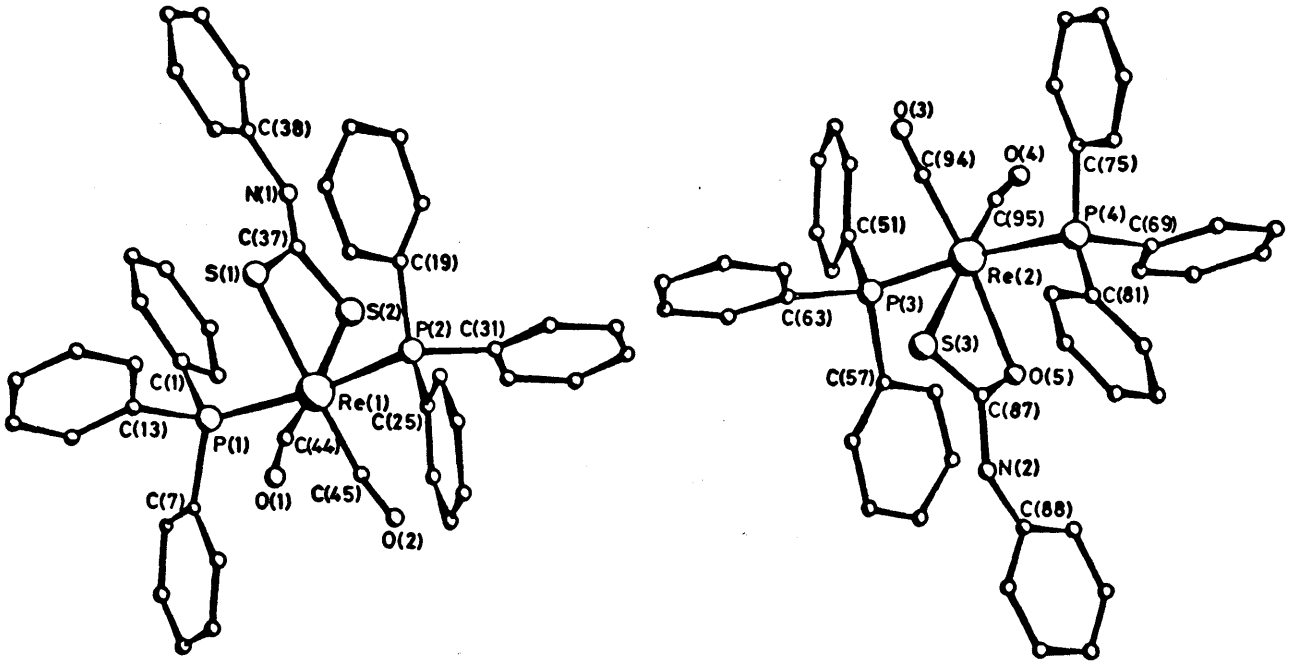

Figure 6.11 Crystal structure of co-crystallised $[Re(CO)_2(PPh_3)_2\{S_2C(NHPh)\}]\bullet[Re(CO)_2(PPh_3)_2\{O(S)C(NHPh)\}]$.[256]

A reaction of isothiocyanates with metal hydrides which involves the migration of the hydride ligand to the carbon atom of the isothiocyanate to form a thioformamido ligand $[SC(H)NR]^-$ has been reported, Figures 6.12 and 6.13.[260,261] A mixture of $Cp_2Zr(H)Cl$ and PhNCS in a 1:1 molar ratio at 10°C in thf for 20 minutes afforded the N,S-containing zirconacycle complex $[ZrCl(\eta^5\text{-}Cp)_2\{\eta^2\text{-}SC(H)NPh\}]$ in 68% yield, Figure 6.12.[261]

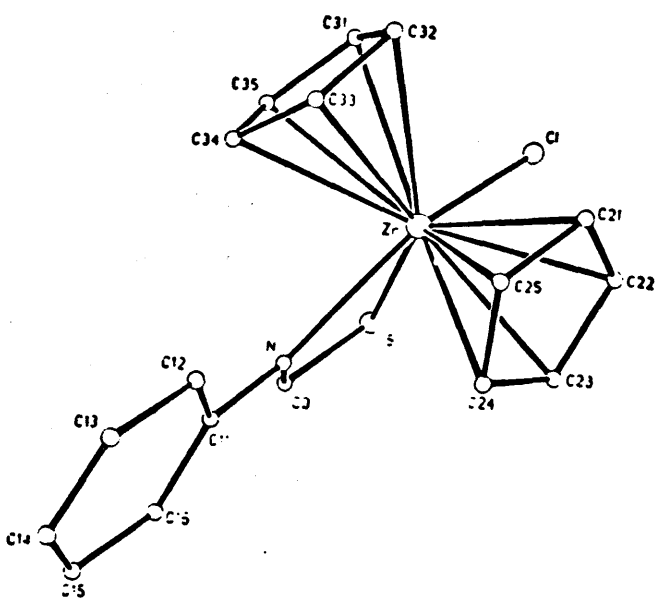

Figure 6.12 Molecular structure of $[ZrCl(\eta^5\text{-}Cp)_2\{\eta^2\text{-}SC(H)NPh\}]$.[261]

Reaction of $[Ru_2H(CO)_5\{\mu\text{-}(Pr^iO)_2PN(Et)P(OPr^i)_2\}_2][PF_6]$ with PhNCS in a 1:1 molar ratio in 1,2-dichloroethane under reflux gives $[Ru_2\{\mu\text{-}\eta^2\text{-}SC(H)NPh\}(CO)_4\{\mu\text{-}(Pr^iO)_2PN(Et)P(OPr^i)_2\}_2][PF_6]$ (227) Figure 6.13.[260] The unusual feature of (227) is that the cation adopts a staggered conformation such that the RuNCSRu ring is puckered.

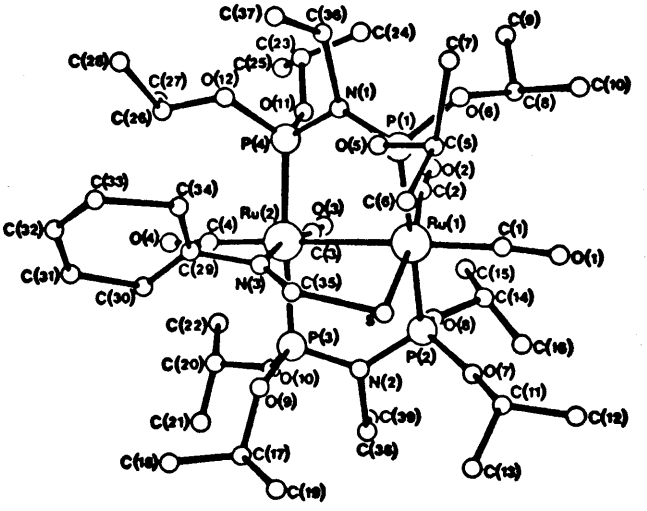

Figure 6.13 The stereochemistry of $[Ru_2\{\mu\text{-}\eta^2\text{-}SC(H)NPh\}(CO)_4\{\mu\text{-}(Pr^iO)_2P\text{-}N(Et)P(OPr^i)_2\}_2]^+$ (227).[260]

The reactions of $[H_2Os_3(CO)_{10}]$ with the organoisothiocyanates RNCS (R=Ph or C_6H_4-*p*-F) have been investigated.[240] The initial products of the reactions are the compounds $[HOs_3\{\mu\text{-}\eta^1\text{-}SC(H)NR\}(CO)_{10}]$ (228). The compound $[HOs_3\{\mu\text{-}\eta^1\text{-}SC(H)NC_6H_4\text{-}p\text{-}F\}(CO)_{10}]$ has been characterised by X-ray crystallographic methods and contains a thioformamido ligand that bridges an edge of the cluster *via* the sulphur atom, Figure 6.14(a).[240] Under irradiation (228) loses one mole of CO to form the complexes $[HOs_3\{\mu_3\text{-}\eta^2\text{-}SC(H)NR\}(CO)_9]$, which contains a triply-bridging thioformamido ligand in which the sulphur atom bridges two metal atoms and the nitrogen atom is bonded to the third. The compound $[HOs_3\{\mu_3\text{-}\eta^2\text{-}SC(H)NC_6H_4\text{-}p\text{-}F\}(CO)_9]$ has been characterised by X-ray crystallographic methods, Figure 6.14(b). When heated to 125°C, (228) is transformed into the compound $[HOs_3(\mu_3\text{-}S)(\mu\text{-}HCNR)(CO)_9]$ which contains an "open" cluster of three metal atoms with a triply-bridging sulfido ligand and formimidoyl ligand which bridges the open edge of the

cluster. The compound $[HOs_3(\mu_3\text{-}S)(\mu\text{-}HCNC_6H_4\text{-}p\text{-}F)(CO)_9]$ was characterised by X-ray crystallographic methods, Figure 6.14(c). Addition of one mole of PMe_2Ph to (228) afforded the complex $[HOs_3\{\mu\text{-}\eta^2\text{-}SC(H)NR\}(CO)_9(PMe_2Ph)]$. An X-ray crystallographic analysis of $[HOs_3\{\mu\text{-}\eta^2\text{-}SC(H)NPh\}(CO)_9(PMe_2Ph)]$ shows that it contains a N-phenylformamido ligand bridging an edge of the cluster but unlike (228) the ligand is coordinated through both the sulphur and nitrogen atoms, Figure 6.14(d).

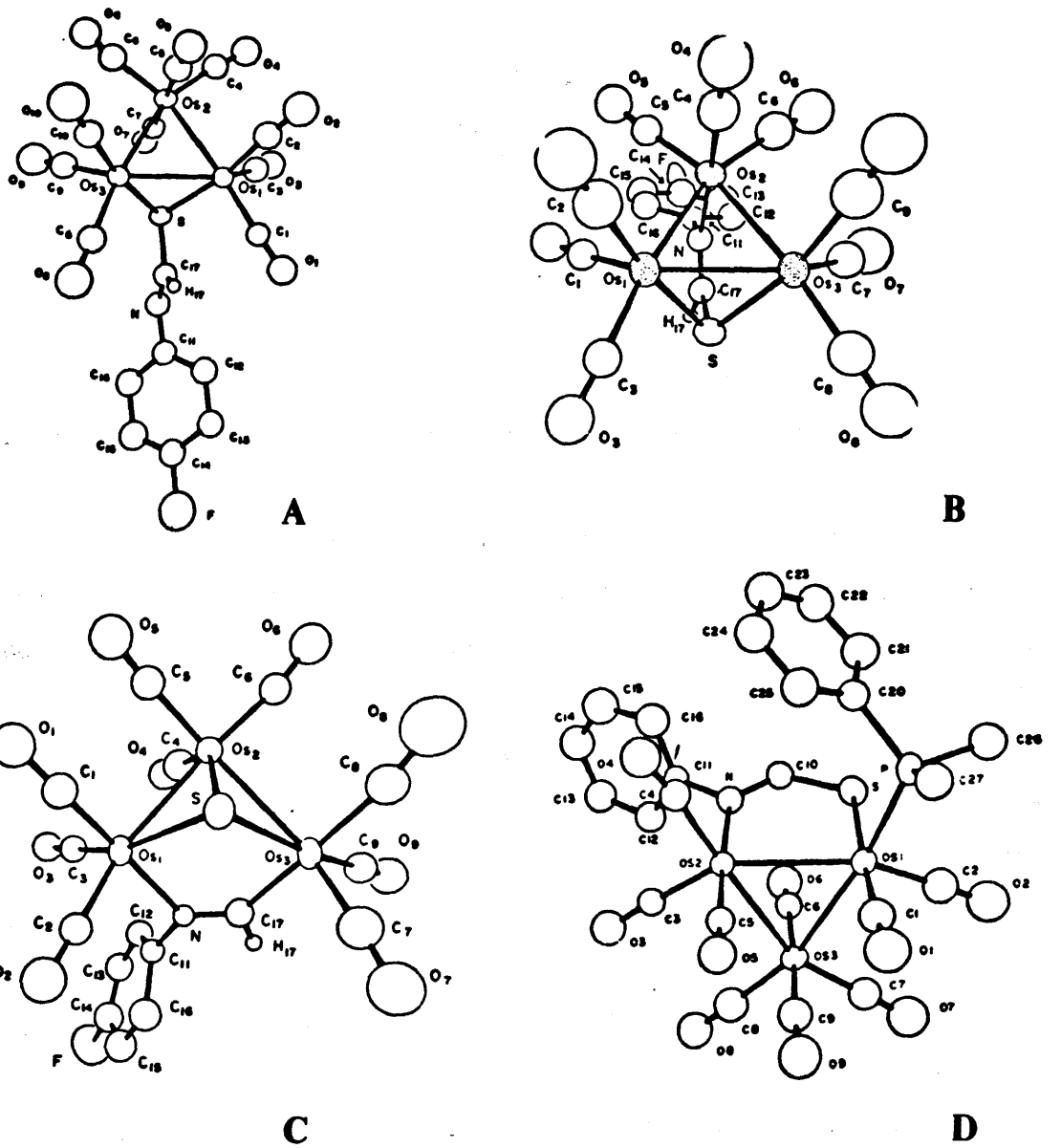

Figure 6.14 Molecular structures, of; (a) $[HOs_3\{\mu\text{-}\eta^1\text{-}SC(H)NC_6H_4\text{-}p\text{-}F\}(CO)_{10}]$, (b) $[HOs_3\{\mu_3\text{-}\eta^2\text{-}SC(H)NC_6H_4\text{-}p\text{-}F\}(CO)_9]$, (c) $[HOs_3(\mu_3\text{-}S)(\mu\text{-}HCNC_6H_4\text{-}p\text{-}F)(CO)_9]$ and (d) $[HOs_3\{\mu\text{-}\eta^2\text{-}SC(H)NPh\}(CO)_9(PMe_2Ph)]$.[240]

The complex $[ReO(OEt)Cl_2(PPh_3)_2]$ reacts with an excess of *p*-tolylisothiocyanate to give the thiazetidine complex $[ReOCl_2(PPh_3)\{SC(OEt)N(p\text{-tol})\}]$ obtained by the formal insertion of the isothiocyanate molecule into the Re-OEt bond, Figure 6.15.[262]

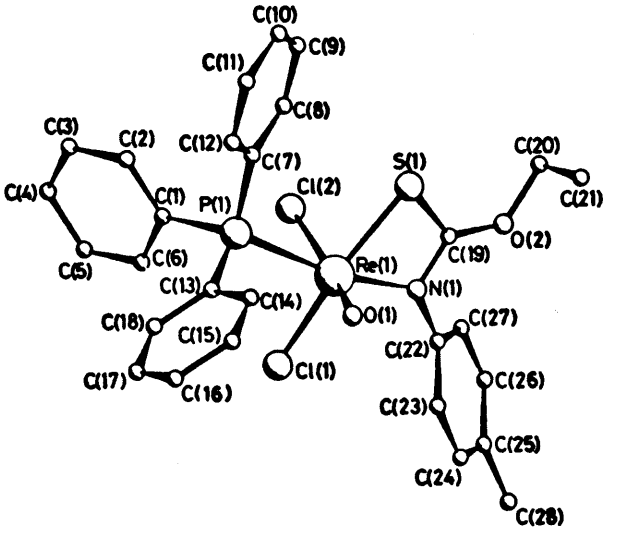

Figure 6.15 Crystal structure of $[ReOCl_2(PPh_3)\{SC(OEt)N(p\text{-tol})\}]$.[262]

The reaction of PhNCS with [CuOAr] (Ar=2,6-dimethylphenoxide) leads to an insertion followed by a rearrangement.[263] In the absence of any other ligand the product oligomerises due to the bridging tendency of sulphur. By using appropriate ligands and steric effects, the syntheses of desired oligomers were described.[263] In the presence of an excess of PPh_3 (3 equiv), PhNCS reacts with copper(I) 2,6-dimethylphenoxide in CH_2Cl_2 to give $[Cu\{\eta^2\text{-}SC(OC_6H_3Me_2\text{-}2,6)(NPh)\}(PPh_3)_2]$ in 89% yield, in which the complex has a simple monomeric structure in which the SC(R)NPh group functions as a chelating ligand, Figure 6.16(a).[263] The reaction of PhNCS with copper(I) 2,6-di-*tert*-butyl-4-methylphenoxide in the presence of $P(OMe)_3$ results in the formation of $[Cu\{\mu\text{-}SC(NPh)(OC_6H_2\text{-}Bu^t_2\text{-}2,6\text{-}Me\text{-}4)\}(P(OMe)_3)]_2$ in 40% yield, Figure 6.16(b). In this molecule the ligand is a bridge between two Cu(I) atoms such that each metal atom has a N, S and P coordinating in a trigonal environment. When the reaction of copper(I) 2,6-dimethylphenoxide was carried out in the presence of $P(OMe)_3$ $[Cu\{\mu\text{-}SC(NPh)(OC_6H_3Me_2\text{-}2,6)\}]_4$ was isolated in 15% yield, which is a tetrameric complex, with copper atoms in trigonal environments with two sulphurs and a nitrogen coordinating each copper, Figure 6.16(c).

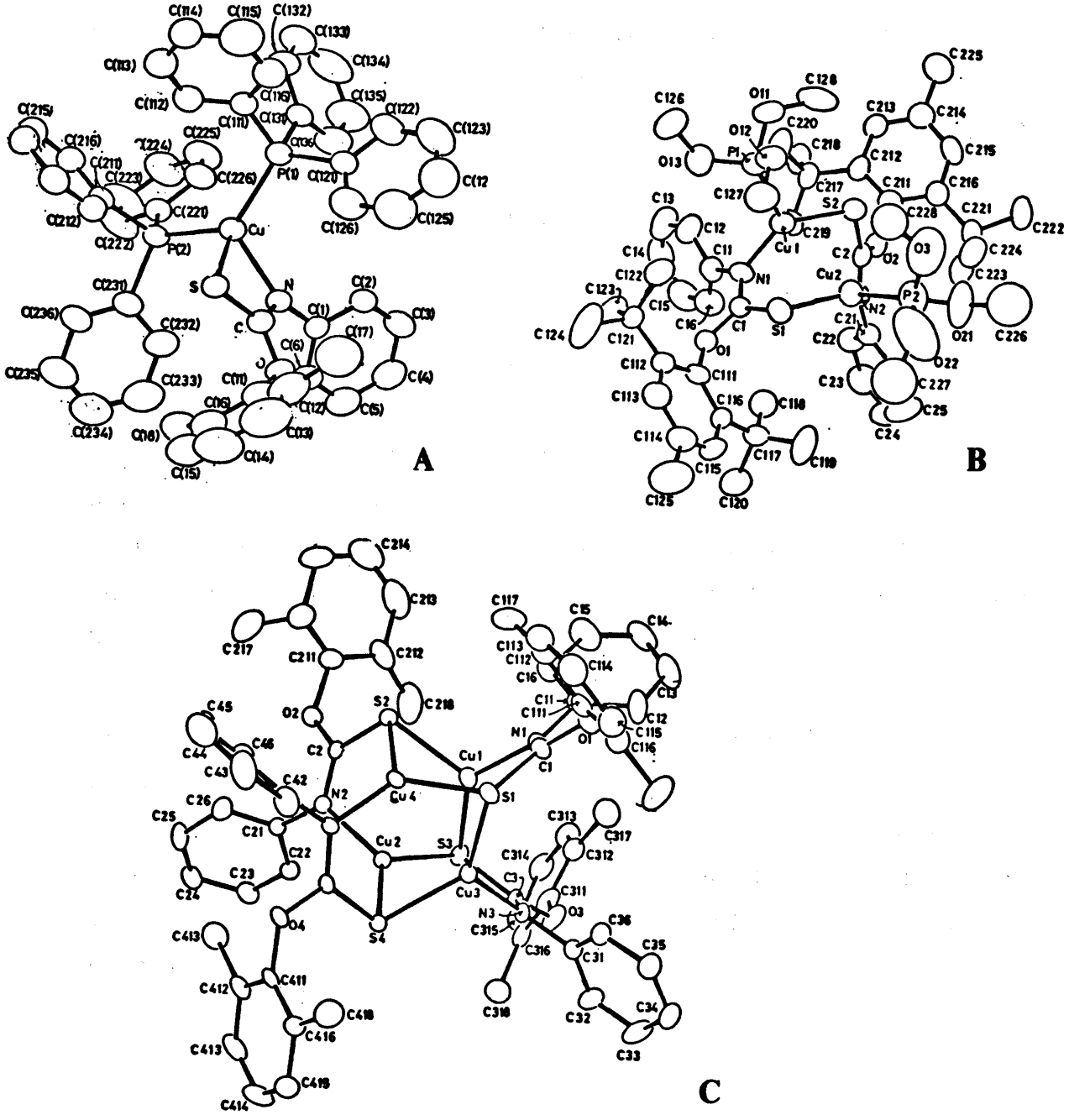

Figure 6.16 (a) Ortep view of $[Cu\{\eta^2\text{-}SC(OC_6H_3(Me)_2\text{-}2,6)(NPh)\}(PPh_3)_2]$.
(b) Ortep view of $[Cu\{\mu\text{-}SC(NPh)(OC_6H_2((t\text{-}Bu)_2\text{-}2,6)\text{-}(Me\text{-}4))\}(P(OMe)_3)]_2$.[263]
(c) Ortep view of $[Cu\{\mu\text{-}SC(NPh)(OC_6H_3(Me)_2\text{-}2,6)\}]_4$.

6.1.3 Summary

A wide variety of ligands can be derived from isothiocyanates *i.e.* RNCS, RNC, S, $S_2C(H)NR$ and $SC(H)NR^-$. These ligands are generated from four main types of reactions described above. In summary these are;

(1) The RNCS molecule can bind to a metal *via* the carbon-sulphur double bond forming a three centred M-C-S metallacycle. This coordination mode (termed η^2) although quite common for CS_2,[2] is somewhat rarer for isothiocyanate molecules.[245]

(2) Isothiocyanates may undergo condensation reactions in the presence of metal complexes yielding species in which two or three isothiocyanate molecules are fused and attached to the metal.[245,248] This often occurs with the extrusion of sulphur.

(3) A more common reaction of isothiocyanates is a disproportionation reaction which can occur to yield isocyanide and sulphide groups which react further in the presence of excess isothiocyanate to afford dithiocarbamato groups.

(4) The reaction of isothiocyanates with metal hydrides can involve the migration of the hydride ligand to the carbon atom of the isothiocyanate to form a thioformamido ligand $[SC(H)NR]^-$.[260,261]

Many methods of analysis are used to identify the types of compounds formed from the reaction of isothiocyanates with metal complexes including IR, ^1H and ^{13}C NMR but X-ray analysis is very important in their characterisation.

In the following chapter reactions of a series of isothiocyanates with rhodaheteroboranes are discussed. Ten new twelve-vertex rhodaheteroboranes were synthesised in this work including thioformamido, $[SC(H)NR]^-$ and dithiocarbamato, $[S_2CN(H)R]$ complexes.

6.2 RESULTS AND DISCUSSION

Of the ten new twelve-vertex rhodaheteroboranes synthesised in this work, two complexes were rhodacarboranes, *closo*-[3-{η^2-SC(H)NPh}-3-(PPh_3)-3,1,2-$RhC_2B_9H_{11}$] (197) and *closo*-[3-{η^2-$S_2CN(H)Ph$}-3-(PPh_3)-3,1,2-$RhC_2B_9H_{11}$] (229), two were rhodatelluraboranes, *closo*-[2-{η^2-$S_2CN(H)Ph$}-2-(PPh_3)-2,1-$RhTeB_{10}H_{10}$] (230) and *closo*-[2-{η^2-SC(H)NPh}-2-(PPh_3)-2,1-$RhTeB_{10}H_{10}$] (231) and six were rhodaarsena-boranes, *closo*-[3-{η^2-$S_2CN(H)Ph$}-3-(PPh_3)-3,1,2-$RhAs_2B_9H_9$] (232), *closo*-[3-{η^2-SC(H)NPh}-3-(PPh_3)-3,1,2-$RhAs_2B_9H_9$] (198), *closo*-[3-{η^2-S_2CNH(*p*-tol)}-3-(PPh_3)-3,1,2-$RhAs_2B_9H_9$] (233), *closo*-[3-{η^2-SC(H)N(*p*-tol)}-3-(PPh_3)-3,1,2-$RhAs_2B_9H_9$] (234), *closo*-[3-{η^2-$S_2CN(H)Bz$}-3-(PPh_3)-3,1,2-$RhAs_2B_9H_9$] (235) and *closo*-[3-{η^2-SC(H)NBz}-3-(PPh_3)-3,1,2-$RhAs_2B_9H_9$] (236). All of these compounds were characterised by spectroscopic methods and in three cases, compounds (198), (230) and (232), the structures were elucidated by single crystal X-ray analyses. The studies of compounds (198) and (232) are the first reported X-ray crystal structures of rhodaarsenaboranes.

6.2.1 Syntheses

Compounds (197), (198) and (229)-(236) were synthesised by the reaction between the hydrido-rhodaheteroboranes *closo*-[3,3-$(PPh_3)_2$-3-H-3,1,2-$RhAs_2B_9H_9$] (58), *closo*-[2,2-$(PPh_3)_2$-2-H-2,1-$RhTeB_{10}H_{10}$] (220), or *closo*-[3,3-$(PPh_3)_2$-3-H-3,1,2-$RhC_2B_9H_{11}$] (59) and RNCS (R=Ph, *p*-tol and Bz) in CH_2Cl_2.

Reaction of (58) with PhNCS in CH_2Cl_2 gave *closo*-[3-{η^2-$S_2CN(H)Ph$}-3-(PPh_3)-3,1,2-$RhAs_2B_9H_9$] (232) and *closo*-[3-{η^2-SC(H)NPh}-3-(PPh_3)-3,1,2-$RhAs_2B_9H_9$] (198). The two different procedures used to effect this reaction are summarised in Table 6.1. In the first procedure, a ten fold excess of PhNCS was added to a solution of (58) in CH_2Cl_2 and the solution was stirred at reflux for 18h. In the second procedure a hundred fold excess of PhNCS was added to a solution of (58) in CH_2Cl_2 and the solution was stirred at room temperature for four days. Both procedures produced about 13 products of various colours, (commonly purple, green, orange and yellow) but unfortunately most were in low yield *ca* 1-2% which is not

sufficient for identification. Only two products were formed in amounts sufficient for them to be isolated and characterised as the orange air-stable compound *closo*-[3-{η^2-SC(H)NPh}-3-(PPh_3)-3,1,2-$RhAs_2B_9H_9$] (198) and the yellow air-stable compound *closo*-[3-{η^2-$S_2CN(H)Ph$}-3-(PPh_3)-3,1,2-$RhAs_2B_9H_9$] (232), Table 6.1.

Table 6.1 Yields of *closo*-[3-{η^2-SC(H)NPh}-3-(PPh_3)-3,1,2-$RhAs_2B_9H_9$] (198) and *closo*-[3-{η^2-$S_2CN(H)Ph$}-3-(PPh_3)-3,1,2-$RhAs_2B_9H_9$] (232) from the reaction of *closo*-[3,3-(PPh_3)$_2$-3-H-3,1,2-$RhAs_2B_9H_9$] (58) with PhNCS.

Procedure	% Yield of (198)	% Yield of (232)
1[a]	64.2	20.2
2[b]	15.2	54.9

[a] 1:10 molar ratio of (58):PhNCS heated at reflux for 18h.

[b] 1:100 molar ratio of (58):PhNCS stirred at room temperature for 4 d.

Reaction of *closo*-[2,2-(PPh_3)$_2$-2-H-2,1-$RhTeB_{10}H_{10}$] (220) with PhNCS in a 1:10 molar ratio in CH_2Cl_2 at reflux for 18h, afforded the air-stable yellow product *closo*-[2-{η^2-$S_2CN(H)Ph$}-2-(PPh_3)-2,1-$RhTeB_{10}H_{10}$] (230) in 9.0% yield, and the air stable orange compound *closo*-[2-{η^2-SC(H)NPh}-2-(PPh_3)-2,1-$RhTeB_{10}H_{10}$] (231) in 52.8% yield.

Reaction of *closo*-[3,3-(PPh_3)$_2$-3-H-3,1,2-$RhC_2B_9H_{11}$] (59) with PhNCS in CH_2Cl_2 in a variety of molar ratios and under various conditions gave *closo*-[3-{η^2-SC(H)NPh}-3-(PPh_3)-3,1,2-$RhC_2B_9H_{11}$](197) and *closo*-[3-{η^2-$S_2CN(H)Ph$}-3-(PPh_3)-3,1,2-$RhC_2B_9H_{11}$] (229), Table 6.2. In the first instance (see section 6.4.7 procedure 1) a 1:10 molar ratio of (59):PhNCS was heated in CH_2Cl_2 at reflux for 18h resulting in the formation of (197) in 22.9% yield and (229) in 1.1% yield. In the second procedure a 1:1 molar ratio of (59):PhNCS was heated in CH_2Cl_2 at reflux for 72h producing (197) in 61.4% yield and (229) in 1.1% yield. In the third procedure a 1:1 molar ratio of (59):PhNCS in CH_2Cl_2 was subjected to microwave irradiation for 5

minutes resulting in the formation of (197) in 98.8% yield. Thus, the reaction carried out in the microwave oven and initiated by microwave irradiation leads not only to a considerable saving in time but also to a marked improvement in the yield of (197). The microwave technique is very efficient for the synthesis of (197) as it is a much "cleaner" reaction than either of the above procedures for the reaction of (59) with PhNCS, this can be clearly seen in the picture of the PLC plates from both the microwave induced reaction and the reflux reaction, Figure 6.17.

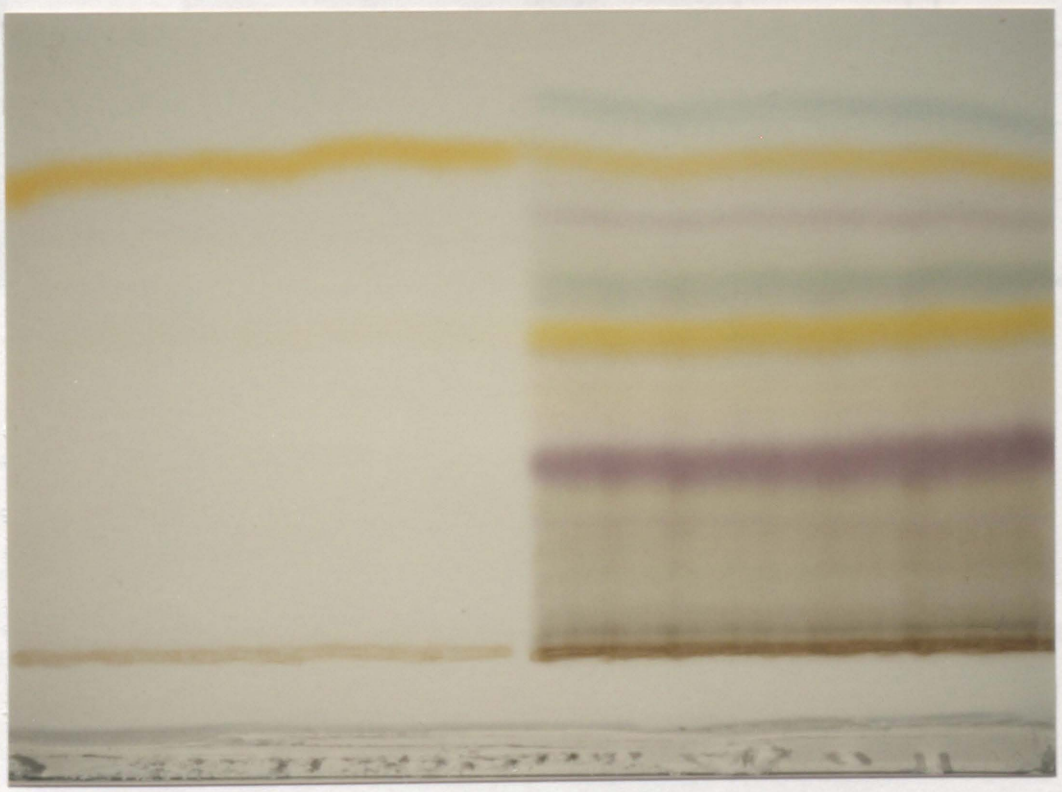

Figure 6.17 Photograph of the PLC plates for the reaction of (59) with PhNCS, on the left the microwave induced reaction and on the right the reaction heated conventionally at reflux.

A solution of *closo*-[3-{η^2-SC(H)NPh}-3-(PPh_3)-3,1,2-$RhC_2B_9H_{11}$] (197) with a ten fold excess of PhNCS in CH_2Cl_2 was subjected to microwave irradiation for 45 minutes, giving (229) in 31.9% yield. The above results for the reaction of (59) and (197) are summarised in Table 6.2.

Table 6.2 Yields of *closo*-[3-{η^2-SC(H)NPh}-3-(PPh_3)-3,1,2-$RhC_2B_9H_{11}$] (197) and *closo*-[3-{η^2-S_2CN(H)Ph}-3-(PPh_3)-3,1,2-$RhC_2B_9H_{11}$] (229) from the reaction of *closo*-[3,3-(PPh_3)$_2$-3-H-3,1,2-$RhC_2B_9H_{11}$] (59) with PhNCS.

Procedure	% Yield of (197)	% Yield of (229)
1[a]	22.9	1.1
2[b]	61.4	1.1
3[c]	98.8	---
4[d]	----	31.9

[a] 1:10 molar ratio of (59):PhNCS heated at reflux for 18h.

[b] 1:1 molar ratio of (59):PhNCS heated at reflux for 72h.

[c] 1:1 molar ratio of (59):PhNCS heated by microwave irradiation for 5 minutes.

[d] 1:10 molar ratio of (229):PhNCS heated by microwave irradiation for 45 minutes.

In order to compare the reactivities of the hydridorhodaheteroboranes *closo*-[3,3-(PPh_3)$_2$-3-H-3,1,2-$RhAs_2B_9H_9$] (58), *closo*-[2,2-(PPh_3)$_2$-2-H-2,1-$RhTeB_{10}H_{10}$] (220) and *closo*-[3,3-(PPh_3)$_2$-3-H-3,1,2-$RhC_2B_9H_{11}$] (59) towards PhNCS, reactions of hydridorhodaheteroborane and PhNCS in a 1:10 molar ratio in CH_2Cl_2 heated at reflux for 18h were investigated. The results are summarised in Table 6.3.

Table 6.3 Yields of {η^2-SC(H)NPh} compounds (198), (231) and (197) and {η^2-S_2CN(H)Ph} compounds (232), (230) and (229) from the reaction between (58), (220) and (59) with a ten fold excess of PhNCS in CH_2Cl_2 at reflux for 18h.

Hydridorhodaheteroborane	% yield of {SC(H)NPh} product	% yield of {S_2CN(H)Ph} product
closo-[3,3-$(PPh_3)_2$-3-H-3,1,2-$RhAs_2B_9H_9$] (58)	64.2	20.2
closo-[2,2-$(PPh_3)_2$-2-H-2,1-$RhTeB_{10}H_{10}$] (220)	52.8	9.0
closo-[3,3-$(PPh_3)_2$-3-H-3,1,2-$RhC_2B_9H_{11}$] (59)	22.9	1.1

Clearly the ligand affects the overall % of products, with the highest yields for the arsenaborane then the telluraborane and the lowest % for the carborane. The heteroborane ligand also affects the product ratios, with the ratios of {SC(H)NPh}:{S_2CN(H)Ph} being approximately 3:1 for the arsenaborane, 6:1 for the telluraborane and 20:1 for the carborane. These results may be significant for the further study of metallaheteroborane reactions.

Reaction between (58) and benzylisothiocyanate in CH_2Cl_2 resulted in the formation of *closo*-[3-{η^2-SC(H)NBz}-3-(PPh_3)-3,1,2-$RhAs_2B_9H_9$] (236) and *closo*-[3-{η^2-S_2CN(H)Bz}-3-(PPh_3)-3,1,2-$RhAs_2B_9H_9$] (235). Two different procedures were used for the reaction. In the first, a ten fold excess of benzylisothiocyanate was used and the solution was heated at reflux for 18h, there were *ca.* ten bands on the PLC plate but only (235) was in significant yield. In the second procedure one equivalent of benzylisothiocyanate was used and the reaction was carried out in a microwave oven and initiated by microwave irradiation. Yields of (235) and (236) are summarised in Table 6.4.

Table 6.4 Yields of *closo*-[3-{η^2-SC(H)NBz}-3-(PPh_3)-3,1,2-$RhAs_2B_9H_9$] (236) and *closo*-[3-{η^2-$S_2CN(H)Bz$}-3-(PPh_3)-3,1,2-$RhAs_2B_9H_9$] (235) from the reaction of *closo*-[3,3-(PPh_3)$_2$-3-H-3,1,2-$RhAs_2B_9H_9$] (58) with benzylisothiocyanate.

Procedure	% Yield of (236)	% Yield of (235)
1[a]	---	19.8
2[b]	53.9	3.3

[a] 1:10 molar ratio of (58):benzylisothiocyanate heated at reflux for 18h.

[b] 1:1 molar ratio of (58):benzylisothiocyanate heated by microwave irradiation for 5 minutes.

Reaction of *closo*-[3,3-(PPh_3)$_2$-3-H-3,1,2-$RhAs_2B_9H_9$] (58) with different molar ratios of *p*-tolylisothiocyanate in refluxing CH_2Cl_2 resulted in the formation of *closo*-[3-{η^2-$S_2CNH(p\text{-tol})$}-3-(PPh_3)-3,1,2-$RhAs_2B_9H_9$] (233) and *closo*-[3-{η^2-SC(H)N(*p*-tol)}-3-(PPh_3)-3,1,2-$RhAs_2B_9H_9$] (234), Table 6.5.

The reaction of (58) with RNCS (R=Ph, *p*-tol and Bz) in refluxing CH_2Cl_2 for 18h affording *closo*-[3-{η^2-$S_2CN(H)R$})-3-(PPh_3)-3,1,2-$RhAs_2B_9H_9$] and *closo*-[3-{η^2-SC(H)NR}-3-(PPh_3)-3,1,2-$RhAs_2B_9H_9$] is summarised in Table 6.6.

Table 6.5 Yields of *closo*-[3-{η^2-SC(H)N(*p*-tol)}-3-(PPh_3)-3,1,2-$RhAs_2B_9H_9$] (234) and *closo*-[3-{η^2-$S_2CNH(p\text{-tol})$}-3-(PPh_3)-3,1,2-$RhAs_2B_9H_9$] (233) from the reaction of *closo*-[3,3-(PPh_3)$_2$-3-H-3,1,2-$RhAs_2B_9H_9$] (58) with *p*-tolylisothiocyanate.

Procedure	% Yield of (234)	% Yield of (233)
1[a]	20.6	26.4
2[b]	47.0	7.7

[a] 1:10 molar ratio of (58):*p*-tolylisothiocyanate heated at reflux for 18h.

[b] 1:1 molar ratio of (58):*p*-tolylisothiocyanate heated at reflux for 18h.

Table 6.6 Yields of *closo*-[3-{η^2-SC(H)NR}-3-(PPh_3)-3,1,2-$RhAs_2B_9H_9$] and *closo*-[3-{η^2-$S_2CNH(R)$}-3-(PPh_3)-3,1,2-$RhAs_2B_9H_9$] from the reaction of *closo*-[3,3-(PPh_3)$_2$-3-H-3,1,2-$RhAs_2B_9H_9$] (58) with a ten fold excess of RNCS (R=Ph, *p*-tol and Bz) in refluxing CH_2Cl_2 for 18h.

R	% yield of *closo*-[3-{η^2-SC(H)NR}-3-(PPh_3)-3,1,2-$RhAs_2B_9H_9$] complex	% yield of *closo*-[3-{η^2-$S_2CNH(R)$}-3-(PPh_3)-3,1,2-$RhAs_2B_9H_9$] complex
Ph	64.2	20.2
p-tol	20.6	26.4
Bz	---	19.8

In summary it was seen that reaction of the hydridorhodaheteroboranes (58), (220) and (59) with an equimolar amount of RNCS (R=Ph, *p*-tol and Bz) results in the major product being the thioformamido {η^2-SC(H)NR} complexes. If an excess of isothiocyanate is used the major product is the dithiocarbamate {η^2-$S_2CNH(R)$} complex. These results are comparable to previous reactions of metal complexes with isothiocyanates as discussed in the introduction. For example the reaction between PhNCS and $Cp_2Zr(H)Cl$ in a 1:1 molar ratio afforded [$Zr(\eta^5$-Cp)$_2${η^2-SC(H)NPh}] in 68% yield,[261] whereas reaction of a 3:1 molar ratio of PhNCS and [(PPh_3)$_2$Cu(BH_4)] resulted in the formation of [Cu(PPh_3)$_2${η^2-$S_2CN(H)Ph$}] in 80% yield.[257]

Microwave irradiation may be used to initiate reactions. The reaction of *closo*-[3,3-(PPh_3)$_2$-3-H-3,1,2-$RhC_2B_9H_{11}$] (59) and PhNCS carried out in the microwave oven and initiated by microwave irradiation leads not only to a considerable saving in time but also to a marked improvement in the yield of *closo*-[3-{η^2-SC(H)NPh}-3-(PPh_3)-3,1,2-$RhC_2B_9H_{11}$] (197).

The composition of the % of products from the reaction of PhNCS and the hydrido-rhodaheteroboranes vary significantly depending on which heteroborane ligand is used, with the highest yields for the arsenaborane, then the telluraborane and

the lowest % for the carborane. The heteroborane ligand also affects the product ratios, with the ratios of {SC(H)NPh}:{S_2CN(H)Ph} being approximately 3:1 for the arsenaborane, 6:1 for the telluraborane and 20:1 for the carborane. These results may be significant for the further study of metallaheteroborane reactions.

The R group of the isothiocyanate RNCS (R=Ph, *p*-tol and Bz) also had an effect on the % products formed. The PhNCS was most reactive followed by *p*-tolNCS with BzNCS being the least reactive.

6.2.2 Infrared Spectra

An important feature of the IR spectra of the compounds (197), (198) and (229)-(236) was the presence of strong absorptions due to terminal B-H stretching bands in the region 2600-2450 cm^{-1}. Other important features were bands due to phosphine ligands arising from C-H stretching in the region 3100-2800 cm^{-1}, P-C stretching in the region 795-650 cm^{-1}, P-Ph stretching in the regions 1600-1425 and 1110-960 cm^{-1} and P-Me stretching in the region 960-835 cm^{-1}. No B-H-B, Rh-H-B or Rh-H bands were observed in the IR spectra of (197), (198) and (229)-(236).

In general, spectra of compounds in which a C=S group is attached to a nitrogen atom show an absorption band in the general C=S stretching region. In addition, several other bands in the broad region of 1600-700 cm^{-1} can be attributed to vibrations involving interaction between C=S stretching and C-N or C=N stretching.[264]

There are four characteristic bands for the dithiocarbamate complexes (229), (230), (232), (233) and (235). These are the N-H stretch in the region 3200-3400 cm^{-1}, the N-H bend in the region 1570-1590 cm^{-1}, the C=S bonds which are also linked to a nitrogen atom in the region 1500-1520 cm^{-1}, and the C-N stretch which occurs in the region 1300-1390 cm^{-1}, Table 6.7.[264]

There are three characteristic bands for the thioformamido complexes (197), (198), (231), (234) and (236). These are the C=N stretch in the region 1480-1550 cm^{-1}, the C-H bend of the thioformamido ligand in the region 1245-1265 cm^{-1}, and the C=S band in the region 860-900 cm^{-1}, Table 6.8.[14,264]

Table 6.7 Infrared bands for the dithiocarbamate complexes *closo*-[3-{η^2-$S_2CN(H)Ph$}-3-(PPh_3)-3,1,2-$RhC_2B_9H_{11}$](229), *closo*-[2-{η^2-$S_2CN(H)Ph$}-2-(PPh_3)-2,1-$RhTeB_{10}H_{10}$](230), *closo*-[3-{η^2-$S_2CN(H)Ph$}-3-(PPh_3)-3,1,2-$RhAs_2B_9H_9$](232), *closo*-[3-{η^2-$S_2CNH(p\text{-tol})$}-3-(PPh_3)-3,1,2-$RhAs_2B_9H_9$] (233) and *closo*-[3-{η^2-$S_2CN(H)Bz$}-3-(PPh_3)-3,1,2-$RhAs_2B_9H_9$] (235).

COMPLEX	N-H stretch cm^{-1}	N-H bend cm^{-1}	C---S linked to N cm^{-1}	C-N stretch cm^{-1}
229	3290	1580	1502	1350
230	3280	1582	1505	1360
232	3235	1582	1518	1380
233	3280	1580	1500	1350
235	3306	1575	1500	1318

Table 6.8 Infrared bands for the thioformamido complexes *closo*-[3-{η^2-$SC(H)NPh$}-3-(PPh_3)-3,1,2-$RhAs_2B_9H_9$] (198), *closo*-[2-{η^2-$SC(H)NPh$}-2-(PPh_3)-2,1-$RhTeB_{10}H_{10}$] (231), *closo*-[3-{η^2-$SC(H)NPh$}-3-(PPh_3)-3,1,2-$RhC_2B_9H_{11}$] (197), *closo*-[3-{$\eta^2$$SC(H)N(p\text{-tol})$}-3-($PPh_3$)-3,1,2-$RhAs_2B_9H_9$] (234) and *closo*-[3-{$\eta^2$-$SC(H)NBz$}-3-($PPh_3$)-3,1,2-$RhAs_2B_9H_9$] (236).

COMPLEX	C---N stretch cm^{-1}	C-H bend cm^{-1}	C---S stretch cm^{-1}
197	1502	1254	880
198	1495	1262	880
231	1493	1260	880
234	1504	1254	891
236	1478	1250	905

6.2.3 Crystal and Molecular Structures of Rhodaheteroboranes

Suitable crystals were grown by the layering technique with hexane slowly diffusing into a CH_2Cl_2 solution of the rhodaheteroborane. The collection of the data and the structure solution were carried out by Professor George Ferguson, University of Guelph, Canada, as stated in the experimental section 3.4.1. Crystal data and relevant structure solution data are given in experimental sections 6.4.4 (198), 6.4.3 (232) and 6.4.6 (230).

6.2.3.1 Crystal and Molecular Structure of *closo*-[3-{η^2-SC(H)NPh}-3-(PPh_3)-3,1,2-$RhAs_2B_9H_9$] (198)

As no single crystal X-ray analysis of a rhodaarsenaborane had been previously reported it was decided to undertake a study of (198). The successful solution and refinement of the molecular structure showed that compound (198) had a *closo* twelve-vertex $RhAs_2B_9$ geometry based on a distorted dodecahedron with the rhodium and arsenic atoms adjacent to one another, Figure 6.18. Important bond distances and angles are given in Table 6.9 and 6.10 respectively.

The orientation of the [Rh{η^2-SC(H)NPh}(PPh_3)] unit above the As_2B_3 face is shown in Figure 6.19 and it is as expected, based on results of a frontier mo study of an "RhL_3" unit above a 7,8-C_2B_9 cage (as discussed in Chapter 2).[162]

Although there appears to be no published {η^2-SC(H)NPh}Rh-containing structure to compare with (198),[206] the Rh-N bond distance of 2.116(5) Å is similar to the value 2.14(3) Å in [(η^5-Cp*)RhHB(pz)$_3$]$^+$ (pz = 1-pyrazolyl),[265] and the Rh-S distance of 2.462(2) Å is slightly longer than the average Rh-S distance of 2.37 Å in rhodium derivatives of dithiocarbamates.[206] Typical examples of Rh-S bond distances are 2.3700(18) and 2.3737(19) Å in [Rh(S_2CNEt_2)(η^5-Cp*){(PPh_2)$_2$C-H_2}][BPh_4],[206,266] and 2.421(2) Å in [Rh_2(S_2CNMe_2)$_5$][BF_4] (237).[267] In a recent study of CS_2 derivatives of rhodadicarboranes the Rh-S bond distance varied from 2.2321(11) Å in *precloso*-[2-{η^2-SC(PPh_3)C(H)S}-2,1,7-$RhC_2B_9H_{11}$] (238) to 2.433(2) Å in *closo*-[2-(η^2-S_2CH)-2-(PPh_3)-2,1,7-$RhC_2B_9H_{11}$](239) with the average Rh-S distance being 2.34 Å,[2] Table 6.11.

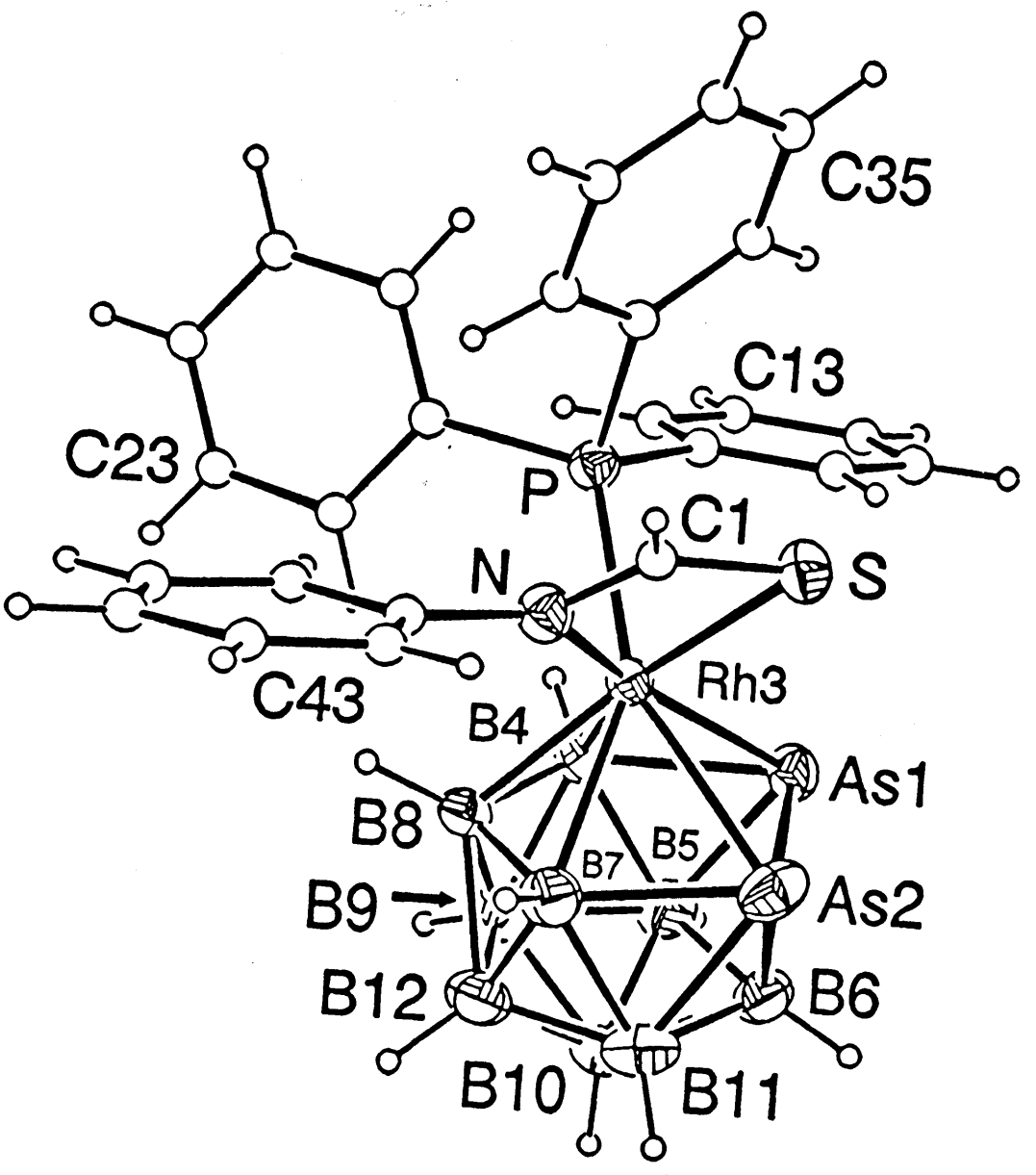

Figure 6.18 Molecular structure of *closo*-[3-{η^2-SC(H)NPh}-3-(PPh_3)-3,1,2-$RhAs_2B_9H_9$] (198).

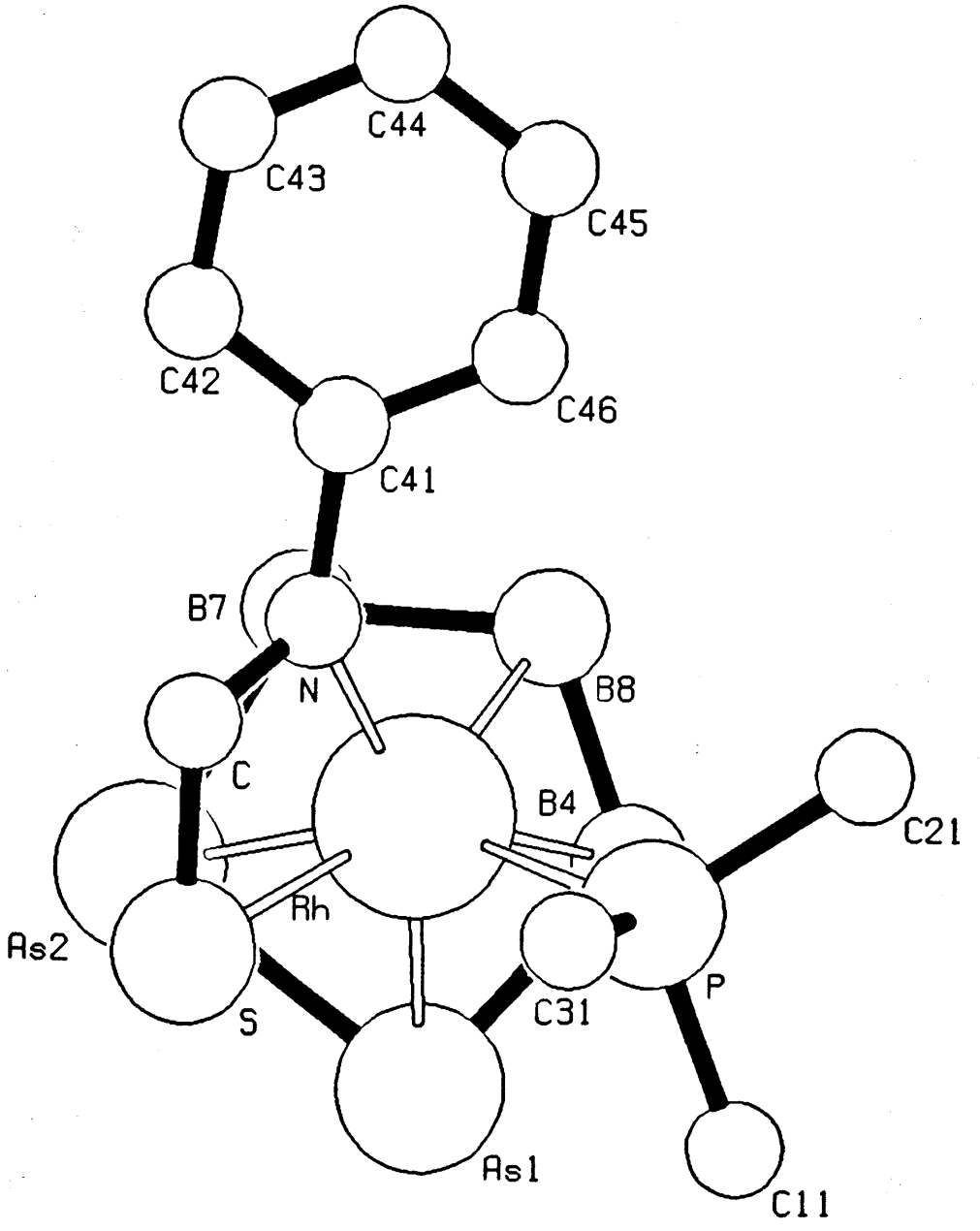

Figure 6.19 A view of the orientation of the [Rh{η^2-SC(H)NPh}(PPh_3)] unit above the As_2B_3 face of *closo*-[3-{η^2-SC(H)NPh}-3-(PPh_3)-3,1,2-$RhAs_2B_9H_9$] (198).

Table 6.9 Important bond distances (Å) for *closo*-[3-{η^2-SC(H)NPh}-3-(PPh_3)-3,1,2-$RhAs_2B_9H_9$] (198).

Rh(3)-As(1)	2.487(1)	N-C(41)	1.422(7)
Rh(3)-As(2)	2.531(1)	B(4)-B(5)	1.889(9)
Rh(3)-S	2.462(2)	B(4)-B(8)	1.782(10)
Rh(3)-P	2.408(1)	B(4)-B(9)	1.755(10)
Rh(3)-N	2.116(5)	B(5)-B(6)	1.827(9)
Rh(3)-B(4)	2.228(7)	B(5)-B(9)	1.784(10)
Rh(3)-B(7)	2.314(7)	B(5)-B(10)	1.783(10)
Rh(3)-B(8)	2.214(7)	B(6)-B(10)	1.777(10)
As(1)-As(2)	2.549(1)	B(6)-B(11)	1.831(11)
As(1)-B(4)	2.189(6)	B(7)-B(8)	1.819(8)
As(1)-B(5)	2.120(7)	B(7)-B(11)	1.866(10)
As(1)-B(6)	2.237(7)	B(7)-B(12)	1.755(11)
As(2)-B(6)	2.226(7)	B(8)-B(9)	1.789(10)
As(2)-B(7)	2.150(7)	B(8)-B(12)	1.794(9)
As(2)-B(11)	2.118(8)	B(9)-B(10)	1.777(8)
S-C(1)	1.695(6)	B(9)-B(12)	1.784(10)
P-C(11)	1.830(6)	B(10)-B(11)	1.756(10)
P-C(21)	1.819(5)	B(10)-B(12)	1.765(10)
P-C(31)	1.827(6)	B(11)-B(12)	1.763(9)
N-C(1)	1.296(7)		

Table 6.10 Important bond angles (°) for *closo*-[3-{η^2-SC(H)NPh}-3-(PPh_3)-3,1,2-$RhAs_2B_9H_9$] (198).

As(1)-Rh(3)-S	96.73(4)	As(1)-Rh(3)-As(2)	61.05(2)
As(1)-Rh(3)-N	160.0.0(1)	As(1)-Rh(3)-P	99.68(4)
As(2)-Rh(3)-S	79.81(4)	As(1)-Rh(3)-B(4)	55.0(2)
As(2)-Rh(3)-N	103.8(1)	As(2)-Rh(3)-P	154.88(5)
S-Rh(3)-P	87.31(5)	As(2)-Rh(3)-B(7)	52.5(2)
S-Rh(3)-B(4)	148.7(2)	S-Rh(3)-N	66.3(1)
S-Rh(3)-B(8)	161.5(2)	S-Rh(3)-B(7)	115.8(2)
P-Rh(3)-B(4)	85.2(2)	P-Rh(3)-N	90.4(1)
P-Rh(3)-B(8)	106.8(2)	P-Rh(3)-B(7)	151.4(2)
N-Rh(3)-B(7)	84.4(2)	N-Rh(3)-B(4)	143.9(2)
B(4)-Rh(3)-B(8)	47.3(3)	N-Rh(3)-B(8)	100.9(2)
Rh(3)-As(1)-As(2)	60.34(2)	B(7)-Rh(3)-B(8)	47.3(2)
As(2)-As(1)-B(4)	95.2(2)	Rh(3)-As(1)-B(4)	56.5(2)
B(4)-As(1)-B(5)	52.0(2)	As(2)-As(1)-B(6)	55.0(2)
Rh(3)-As(2)-As(1)	58.62(2)	B(5)-As(1)-B(6)	49.5(2)
As(1)-As(2)-B(6)	55.4(2)	Rh(3)-As(2)-B(7)	58.6(2)
B(6)-As(2)-B(11)	49.8(3)	As(1)-As(2)-B(7)	96.8(2)
Rh(3)-S-C(1)	78.2(2)	B(7)-As(2)-B(11)	51.8(3)
Rh(3)-N-C(41)	135.7(4)	Rh(3)-N-C(1)	101.2(4)
S-C(1)-N	114.2(5)	C(1)-N-C(41)	123.0(5)
Rh(3)-B(4)-B(8)	65.9(3)	Rh(3)-B(4)-As(1)	68.5(2)

As(1)-B(4)-B(8)	117.8(4)	As(1)-B(4)-B(5)	62.1(3)
B(8)-B(4)-B(9)	60.8(4)	B(5)-B(4)-B(9)	58.5(4)
As(1)-B(5)-B(6)	68.6(3)	As(1)-B(5)-B(4)	65.9(3)
B(9)-B(5)-B(10)	59.8(4)	B(4)-B(5)-B(9)	57.0(4)
B(6)-B(5)-B(10)	58.9(4)	As(1)-B(6)-B(5)	61.9(3)
B(5)-B(6)-B(10)	59.3(4)	As(1)-B(6)-As(2)	69.6(2)
B(10)-B(6)-B(11)	58.2(4)	As(2)-B(6)-B(11)	62.0(3)
Rh(3)-B(7)-B(8)	63.5(3)	Rh(3)-B(7)-As(2)	69.0(2)
As(2)-B(7)-B(11)	63.2(3)	As(2)-B(7)-B(8)	117.1(4)
B(11)-B(7)-B(12)	58.2(4)	B(8)-B(7)-B(12)	60.2(4)
Rh(3)-B(8)-B(7)	69.2(3)	Rh(3)-B(8)-B(4)	66.8(3)
B(4)-B(8)-B(9)	58.9(4)	B(7)-B(8)-B(12)	58.1(4)
B(9)-B(8)-B(12)	59.7(4)	B(4)-B(9)-B(5)	64.5(4)
B(4)-B(9)-B(8)	60.4(4)	B(5)-B(9)-B(10)	60.1(4)
B(10)-B(9)-B(12)	59.4(4)	B(8)-B(9)-B(12)	60.3(4)
B(5)-B(10)-B(9)	60.1(4)	B(5)-B(10)-B(6)	61.8(4)
B(9)-B(10)-B(12)	60.5(4)	B(6)-B(10)-B(11)	62.4(4)
As(2)-B(11)-B(6)	68.2(4)	B(11)-B(10)-B(12)	60.1(4)
B(6)-B(11)-B(10)	59.3(4)	As(2)-B(11)-B(7)	65.0(3)
B(7)-B(11)-B(12)	57.8(4)	B(10)-B(11)-(12)	60.2(4)
B(7)-B(12)-B(8)	61.7(4)	B(8)-B(12)-B(9)	60.0(4)
B(7)-B(12)-B(11)	64.1(4)	B(9)-B(12)-B(10)	60.1(4)
B(10)-B(12)-B(11)	59.7(4)		

The Rh-P distance of 2.408(1) Å is considerably longer than the reported "normal" Rh-P bond distance of 2.33 Å for rhodium triphenylphosphine complexes.[206] The value in (198) is similar to the Rh-P distance of 2.4020(6) Å found in *closo*-[2-{η^2-$S_2CN(H)Ph$}-2-(PPh_3)-2,1-$RhTeB_{10}H_{10}$] (230) *vide infra*, Table 6.11 (see also section 6.2.3.3).

Table 6.11 Bond distances for compound (198) and four related 12 vertex rhodaheteroboranes, *closo*-[2-{η^2-$S_2CN(H)Ph$}-2-(PPh_3)-2,1-$RhTeB_{10}H_{10}$] (230), *closo*-[3-{η^2-$S_2CN(H)Ph$}-3-(PPh_3)-3,1,2-$RhAs_2B_9H_9$] (232), *precloso*-[2-{η^2-SC(PPh_3)C(H)S}-2,1,7-$RhC_2B_9H_{11}$] (238),[2] and *closo*-[2-(η^2-S_2CH)-2-(PPh_3)-2,1,7-$RhC_2B_9H_{11}$] (239).[2]

No.	Rh-S/Å	Rh-P/Å	Rh-B/Å	N-C/Å	C-S/Å
198	2.462(2)	2.408(1)	2.214(7)- 2.314(7)	1.296(7)	1.695(6)
230	2.4132(6) 2.4020(6)	2.4020(6)	2.2038(24)- 2.2897(22)	1.320(3)	1.6980(21) 1.7100(20)
232(a) --- 232(b)	2.3919(14) 2.4117(13) --- 2.3910(13) 2.4104(15)	2.3854(14) --- 2.3974(14)	2.245(5)- 2.298(5) --- 2.239(5)- 2.264(5)	1.339(6) --- 1.324(6)	1.701(5) 1.712(5) --- 1.715(5) 1.708(5)
238	2.2387(12) 2.2321(11)	---	2.126(5)- 2.172(5)	---	1.711(4) 1.741(4)
239	2.352(1) 2.433(2)	2.315(1)	2.172(5)- 2.196(6)	---	1.657(5) 1.651(5)

The C-S distance in (198) of 1.695(6) Å is notably shorter than the typical C-S single bond distance of 1.82 Å[268] but longer than the typical C=S double bond of 1.61 Å.[269] The C-S distance in (198) is very similar to those in other η^2-isothiocyanate compounds, Table 6.11, and the zirconium compound [$ZrCl(\eta^5$-$Cp)_2\{\eta^2$-$SC(H)NPh\}$] (240), of 1.700(15) Å,[261] the copper compound [$Cu\{\eta^2$-$SC(OC_6H_3Me_2$-2,6)$NPh\}(PPh_3)_2$] (241), of 1.703(3) Å,[270] the ruthenium compound [$Ru\{\eta^2$-$SC(H)NPh\}(CO)PPh_3)]_2[WS_4]$ (242), of 1.69(1) Å,[271] or the osmium compound [$HOs_3\{\mu$-η^2-$SC(H)NPh\}(CO)_9(PMe_2Ph)$] (243), of 1.69(1) Å.[240] The C-S distance in (198) is slightly shorter than that observed in the rhenium compound [$ReOCl_2\{\eta^2$-$SC(OEt)NC_6H_4Me$-4$\}(PPh_3)$] (244) of 1.735(6) Å.[262] It is similar to the longer C-S bond distances in [$RhC_2S_4(\eta^5$-$Cp^*)(PMe_3)$] (245) which range from 1.650(15)-1.688(15) Å.[272] In (245) it was suggested that the chelating C_2S_4 ligand formed a highly delocalised π electron system.

The N-C bond distance in (198) of 1.296(7) Å is close to the typical N=C double bond length of 1.287 Å.[273] The value in (198) is similar to the N=C distances in (240) of 1.284(20) Å, (241) of 1.278(6) Å, (242) of 1.30(2) Å and (243) of 1.319(8) Å.

The Rh-B bond distances range from 2.214(7)-2.314(7) Å which are within the standard range of Rh-B bond distances, and are similar to the distances of the typical 12 vertex rhodaheteroboranes in Table 6.11, (Section 6.2.3.3, Table 6.18).[206]

The Rh-As distances of 2.487(1) and 2.531(1) Å are similar to the Rh-As bond distances in the only other known X-ray crystal structure of a rhodaarsenaborane, *closo*-[3-$\{\eta^2$-$S_2CN(H)Ph\}$-3-PPh_3-3,1,2-$RhAs_2B_9H_9$] (232) which range from 2.438(3)-2.5150(9) Å *vide infra* (see section 6.2.3.2). These Rh-As distances are similar to values reported in the literature for the skutterudite type structure of [$RhAs_3$] of 2.434, 2.468 and 2.569 Å,[274] [$RhCl_3(nas)_2$] (nas = *o*-dimethylaminophenyldimethyl-arsine) of 2.342(4) and 2.529(5) Å,[275] or the Rh(I) complex [$Rh(\mu$-$Bu^t_2As)(CO)_2]_2$ of 2.496 Å.[276]

The As-As bond distance of 2.549(1) Å is slightly longer than the As-As bond distances reported for the few published arsenaborane structures, Table 6.12, which are 2.435(2) and 2.421(2) Å in $As_2B_{10}H_8I_2$ (9),[15] 2.477(3) Å in *closo*-[3-Cl-3,8-$(PPh_3)_2$-3,1,2-$PdAs_2B_9H_8$] (64),[53] 2.4885(5) Å in [1,1-$(PMe_2Ph)_2$-1,2,3-$PdAs_2B_9H_9$]

(65),[44] 2.517(5) Å in [1,6-Cl_2-1,5-$(PMe_2Ph)_2$-1,2,3-$PdAs_2B_9H_7$] (68),[44] and 2.497(3) Å in *closo*-[3,3-$(PPh_3)_2$-3,1,2-$PtAs_2B_9H_9$] (69).[53] However, the value in (198) is exactly the same as in *closo*-[8-{OPr^i(Et)}-3-PPh_3-3,1,2-$CuAs_2B_9H_8$] (71) which is 2.549(4) Å.[58] A "normal" range of As-As bond distances of 2.3-2.8 Å has been suggested.[17]

The B-As bond distances which range from 2.118(8)-2.237(7) Å are very similar to those in (71) which range from 2.125(11)-2.231(11) Å, and are similar to the B-As bond distances in [1-Cl-2,3-Me_2-1,2,3-$AsC_2B_9H_9$] (29) which range from 2.129(18)-2.243(21) Å.[33] These values are similar to the distances of the typical arsenaboranes in Table 6.12. These B-As values are longer than those reported from a recent study of B-As bond distances in non-cluster two-centre two-electron compounds which range from 1.926(6) Å in $[(Me_5)_2BAsPhLi(thf)_3]$ to 2.00(5) Å in $[PhB(Cl)As(Bu^t)_2]_2$.[277]

In compound (198) the shortest B-As bond distances are for As(1)-B(5) and As(2)-B(11). Atoms B(5) and B(11) are each bonded to an arsenic atom with bonding interactions from other cage boron atoms only. Intermediate B-As bond distances are observed for As(1)-B(4) and As(2)-B(7), and B(4) and B(7) are bonded to one arsenic and the rhodium atom, while the longest are As(1)-B(6) and As(2)-B(6) where B(6) is bonded to both arsenic atoms. This pattern in bond lengths is similar to that found in *closo*-[8-{OPr^i(Et)}-3-PPh_3-3,1,2-$CuAs_2B_9H_8$] (71),[58] and *closo*-[3-{η^2-$S_2CN(H)Ph$}-3-(PPh_3)-3,1,2-$RhAs_2B_9H_9$] (232).

The B-B bond distances range from 1.755(10)-1.889(9) Å and are similar to those in (9), (29), (64), (65), (68), (69), (70) and (71) and are within the normal B-B range for metallaboranes, Table 6.12.[103]

Table 6.12 Bond distances for compound (198), $As_2B_{10}H_8I_2$ (9),[15] and eight related 12 vertex metallaarsenaboranes *closo*-[3-{η^2-$S_2CN(H)Ph$}-3-(PPh_3)-3,1,2-$RhAs_2B_9H_9$] (232), *closo*-[1-Cl-2,3-Me_2-1,2,3-$AsC_2B_9H_9$] (29),[33] *closo*-[3-Cl-3,8-(PPh_3)$_2$-3,1,2-$PdAs_2B_9H_8$] (64),[53] [1,1-(PMe_2Ph)$_2$-1,2,3-$PdAs_2B_9H_9$] (65),[44] [1,6-Cl_2-1,5-(PMe_2Ph)$_2$-1,2,3-$PdAs_2B_9H_7$] (68),[44] *closo*-[3,3-(PPh_3)$_2$-3,1,2-$PtAs_2B_9H_9$] (69),[53] *closo*-[3,3-(PMe_2Ph)$_2$-3,1,2-$PtAs_2B_9H_9$] (70),[53] and *closo*-[8-{$OPr^i(Et)$}-3-PPh_3-3,1,2-$CuAs_2B_9H_8$] (71).[58]

No.	As-As/Å	B-As/Å	B-B/Å
198	2.549(1)	2.118(8)-2.237(7)	1.755(10)-1.889(9)
9	2.258(7)-2.435(2)	1.872(10)-2.435(2)	1.763(10)-1.852(11)
232(a)	2.308(3)-2.5089(11)	1.911(6)-2.308(3)	1.751(9)-1.882(9)
-------	----------	----------	----------
232(b)	2.342(3)-2.5315(10)	1.880(7)-2.342(3)	1.729(10)-1.879(8)
29	----	2.129(18)-2.250(22)	1.733(33)-1.897(26)
64	2.477(3)	2.101(9)-2.281(8)	1.739(12)-1.896(10)
65	2.4885(15)	2.119(12)-2.259(12)	1.740(16)-1.881(17)
68	2.517(5)	2.11(5)-2.26(5)	1.65(6)-1.92(7)
69	2.435(6)-2.515(6)	2.076(19)-2.515(6)	1.683(24)-1.919(25)
70	2.497(3)	2.104(12)-2.257(11)	1.730(17)-1.861(16)
71	2.549(4)	2.125(11)-2.231(11)	1.753(14)-1.869(15)

6.2.3.2 Crystal and Molecular Structure of *closo*-[3-{η^2-$S_2CN(H)Ph$}-3-(PPh_3)-3,1,2-$RhAs_2B_9H_9$] (232)

In order to elucidate the structural features of the rhodaarsenaborane (232), it was decided to undertake a single crystal X-ray analysis of the above compound. The X-ray study showed that compound (232) had a *closo* twelve vertex $RhAs_2B_9$ geometry based on a distorted dodecahedron with the rhodium and arsenic atoms adjacent to one another Figure 6.20. The unit cell contained two independent molecules which did not differ significantly, Tables 6,13 and 6,14. In each molecule one of the arsenic atoms in the cage is disordered over two sites which leads to some complication in the discussion of the structure, however, the same population parameters were calculated in both molecules.

The orientation of the Rh{η^2-$S_2CN(H)Ph$}(PPh_3) unit above the As_2B_3 face is shown in Figure 6.21. The PPh_3 unit is above B(8)-B(4) but nearer B(4). The S(1)-Rh-S(2) bond angle of 71.74(4)° in molecule A {and 71.82(5)° in molecule B} is slightly smaller than corresponding angles for rhodiumdithiocarbamates reported in the literature. For example in [(η^5-Cp*)(η^2-S_2CNEt_2)Rh(μ-$Ph_2PCH_2CH_2PPh_2$)Rh(η^2-S_2CNEt_2)(η^5-Cp*)][BPh_4]$_2$ (246) the S-Rh-S angles were identical at 73.69(6)°,[278] and in [Rh{$(Ph_2P)_2CH_2$}(η^2-S_2CNEt_2)(η^5-Cp*)][Ph_4B] (247) S-Rh-S was 73.22(6)°.[266] The S(1)-Rh-S(2) bond angle in (232) is also slightly smaller than that of 72.639(19)° in *closo*-[2-{η^2-$S_2CN(H)Ph$}-2-(PPh_3)-2,1-$RhTeB_{10}H_{10}$](230), Table 6.15 *vide infra*, (see also section 6.2.3.3), but very similar to those reported in *closo*-[3-{η^2-S_2CH}-3-(PPh_3)-3,1,2-$RhC_2B_9H_{11}$](248) of 71.84(3)°,[2] and *closo*-[2-{η^2-S_2CH}-2-(PPh_3)-2,1,7-$RhC_2B_9H_{11}$] (239) of 71.64(3) and 71.67(3)°.[279]

The Rh-S distances in (232) of 2.3919(14){2.3910(13)} Å and 2.4117(13) {2.4104(15)} Å are slightly longer than the typical value of 2.37 Å for Rh-S distances in dithiocarbamates, Table 6.15 (see also section 6.2.4.1, Table 6.11).[206] The Rh-S distances in (232) are similar to the Rh-S distance in [(pp_3)RhSC(S)SCH_3] (249) [pp_3=tris{2-(diphenylphosphino)ethyl}phosphine] of 2.409(5) Å,[280] and three in [$Rh_2(S_2CNMe_2)_5$][BF_4] (237) which are in the range 2.35-2.42 Å.[267]

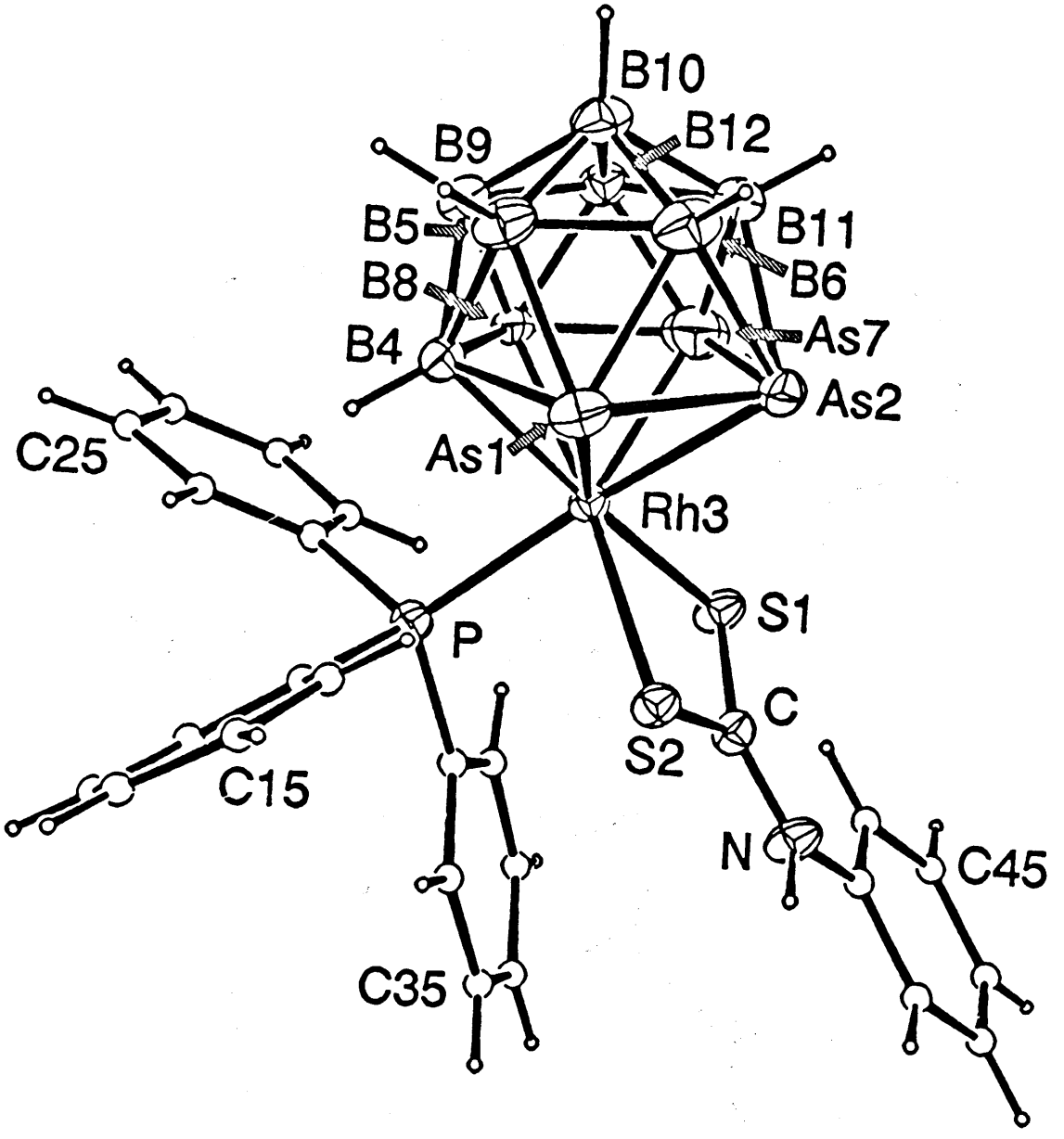

Figure 6.20 An ORTEP view of molecule A of *closo*-[3-{η^2-$S_2CN(H)Ph$}-3-(PPh_3)-3,1,2-$RhAs_2B_9H_9$] (232) with atom numbering scheme.

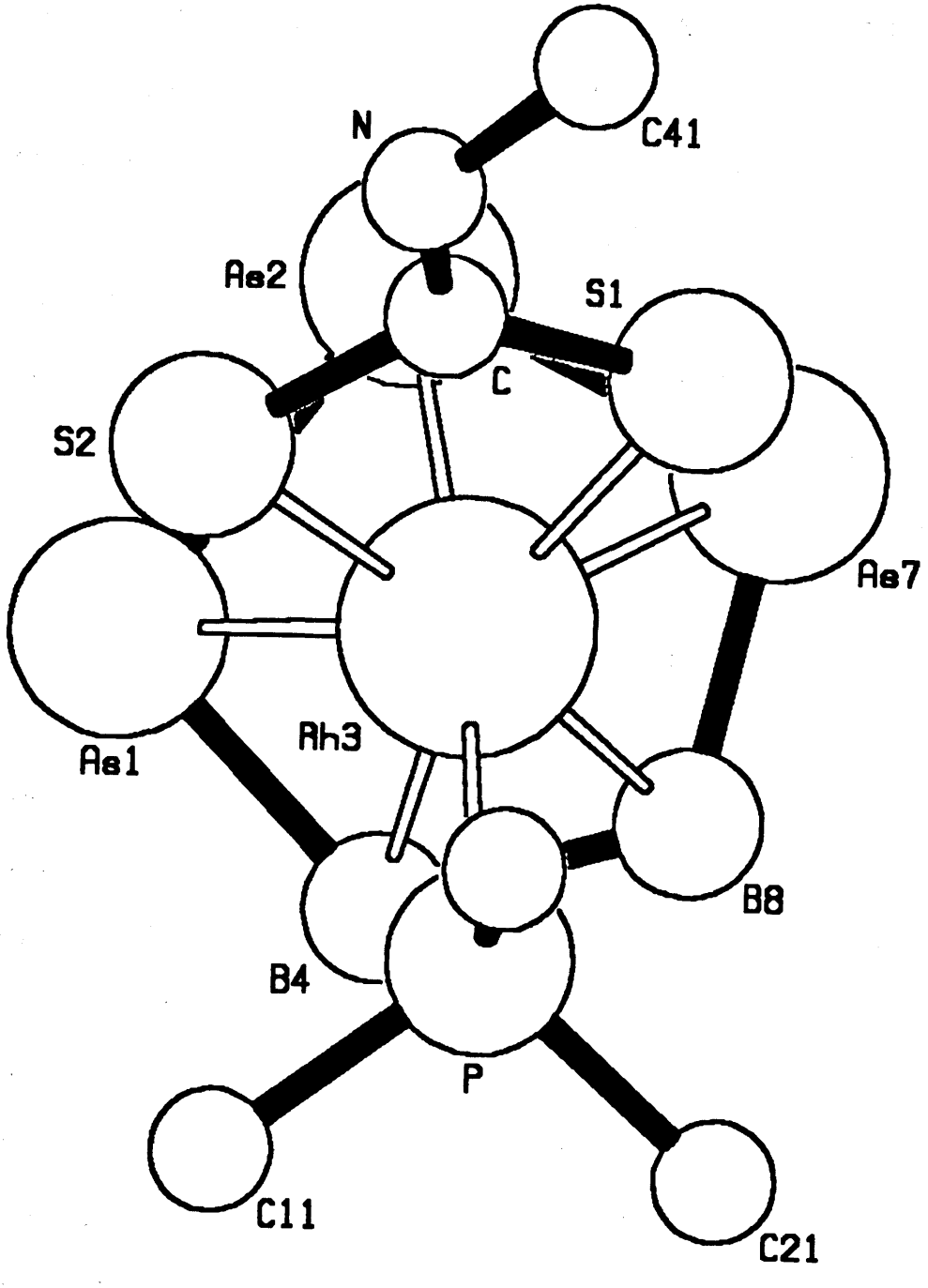

Figure 6.21 A view of the Rh{η^2-$S_2CN(H)Ph$}(PPh_3) unit above the As_2B_3 face of molecule A of *closo*-[3-{η^2-$S_2CN(H)Ph$}-3-(PPh_3)-3,1,2-$RhAs_2B_9H_9$] (232).

Table 6.13 Important bond distances (Å) for *closo*-[3-{η^2-$S_2CN(H)Ph$}-3-(PPh_3)-3,1,2-$RhAs_2B_9H_9$] (232).

Rh(3A)-As(1A)	2.5024(12)	Rh(3B)-As(1B)	2.4966(9)
Rh(3A)As(2A)	2.5130(9)	Rh(3B)-As(2B)	2.5150(9)
Rh(3A)-S(1A)	2.3919(14)	Rh(3B)-S(1B)	2.3910(13)
Rh(3)-S(2A)	2.4117(13)	Rh(3B)-S(2B)	2.4104(15)
Rh(3A)-P(A)	2.3854(14)	Rh(3B)-P(B)	2.3974(14)
Rh(3A)-B(4A)	2.298(5)	Rh(3B)-B(4B)	2.264(5)
Rh(3A)-As(7A)	2.438(3)	Rh(3B)-As(7B)	2.494(3)
Rh(3A)-B(8A)	2.245(5)	Rh(3B)-B(8B)	2.239(5)
As(1A)-As(2A)	2.5089(11)	As(1B)-As(2B)	2.5315(10)
As(1A)-B(4A)	2.146(6)	As(1B)-B(4B)	2.130(6)
As(1A)-B(5A)	2.091(6)	As(1B)-B(5B)	2.097(7)
As(1A)-B(6A)	2.197(7)	As(1B)-B(6B)	2.215(7)
As(2A)-B(6A)	2.220(6)	As(2B)-B(6B)	2.242(6)
As(2A)-As(7A)	2.308(3)	As(2B)-As(7B)	2.342(3)
As(2A)-B(11A)	2.146(6)	As(2B)-B(11B)	2.154(6)
S(1A)-C(A)	1.701(5)	S(1B)-C(B)	1.715(5)
S(2A)-C(A)	1.712(5)	S(2B)-C(B)	1.708(5)
P(A)-C(11A)	1.833(5)	P(B)-C(11B)	1.831(5)
P(A)-C(21A)	1.848(5)	P(B)-C(21B)	1.836(5)
P(A)-C(31A)	1.842(5)	P(B)-C(31B)	1.845(5)
N(A)-C(A)	1.339(6)	N(B)-C(B)	1.324(6)

N(A)-C(41A)	1.403(6)	N(B)-C(41B)	1.421(6)
B(4A)-B(5A)	1.882(9)	B(4B)-B(5B)	1.879(8)
B(4A)-B(8A)	1.850(8)	B(4B)-B(8B)	1.806(7)
B(4A)-B(9A)	1.787(8)	B(4B)-B(9B)	1.782(8)
B(5A)-B(6A)	1.837(10)	B(5B)-B(6B)	1.815(9)
B(5A)-B(9A)	1.762(9)	B(5B)-B(9B)	1.771(9)
B(5A)-B(10A)	1.762(10)	B(5B)-B(10B)	1.757(9)
B(6A)-B(10A)	1.751(9)	B(6B)-B(10B)	1.729(10)
B(6A)-B(11A)	1.816(10)	B(6B)-B(10B)	1.823(9)
As(7A)-B(8A)	1.996(6)	As(7B)-B(8B)	2.028(6)
As(7A)-B(11A)	2.004(7)	As(7B)-B(11B)	2.002(7)
As(7A)-B(12A)	1.911(6)	As(7B)-B(12B)	1.880(7)
B(8A)-B(9A)	1.798(8)	B(8B)-B(9B)	1.787(8)
B(8A)-B(12A)	1.811(8)	B(8B)-B(12B)	1.804(8)
B(9A)-B(10A)	1.771(9)	B(9B)-B(10B)	1.781(9)
B(9A)-B(12A)	1.772(8)	B(9B)-B(12B)	1.783(8)
B(10A)-B(11A)	1.768(9)	B(10B)-B(11B)	1.745(9)
B(10A)-B(12A)	1.765(9)	B(10B)-B(12B)	1.785(9)
B(11A)-B(12A)	1.771(9)	B(11B)-B(12B)	1.759(10)

Table 6.14 Important bond angles (°) for *closo*-[3-{η^2-$S_2CN(H)Ph$}-3-(PPh_3)-3,1,2-$RhAs_2B_9H_9$] (232).

As(1A)-Rh(3A)-As(2A)	60.03(3)	As(1B)-Rh(3B)-As(2B)	60.68(3)
As(1A)-Rh(3A)-S(1A)	142.27(4)	As(1B)-Rh(3B)-S(1B)	143.60(4)
As(1A)-Rh(3A)-S(2A)	85.59(4)	As(1B)-Rh(3B)-S(2B)	86.05(4)
As(1A)-Rh(3A)-P(A)	116.02(4)	As(1B)-Rh(3B)-P(B)	114.80(4)
As(1A)-Rh(3A)-B(4A)	52.90(14)	As(1B)-Rh(3B)-B(4B)	52.90(14)
As(2A)-Rh(3A)-S(1A)	89.55(5)	As(2B)-Rh(3B)-S(1B)	90.14(4)
As(2A)-Rh(3A)-S(2A)	90.12(4)	As(2B)-Rh(3B)-S(2B)	90.16(4)
As(2A)-Rh(3A)-P(A)	174.06(4)	As(2B)-Rh(3B)-P(B)	174.26(3)
As(2A)-Rh(3A)-B(4A)	94.71(14)	As(2B)-Rh(3B)-B(4B)	94.40(14)
As(2A)-Rh(3A)-As(7A)	55.54(6)	As(2B)-Rh(3B)-As(7B)	55.75(7)
S(1A)-Rh(3A)-S(2A)	71.74(4)	S(1B)-Rh(3B)-S(2B)	71.82(5)
S(1A)-Rh(3A)-P(A)	92.19(5)	S(1B)-Rh(3B)-P(B)	92.58(5)
S(1A)-Rh(3A)-B(4A)	161.22(14)	S(1B)-Rh(3B)-B(4B)	159.80(14)
S(1A)-Rh(3A)-As(7A)	78.95(7)	S(1B)-Rh(3B)-As(7B)	78.42(8)
S(1A)-Rh(3A)-B(8A)	113.63(14)	S(1B)-Rh(3B)-B(8B)	112.94(14)
S(2A)-Rh(3A)-P(A)	85.04(5)	S(2B)-Rh(3B)-P(B)	85.89(5)
S(2A)-Rh(3A)-B(4A)	126.42(14)	S(2B)-Rh(3B)-B(4B)	127.74(14)
S(2A)-Rh(3A)-As(7A)	134.84(7)	S(2B)-Rh(3B)-As(7B)	134.42(7)
S(2A)-Rh(3A)-B(8A)	174.19(14)	S(2B)-Rh(3B)-B(8B)	174.70(14)
P(A)-Rh(3A)-B(4A)	85.44(15)	P(B)-Rh(3B)-B(4B)	84.77(15)
P(A)-Rh(3A)-As(7A)	130.38(7)	P(B)-Rh(3B)-As(7B)	129.81(7)

P(A)-Rh(3A)-B(8A)	92.40(14)	P(B)-Rh(3B)-B(8B)	91.46(15)
B(4A)-Rh(3A)-As(7A)	88.41(15)	B(4B)-Rh(3B)-As(7B)	87.90(15)
B(4A)-Rh(3A)-B(8A)	48.03(19)	B(4B)-Rh(3B)-B(8B)	47.30(19)
As(7A)-Rh(3A)-B(8A)	50.25(15)	As(7B)-Rh(3B)-B(8B)	50.38(15)
Rh(3A)-As(1A)-As(2A)	60.19(3)	Rh(3B)-As(1B)-As(2B)	60.02(3)
Rh(3A)-As(1A)-B(4A)	58.67(15)	Rh(3B)-As(1B)-B(4B)	57.93(14)
As(2A)-As(1A)-B(4A)	98.79(15)	As(2B)-As(1B)-B(4B)	97.33(14)
As(2A)-As(1A)-B(6A)	55.83(18)	As(2B)-As(1B)-B(6B)	55.89(16)
B(4A)-As(1A)-B(5A)	52.74(23)	B(4B)-As(1B)-B(5B)	52.76(22)
B(5A)-As(1A)-B(6A)	50.6(3)	B(5B)-As(1B)-B(6B)	49.67(24)
Rh(3A)-As(2A)-As(1A)	59.77(3)	Rh(3B)-As(2B)-As(1B)	59.30(3)
Rh(3A)-As(2A)-As(7A)	60.58(7)	Rh(3B)-As(2B)-As(7B)	61.67(7)
As(1A)-As(2A)-B(6A)	54.96(20)	As(1B)-As(2B)-B(6B)	54.90(17)
As(1A)-As(2A)-As(7A)	101.60(8)	As(1B)-As(2B)-As(7B)	102.29(8)
B(6A)-As(2A)-B(11A)	49.1(3)	B(6B)-As(2B)-B(11B)	49.0(3)
As(7A)-As(2A)-B(11A)	53.33(19)	As(7B)-As(2B)-B(11B)	52.68(21)
Rh(3A)-S(1A)-C(A)	89.00(16)	Rh(3B)-S(1B)-C(B)	88.88(15)
Rh(3A)-S(2A)-C(A)	88.09(16)	Rh(3B)-S(2B)-C(B)	88.40(16)
S(1)-C(A)-S(2A)	111.09(25)	S(1B)-C(B)-S(2B)	110.73(25)
S(1A)-C(A)-N(A)	128.7(4)	S(1B)-C(B)-N(B)	128.4(3)
S(2A)-C(A)-N(A)	120.2(3)	S(2B)-C(B)-N(B)	120.9(3)
Rh(3A)-B(4A)-As(1A)	68.43(16)	Rh(3B)-B(4B)-As(1B)	69.17(16)
Rh(3A)-B(4A)-B(8A)	64.46(23)	Rh(3B)-B(4B)-B(8B)	65.63(23)

As(1A)-B(4A)-B(5A)	62.1(3)	As(1B)-B(4B)-B(5B)	62.7(3)
As(1A)-B(4A)-B(8A)	115.7(3)	As(1B)-B(4B)-B(8B)	118.1(3)
B(5A)-B(4A)-B(9A)	57.3(3)	B(5B)-B(4B)-B(9B)	57.8(3)
B(8A)-B(4)-B(9A)	59.2(3)	B(8B)-B(4B)-B(9B)	59.7(3)
As(1A)-B(5A)-B(4A)	65.14(25)	As(1B)-B(5B)-B(4B)	64.5(3)
As(1A)-B(5A)-B(6A)	67.7(3)	As(1B)-B(5B)-B(6B)	68.6(3)
B(4A)-B(5A)-B(9A)	58.6(3)	B(4B)-B(5B)-B(9B)	58.3(3)
B(6A)-B(5A)-B(10A)	58.2(4)	B(6B)-B(5B)-B(10B)	57.9(4)
B(9A)-B(5A)-B(10A)	60.3(4)	B(9B)-B(5B)-B(10B)	60.6(4)
As(1A)-B(6A)-As(2A)	69.21(19)	As(1B)-B(6B)-As(2B)	69.21(19)
As(1A)-B(6A)-B(5A)	61.7(3)	As(1B)-B(6B)-B(5B)	61.8(3)
As(2A)-B(6A)-B(11A)	63.3(3)	As2(B)-B(6B)-B(11B)	63.0(3)
B(5A)-B(6A)-B(10A)	58.8(4)	B(5B)-B(6B)-B(10B)	59.4(4)
B(10A)-B(6A)-B(11A)	59.4(4)	B(10B)-B(6B)-B(11B)	58.8(4)
Rh(3A)-As(7A)-As(2A)	63.87(7)	Rh(3B)-As(7B)-As(2B)	62.58(7)
Rh(3A)-As(7A)-B(8A)	59.84(16)	Rh(3B)-As(7B)-B(8B)	58.27(17)
As(2A)-As(7A)-B(8A)	105.46(20)	As(2B)-As(7B)-B(8B)	103.16(20)
As(2A)-As(7A)-B(11A)	59.19(19)	As(2B)-As(7B)-B(11B)	58.83(21)
B(8A)-As(7A)-B(12A)	55.18(24)	B(8B)-As(7B)-B(12B)	54.8(3)
B(11A)-As(7A)-B(12A)	53.7(3)	B(11B)-As(7B)-B(12B)	53.8(3)
Rh(3A)-B(8A)-B(4A)	67.50(23)	Rh(3B)-B(8B)-B(4B)	67.07(24)
Rh(3A)-B(8A)-As(7A)	69.91(17)	Rh(3B)-B(8B)-As(7B)	71.35(18)
B(4A)-B(8A)-As(7A)	118.4(3)	B(4B)-B(8B)-As(7B)	119.0(3)

B(4A)-B(8A)-B(9A)	58.6(3)	B(4B)-B(8B)-B(9B)	59.4(3)
As(7A)-B(8A)-B(12A)	60.02(25)	As(7B)-B(8B)-B(12B)	58.4(3)
B(9A)-B(8A)-B(12A)	58.8(3)	B(9B)-B(8B)-B(12B)	59.5(3)
B(4A)-B(9A)-(B5A)	64.1(3)	B(4B)-B(9B)-B(5B)	63.9(3)
B(4A)-B(9A)-B(8A)	62.1(3)	B(4B)-B(9B)-B(8B)	60.8(3)
B(5A)-B(9A)-B(10A)	59.8(4)	B(5B)-B(9B)-B(10B)	59.3(4)
B(8A)-B(9A)-B(12A)	61.0(3)	B(8B)-B(9B)-B(12B)	60.7(3)
B(10A)-B(9A)-B(12A)	59.8(4)	B(10B)-B(9B)-B(12B)	60.1(3)
B(5A)-B(10A)-B(6A)	63.0(4)	B(5B)-B(10B)-B(6B)	62.7(4)
B(5A)-B(10A)-B(9A)	59.8(4)	B(5B)-B(10B)-B(9B)	60.1(3)
B(6A)-B(10A)-B(11A)	62.1(4)	B(6B)-B(10B)-B(11B)	63.3(4)
B(9A)-B(10A)-B(12A)	60.1(3)	B(9B)-B(10B)-B(12B)	60.0(3)
B(11A)-B(10A)-B(12A)	60.2(3)	B(11B)-B(10B)-B(12B)	59.8(4)
As(2A)-B(11A)-B(6A)	67.6(3)	As(2B)-B(11B)-B(6B)	68.0(3)
As(2A)-B(11A)-As(7A)	67.48(19)	As(2B)-B(11B)-As(7B)	68.49(21)
B(6A)-B(11A)-B(10A)	58.5(4)	B(6B)-B(11B)-B(10B)	57.9(4)
As(7A)-B(11A)-B(12A)	60.5(3)	As(7B)-B(11B)-B(12B)	59.5(3)
B(10A)-B(11A)-B(12A)	59.8(3)	B(10B)-B(11B)-B(12B)	61.2(4)
As(7A)-B(12A)-B(8A)	64.8(3)	As(7B)-B(12B)-B(8B)	66.8(3)
As(7A)-B(12A)-B(11A)	65.8(3)	As(7B)-B(12B)-B(11B)	66.7(3)
B(8A)-B(12A)-B(9A)	60.2(3)	B(8B)-B(12B)-B(9B)	59.8(3)
B(9A)-B(12A)-B(10A)	60.1(4)	B(9B)-B(12B)-B(10B)	59.9(3)
B(10A)-B(12A)-B(11A)	60.0(4)	B(10B)-B(12B)-B(11B)	59.0(4)

Table 6.15 Bond distances and angles for compounds (232) and *closo*-[2-{η^2-$S_2CN(H)Ph$}-2-(PPh_3)-2,1-$RhTeB_{10}H_{10}$] (230), and three rhodium dithiocarbamate complexes, [$Rh_2(\eta^2$-$S_2CNMe_2)_5$][BF_4] (237),[267] [(η^5-Cp*)(η^2-S_2CNEt_2)Rh(μ-$Ph_2PCH_2CH_2PPh_2$)Rh(η^2-S_2CNEt_2)(η^5-Cp*)][BPh_4]$_2$ (246),[278] and [Rh{$(Ph_2P)_2CH_2$}(η^2-S_2CNEt_2)(η^5-Cp*)][Ph_4B] (247).[266]

No.	S(1)-Rh-S(2)/°	Rh-S/Å	S-C/Å	C-N/Å
232(a)	71.44(4)	2.3919(14) 2.4117(13)	1.701(5) 1.712(5)	1.339(6)
---	---	---	---	---
232(b)	71.82(5)	2.3910(13) 2.4104(15)	1.715(5) 1.708(5)	1.324(6)
230	72.639(19)	2.4132(6) 2.3577(6)	1.6980(21) 1.7100(20)	1.320(3)
237	[a]	2.337(2)- 2.421(2)	1.688(10)- 1.771(10)	1.300(11)- 1.503(11)
246	73.69(6)	2.3493(18) 2.3638(18)	1.720(6) 1.704(6)	1.437(9) 1.481(10)
247	73.22(6)	2.3700(18) 2.3737(19)	1.729(7) 1.715(7)	1.313(9)

[a] Data not given

The two S-C distances of 1.701(5){1.715(5)} and 1.712(5){1.708(5)} Å are the same within twice the esd (estimated standard deviation). Other S-C distances are 1.725 Å in [$RhCl_2(S_2CO)(PMe_2Ph)_2$][K],[281] and those in other rhodiumdithiocarbamate complexes given above in Table 6.15.

The N-C bond distances of 1.339(6) {1.324(6)} Å correspond with the average bond distance of 1.324 Å in dithiocarbamates (within twice the esd), and are similar to the N-C distances of the rhodiumdithiocarbamate complexes in Table 6.15.[206]

The Rh-P distances of 2.3854(14){2.3974(14)} Å are slightly longer than the average Rh-P bond distance of 2.33 Å for rhodium triphenylphosphine complexes, but shorter than the Rh-P distances of 2.408(1) Å in *closo*-[3-{η^2-SC(H)NPh}-3-(PPh_3)-3,1,2-$RhAs_2B_9H_9$] (198) and 2.4020(6) Å in *closo*-[2-{η^2-$S_2CN(H)Ph$}-2-(PPh_3)-2,1-$RhTeB_{10}H_{10}$] (230), Table 6.11.[206]

The Rh-As(2) distances of 2.5130(9){2.5150(9)} Å are similar to the Rh-As bond distances in *closo*-[3-{η^2-SC(H)NPh}-3-(PPh_3)-3,1,2-$RhAs_2B_9H_9$] (198) (see section 6.2.3.1, Table 6.12), and are similar to the Rh-As bond distances in the skutterudite type structure, [$RhAs_3$] of 2.434, 2.468 and 2.569 Å.[274]

The Rh-B distances of 2.298(5){2.264(5)} and 2.245(5){2.239(5)} Å are within the standard range of Rh-B bond distances, and are similar to the Rh-B distances in the 12 vertex rhodaheteroboranes in Table 6.11.[206]

The As-As bond distances vary from 2.5089(11){2.5315(10)} to 2.308(3){2.3-42(3)} and are within the normal range of As-As bond distances of 2.3-2.8 Å, which are within the range of the few published arsenaborane complexes, Table 6.12.[17]

The B-As bond distances which range from 1.911(6){1.880(7)} to 2.220(6){2.242(6)} Å have a wider range than those found in a recent study of B-As bond distances in non cluster compounds which range from 1.926(6) Å in [$(Me_5)_2BAsPhLi(thf)_3$] to 2.200(5) Å in [$PhB(Cl)As(Bu^t)_2]_2$.[277] The shortest B-As distances are As(1)-B(5) and As(2)-B(11). Atoms B(5) and B(11) are each bonded to an arsenic atom with bonding interactions from other cage borons. Intermediate B-As bond distances are those of As(1)-B(4) and As(2)-B(11) while the longest are As(1)-B(6) and As(2)-B(6) where B(6) is bonded to both arsenic atoms but not to rhodium and B(4) and B(7) are bonded to one arsenic and the rhodium atom. This pattern of bond distances is the same as that found in (198) (see section 6.4.2.1) and in *closo*-[8-{$OPr^i(Et)$}-3-PPh_3-3,1,2-$CuAs_2B_9H_8$] (71).[58]

The B-B bond distances range from 1.751(9){1.729(10)} to 1.882(9){1.879(8)} Å and are very similar to those found in (198) (see section 6.2.3.1, Table 6.12) and are within the normal B-B range for metallaboranes.[103]

6.2.3.3 Crystal and Molecular Structure of *closo*-[2-{η^2-$S_2CN(H)Ph$}-2-(PPh_3)-2,1-$RhTeB_{10}H_{10}$] (230)

For complete structural characterisation of the rhodatelluraborane (230), it was decided to undertake a single crystal X-ray analysis of the compound. The analysis showed that compound (230) had a *closo* twelve vertex $RhTeB_{10}$ geometry based on a distorted dodecahedron with rhodium and tellurium atoms in adjacent positions, Figure 6.22. Important bond distances and angles are given in Tables 6.16 and 6.17 respectively.

The conformation of the [(S_2CNHPh)Rh(PPh_3)] unit above the TeB_4 face, Figure 6.23, is not unexpected in terms of the postulated molecular orbital interactions that occur between $TeB_{10}H_{10}$ ligands and Rh(L)L_2' moieties,[97] but is strongly affected by the fact that the S(1)-Rh-S(2) angle is 72.639(19)°. The conformation is similar to that of the {(η^2-S_2CH)Rh(PPh_3)} unit above the SeB_4 face in *closo*-[2,2-(η^2-S_2CH)-2-(PPh_3)-1,2-$SeRhB_{10}H_{10}$].[282]

The Rh-Te bond length, 2.5812(3) Å, is shorter than the value of 2.6172(4) Å in *closo*-[2,2-(PPh_3)$_2$-2-H-1,2-$TeRhB_{10}H_{10}$] (220),[97] but longer than the Rh-Te bond distances in [2-(η^5-Cp*)-2,1-$RhTeB_{10}H_{10}$] (221),[236] and *closo*-[2-(PPh_3)-2-H-2-($Ph_2PC_6H_4$)-2,1-$RhTeB_{10}H_9$] (222),[237] Table 6.18.

The Rh-B bond distances range from 2.2038(24)-2.2897(22) Å which are within the standard range of Rh-B distances, and are similar to the distances of the published 12 vertex rhodatelluraboranes, Table 6.18.[206]

Within the TeB_{10} cage, the B-B distances vary from 1.747(4)-1.956(4) Å and the Te-B distances range from 2.293(3)-2.3924(23) Å, which are similar to those distances in other 12 vertex rhodatelluraboranes, Table 6.18, and these ranges are typical of metallatelluraboranes in general.[3,197]

In section 6.2.3.2 the bond distances in rhodium-dithiocarbamate complexes are discussed in detail and Table 6.15 contains the bond distances and angles for (230) and four other rhodium-dithiocarbamate complexes.

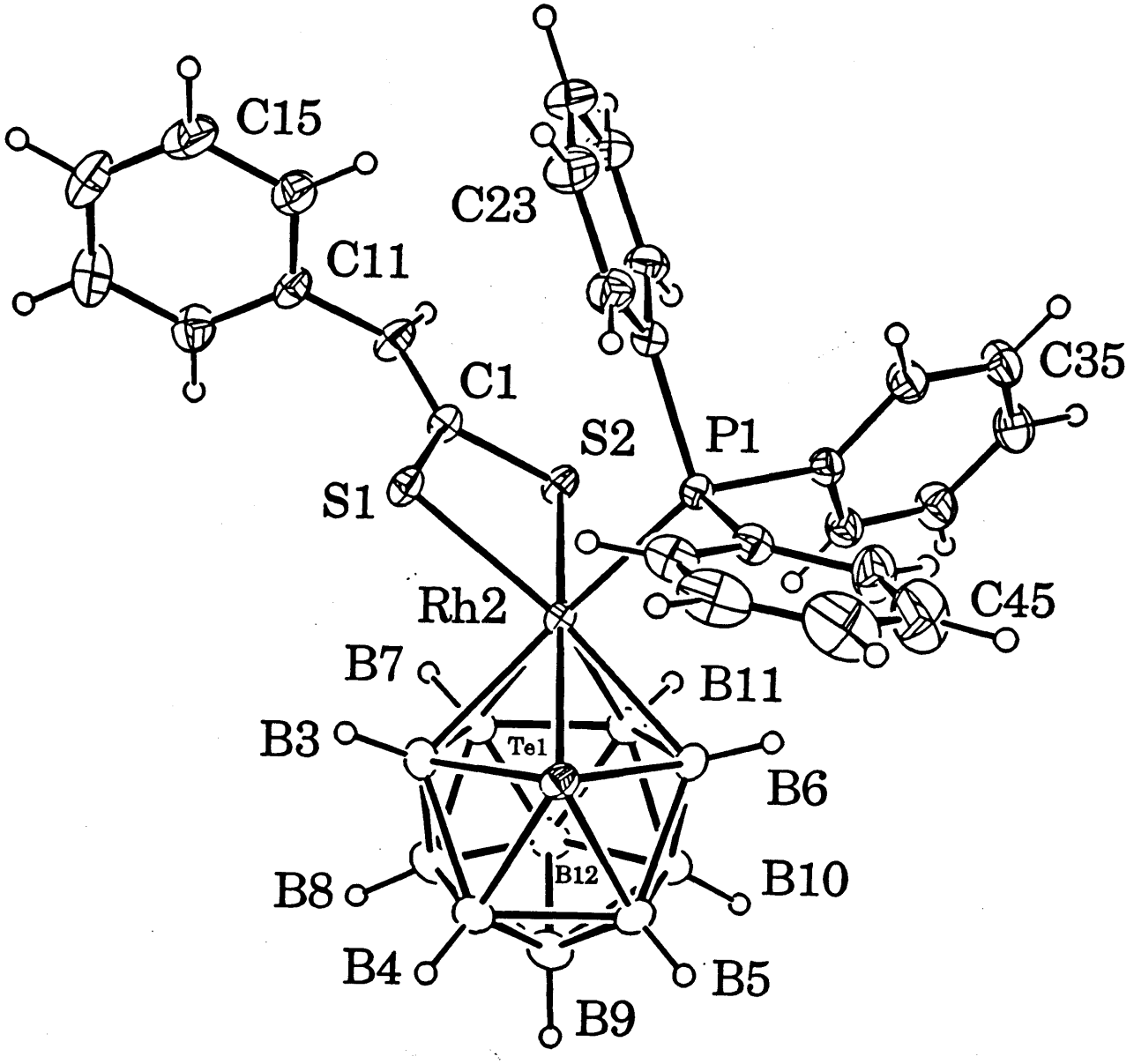

Figure 6.22 A view of *closo*-[2-{η^2-$S_2CN(H)Ph$}-2-(PPh_3)-2,1-$RhTeB_{10}H_{10}$] (230) with atom numbering scheme.

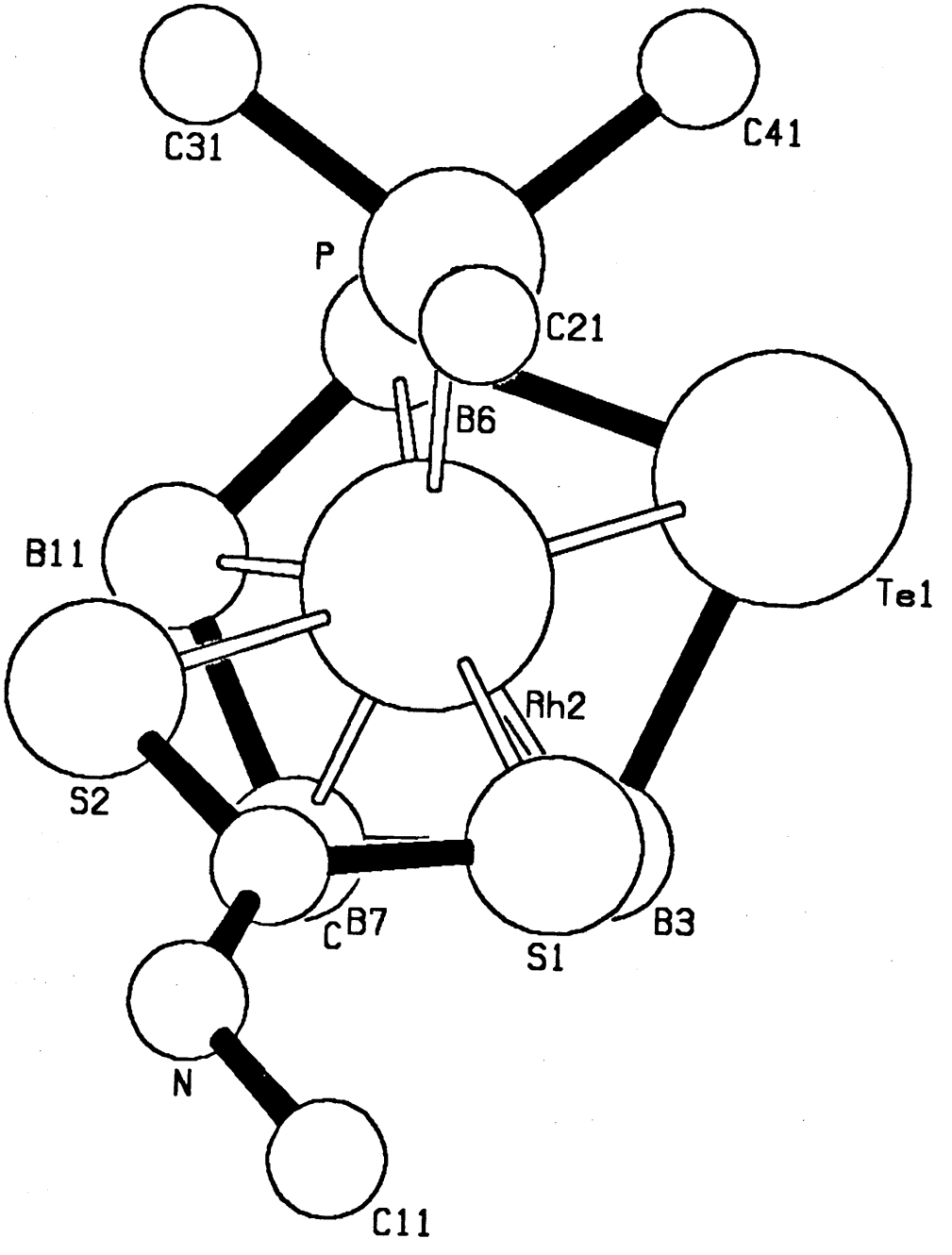

Figure 6.23 A view of the $[(S_2CNHPh)Rh(PPh_3)]$ unit above the TeB_4 face of *closo*-[2-{η^2-$S_2CN(H)Ph$}-2-(PPh_3)-2,1-$RhTeB_{10}H_{10}$] (230).

Table 6.16 Important bond distances (Å) for *closo*-[2-{η^2-$S_2CN(H)Ph$}-2-(PPh_3)-2,1-$RhTeB_{10}H_{10}$] (230).

Te1-Rh2	2.5812(3)	Te1-B3	2.3816(25)
Te1-B4	2.293(3)	Te1-B5	2.304(3)
Te1-B6	2.3924(23)	Rh2-B6	2.2897(22)
Rh2-B7	2.2379(25)	Rh2-B11	2.2038(24)
Rh2-S1	2.4132(6)	Rh2-S2	2.3577(6)
Rh2-P1	2.4020(6)	B3-B4	1.942(4)
B3-B7	1.766(4)	B3-B8	1.747(4)
B4-B5	1.887(4)	B4-B8	1.763(4)
B4-B9	1.756(4)	B5-B6	1.956(4)
B5-B9	1.756(4)	B5-B10	1.751(4)
B6-B10	1.761(4)	B6-B11	1.780(4)
B7-B8	1.791(4)	B7-B11	1.832(4)
B7-B12	1.776(4)	B8-B9	1.776(4)
B8-B12	1.774(4)	B9-B10	1.785(4)
B9-B12	1.768(4)	B10-B11	1.794(4)
B10-B12	1.783(4)	B11-B12	1.770(4)
S1-C1	1.6980(21)	S2-C1	1.7100(20)
C1-N1	1.320(3)	N1-C11	1.441(3)
N1-H1	0.9500(19)	P1-C21	1.8422(21)
P1-C31	1.8306(21)	P1-C41	1.8255(22)

Table 6.17 Important bond angles (°) for *closo*-[2-{η^2-$S_2CN(H)Ph$}-2-(PPh_3)-2,1-$RhTeB_{10}H_{10}$] (230).

Rh2-Te1-B3	55.83(6)	Rh2-Te1-B6	54.66(6)
B3-Te1-B6	83.91(8)	B4-Te1-B5	48.45(10)
B4-Te1-B6	84.19(9)	Te1-Rh2-B6	58.47(6)
Te1-Rh2-B7	93.90(7)	Te1-Rh2-B11	94.49(7)
Te1-Rh2-S1	108.380(16)	Te1-Rh2-S2	178.121(15)
Te1-Rh2-P1	96.614(15)	B6-Rh2-B7	83.52(10)
B6-Rh2-B11	46.63(9)	B6-Rh2-S1	166.84(6)
B6-Rh2-S2	120.52(6)	B6-Rh2-P1	90.25(6)
B7-Rh2-B11	48.71(10)	B7-Rh2-S1	98.67(7)
B7-Rh2-S2	84.36(7)	B7-Rh2-P1	162.64(7)
B11-Rh2-S1	142.10(7)	B11-Rh2-S2	83.83(7)
B11-Rh2-P1	116.45(7)	S1-Rh2-S2	72.639(19)
S1-Rh2-P1	91.083(20)	S2-Rh2-P1	84.909(20)
Te1-B3-B4	63.11(11)	Te1-B3-B7	115.85(14)
B4-B3-B8	56.80(16)	B7-B3-B8	61.30(16)
Te1-B4-B3	67.85(11)	Te1-B4-B5	66.08(12)
B3-B4-B8	56.01(15)	B5-B4-B9	57.52(16)
B8-B4-B9	60.61(18)	Te1-B5-B4	65.47(11)
Te1-B5-B6	67.75(10)	B4-B5-B9	57.50(16)
B6-B5-B10	56.39(14)	B9-B5-B10	61.17(17)
Te-B6-Rh2	66.87(6)	Te1-B6-B5	63.06(10)

Te1-B6-B11	114.38(13)	Rh2-B6-B11	64.15(11)
B5-B6-B10	55.93(15)	B10-B6-B11	60.87(15)
Rh2-B7-B3	70.05(12)	Rh2-B7-B11	64.67(11)
B3-B7-B8	58.83(15)	B3-B7-B11	111.90(17)
B8-B7-B12	59.64(16)	B11-B7-B12	58.73(15)
B3-B8-B4	67.19(16)	B3-B8-B7	59.87(15)
B4-B8-B9	59.51(17)	B7-B8-B12	59.75(16)
B9-B8-B12	59.77(17)	B4-B9-B5	64.98(16)
B4-B9-B8	59.88(17)	B5-B9-B10	59.28(16)
B8-B9-B12	60.06(17)	B10-B9-B12	60.24(17)
B5-B10-B6	67.68(16)	B5-B10-B9	59.55(16)
B6-B10-B11	60.10(14)	B9-B10-B12	59.42(17)
B11-B10-B12	59.31(15)	Rh2-B11-B6	69.22(11)
Rh2-B11-B7	66.62(11)	B6-B11-B7	113.19(17)
B6-B11-B10	59.03(15)	B7-B11-B12	59.04(15)
B10-B11-B12	60.04(16)	B7-B12-B8	60.60(16)
B7-B12-B11	62.23(15)	B8-B12-B9	60.17(17)
B9-B12-B10	60.34(17)	B10-B12-B11	60.65(15)
Rh2-S1-C1	86.83(7)	Rh2-S1-C1	88.37(7)
S1-C1-S2	112.05(11)	S1-C1-N1	125.55(16)
S2-C1-N1	122.40(16)	C1-N1-C11	124.02(18)
Rh2-P1-C21	116.80(7)	Rh2-P1-C31	115.69(71)
Rh2-P1-C41	113.31(7)	C21-P1-C31	100.72(10)

Table 6.18 Bond distances for compound (230) and three related 12 vertex rhodatelluraboranes *closo*-[2,2-$(PPh_3)_2$-2-H-1,2-$TeRhB_{10}H_{10}$] (220),[97] *closo*-[2-(η^5-Cp')-2,1-$RhTeB_{10}H_{10}$] (221),[236] and *closo*-[2-(PPh_3)-2-H-2-$(Ph_2PC_6H_4)$-2,1-RhTe-$B_{10}H_9$] (222).[237]

No.	Rh-Te/Å	Rh-B/Å	Te-B/Å	B-B/Å
230	2.5812(3)	2.2038(24)-2.2897(22)	2.293(3)-2.3924(23)	1.747(4)-1.956(4)
220	2.6172(4)	2.238(4)-2.333(5)	2.296(4)-2.399(4)	1.743(5)-1.962(7)
221(a)	2.529(4)	2.187(12)-2.286(13)	2.264(13)-2.407(12)	1.724(17)-1.982(17)
-------	---------	----------	----------	----------
221(b)	2.536(4)	2.214(11)-2.312(12)	2.302(13)-2.392(12)	1.735(16)-1.967(16)
222	2.5656(4)	2.263(5)-2.331(4)	2.294(5)-2.439(5)	1.725(8)-1.970(6)

The Rh-S distances of 2.4132(6) and 2.3577(6) Å are significantly different and show a *trans* effect with Rh-S(2) *trans* to Te being shorter than Rh-S(1) *trans* to B(5) [2.3577(6) and 2.4132(6) Å respectively] this is also the case with other dithiocarbamates, Table 6.15.

The S-C distances of 1.6980(21) and 1.7100(20) Å are similar to those in $[Rh_2(\eta^2\text{-}S_2CNMe_2)_5][BF_4]$ (237) which range from 1.688(10)-1.771(10) Å, Table 6.15. The S-C distances in (230) are notably shorter than the typical S-C single bond distance of 1.82 Å[268] but longer than the typical S=C double bond of 1.61 Å.[269] There is also an effect on the S-C bond lengths, the longer S-C bond being associated with the shorter Rh-S bond and *vice versa* [S(1)-C(1) 1.6980(21) Å and S(2)-C(1) 1.7100(20) Å].

The C-N bond distance of 1.320(3) Å corresponds to the average C-N bond distance of 1.324 Å in dithiocarbamates and is comparable with C-N distances of rhodium-dithiocarbamate complexes given in Table 6.15.[206]

The Rh-P distance of 2.4020(6) Å is similar to the distance of 2.408(1) Å in *closo*-[3-{η^2-SC(H)NPh}-3-(PPh_3)-3,1,2-$RhAs_2B_9H_9$] (198), but longer than the average Rh-P distance of 2.33 Å for rhodium-triphenylphosphine complexes, Table 6.11.[206]

6.2.4 NMR Spectroscopy

The NMR spectra of compounds *closo*-[3-{η^2-SC(H)NPh}-3-(PPh_3)-3,1,2-$RhC_2B_9H_{11}$] (197), *closo*-[2-{η^2-S_2CN(H)Ph}-2-(PPh_3)-2,1-$RhTeB_{10}H_{10}$] (230) and *closo*-[3-{η^2-SC(H)N(*p*-tol)}-3-(PPh_3)-3,1,2-$RhAs_2B_9H_9$] (234) were kindly recorded on a BRUKER AM 400 MHz instrument by Dr. J. D. Kennedy, University of Leeds, England. All the other spectra including all ^{13}C spectra were recorded on a JEOL FT GSX 270 MHz spectrometer by Mr. D. O'Leary, University College, Cork. In general the NMR data were not very informative.

6.2.4.1 NMR spectra of the thioformamido rhodacarborane *closo*-[3-{η^2-SC(H)NPh}-3-(PPh_3)-3,1,2-$RhC_2B_9H_{11}$] (197) and the dithiocarbamato rhodacarborane *closo*-[3-{η^2-S_2CN(H)Ph}-3-(PPh_3)-3,1,2-$RhC_2B_9H_{11}$] (229)

The measured NMR parameters for the thioformamido rhodacarborane (197) are given in Table 6.19 and the ^{11}B and $^{11}B\{^1H\}$ NMR spectra are illustrated in Figure 6.24. The 400 MHz $^{11}B\{^1H\}$ NMR spectrum of (197) displayed nine resonances of unit relative intensity consistent with a fully asymmetric metallacarborane cage. All boron atom positions had *exo*-terminal hydrogen atoms bound to them and the borane ^1H resonances were assigned to their directly bound boron atoms by $^1H\{^{11}B$(selective)$\}$ spectroscopy. In general the ^{11}B shielding pattern for (197) shows some similarities with *closo*-[3,3-(PPh_3)$_2$-3-H-3,1,2-$RhC_2B_9H_{11}$] (59)[205] and *closo*-[3-{η^2-S_2CN(H)Ph}-3-(PPh_3)-3,1,2-$RhC_2B_9H_{11}$] (229). Figure 6.25 gives the chemical shifts and relative intensities in the ^{11}B NMR spectra of (59), (197) and (229).

Table 6.19 ^{1}H and ^{11}B data for *closo*-[3-{η^2-SC(H)NPh}-3-PPh_3-3,1,2-$RhC_2B_9H_{11}$] (197) at 297K.

$\delta(^{11}B)$/ppm	$\delta(^{1}H)$/ppm
+7.4	3.80
+4.1	2.82
-3.4	2.29
-4.8	2.64
-6.9	2.39
-8.0	2.00
-12.1	2.01
-15.6	1.78
-23.1	1.67
CH	4.12 4.32

at 219K $\delta(^{31}P)$ +42.7 $^{1}J(^{103}Rh\text{-}^{31}P)$ 154Hz

$\delta(^{1}H)$ +8.84 {SC(*H*)NPh}

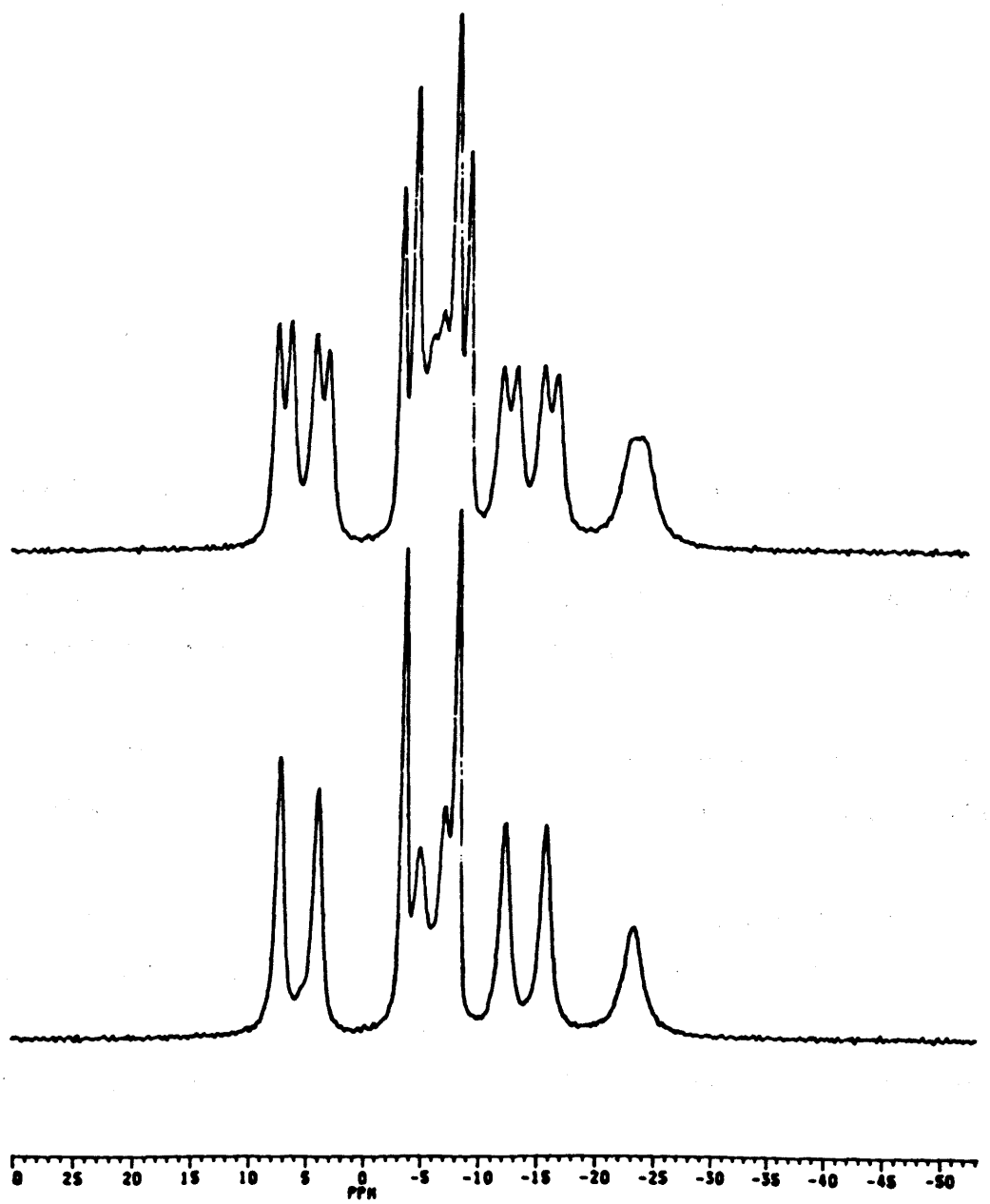

Figure 6.24 ^{11}B(top trace) and $^{11}B\{^1H\}$ (lower trace) NMR spectra of *closo*-[3-{η^2-SC(H)NPh}]-3-(PPh_3)-3,1,2-$RhC_2B_9H_{11}$] (197).

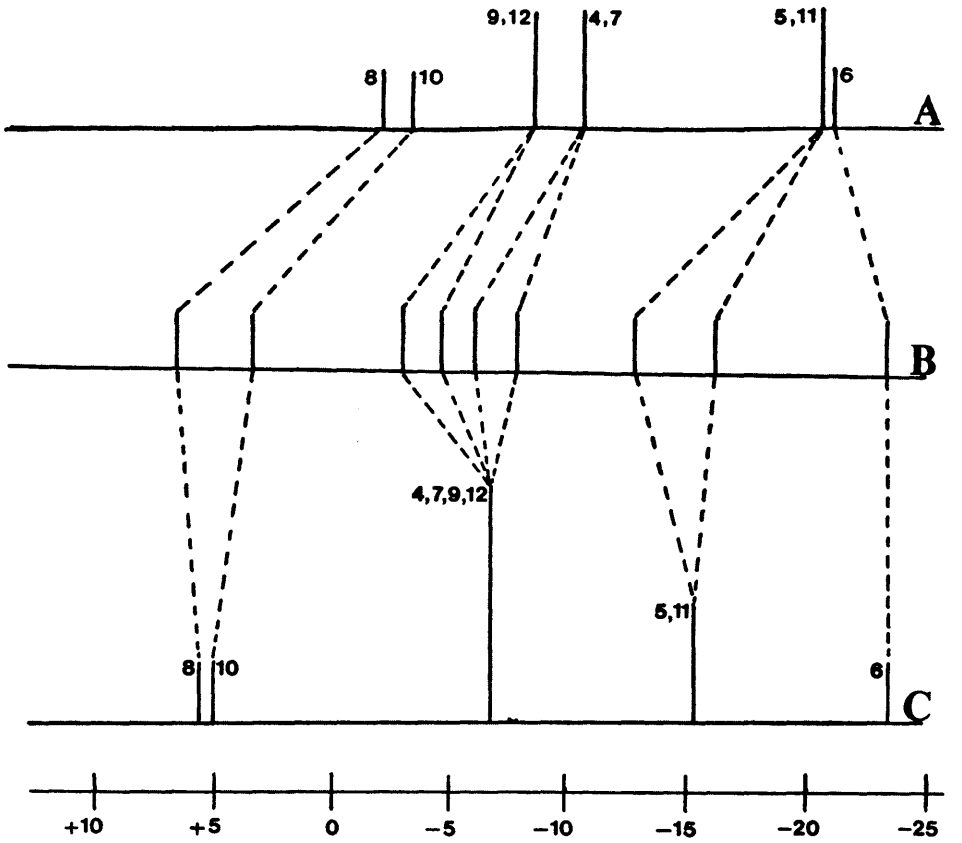

Figure 6.25 Stick diagrams of the chemical shifts and relative intensities in the ^{11}B NMR spectra of (A) *closo*-[3,3-$(PPh_3)_2$-3-H-3,1,2-$RhC_2B_9H_{11}$] (59),[205] (B) *closo*-[3-{η^2-SC(H)NPh}-3-(PPh_3)-3,1,2-$RhC_2B_9H_{11}$] (197) and (C) *closo*-[3-{η^2-$S_2CN(H)Ph$}-3-(PPh_3)-3,1,2-$RhC_2B_9H_{11}$] (229) with tentative assignments.

6.2.4.2 NMR spectra of the dithiocarbamato rhodaarsenaboranes *closo*-[3-{η^2-$S_2CN(H)R$}-3-(PPh_3)-3,1,2-$RhAs_2B_9H_9$] {R=Ph (232), *p*-tol (233) and Bz (235)}

The NMR properties of compounds (232), (233) and (235) are strikingly similar. The ^{11}B and $^{11}B\{^1H\}$ NMR spectra of (232) are illustrated in Figure 6.26. The $^{11}B\{^1H\}$ NMR spectrum displayed three resonances of relative intensity 4:2:3. The $^{11}B\{^1H\}$ NMR spectra of (232), (233) and (235) can be compared to that of the parent rhodaarsenaborane *closo*-[3,3-$(PPh_3)_2$-3-H-3,1,2-$RhAs_2B_9H_9$] (58)[6,22] in stick diagram form, Figure 6.27. No bridging hydrogens were observed in the ^1H NMR spectra of (232), (233) and (235) which is consistent with the *closo* nature of the compounds. Comparison of the NMR spectra of (232), (233) and (235) with the NMR spectrum of (58) allows "tentative" assignment of the peaks as illustrated in Figure 6.27.

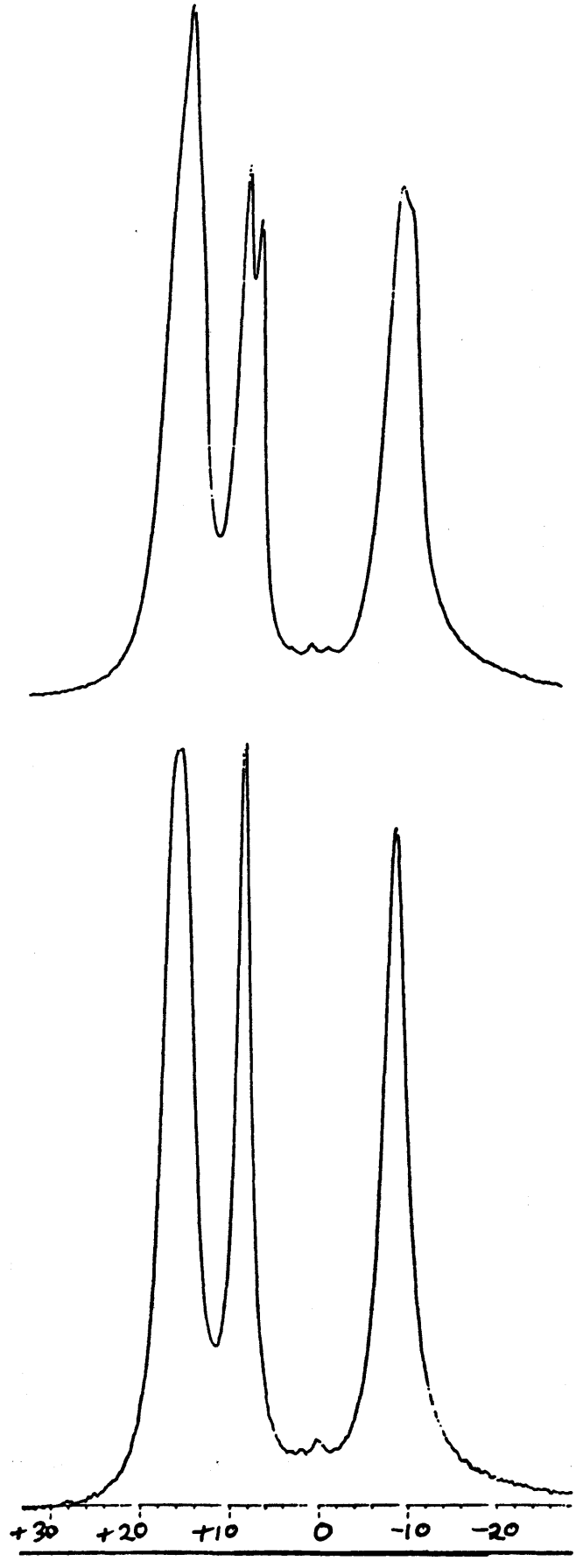

Figure 6.26 ^{11}B(top trace) and $^{11}B\{^1H\}$ (lower trace) NMR spectra of *closo*-[3-{η^2-$S_2CN(H)Ph$}-3-(PPh_3)-3,1,2-$RhAs_2B_9H_9$] (232).

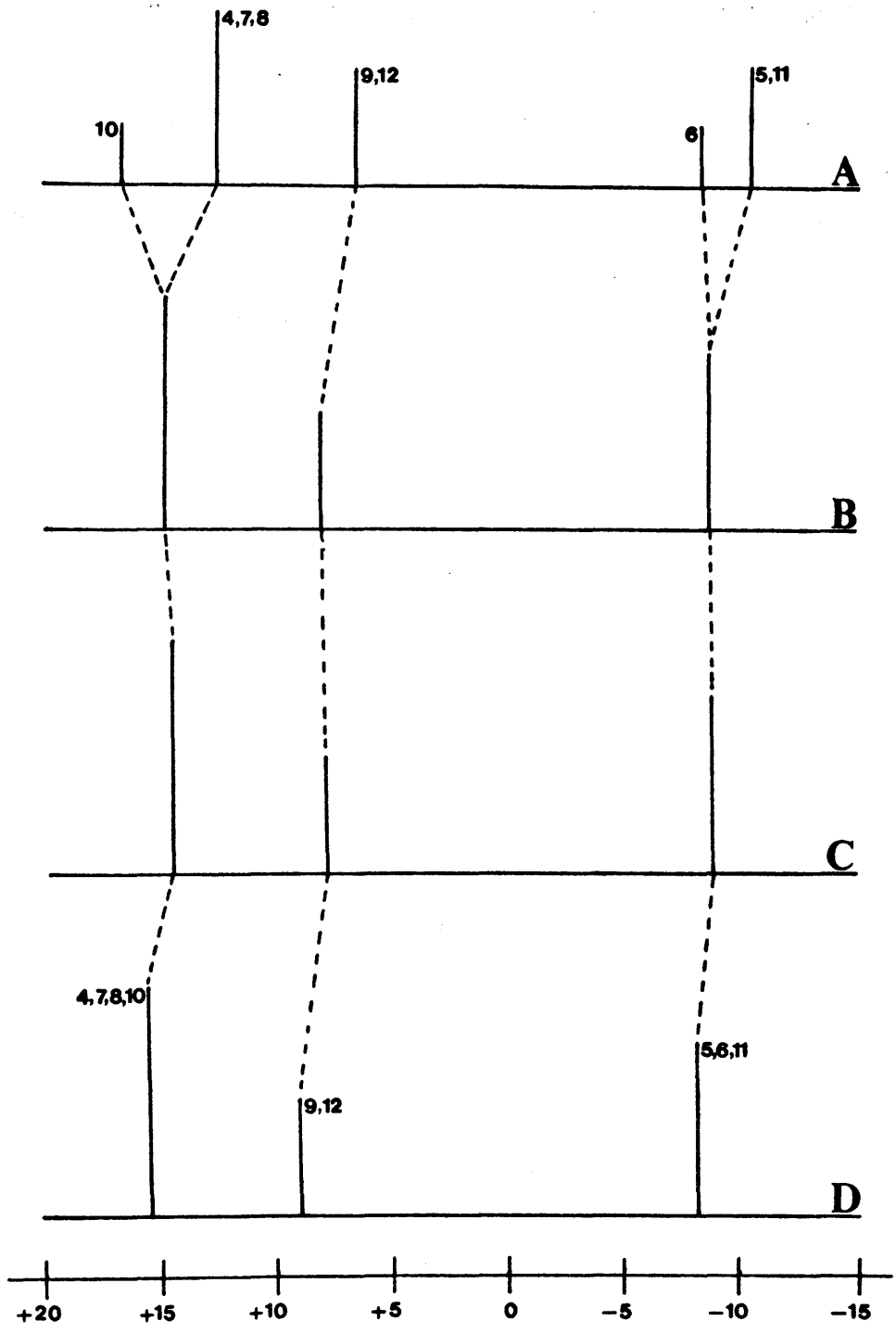

Figure 6.27 Stick diagrams of the chemical shifts and relative intensities in the ^{11}B NMR spectra of (A) *closo*-[3,3-(PPh$_3$)$_2$-3-H-3,1,2-RhAs$_2$B$_9$H$_9$] (58),[6,22] (B) *closo*-[3-{η^2-S$_2$CN(H)Bz}-3-(PPh$_3$)-3,1,2-RhAs$_2$B$_9$H$_9$] (235), (C) *closo*-[3-{η^2-S$_2$CNH(*p*-tol)}-3-(PPh$_3$)-3,1,2-RhAs$_2$B$_9$H$_9$] (233) and (D) *closo*-[3-{η^2-S$_2$CN(H)Ph}-3-(PPh$_3$)-3,1,2-RhAs$_2$B$_9$H$_9$] (232) with tentative assignments.

6.2.4.3 NMR spectra of the thioformamido rhodaarsenaboranes *closo*-[3-{η^2-SC(H)NR}-3-(PPh_3)-3,1,2-$RhAs_2B_9H_9$] {R=Ph (198), *p*-tol (234) and Bz (236)}

The $^{11}B\{^1H\}$ NMR spectra of (198), Figure 6.28 and (234) had 2:2:2:3 relative intensity patterns, whilst (236) had a 2:2:2:2:1 relative intensity sequence. No bridging hydrogens were observed in the ^1H NMR spectra of (198), (234) and (236). The $^{11}B\{^1H\}$ NMR spectra of (198), (234) and (236) can be compared to each other in stick diagram form, Figure 6.29.

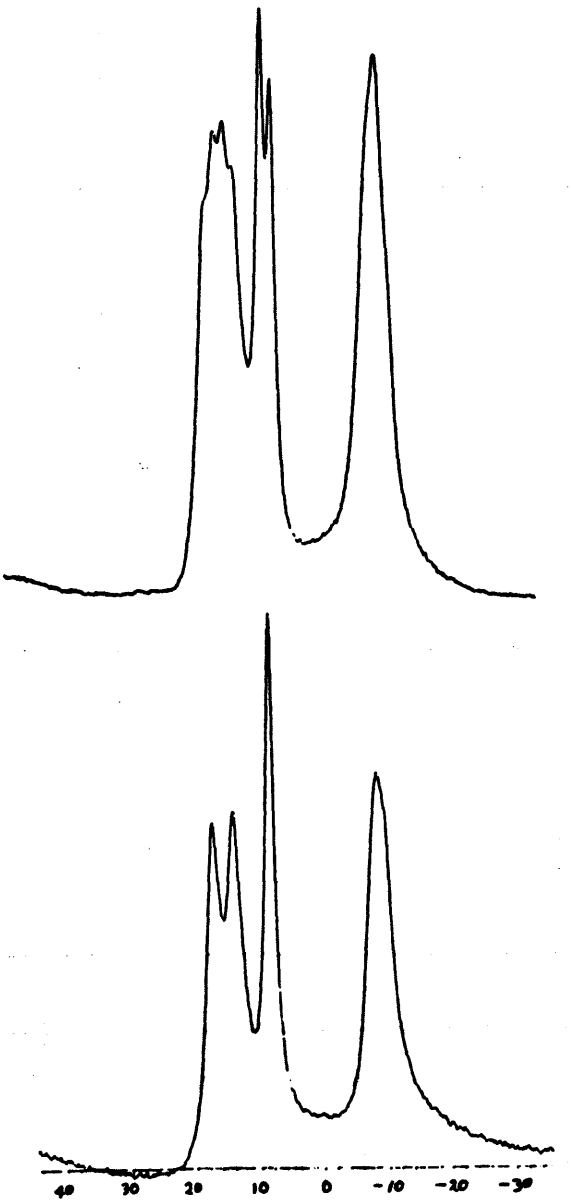

Figure 6.28 ^{11}B(top trace) and $^{11}B\{^1H\}$ (lower trace) NMR spectra of *closo*-[3-{η^2-SC(H)NPh}-3-(PPh_3)-3,1,2-$RhAs_2B_9H_9$] (198).

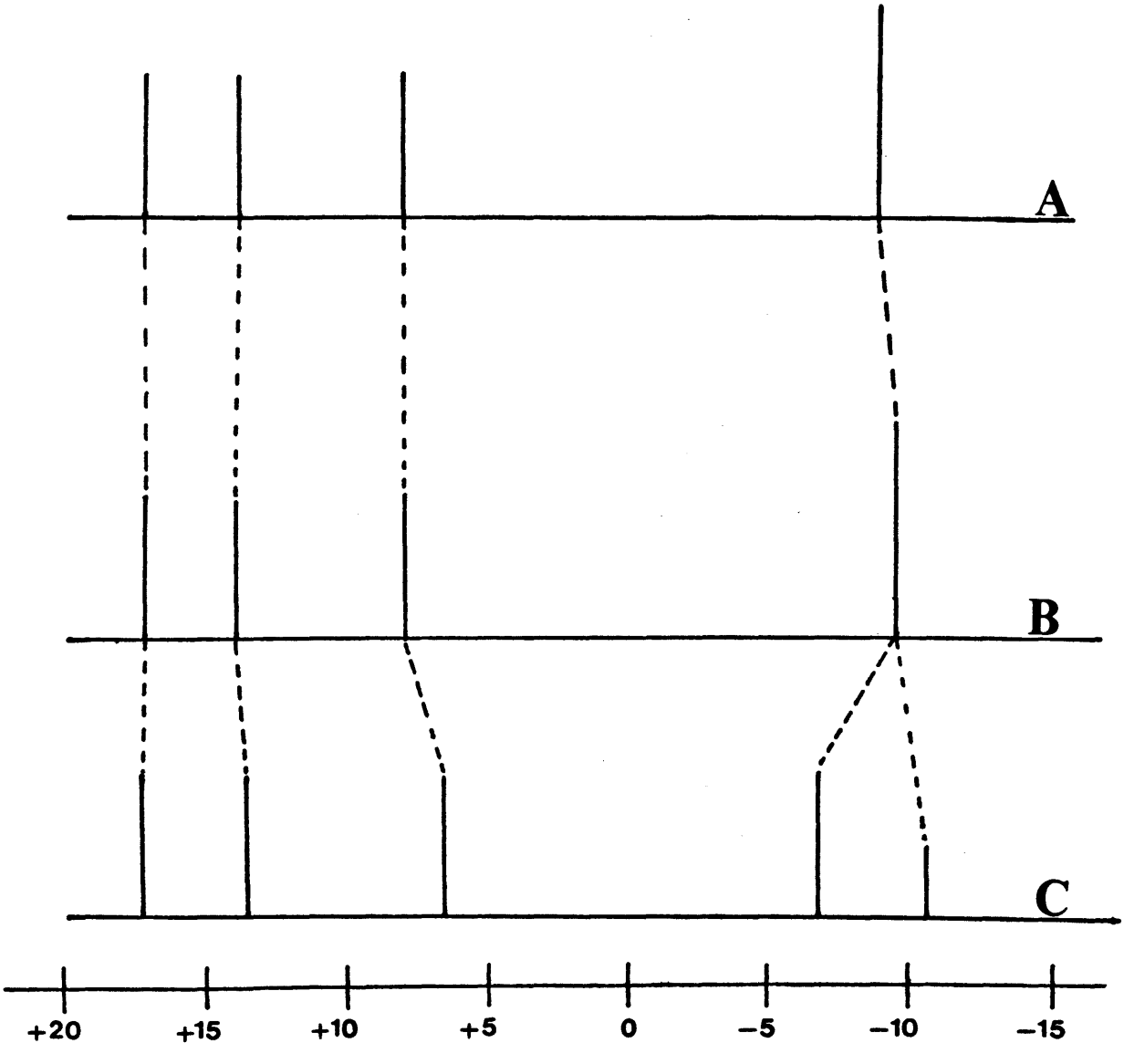

Figure 6.29 Stick diagrams of the chemical shifts and relative intensities in the ^{11}B NMR spectra of (A) *closo*-[3-{η^2-SC(H)NPh}-3-(PPh_3)-3,1,2-$RhAs_2B_9H_9$] (198), (B) *closo*-[3-{η^2-SC(H)N(*p*-tol)}-3-(PPh_3)-3,1,2-$RhAs_2B_9H_9$] (234) and (C) *closo*-[3-{η^2-SC(H)NBz}-3-(PPh_3)-3,1,2-$RhAs_2B_9H_9$] (236).

6.2.4.4 NMR spectra of the dithiocarbamato rhodatelluraborane *closo*-[2-{η^2-$S_2CN(H)Ph$}-2-(PPh_3)-2,1-$RhTeB_{10}H_{10}$] (230)

The $^{11}B\{^1H\}$ NMR spectrum of (230) had a 2:4:2:2 relative intensity pattern Figure 6.30. The thioformamido rhodatelluraborane *closo*-[2-{η^2-SC(H)NPh}-2-(PPh_3)-2,1-$RhTeB_{10}H_{10}$] (231) had a 2:3:1:2:2 pattern. No bridging hydrogens were observed in the ^1H NMR spectrum of (230) or (231).

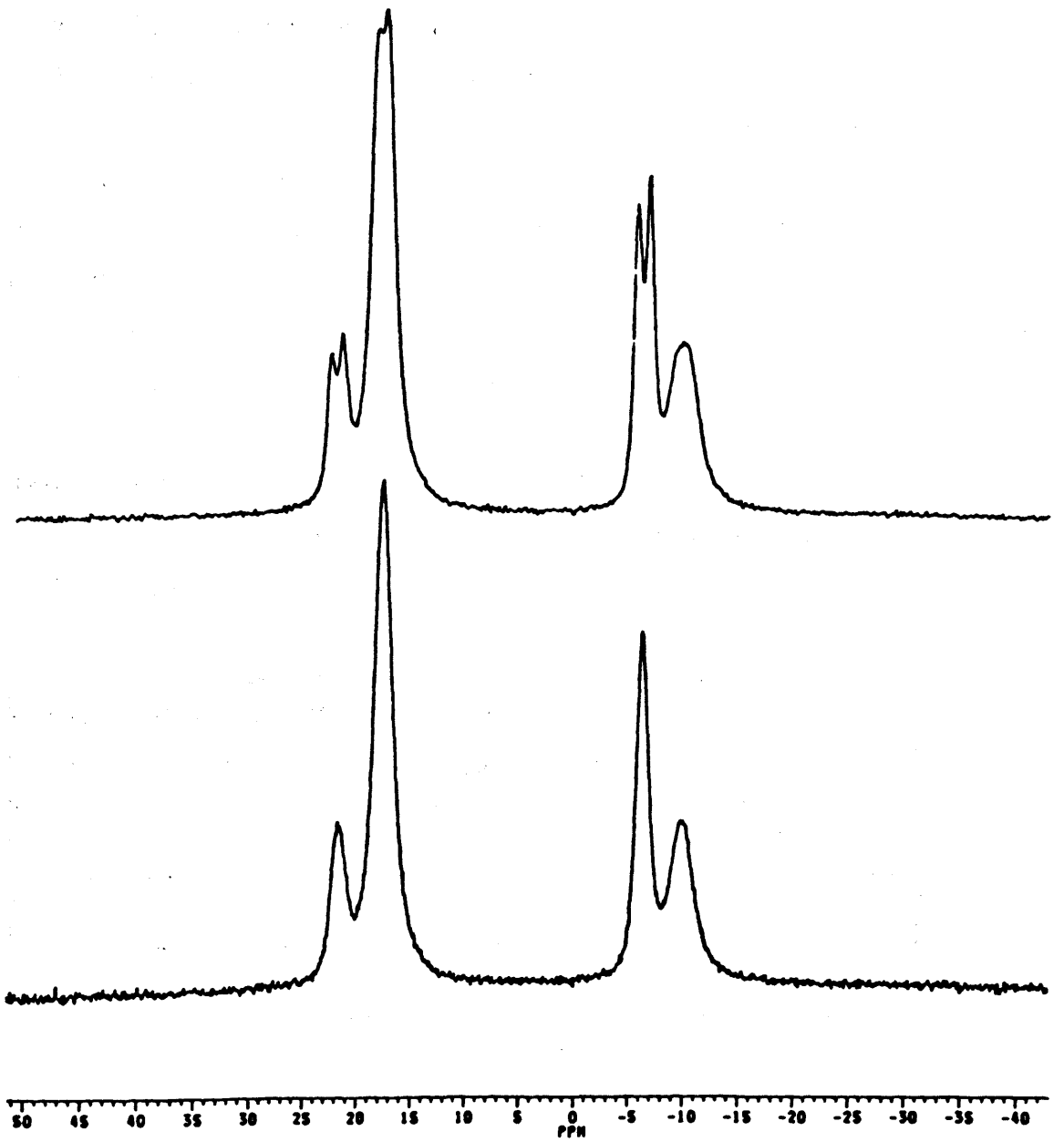

Figure 6.30 ^{11}B(top trace) and $^{11}B\{^1H\}$ (lower trace) NMR spectra of *closo*-[2-{η^2-$S_2CN(H)Ph$}-2-(PPh_3)-2,1-$RhTeB_{10}H_{10}$] (230).

6.2.4.5 ^{13}C NMR of dithiocarbamate and thioformamido complexes

From a study of over seventy metal dithiocarbamate complexes, the chemical shift of the carbon atom in the NCS_2 moiety bonded to a rhodium atom has been assigned a δ value of $\approx +208 \pm 2$ ppm.[283] For the four dithiocarbamate complexes *closo*-[3-{η^2-$S_2CN(H)Ph$}-3-(PPh_3)-3,1,2-$RhC_2B_9H_{11}$] (229) and *closo*-[3-{η^2-S_2C-N(H)R}-3-(PPh_3)-3,1,2-$RhAs_2B_9H_9$] {R=Ph (232), *p*-tol (233) and Bz (235)} the δ values of the carbon atoms in the {η^2-$S_2CN(H)R$} ligands have been measured, Table 6.20. These values are between 207.1-209.9 ppm.

For the thioformamido complexes *closo*-[3-{η^2-SC(H)NPh}-3-(PPh_3)-3,1,2-$RhC_2B_9H_{11}$] (197), *closo*-[3-{η^2-SC(H)NR}-3-(PPh_3)-3,1,2-$RhAs_2B_9H_9$] {R=Ph (198), *p*-tol (234) and Bz (236)} and *closo*-[2-{η^2-SC(H)NPh}-2-(PPh_3)-2,1-$RhTeB_{10}H_{10}$] (231), the δ values of the carbon atom in the {η^2-SC(H)NR} ligand are $\approx$ 180 ppm, Table 6.20. Hence, from a ^{13}C NMR study dithiocarbamate complexes can be distinguished from thioformamido complexes.

Table 6.20 ^{13}C values for the {η^2-$S_2CN(H)R$} ligand in complexes (229), (232), (233) and (235) and for the {η^2-SC(H)NR} ligand in complexes (197), (198), (234), (236) and (231).

COMPOUND {η^2-$S_2CN(H)R$}	$\delta(^{13}C)$/ppm	COMPOUND {η^2-SC(H)NR}	$\delta(^{13}C)$/ppm
229	209.9	197	180.9
232	207.6	198	179.8
233	207.1	234	178.7
235	207.9	236	181.1
		231	179.6

6.3 SUMMARY AND CONCLUSIONS

Reactions between RNCS (R=Ph, *p*-tol and Bz) and Rh-H bonds in *closo*-[3,3-$(PPh_3)_2$-3-H-3,1,2-$RhAs_2B_9H_9$] (58), *closo*-[2,2-$(PPh_3)_2$-2-H-2,1-$RhTeB_{10}H_{10}$] (220) and *closo*-[3,3-$(PPh_3)_2$-3-H-3,1,2-$RhC_2B_9H_{11}$] (59) were studied. The rhodaarsenaborane *closo*-[3,3-$(PPh_3)_2$-3-H-3,1,2-$RhAs_2B_9H_9$] (58) was reacted with RNCS (R=Ph, *p*-tol and Bz) in CH_2Cl_2 to form three dithiocarbamato rhodaarsenaboranes *closo*-[3-{η^2-$S_2CN(H)R$}-3-(PPh_3)-3,1,2-$RhAs_2B_9H_9$]{R=Ph (232), *p*-tol (233) and Bz (235)} and three thioformamido rhodaarsenaboranes *closo*-[3-{η^2-SC(H)NR}-3-(PPh_3)-3,1,2-$RhAs_2B_9H_9$] {R=Ph (198), *p*-tol (234) and Bz (236)}.

Reaction of the rhodatelluraborane *closo*-[2,2-$(PPh_3)_2$-2-H-2,1-$RhTeB_{10}H_{10}$] (220), and the rhodacarborane *closo*-[3,3-$(PPh_3)_2$-3-H-3,1,2-$RhC_2B_9H_{11}$] (59) respectively with PhNCS afforded the two new rhodatelluraboranes, *closo*-[2-{η^2-$S_2CN(H)Ph$}-2-(PPh_3)-2,1-$RhTeB_{10}H_{10}$] (230) and *closo*-[2-{η^2-SC(H)NPh}-2-(PPh_3)-2,1-$RhTeB_{10}H_{10}$] (231), and two new rhodacarboranes *closo*-[3-{η^2-SC(H)NPh}-3-(PPh_3)-3,1,2-$RhC_2B_9H_{11}$] (197) and *closo*-[3-{η^2-$S_2CN(H)Ph$}-3-(PPh_3)-3,1,2-$RhC_2B_9H_{11}$] (229).

The reaction conditions were varied in order to maximise the yields of either the thioformamido or dithiocarbamato complexes, Table 6.21. Under thermally induced reflux conditions, the reaction between the rhodium hydride complexes (58), (220) and (59) and RNCS (R=Ph, *p*-tol and Bz) in a 1:1 mole ratio afforded thioformamido {η^2-SC(H)NR} complexes as the major products. If an excess of isothiocyanate was used the major product was the dithiocarbamate {η^2-$S_2CNH(R)$} complex. These results are comparable with previous reactions of metal complexes with isothiocyanates as discussed in the introduction.[256,261]

Subjecting the reaction of the rhodacarborane *closo*-[3,3-$(PPh_3)_2$-3-H-3,1,2-$RhC_2B_9H_{11}$] (59) with PhNCS in a 1:1 mole ratio in CH_2Cl_2 to microwave irradiation for 5 minutes produced *closo*-[3-{η^2-SC(H)NPh}-3-(PPh_3)-3,1,2-$RhC_2B_9H_{11}$] (197) in 98.8% yield. Clearly the reaction carried out in the microwave oven afforded a marked improvement in the yield of (197), required much less time and afforded fewer side products.

Table 6.21 Maximised Yields of {$S_2CN(H)R$} and {SC(H)NR} products for the reactions of (58), (220) and (59) with RNCS (R=Ph, *p*-tol and Bz) in CH_2Cl_2.

Rhodaheteroborane	RNCS	% yield of {SC(H)NPh} product	% yield of {$S_2CN(H)Ph$} product
closo-[3,3-$(PPh_3)_2$-3-H-3,1,2-$RhC_2B_9H_{11}$] (59)	PhNCS	98.8[a]	31.9[b]
closo-[2,2-$(PPh_3)_2$-2-H-2,1-$RhTeB_{10}H_{10}$] (220)	PhNCS	52.8[c]	9.0[c]
closo-[3,3-$(PPh_3)_2$-3-H-3,1,2-$RhAs_2B_9H_9$] (58)	PhNCS	64.2[c]	54.9[d]
closo-[3,3-$(PPh_3)_2$-3-H-3,1,2-$RhAs_2B_9H_9$] (58)	*p*-tolNCS	47.0[e]	26.4[c]
closo-[3,3-$(PPh_3)_2$-3-H-3,1,2-$RhAs_2B_9H_9$] (58)	BzNCS	53.9[a]	19.8[c]

[a] 1:1 mole ratio of heteroborane:RNCS heated by microwave irradiation for 5 minutes.

[b] 1:10 mole ratio of (229):PhNCS heated by microwave irradiation for 45 minutes.

[c] 1:10 mole ratio of heteroborane:RNCS heated at reflux for 18h.

[d] 1:100 mole ratio of (58):PhNCS stirred at room temperature for 4 d.

[e] 1:1 mole ratio of (58):*p*-tolNCS heated at reflux for 18h.

All of the compounds (197), (198) and (229)-(236) were yellow/orange in colour and air-stable and were characterised by spectroscopic methods. In three cases, compounds (232), (198) and (230), the structures were elucidated by single crystal X-ray analysis.

The successful solution and refinement of the molecular structures *closo*-[3-{η^2-SC(H)NPh}-3-(PPh_3)-3,1,2-$RhAs_2B_9H_9$] (198), *closo*-[3-{η^2-$S_2CN(H)Ph$}-3-(PPh_3)-3,1,2-$RhAs_2B_9H_9$](232)and*closo*-[2-{η^2-$S_2CN(H)Ph$}-2-(PPh_3)-2,1-$RhTeB_{10}H_{10}$](230) showed that all three compounds had a *closo* twelve-vertex geometry based on a distorted dodecahedron. Compounds (232) and (198) are the first reported X-ray crystal structures of rhodaarsenaboranes. Compound (198) appears to be the first reported {η^2-SC(H)NPh}Rh-containing structure. The Rh-P distance in (198) of 2.408(1) Å is considerably longer than the reported "normal" Rh-P bond distance of 2.33 Å for rhodium triphenylphosphine complexes.[206] The C-S distance in (198) of 1.695(6) Å is notably shorter than the typical C-S single bond distance of 1.82 Å[268] but longer than the typical C=S double bond of 1.61 Å.[269] The C-S distance in (198) is very similar to those in other η^2-isothiocyanate compounds, Table 6.11. The N-C bond distance in (198) of 1.296(7) Å is close to the typical N=C double bond length of 1.287 Å.[273] The Rh-As distances of in (198) of 2.487(1) and 2.531(1) Å are similar to the Rh-As bond distances in *closo*-[3-{η^2-$S_2CN(H)Ph$}-3-PPh_3-3,1,2-$RhAs_2B_9H_9$] (232) which range from 2.438(3)-2.5150(9) Å.

The unit cell for compound (232) contained two independent molecules which did not differ significantly. In each molecule one of the arsenic atoms in the boron cage is disordered over two sites with the same population parameters in both molecules which leads to some complication in the discussion of the structure.

Compounds (230) and (232) are both {η^2-$S_2CN(H)Ph$}Rh(PPh_3)} rhodium dithiocarbamate complexes. The Rh-S distances of 2.4132(6) and 2.3577(6) Å in (230) are significantly different and show a *trans* effect with Rh-S(2) *trans* to Te being shorter than Rh-S(1) *trans* to B(5) [2.4020(6) and 2.4132(6) Å respectively] this is also the case with other dithiocarbamates, Table 6.15. The S-C distances in (230) and (232) are notably shorter than the typical S-C single bond distance of 1.82 Å[268] but longer than the typical S=C double bond of 1.61 Å.[269] There is also an effect on the S-C bond lengths, the longer S-C bond being associated with the shorter Rh-S

bond and *vice versa*. The N-C bond distances of 1.339(6) {1.324(6)} Å in (232) and 1.320(3) Å in (230) correspond with the average bond distance of 1.324 Å in dithiocarbamates (within twice the esd), and are similar to the N-C distances of the rhodiumdithiocarbamate complexes in Table 6.15.[206]

For the rhodatelluraborane compound (230) the Rh-Te bond length is similar to those distances in other 12 vertex rhodatelluraboranes, Table 6.18, and these ranges are typical of metallatelluraboranes in general.[3,197] Within the TeB_{10} cage, the B-B distances vary from 1.747(4)-1.956(4) Å and the Te-B distances range from 2.293(3)-2.3924(23) Å, which are similar to those distances in other 12 vertex rhodatelluraboranes, Table 6.18, and these ranges are typical of metallatelluraboranes in general.[3,197]

The Rh-B bond distances in (198) (230) and (232) are within the standard range of Rh-B bond distances, and are similar to the distances of the typical 12 vertex rhodaheteroboranes.[206]

Infrared spectra of the compounds (197), (198) and (229)-(236) contained characteristic B-H bands and bands due to phosphine ligands. No B-H-B, Rh-H-B or Rh-H bands were observed in the IR spectra of (197), (198) and (229)-(236). There were four characteristic bands for the dithiocarbamate complexes (229), (230), (232), (233) and (235). These were the N-H stretch, the N-H bend, the C---S bonds which are also linked to a nitrogen atom and the C-N stretch. There were three characteristic bands for the thioformamido complexes (197), (198), (231), (234) and (236). These were the C---N stretch, the C-H bend of the thioformamido ligand and the C---S band.

The NMR properties of compounds (232), (233) and (235) were strikingly similar. Each spectrum displayed three resonances of relative intensity 4:2:3. The $^{11}B\{^1H\}$ NMR spectra of the rhodaarsenaborane thioformamido derivative (198), (234) and (236) showed a 2:2:2:1:1:1, a 2:2:2:2:3 and a 2:2:2:2:1 relative intensity sequence respectively. The $^{11}B\{^1H\}$ NMR spectrum of the thioformamido compound (197) displayed nine resonances of unit relative intensity consistent with a fully asymmetric metallacarborane cage. The $^{11}B\{^1H\}$ NMR spectra of the dithiocarbamato compound (230) had a 2:4:2:2 relative intensity pattern whilst the thioformamido derivative (231) had a 2:3:1:2:2 pattern. For compounds (197), (198) and (229)-

(236) all boron atom positions had *exo*-terminal hydrogen atoms bound to them and no bridging hydrogens were observed in the ^{1}H NMR spectra which is consistent with the *closo* nature of the compounds.

For the four dithiocarbamate complexes (229), (232), (233) and (235) the ^{13}C δ values of the carbon atom in the $\{\eta^2\text{-}S_2CN(H)R\}$ ligand has been measured, and ranges from 207.1-209.9 ppm, these values are similar to each other and provide a method of distinguishing the manner in which the isothiocyanate ligand is bonded to the metal. For the thioformamido complexes (197), (198), (231), (234) and (236) the δ values of the carbon atom in the $\{\eta^2\text{-}SC(H)NR\}$ ligand has also been measured and are $\approx$ 180 ppm. Hence, from ^{13}C NMR spectroscopy it is very easy to distinguish dithiocarbamate complexes from thioformamido complexes.

6.4 EXPERIMENTAL

6.4.1 General Methodology

All reactions and recrystallisations were carried out under an inert atmosphere but products were isolated and manipulated in air. Thin layer chromatography (tlc), preparative thin layer chromatography (plc) and all spectroscopic and analytical analyses were carried out as stated in section 4.3.1.

Single crystal X-ray analyses were performed by Professor George Ferguson and Dr. John Gallagher, University of Guelph, Canada (see section 4.3.1 for details).

Dr. J. D. Kennedy, University of Leeds, recorded the ^{1}H, ^{11}B and ^{31}P NMR spectra for compounds (230), (197) and (234) on a BRUKER AM 400 MHz instrument. All the other spectra including all ^{13}C spectra were recorded on a JEOL FT GSX 270 MHz spectrometer by Mr. D. O'Leary, University College, Cork. Elemental analyses (C, H, N, S and B) were performed by Mrs. H. Kelly and Mr. B. O'Mahoney at the Microanalytical Laboratory, University College, Cork.

The compounds *closo*-$[3,3\text{-}(PPh_3)_2\text{-}3\text{-}H\text{-}3,1,2\text{-}RhAs_2B_9H_9]$ (58),[6] *closo*-$[2,2\text{-}(PPh_3)_2\text{-}2\text{-}H\text{-}2,1\text{-}RhTeB_{10}H_{10}]$ (220)[97] and *closo*-$[3,3\text{-}(PPh_3)_2\text{-}3\text{-}H\text{-}3,1,2\text{-}RhC_2B_9H_{11}]$ (59)[33] were prepared according to literature methods and characterised spectroscopically and by (C,H) microanalysis. The isothiocyanates (RNCS, R = Ph,

p-tol and Bz) were obtained from the Aldrich Chemical Company Ltd., England and used as supplied.

6.4.2 Reaction between PhNCS and *closo*-[3,3-$(PPh_3)_2$-3-H-3,1,2-$RhAs_2B_9H_9$] (58)

Procedure 1

To a solution of *closo*-[3,3-$(PPh_3)_2$-3-H-3,1,2-$RhAs_2B_9H_9$] (58) (0.10g, 0.113mmol) in CH_2Cl_2 (20ml) was added PhNCS (0.15g, 1.13mmol). The mixture was heated at reflux for 18h. The dark orange solution was concentrated under reduced pressure (rotatory film evaporator, 25°C). Preparative tlc {CH_2Cl_2 - hexane (3:2)} produced *ca.* thirteen bands of which two were in significant amount and were isolated: (a) a yellow band (R_f = 0.4) and (b) an orange band (R_f = 0.8).

(a) The yellow band was extracted into CH_2Cl_2 and recrystallised from CH_2Cl_2 - hexane (3:2) as pale orange prisms of *closo*-[3-{η^2-$S_2CN(H)Ph$}-3-(PPh_3)-3,1,2-$RhAs_2B_9H_9$] (232) (0.018g, 20.2%). (Found: C, 37.5; H, 4.0; N, 1.9; S, 8.3, $C_{25}H_{30}As_2B_9NPRhS_2$ requires: C, 38.0; H, 3.9; N, 1.8; S, 8.1%). IR: ν_{max}(KBr) 3235(m) (NH), 3015(vw), 2925(vw), 2900(w), 2830(w), 2518(vs) (BH), 1582(m), 1518(s), 1485(s), 1468(w), 1428(s), 1422(s), 1380(s,br), 1322(vw), 1178(vw), 1152(vw), 1084(m), 990(s), 820(vw), 740(s), 718(vw), 690(vs) cm^{-1}. NMR data $^{11}B\{^1H\}$ (CH_2Cl_2, 298K) {ordered as: δ ppm (multiplicity, intensity)} +15.6 (s,4B), +8.9 (s,2B), -8.3 (s,3B). ^{13}C (S_2CNHPh) 207.6 ppm, ^1H (*NH*) 8.3 ppm.

(b) The orange band was extracted into CH_2Cl_2 and recrystallised from CH_2Cl_2-hexane (3:2) as orange-red block crystals of *closo*-[3-{η^2-SC(H)NPh}-3-(PPh_3)-3,1,2-$RhAs_2B_9H_9$] (198) (0.055g, 64.2%). (Found: C, 40.1; H, 4.2; N, 2.0, $C_{25}H_{30}As_2B_9NPRhS$ requires C, 39.6; H, 4.0; N, 1.85%). IR: ν_{max}(KBr) 3030(w), 2900(w), 2830(w), 2540(s,sh) (BH), 2515(vs) (BH), 2505(vs,sh) (BH), 2482(s,sh) (BH), 1580(w), 1570(w), 1504(s), 1495(s,sh), 1470(m), 1440(w), 1428(m,sh), 1422(s), 1262(w), 1200(w), 1175(vw), 1150(vw), 1082(m), 1001(m,sh), 993(s), 910(w), 900(vw), 880(w), 840(vw), 815(vw), 750(m,sh), 740(s), 689(s) cm^{-1}. NMR data $^{11}B\{^1H\}$ (CH_2Cl_2, 298K) {ordered as: δ ppm (multiplicity, intensity)} +16.95 (s,2B), +13.8 (s,2B), +8.02 (s,2B), -8.7 (s,1B), -9.1 (s,1B), -9.7 (s,1B). ^{13}C {S*C*(H)NPh} 179.8 ppm, ^1H {SC(*H*)NPh} 8.6 ppm.

Procedure 2

To a solution of *closo*-[3,3-$(PPh_3)_2$-3-H-3,1,2-$RhAs_2B_9H_9$] (58) (0.10g, 0.113mmol) in CH_2Cl_2 (20ml) was added PhNCS (1.50g, 11.3mmol). The mixture was stirred at room temperature for 4 days. The dark orange solution was concentrated under reduced pressure (rotatory film evaporator, 25°C). Preparative tlc {CH_2Cl_2 - hexane (3:2)} produced *ca.* 13 bands. Two bands were isolated: (a) a yellow band (R_f = 0.4) and (b) an orange band (R_f = 0.8) (as in procedure 1 above).

(a) The yellow band was extracted into CH_2Cl_2 and recrystallised from CH_2Cl_2-hexane (3:2) as pale orange prisms of *closo*-[3-{η^2-$S_2CN(H)Ph$}-3-(PPh_3)-3,1,2-$RhAs_2B_9H_9$] (232) (0.049g, 54.9%). IR and NMR data were identical to those reported in procedure 1.

(b) The orange band was extracted into CH_2Cl_2 and recrystallised from CH_2Cl_2-hexane (3:2) as orange-red block crystals of *closo*-[3-{η^2-SC(H)NPh}-3-(PPh_3)-3,1,2-$RhAs_2B_9H_9$] (198) (0.013g, 15.2%). IR and NMR data were identical to those reported in procedure 1.

6.4.3 X-ray analysis of *closo*-[3-{η^2-$S_2CN(H)Ph$}-3-(PPh_3)-3,1,2-$RhAs_2B_9H_9$] (232)

Crystal Data: $C_{25}H_{30}As_2B_9NPRhS_2$, M = 789.67, triclinic, $P\bar{1}$, a = 12.370(3), b = 14.380(3), c = 18.865(4) Å, α = 99.16(2), β = 95.04(2), γ = 107.40(3)°, U = 3128.6(12) Å^3, Z = 4, D_c = 1.68g cm^{-3}, λ(Mo-K_α) = 0.7093 Å, μ(Mo-K_α) = 28.31 cm^{-1}, F(000) = 1560, T = 291K, R = 0.036, R_w = 0.041 for 8613 observed reflections. The unit cell contained two independent molecules which do not differ significantly. One of the arsenic atoms in the boron cage is disordered over two sites with the same occupancy factors (As1 0.864 and As7 0.287) in both molecules.

6.4.4 X-ray analysis of *closo*-[3-{η^2-SC(H)NPh}-3-(PPh_3)-3,1,2-$RhAs_2B_9H_9$] (198)

Crystal Data: $C_{25}H_{30}As_2B_9NPRhS$, M = 757.61, monoclinic, $C2/c$, a = 30.874(5), b = 9.860(2), c = 21.333(3) Å, β = 106.66(1), U = 6221(4) Å^3, Z = 8, D_c = 1.62g cm^{-3}, λ(Mo-K_α) = 0.71073 Å, μ(Mo-K_α) = 27.8 cm^{-1}, F(000) = 2992, T = 294 K, R = 0.033, R_w = 0.036 for 3343 observed reflections.

6.4.5 Reaction of *closo*-[2,2-$(PPh_3)_2$-2-H-2,1-$RhTeB_{10}H_{10}$] (220) with PhNCS.

To a solution of *closo*-[2,2-$(PPh_3)_2$-2-H-2,1-$RhTeB_{10}H_{10}$] (220) (0.10g, 0.114mmol) in CH_2Cl_2 (20mls) was added PhNCS (0.154g, 1.14mmol). The mixture was heated at reflux for 18h. The orange solution was concentrated under reduced pressure (rotatory film evaporator, 25°C). Preparative tlc {CH_2Cl_2 - hexane (3:2)} produced two major components: (a) a yellow band (R_f = 0.4) and (b) an orange band (R_f = 0.8).

(a) The yellow band was extracted into CH_2Cl_2 and recrystallised from CH_2Cl_2-hexane (3:2) to give pale orange crystals of *closo*-[2-{η^2-$S_2CN(H)Ph$}-2-(PPh_3)-2,1-$RhTeB_{10}H_{10}$] (230) (0.008g, 9.0%). (Found: C, 38.1; H, 4.0; N, 1.9, $C_{25}H_{31}B_{10}NPRhS_2Te$ requires C, 38.5; H, 4.0; N, 1.8%). IR: ν_{max}(KBr) 3280(w) (NH), 3030(w), 2930(w,sh), 2903(m), 2838(w), 2520(vs) (BH), 1582(m), 1505(m), 1485(s), 1468(m), 1428(s,sh), 1424(s), 1360(s,br), 1322(vw), 1256(vw), 1180(vw), 1152(vw), 1088(m), 1022(w), 1000(vs), 910(vw), 880(m), 748(s), 690(vs) cm^{-1}. NMR data $^{11}B\{^1H\}$ (CH_2Cl_2, 298K) {ordered as: δ ppm (multiplicity, intensity)} +21.2 (s,2B), +17.2 (s,4B), -6.3 (s,2B), -10.1 (s,2B). $\delta(^{31}P)$ +36 ppm (broad) at 294K.

(b) The orange band was extracted into CH_2Cl_2 and recrystallised from CH_2Cl_2-hexane (3:2) to give dark orange-red crystals of *closo*-[2-{η^2-SC(H)NPh}-2-(PPh_3)-2,1-$RhTeB_{10}H_{10}$] (231) (0.045g, 52.8%). (Found: C, 39.7; H, 4.2; N, 1.7, $C_{25}H_{31}B_{10}NPRhSTe$ requires C, 40.2; H, 4.2; N 1.9%). IR: ν_{max}(KBr) 3030(w), 2930(w,sh), 2903(m), 2838(w), 2520(vs), 1580(w), 1499(vs,sh), 1493(vs), 1470(m), 1440(w), 1430(m,sh), 1423(s), 1260(w), 1199(w), 1085(m), 1008(s), 995(s), 880(m,br), 748(s), 690(vs) cm^{-1}. NMR data $^{11}B\{^1H\}$ (CH_2Cl_2, 298K) {ordered as: δ ppm (multiplicity, intensity)} +17.9 (s,2B), +12.7 (s,3B), +8.9 (s,1B), -11.4 (s,2B), -14.8 (s,2B). ^{13}C (*SC*(H)NPh) 179.6 ppm, ^1H (SC(*H*)NPh) 8.4 ppm.

6.4.6 X-ray analysis of *closo*-[2-{η^2-$S_2CN(H)Ph$}-2-(PPh_3)-2,1-$RhTeB_{10}H_{10}$] (230)

Crystal Data: $C_{25}H_{31}B_{10}NPRhS_2Te$, M = 779.22, triclinic, $P\bar{1}$, a = 11.2314(10), b = 11.2743(9), c = 13.5928(10) Å, α = 89.322(6), β = 69.114(7), γ = 81.043(7)°, U = 1586.72(22) Å^3, Z = 2, D_c = 1.631g cm^{-3}, λ(Mo-K$_\alpha$) = 0.7093 Å, μ(Mo-K$_\alpha$) = 1.63 cm^{-1}, F(000) = 760.69, T = 293K, R = 0.018, R_w = 0.035 for 6126 observed reflections.

6.4.7 Reaction of *closo*-[3,3-(PPh_3)$_2$-3-H-3,1,2-$RhC_2B_9H_{11}$] (59) with PhNCS.

Procedure 1

To a solution of *closo*-[3,3-(PPh_3)$_2$-3-H-3,1,2-$RhC_2B_9H_{11}$] (59) (0.10g, 0.131mmol) in CH_2Cl_2 (20mls) was added PhNCS (0.178g, 1.31mmol). The mixture was heated at reflux for 18h. The orange solution was concentrated under reduced pressure (rotatory film evaporator, 25°C). Preparative tlc {CH_2Cl_2 - hexane (3:2)} produced two components: (a) a major orange band (R_f = 0.8) and (b) a minor yellow band (R_f = 0.4).

(a) The orange band was extracted into CH_2Cl_2 and recrystallised as orange-red crystals of *closo*-[3-{η^2-SC(H)NPh}-3-(PPh_3)-3,1,2-$RhC_2B_9H_{11}$] (197) (0.019g, 22.9%). (Found: C, 51.2; H, 5.3; N, 2.0; S, 4.95; B, 15.6, $C_{27}H_{32}B_9NPRhS$ requires C, 51.2; H, 5.1; N, 2.2; S, 5.1; B, 15.35%). IR: ν_{max}(KBr) 3030(w), 2940(w), 2900(vw), 2590(m,sh) (BH), 2560(vs,sh) (BH), 2540(vs) (BH), 2530(vs,sh) (BH), 1580(w), 1502(vs), 1460(m), 1440(w), 1425(m), 1265(w,sh), 1254(m), 1200(w), 1178(w), 1088(s), 1015(w,br), 996(vw), 978(vw), 910(vw), 902(w), 880(w), 844(vw), 800(m,br), 752(s,sh), 743(s), 691(vs) cm^{-1}. ^{11}B and ^{1}H NMR data are given in Table 6.19. ^{13}C {S*C*(H)NPh} 180.9 ppm.

(b) The minor yellow band was extracted into CH_2Cl_2 and recrystallised from CH_2Cl_2 - hexane (3:2) to give pale orange crystals of *closo*-[3-{η^2-$S_2CN(H)Ph$}-3-(PPh_3)-3,1,2-$RhC_2B_9H_{11}$] (229) (0.001g 1.1%). (Found C, 48.3; H, 5.3; N, 2.55, $C_{27}H_{32}B_9NPRhS_2$ requires C, 48.7; H, 4.8; N, 2.1%). IR: ν_{max}(KBr) 3290(w) (NH), 3030(w), 2938(w), 2900(w), 2830(vw), 2530(vs) (BH), 1680(w), 1580(w), 1502(m),

1482(m), 1470(w), 1428(s,sh), 1422(s), 1350(m,br), 1252(w), 1178(vw), 1152(vw), 1089(s), 1020(w), 1010(w), 998(w), 976(w), 800(w,br), 745(m), 690(vs) cm^{-1}. NMR data $^{11}B\{^1H\}$ (CH_2Cl_2, 298K) {ordered as: δ ppm, (multiplicity, intensity)} +5.6 (s,1B), +5.0(s,1B), -6.9(s,4B), -15.3(s,2B), -23.8(s,1B). ^{13}C {$S_2CN(H)Ph$} 209.9 ppm, ^1H (N*H*) 8.2 ppm.

Procedure 2

To a solution of *closo*-[3,3-$(PPh_3)_2$-3-H-3,1,2-$RhC_2B_9H_{11}$] (59) (0.10g, 0.131mmol) in CH_2Cl_2 (20mls) was added PhNCS (0.018g, 0.131mmol). The mixture was heated at reflux for 72h. The reaction mixture was treated as in procedure 1.

(a) The orange band was extracted into CH_2Cl_2 and recrystallised as orange-red crystals of *closo*-[3-{η^2-SC(H)NPh}-3-(PPh_3)-3,1,2-$RhC_2B_9H_{11}$] (197) (0.051g, 61.4%). IR and NMR data were identical to those reported in procedure 1.

(b) The minor yellow band was extracted into CH_2Cl_2 and recrystallised from CH_2Cl_2 - hexane (3:2) to give pale orange crystals of *closo*-[3-{η^2-S_2CN(H)Ph}-3-(PPh_3)-3,1,2-$RhC_2B_9H_{11}$] (229) (0.001g 1.1%). IR and NMR data were identical to those reported in procedure 1.

Procedure 3

Closo-[3,3-$(PPh_3)_2$-3-H-3,1,2-$RhC_2B_9H_{11}$] (59) (0.10g, 0.131mmol), CH_2Cl_2 (20mls) and PhNCS (0.018g, 0.131mmol) were introduced into the glass microwave reaction vessel as described in section 3.4.3. The solution was subjected to microwave irradiation (650W) for 5 minutes. The reaction mixture was treated as in procedure 1. Preparative tlc CH_2Cl_2 - hexane (3:2) produced only one orange band (R_f = 0.8). The orange band was extracted into CH_2Cl_2 and recrystallised as orange-red crystals of *closo*-[3-{η^2-SC(H)NPh}-3-(PPh_3)-3,1,2-$RhC_2B_9H_{11}$] (197) (0.082g, 98.8%). IR and NMR data were identical to those reported in procedure 1.

6.4.8 Reaction of *closo*-[3-{η^2-SC(H)NPh}-3-(PPh_3)-3,1,2-$RhC_2B_9H_{11}$] (197) with PhNCS.

Closo-[3-{η^2-SC(H)NPh}-3-(PPh_3)-3,1,2-$RhC_2B_9H_{11}$] (197) (0.051g, 0.08mmol), CH_2Cl_2 (20ml) and PhNCS (0.108g, 0.80mmol) were introduced into the glass microwave reaction vessel as described in section 3.4.3. The solution was subjected to microwave irradiation (650W) for 45 minutes. The orange solution was concentrated under reduced pressure (rotatory film evaporator, 25°C) and subjected to preparative tlc {CH_2Cl_2 - hexane (3:2)}. The single major band was extracted into CH_2Cl_2 and recrystallised from CH_2Cl_2 - hexane (3:2) as pale orange crystals of *closo*-[3-{η^2-$S_2CN(H)Ph$}-3-(PPh_3)-3,1,2-$RhC_2B_9H_{11}$](229) (0.017g, 31.9%). IR and NMR were identical to those reported in section 6.4.7.

6.4.9 Reaction between *p*-tolylisothiocyanate and *closo*-[3,3-(PPh_3)$_2$-3-H-3,1,2-$RhAs_2B_9H_9$] (58)

Procedure 1

To a solution of *closo*-[3,3-(PPh_3)$_2$-3-H-3,1,2-$RhAs_2B_9H_9$] (58) (0.10g, 0.113mmol) in CH_2Cl_2 (20ml) was added *p*-tolylisothiocyanate (0.169g, 1.13mmol). The mixture was heated at reflux for 18h. The orange solution was concentrated under reduced pressure (rotatory film evaporator, 25°C). Preparative tlc {CH_2Cl_2 - hexane (3:2)} produced two major components: (a) a yellow band (R_f = 0.7) and (b) an orange band (R_f = 0.8)

(a) The yellow band was extracted into CH_2Cl_2 and recrystallised from CH_2Cl_2 - hexane (3:2) as pale orange crystals of *closo*-[3-{η^2-$S_2CNH(p\text{-tol})$}-3-(PPh_3)-3,1,2-$RhAs_2B_9H_9$] (233) (0.024g, 26.4%). (Found: C, 39.2; H, 4.3; N, 1.7, $C_{26}H_{32}As_2B_9NPRhS_2$ requires C, 38.9; H, 4.0; N, 1.7%). IR: ν_{max}(KBr) 3280(m) (NH), 3015(vw), 2925(vw), 2900(w), 2830(vw), 2520(vs) (BH), 1580(m), 1500(s), 1469(w), 1428(m,sh), 1422(s), 1350(s,br), 1305(vw), 1175(vw), 1154(vw), 1087(m), 992(s), 912(w), 881(vw), 868(vw), 809(m), 741(s), 690(vs) cm^{-1}. NMR data $^{11}B\{^1H\}$

(CH_2Cl_2, 298K) {ordered as: δ ppm, (multiplicity, intensity)} +14.7 (s,4B), +7.8 (s,2B), -9.1 (s,3B). ^{13}C {$S_2CNH(p\text{-tol})$} 207.1 ppm, ^1H (N*H*) 7.9 ppm.

(b) The orange band was extracted into CH_2Cl_2 and recrystallised from CH_2Cl_2-hexane (3:2) as orange-red crystals of *closo*-[3-{η^2-SC(H)N(*p*-tol)}-3-(PPh_3)-3,1,2-$RhAs_2B_9H_9$] (234) (0.018g, 20.6%). (Found: C, 40.1; H, 4.4; N, 2.2, $C_{26}H_{32}As_2B_9NPRhS$ requires C, 40.5; H, 4.2; N, 1.8%). IR: ν_{max}(KBr) 3030(w), 2900(w), 2830(w), 2540(vs,sh) (BH), 2518(vs) (BH), 2500(vs,sh) (BH), 1575(vw), 1560(w), 1504(s), 1495(s,sh), 1469(m), 1430(s,sh) 1422(s), 1254(w), 1199(w), 1180(vw), 1081(s), 1001(s,sh), 992(s), 910(vw), 891(s), 848(w), 821(s), 745(s,sh), 739(s), 689(vs), cm^{-1}. NMR data $^{11}B\{^1H\}$ (CH_2Cl_2, 298K) {ordered as: δ ppm, (multiplicity, intensity)} +16.95 (s,2B), +13.8 (s,2B), +7.9 (s,2B), -9.8 (s,3B). ^{13}C {S*C*(H)N(*p*-tol)} 178.7 ppm, ^1H {SC*H*N(*p*-tol)} 8.54 ppm.

Procedure 2

To a solution of *closo*-[3,3-(PPh_3)$_2$-3-H-3,1,2-$RhAs_2B_9H_9$] (58) (0.10g, 0.113mmol) in CH_2Cl_2 (20ml) was added *p*-tolylisothiocyanate (0.0169g, 0.113mmol). The mixture was heated at reflux for 18h. The orange solution was concentrated under reduced pressure (rotatory film evaporator, 25°C). Preparative tlc {CH_2Cl_2 - hexane (3:2)} produced two major components: (a) a yellow band (R_f = 0.7) and (b) an orange band (R_f = 0.8).

a) The yellow band was extracted into CH_2Cl_2 and recrystallised from CH_2Cl_2-hexane (3:2) as pale orange crystals of *closo*-[3-{η^2-$S_2CNH(p\text{-tol})$}-3-(PPh_3)-3,1,2-$RhAs_2B_9H_9$] (233) (0.007g, 7.7%). IR and NMR data were identical to those reported in procedure 1.

(b) The orange band was extracted into CH_2Cl_2 and recrystallised from CH_2Cl_2-hexane (3:2) as orange-red crystals of *closo*-[3-{η^2-SC(H)N(*p*-tol)}-3-(PPh_3)-3,1,2-$RhAs_2B_9H_9$] (234) (0.041g, 47.0%). IR and NMR data were as stated in procedure 1.

6.4.10 Reaction between benzylisothiocyanate and *closo*-[3,3-$(PPh_3)_2$-3-H-3,1,2-$RhAs_2B_9H_9$] (58)

Procedure 1

To a solution of *closo*-[3,3-$(PPh_3)_2$-3-H-3,1,2-$RhAs_2B_9H_9$] (58) (0.10g, 0.113mmol) in CH_2Cl_2 (20ml) was added benzylisothiocyanate (0.168g, 1.130mmol). The mixture was heated at reflux for 18h. The orange solution was concentrated under reduced pressure (rotatory film evaporator, 25°C). Preparative tlc {CH_2Cl_2 - hexane (3:2)} produced *ca.* 10 bands. The single major band was extracted into CH_2Cl_2 and recrystallised from CH_2Cl_2 - hexane (3:2) as pale orange crystals of *closo*-[3-{η^2-$S_2CN(H)Bz$}-3-(PPh_3)-3,1,2-$RhAs_2B_9H_9$] (235) (0.018g, 19.8%). (Found: C, 39.2; H, 4.3; N, 1.8; S, 7.6, $C_{26}H_{32}As_2B_9NPRhS_2$ requires C, 38.9; H, 4.0; N, 1.7; S, 8.0%). IR: ν_{max}(KBr) 3306(m) (NH), 3035(vw), 2900(w), 2830(vw), 2520(vs) (BH), 1595(vw), 1575(vw), 1500(s,br), 1470(s), 1442(m), 1423(s), 1378(m), 1318(m,br), 1230(w), 1180(vw), 1155(vw), 1088(m), 1022(w), 993(s), 740(s), 692(vs) cm^{-1}. NMR data $^{11}B\{^1H\}$ (CH_2Cl_2, 298K) {ordered as: δ ppm, (multiplicity, intensity)} +14.87 (s,4B), +7.9 (s,2B), -8.9 (s,3B). ^{13}C {$S_2CN(H)Bz$} 207.9 ppm, ^1H (N*H*) 6.4 ppm.

Procedure 2

Closo-[3,3-$(PPh_3)_2$-3-H-3,1,2-$RhAs_2B_9H_9$] (58) (0.10g, 0.113mmol), CH_2Cl_2 (20ml) and benzylisothiocyanate (0.0168g, 0.113mmol) were introduced into the glass microwave reaction vessel as described in section 3.4.3. The solution was subjected to microwave irradiation (650W) for 5 minutes. The orange solution was concentrated under reduced pressure (rotatory film evaporator, 25°C). Preparative tlc {CH_2Cl_2 - hexane (3:2)} produced *ca.* 10 bands of which two were in significant amount and were isolated: (a) a major orange band (R_f = 0.8) and (b) a minor yellow band (R_f = 0.4).

(a) The orange band was extracted into CH_2Cl_2 and recrystallised from

CH_2Cl_2-hexane, (3:2) as orange crystals of *closo*-[3-{η^2-SC(H)NBz}-3-(PPh_3)-3,1,2-$RhAs_2B_9H_9$] (236) (0.047g 53.9%). (Found: C, 40.6; H, 4.4; N, 2.0, $C_{26}H_{32}As_2B_9NPRhS$ requires C, 40.5; H, 4.2; N, 1.8%). IR: ν_{max}(KBr) 3030(vw), 2915(w,sh), 2900(w), 2820(w), 2530(s,sh) (BH), 2510(vs) (BH), 2495(s,sh) (BH), 2475(m,sh) (BH), 1543(m), 1478(vw), 1462(m), 1439(m), 1418(s), 1411(w,sh), 1250(m), 1175(vw), 1148(vw), 1081(m), 1018(vw), 992(s,sh), 982(s), 905(vw), 863(m), 745(m,sh), 736(s), 688(s) cm^{-1}. NMR data $^{11}B\{^1H\}$ (CH_2Cl_2, 298K) {ordered as: δ ppm, (multiplicity, intensity)} +17.1 (s,2B), +13.6 (s,2B), +10.7 (s,1B), +6.9 (s,1B), -6.4 (s,2B), -10.7 (s,2B). ^{13}C {S*C*(H)NBz} 181.1 ppm, ^1H {SC*(H)*NBz} 5.3 ppm.

(b) The yellow band was extracted into CH_2Cl_2 and recrystallised from CH_2Cl_2-hexane, (3:2) as pale orange crystals of *closo*-[3-{η^2-S_2CN(H)Bz}-3-(PPh_3)-3,1,2-$RhAs_2B_9H_9$] (235) (0.003g 3.3%). IR and NMR data were identical to those reported in procedure 1.

REFERENCES

1. N. S. Hosmane and J. A. Maguire, *Adv. Organomet. Chem.*, 1990, 30, 99.
2. S. M. Coughlan, Ph.D. Thesis, University College, Cork, 1991.
3. J. P. Sheehan, Ph.D. Thesis, University College, Cork, 1992.
4. Faridoon, Ph.D. Thesis, University College Cork, 1988.
5. J. L. Little, S. S. Pao and K. K. Sugathan, *Inorg. Chem.*, 1974, 13, 1752.
6. X. L. R. Fontaine, J. D. Kennedy, M. McGrath and T. R. Spalding, *Magn. Reson. Chem.*, 1991, 29, 711.
7. G. D. Friesen and L. J. Todd, *J. Chem. Soc., Chem. Commun.*, 1978, 349.
8. G. B. Dunks, K. Barker, E. Hedaya, C. Hefner, K. Palmer-Ordonez and P. Remec, *Inorg. Chem.*, 1981, 20, 1692.
9. T. P. Hanusa, N. Roig de Parisi, J. G. Kester, A. Arafat and L. J. Todd, *Inorg. Chem.*, 1987, 26, 4100.
10. M. F. Hawthorne, D. C. Young, P. M. Garrett, D. A. Owen, S. G. Schwerin, F. N. Tebbe and P. A. Wegner, *J. Am. Chem. Soc.*, 1968, 90, 862.
11. L. J. Todd, A. R. Burke, A. R. Garber, H. T. Silverstein and B. N. Storhoff, *Inorg. Chem.*, 1970, 9, 2175.
12. L. J. Todd, J. L. Little and H. T. Silverstein, *Inorg. Chem.*, 1969, 8, 1698.
13. J. Buchanan, E. J. M. Hamilton, D. Reed and A. J. Welch, *J. Chem. Soc., Dalton Trans.*, 1990, 677.
14. G. Socrates, "Infrared Characteristic Group Frequencies", John Wiley and Sons, New York, 1980.
15. D. O'Connell, T. R. Spalding and G. Ferguson, *Acta Cryst.*, 1991, C47, 492.
16. L. V. Vilkov, L. S. Khaikin, A. F. Zhigach and V. N. Siryatskaya, *Zh. Strukt. Khim.*, 1968, 9, 889.
17. A. L. Rheingold and P. J. Sullivan, *Organometallics*, 1983, 2, 327.
18. O. Ni Dhubhghaill, J. MacCurtain, M. Myers, T. R. Spalding, P. Brint, T. McCabe, G. Ferguson and D. Reed, *Proc. R. Ir. Acad., Sect. B*, 1989, 89, 461.
19. A. Sequeira and W. C. Hamilton, *Inorg. Chem.*, 1967, 6, 1281.

20. W. H. Knoth, J. L. Little, J. R. Lawrence, F. R. Scholer and L. J. Todd, *Inorg. Synthesis*, 1968, 11, 39.

21. L. J. Todd, A. R. Burke, H. T. Silverstein, J. L. Little and G. S. Wikholm, *J. Am. Chem. Soc.*, 1969, 91, 3376.

22. M. McGrath, Ph.D. Thesis, University College, Cork, 1990.

23. L. A. Fedorov, V. I. Kyskin and L. I. Zakharkin, *Izv. Akad. Nauk. SSSR, Ser. Khim.*, 1972, 536.

24. L. I. Zakharkin and V. I. Kyskin, *Izv. Akad. Nauk. SSSR, Ser. Khim.*, 1971, 2053.

25. L. J. Todd in "Comprehesive Organometallic Chemistry", ed. G. Wilkinson, F. G. A. Stone and E. W. Abel, Pergamon Press, Oxford, Vol. 1., 1982, p543.

26. D. C. Beer, A. R. Burke, T. R. Engelmann, B. N. Storhoff and L. J. Todd, *Chem. Commun.*, 1971, 1611.

27. L. I. Zakharkin and V. I. Kyskin, *Zh. Obshch. Khim.*, 1971, 41, 205.

28. A. M. Barriola, T. P. Hanusa and L. J. Todd, *Inorg. Chem.*, 1980, 19, 2801.

29. H. D. Smith, and M. F. Hawthorne, *Inorg. Chem.*, 1974, 13, 2312.

30. A. R. Siedel and L. J. Todd, *J. Chem. Soc., Chem. Commun.*, 1973, 914.

31. H. M. Colquhoun, T. J. Greenhough and M. G. H. Wallbridge, *J. Chem. Research (S)*, 1979, 248.

32. D. A. T. Young, R. J. Wiersema and M. F. Hawthorne, *J. Am. Chem. Soc.*, 1971, 93, 5687.

33. P. Jutzi, D. Wegener and M. Hursthouse, *J. Organomet. Chem.*, 1991, 418, 277.

34. R. B. Maynard, Z-T. Wang, E. Sinn and R. N. Grimes, *Inorg. Chem.*, 1983, 22, 873.

35. J. L. Little, G. D. Friesen and L. J. Todd, *Inorg. Chem.*, 1977, 16, 869.

36. T. Yamamoto and L. J. Todd, *J. Organomet. Chem.*, 1974, 67, 75.

37. J. L. Little and S. S. Pao, *Inorg. Chem.*, 1978, 17, 584.

38. R. R. Rietz, D. F. Dustin and M. F. Hawthorne, *Inorg. Chem.*, 1974, 13, 1580.

39. R. N. Grimes, "Metal Interactions with Boron Clusters", Plenum Press, New York, 1982.

40. D. C. Beer and L. J. Todd, *J. Organomet. Chem.*, 1973, 50, 93.

41. M. F. Hawthorne and T. D. Andrews, *Chem. Commun.*, 1965, 443.

42. C. J. Jones and M. F. Hawthorne, *Inorg. Chem.*, 1973, 12, 608.

43. T. E. Paxson and M. F. Hawthorne, *J. Am. Chem. Soc.*, 1974, 96, 4674.

44. S. A. Jasper, S. Roach, J. N. Stipp, J. C. Huffman and L. J. Todd, *Inorg. Chem.*, 1993, 32, 3072.

45. S. B. Miller and M. F. Hawthorne, *J. Chem. Soc., Chem. Commun.*, 1976, 786.

46. R. E. King, S. B. Miller, C. B. Knobler and M. F. Hawthorne, *Inorg. Chem.*, 1983, 22, 3548.

47. G. K. Barker, M. Green, F. G. A. Stone, A. J. Welch and W. C. Wolsey *J. Chem. Soc., Chem. Commun.*, 1980, 627.

48. R. T. Baker, M. S. Delaney, R. E. King, C. B. Knobler, J. A. Long, T. B Marder, T. E. Paxon, R. G. Teller and M. F. Hawthorne, *J. Am. Chem. Soc.*, 1984, 106, 2965.

49. C. W. Jung and M. F. Hawthorne, *J. Am. Chem. Soc.*, 1980, 102, 3024.

50. C. W. Jung, R. T. Baker and M. F. Hawthorne, *J. Am. Chem. Soc.*, 1981, 103, 810.

51. J. P. Collman and L. S. Hegedus, "Principles and Applications of Organotransition Metal Chemistry", University Science Books, Mill Valley, California, 1980.

52. T. B. Marder, R. T. Baker, J. A. Long, J. A. Doi and M. F. Hawthorne, *J. Am. Chem. Soc.*, 1981, 103, 2988.

53. M. McGrath, T. R. Spalding, X. L. R. Fontaine, J. D. Kennedy and M. Thornton-Pett, *J. Chem. Soc., Dalton Trans.*, 1991, 3223.

54. G. K. Barker, M. Green, F. G. A. Stone, W. C. Wolsey and A. J. Welch, *J. Chem. Soc., Dalton Trans.*, 1983, 2063.

55. L. J. Todd and A. R. Siedle, *Prog. Nucl. Magn. Reson. Spectrosc.*, 1979, 13, 87.

56. M. Green, J. L. Spencer, F. G. A. Stone and A. J. Welch, *J. Chem. Soc., Dalton Trans.*, 1975, 179.

57. M. Green, J. L. Spencer, F. G. A. Stone and A. J. Welch, *J. Chem. Soc., Chem. Commun.*, 1974, 571.

58. J. P. Breen, M.Sc. Thesis, University College, Cork, 1991.

59. J. L. Little, *Inorg. Chem.*, 1979, 18, 1598.

60. J. L. Little, M. A. Whitesell, J. G. Kester, K. Folting and L. J. Todd, *Inorg. Chem.*, 1990, 29, 804.

61. J. L. Little and A. C. Wong, *J. Am. Chem. Soc.*, 1971, 93, 522.

62. J. L. Little, J. T. Moran and L. J. Todd, *J. Am. Chem. Soc.*, 1967, 89, 5495.

63. T. D. Getman, Hai-Bin Deng, Leh-Yea Hsu and S. G. Shore, *Inorg. Chem.*, 1989, 28, 3612.

64. J. L. Little, *Inorg. Chem.*, 1976, 15, 114.

65. J. L. Little, J. G. Kester, J. C. Huffman and L. J. Todd, *Inorg. Chem.*, 1989, 28, 1087.

66. J. L. Little, M. A. Whitesell, R. W. Chapman, J. G. Kester, J. C. Huffman and L. J. Todd, *Inorg. Chem.*, 1993, 32, 3369.

67. W. Haubold, W. Keller and G. Sawitzki, *Angew. Chem. Int. Ed. Engl.*, 1988, 27, 925.

68. F. Meyer, P. Paetzold and U. Englert, *Chem. Ber.*, 1994, 127, 93.

69. L. B. Friedman and S. L. Perry, *Inorg. Chem.*, 1973, 12, 288.

70. M. A. Beckett and J. D. Kennedy, *J. Chem. Soc., Chem. Commun.*, 1983, 575.

71. D. E. Coons and D. F. Gaines, *Inorg. Chem.*, 1987, 26, 1985.

72. R. W. Miller, K. J. Donaghy and J. T. Spencer, *Organometallics*, 1991, 10, 1161.

73. J. A. Glass, T. A. Whelan and J. T. Spencer, *Organometallics*, 1991, 10, 1148.

74. J. Feilong, T. P. Fehlner and A. L. Rheingold, *J. Chem. Soc., Chem. Commun.*, 1987, 1395.

75. S. R. Bunkhall, X. L. R. Fontaine, N. N. Greenwood, J. D. Kennedy and M. Thornton-Pett, *J. Chem. Soc., Dalton Trans.*, 1990, 73.

76. F. R. Schloer and L. J. Todd, "Preparative Inorganic Reactions", ed. W. J. Jolly, John Wiley and Sons, New York, 1971.
77. L. I. Zakharkin and V. I. Kyskin, *Zh. Obshch. Khim.*, 1970, 40, 2241.
78. L. I. Zakharkin and V. I. Kyskin, *Zh. Obshch. Khim.*, 1969, 39, 928.
79. L. I. Zakharkin and V. I. Kyskin, *Izv. Akad. Nauk. SSSR, Ser. Khim.*, 1969, 1197.
80. L. I. Zakharkin and V. I. Kyskin, *Zh. Obshch. Khim.*, 1970, 40, 2234.
81. H. S. Wong and W. N. Lipscomb, *Inorg. Chem.*, 1975, 14, 1350.
82. P. S. Welcker and L. J. Todd, *Inorg. Chem.*, 1970, 9, 286.
83. L. J. Todd, I. C. Paul, J. L. Little, P. S. Welker and C. R. Peterson, *J. Am. Chem. Soc.*, 1968, 90, 4489.
84. W. F. Wright, J. C. Huffman and L. J. Todd, *J. Organomet. Chem.*, 1978, 148, 7.
85. N. S. Hosmane, K. Lu, A. H. Cowley and M. A. Mardones, *Inorg. Chem.*, 1991, 30, 1325.
86. W. Keller, B. A. Barnum, J. W. Bausch and L. G. Sneddon, *Inorg. Chem.*, 1993, 32, 5058.
87. W. N. Lipscomb, "Boron Hydrides", Benjamin, New York, 1963, p275.
88. K. Wade, *Adv. Inorg. Chem. Radiochem.*, 1976, 18, 1.
89. A. J. Stone, *Mol. Phys.*, 1980, 41, 1339.
90. A. J. Stone, *Inorg. Chem.*, 1981, 20, 563.
91. M. J. S. Dewar and W. Thiel, *J. Am. Chem. Soc.*, 1977, 99, 4899.
92. D. M. P. Mingos, P. C. Minshall, M. B. Hursthouse, K. M. A. Malik and S. D. Willoughby, *J. Organomet. Chem.*, 1979, 181, 169.
93. D. G. Evans and D. M. P. Mingos, *J. Organomet. Chem.*, 1982, 240, 321.
94. M. J. S. Dewar and M. L. McKee *Inorg. Chem.*, 1980, 19, 2662.
95. D. Hnyk, E. Vajda, M. Buhl and P. von Rague Schleyer, *Inorg. Chem.*, 1992, 31, 2464.
96. P. Brint, B. Sangchakr, M. McGrath, T. R. Spalding and R. J. Suffolk, *Inorg. Chem.*, 1990, 29, 47.

97. Fairdoon, O. Ni Dhubhghaill, T. R. Spalding, G. Ferguson, B. Kaitner, X. L. R. Fontaine, J. D. Kennedy and D. Reed, *J. Chem. Soc., Dalton Trans.*, 1988, 2739.

98. J. MacCurtain, P. Brint and T. R. Spalding, *J. Chem. Soc., Dalton Trans.*, 1985, 2591.

99. O. Ni Dhubhghaill, D. Reed and T. R. Spalding, *Polyhedron*, 1993, 12, 1977.

100. M. J. S. Dewar and M. L. McKee, *Inorg. Chem.*, 1978, 17, 1569.

101. B. Stibr, T. Jelinek, J. D. Kennedy, X. L. R. Fontaine and M. Thornton-Pett, *J. Chem. Soc., Dalton Trans.*, 1993, 1261.

102. B. Stibr, K. Base, T. Jelinek, X. L. R. Fontaine, J. D. Kennedy and M. Thornton-Pett, *Collect. Czech. Chem. Commun.*, 1991, 56, 646.

103. J. D. Kennedy, *Prog. Inorg. Chem.*, 1986, 34, 211.

104. G. Ferguson, M. C. Jennings, A. J. Lough, S. Coughlan, T. R. Spalding, J. D. Kennedy, X. L. R. Fontaine and B. Stibr, *J. Chem. Soc., Chem. Commun.*, 1990, 891.

105. D. M. P. Mingos and D. R. Baghurst, *Chem. Soc. Rev.*, 1991, 20, 1.

106. H. Frohlich, "Theory of Dieletrics", Oxford University Press, London, 1958.

107. A. R. von Hippel, "Dieletric Materials and Applications", John Wiley and Sons, New York, 1954.

108. A. R. von Hippel, "Dieletrics and Waves", John Wiley and Sons, New York, 1954.

109. R. N. Gedye, F. E. Smith, K. G. Westaway, H. Ali, L. Balderisa, L. Laberge and J. Rousell, *Tet. Lett.*, 1986, 27, 279.

110. R. J. Giguere, T. L. Bray, S. N. Duncan and G. Majetich, *Tet. Lett.*, 1986, 27, 4945.

111. R. A. Abramovich, *Org. Prep. Proced. Int.*, 1991, 23, 685.

112. A. K. Bose, M. S. Manhas, M. Ghosh, M. Shah, V. S. Raju, S. S. Bari, S. N. Newaz, B. K. Banik, A. G. Chaudharry and K. J. Barakat, *J. Organic Chem.*, 1991, 56, 6968.

113. A. K. Bose, M. S. Manhas, M. Ghosh, V. S. Raju, K. Tabei and Z. Urbanczyk-Lipkowska, *Heterocycles*, 1990, 30, 471.

114. D. R. Baghurst and D. M. P. Mingos, *J. Organomet. Chem.*, 1990, 384, C57.

115. Simson 380 M Microwave Leakage Detector, Simpson Eletric Company Eglin, Illinois 60120, USA.

116. Q. Dabirmanesh and R. M. G. Roberts, *J. Organomet. Chem.*, 1993, 460, C28.

117. D. R. Baghurst and D. M. P. Mingos, *J. Chem. Soc., Dalton Trans.*, 1992, 1151.

118. Instrument workshop, (Mr. Mick O'Shea), Chemistry Deptartment, University College, Cork, Ireland.

119. Glassblowing workshop, (Mr. Derry Kearney), Chemistry Department, University College, Cork, Ireland.

120. Radionics, Dublin 12, Ireland.

121. Swagelock Co., Solon Ohio, 44139, U.S.A.

122. Kemtron (Ireland) Ltd., South Cork Industrial Estate, Cork, Ireland.

123. Instrument workshop, (Mr. Tony Hogan), Chemistry Department, University College, Cork, Ireland.

124. Instrument workshop, (Mr. Johnny Ryan), Chemistry Department, University College, Cork, Ireland.

125. Kane-May Infratrace 800, C.P. Instrument Co. Ltd., Herts., England.

126. J. A. Hesek and R. C. Wilson, *Anal. Chem.*, 1974, 46, 1160.

127. G. Schnitzer, C. Pellerin and G. Clouet, *Laboratory Practice,* 1988, 37, 63.

128. W. Van Delft and G. Vos, *Anal. Chim. Acta.*, 1988, 209, 147.

129. D. R. Baghurst, D. Phil. Thesis, University of Oxford, 1992.

130. J. Nieuwenhuize, C. H. Poley-Vos, A. H. Van den Akker and W. Van Delft, *Analyst,* 1991, 116, 347.

131. P. J. Lamothe, T. L. Fries and J. J. Consul, *Anal. Chem.* 1986, 58, 1881.

132. N. Ybanez, M. L. Cervera, R. Montoro and M. De la Guardia, *J. Anal. Atomic Spectrom.*, 1991, 6, 379.

133. P. Hocquellet and M. P. Candillier, *Analyst*, 1991, 116, 505.

134. L. B. Fischer, *Anal. Chem.*, 1986, 58, 261.

135. R. N. Gedye, F. E. Smith and K. G. Westaway, *Can. J. Chem.*, 1988, 66, 17.

136. R. N. Gedye, F. E. Smith and K. G. Westaway, *Educ. Chem.*, 1988, 25, 55.

137. R. J. Giguere, A. M. Namen, B. O. Lopez, A. Arepally, D. E. Ramos, G. Majetich and J. Defauw, *Tet. Lett.*, 1987, 28, 6553.

138. G. Giordano and R. H. Crabtree, *Inorg. Synth.*, 1979, 19, 218.

139. E. W. Abel, M. A. Bennett and G. Wilkinson, *J. Chem. Soc.*, 1959, 3178.

140. J. L. Herde, J. C. Lambert and C. V. Senoff, *Inorg. Synth.*, 1974, 15, 18.

141. D. R. Baghurst, D. M. P. Mingos and M. J. Watson, *J. Organomet. Chem.*, 1989, 368, C43.

142. D. R. Baghurst, S. R. Cooper, D. L. Green, D. M. P. Mingos and S. M. Reynolds, *Polyhedron*, 1990, 9, 893.

143. A. G. Whittaker and D. M. P. Mingos, *J. Chem. Soc., Dalton Trans.*, 1993, 2541.

144. J. Emsley, *New Scientist*, 12th Nov. 1988, p. 56.

145. D. R. Baghurst and D. M. P. Mingos, *J. Chem. Soc., Chem. Commun.*, 1992, 674.

146. C. Peterson, *New Scientist*, 9th September, 1989, 123, 44.

147. D. R. Baghurst, R. C. B. Copley, H. Fleischer, D. M. P. Mingos, G. O. Kyd, L. J. Yellowlees, A. J. Welch, T. R. Spalding and D. O'Connell, *J. Organomet. Chem.*, 1993, 447, C14.

148. E. I. Topin and W. N. Lipscomb, *J. Am. Chem. Soc.*, 1973, 95, 2384.

149. H. Beall and C. H. Bushweller, *Chem. Rev.*, 1973, 73, 465.

150. J. Borlin and D. F. Gaines, *J. Am. Chem. Soc.*, 1972, 94, 1367.

151. J. D. Kennedy, Ch 8 in "Multinuclear NMR" ed. J. Mason, Plenum, New York, 1987.

152. G. Ferguson, J. D. Kennedy, X. L. R. Fontaine, Faridoon and T. R. Spalding, *J. Chem. Soc., Dalton Trans.*, 1988, 2555.

153. H. Kessler, *Angew. Chem. Int. Ed. Engl.*, 1970, 9, 219.

154. J. A. Pople, W. G. Schneider and H. J. Bernstein, "High Resolution Nuclear Magnetic Resonance", McGraw-Hill, New York, 1959.

155. F. A. L. Anet and A. J. R. Bourn, *J. Am. Chem. Soc.*, 1967, 89, 760.

156. A. Rauk, L. C. Allen and K. Mislow, *Angew. Chem. Int. Ed. Engl.*, 1970, 9, 400.

157. D. Kost, E. H. Carlson and M. Raban, *Chem. Commun.*, 1971, 656.

158. M. Takeda and E. O. Stejskal, *J. Am. Chem. Soc.*, 1960, 82, 25.

159. A. Allerhand, H. S. Gutowsky, J. Jonas and R. A. Meinzer, *J. Am. Chem. Soc.*, 1966, 88, 3185.

160. J. D. Kennedy, University of Leeds, England, personal communication, 1993.

161. X. L. R. Fontaine, N. N. Greenwood, J. D. Kennedy, K. Nestor, M. Thornton-Pett, S. Hermanek, T. Jelinek and B. Stibr, *J. Chem. Soc., Dalton Trans.*, 1990, 681.

162. D. M. P. Mingos, M. I. Forsyth and A. J. Welch, *J. Chem. Soc., Dalton Trans.*, 1978, 1363.

163. A. J. Welch, *J. Chem. Soc., Dalton Trans.*, 1975, 1473.

164. Faridoon, O. Ni Dhubhghaill, T. R. Spalding, G. Ferguson, B. Kaitner, X. L. R. Fontaine and J. D. Kennedy, *J. Chem. Soc., Dalton Trans.*, 1989, 1657.

165. L. Pauling, "The Nature of the Chemical Bond", 3rd ed., Cornell University Press, Ithaca, New York, 1960.

166. N. W. Alcock, J. G. Taylor and M. G. H. Wallbridge, *J. Chem. Soc., Dalton Trans*, 1987, 1805.

167. D.M.P. Mingos, M. I. Forsyth and A. J. Welch, *J. Chem. Soc., Chem. Commun.*, 1977, 605.

168. D. M. P. Mingos, *J. Chem. Soc., Dalton Trans.*, 1977, 602.

169. R. N. Grimes, "Carboranes", Academic Press, New York and London, 1970.

170. D. J. Wales and A. J. Stone, *Inorg. Chem.*, 1987, 26, 3845.

171. B. M. Gimarc, D. S. Warren, J. J. Ott and C. Brown, *Inorg. Chem.*, 1991, 30, 1598.

172. G. M. Edvenson and D. F. Gaines, *Inorg. Chem.*, 1990, 29, 1210.

173. B. F. G. Johnson, Y. V. Roberts and E. Parisini, *Inorg. Chim. Acta*, 1993, 211, 17.

174. D. J. Wales, *J. Am. Chem. Soc.*, 1993, 115, 1557.

175. S. A. Brew, J. C. Jeffrey, M. U. Pilotti and F. G. A. Stone, *J. Am. Chem. Soc.*, 1990, 112, 6148.

176. J. A. Doi, E. A. Mizusawa, C. B. Knobler and M. F. Hawthorne, *Inorg. Chem.*, 1984, 23, 1482.

177. M. K. Kaloustian, R. J. Wiersema and M. F. Hawthorne, *J. Am. Chem. Soc.*, 1972, 94, 6679.

178. M. K. Kaloustian, R. J. Wiersema and M. F. Hawthorne, *J. Am. Chem. Soc.*, 1971, 93, 4912.

179. Z. G. Lewis and A. J. Welch, *J. Organomet. Chem.*, 1992, 430, C45.

180. Commission on Nomenclature of Inorganic Chemistry, *Pure Appl. Chem.*, 1972, 30, 683.

181. S. Wu and M. Jones, *J. Am. Chem. Soc.*, 1989, 111, 5373.

182. W. N. Lipscomb, *Science*, 1966, 153, 373.

183. H. D. Kaesz, R. Bau, H. A. Beall and W. N. Lipscomb, *J. Am. Chem. Soc.*, 1967, 89, 4218.

184. D. Grafstein and J. Dvorak, *Inorg. Chem.*, 1963, 2, 1128.

185. L. I. Zakharkin and V. N. Kalinin, *Dokl. Akad. Nauk. SSSR.*, 1966, 169, 590.

186. E. L. Muetterties and W. H. Knoth, "Polyhedral Boranes", Marcel Deker, New York, 1968.

187. D. D. Perrin, W. L. F. Amatego and D. R. Perrin, "Purification of Laboratory Chemicals", Pergamon Press, 1966.

188. M. B. Hursthouse, R. A. Jones, K. M. A. Malik and G. Wilkinson, *J. Am. Chem. Soc.*, 1979, 101, 4128.

189. G. M. Sheldrick, SHELX-76, Program System for X-Ray Structure Determination, University of Cambridge, 1976.

190. E. J. Gabe, Y. LePage, J. P. Charland, F. L. Lee and P. S. White, *J. Appl. Cryst.*, 1989, 22, 384.

191. Supplied in Ireland by Radionics, Dublin 12.

192. J. Plesek, S. Hermanek and B. Stibr, *Inorg. Synth.*, 1983, 22, 231.

193. G. B. Kaufman and D. O. Cowan, *Inorg. Synth.*, 1960, 6, 211.

194. C. E. Housecroft, Chap. 4 in "Organometallic Chemistry", Ed. E. W. Able, S. P. R., The Royal Society of Chemistry, London, 1992, vol 21.

195. C. E. Housecroft, Chap. 4, in "Organometallic Chemistry", Eds. E. W. Able and F. G. A. Stone, S. P. R., The Royal Society of Chemistry, London, 1991, vol 20.

196. M. A. Beckett, *Annu. Rep. Prog. Chem., Sect. A.*, 1990, 87, 3.

197. J. P. Sheehan, T. R. Spalding, G. Ferguson, J. F. Gallagher, B. Kaitner and J. D. Kennedy, *J. Chem. Soc., Dalton Trans.*, 1993, 35.

198. C. J. Jones, J. N. Francis and M. F. Hawthorne, *J. Am. Chem. Soc.*, 1973, 95, 7633.

199. M. F. Hawthorne, L. F. Warren, K. P. Callahan and N. F. Travers, *J. Am. Chem. Soc.*, 1971, 93, 2407.

200. H. C. Kang, S. S. Lee, C. B. Knobler and M. F. Hawthorne, *Inorg. Chem.*, 1991, 30, 2024.

201. N. L. Douek and A. J. Welch, *J. Chem. Soc., Dalton Trans.*, 1993, 1917.

202. I. T. Chizhevsky, I. V. Pisareva, P. V. Petrovski, V. I. Bregadze, A. I. Yanovsky, Y. T. Struchkov, C. B. Knobler and M. F. Hawthorne, *Inorg. Chem.*, 1993, 32, 3393.

203. O. J. Scherer and H. Jungmann, *J. Organomet. Chem.*, 1981, 208, 153.

204. M. A. Bennett, R. J. H. Clark and D. L. Milner, *Inorg. Chem.*, 1967, 6, 1647.

205. W. C. Kalb, C. W. Kreimendahl, D. C. Busby and M. F. Hawthorne, *Inorg. Chem.*, 1980, 19, 1590.

206. A. G. Orpen, L. Brammer, F. H. Allen, O. Kennard, D. G. Watson and R. Taylor, *J. Chem. Soc., Dalton Trans.*, 1989, S1.

207. M. Kubota, S. Ohba and Y. Saito, *Acta. Cryst.*, 1991, C47, 1727.

208. N. A. Bailey, N. W. Walker and J. A. W. Williams, *J. Organomet. Chem.*, 1972, 37, C49.

209. N. A. Bailey and R. Mason, *J. Chem. Soc., (A),* 1968, 2594.

210. G. Ferguson, J. F. Gallagher, M. McGrath, J. P. Sheehan, T. R. Spalding and J. D. Kennedy, *J. Chem. Soc., Dalton Trans.*, 1993, 27.

211. J. C. Patterson, University College, Cork, unpublished results 1994.

212. W. E. Carroll, M. Green, F. G. A. Stone and A. J. Welch, *J. Chem. Soc., Dalton Trans.*, 1975, 2263.

213. E. J. M. Hamilton and A. J. Welch, *Acta. Cryst.*, 1990, C46, 1228.

214. E. Mizusawa, S. E. Rudnick and K. Eriks, *Inorg. Chem.*, 1980, 19, 1188.

215. K. D. Schramm and J. A. Ibers, *Inorg. Chem.*, 1977, 16, 3287.

216. E. J. M. Hamilton and A. J. Welch, *Polyhedron*, 1991, 10, 471.

217. V. Subrtova, C. Novak, A. Linek and J. Hasek, *Acta. Cryst.*, 1984, C40, 1955.

218. C. J. M. Stirling, "The Chemistry of the Sulphonium Group", John Wiley and sons, New York, 1981.

219. V. G. Adrianov and Yu. T. Struchkov, *Izv. Akad. Nauk SSSR*, 1977, 26, 687.

220. V. G. Adrianov and Yu. T. Struchkov, *Bull. Acad. Sci. USSR*, 1977, 26, 624.

221. D. E. Smith and A. J. Welch, *Acta. Cryst.*, 1986, C42, 1717.

222. H. M. Colquhoun, T. J. Greenhough and M. G. H. Wallbridge, *J. Chem. Soc., Dalton Trans.*, 1985, 761.

223. M. Murphy, University College, Cork, unpublished results 1994.

224. F. Teixidor, A. Romerosa, C. Vinas, J. Rius, C. Miravittles and J. Casabo, *J. Chem. Soc., Chem. Commun.*, 1991, 192

225. C. B. Knobler, T. B. Marder, E. A. Mizusawa, R. G. Teller, J. A. Long, P. E. Benken and M. F. Hawthorne, *J. Am. Chem. Soc.*, 1984, 106, 2990.

226. J. A. Walker, L. Zheng, C. B. Knobler, J. Soto and M. F. Hawthorne, *Inorg. Chem.*, 1987, 26, 1608.

227. S. Z. Goldberg, C. Kubiak, C. D. Meyer and R. Eisenberg, *Inorg. Chem.*, 1975, 14, 1650.

228. M. R. Churchill, S. A. Julis and F. J. Rotella, *Inorg. Chem.*, 1977, 16, 1137.

229. W. H. Knoth, H. C. Miller, J. C. Sauer, J. H. Balthis, Y. T. Chia and E. L. Muetterties, *Inorg. Chem.*, 1964, 3, 159.

230. J. A. Belmont, J. Soto, R. E. King, A. J. Donaldson, J. D. Hewes and M. F. Hawthorne, *J. Am. Chem. Soc.*, 1989, 111, 7475.

231. M. F. Hawthorne, A. Varadarajan, C. B. Knobler and S. Chakrabarti, *J. Am. Chem. Soc.*, 1990, 112, 5365.

232. M. F. Hawthorne, *Angew. Chem. Int. Ed. Engl.*, 1993, 32, 950.

233. G. E. Hardy, K. P. Callahan, C. E. Strouse and M. F. Hawthorne, *Acta. Cryst.*, 1976, B32, 264.

234. J. A. Long, T. B. Marder, P. E. Behnken and M. F. Hawthorne, *J. Am. Chem. Soc.*, 1984, 106, 2979.

235. L. N. Lewis, *Chem. Rev.*, 1993, 93, 2693.

236. Faridoon, M. McGrath, T. R. Spalding, X. L. R. Fontaine, J. D. Kennedy and M. Thornton-Pett, *J. Chem. Soc., Dalton Trans.*, 1990, 1819.

237. G. Ferguson, Faridoon and T. R. Spalding, *Acta Cryst.*, 1988, C44, 1371.

238. P. Braunstein and D. Nobel, *Chem. Rev.*, 1989, 89, 1927.

239. J. D. Wilkins, *J. Organomet. Chem.*, 1974, 65, 383.

240. R. D. Adams, Z. Dawoodi, D. F. Foust and B. E. Segmuller, *Organometallics*, 1983, 2, 315.

241. V. Crocq, J. Daran and Y. Jeannin, *J. Organomet. Chem.*, 1989, 373, 85.

242. D. Seyferth, G. B. Womack, C. M. Archer, J. P. Fackler and D. O. Marler, *Organometallics*, 1989, 8, 443.

243. G. Hogarth and E. Skordalakis, *J. Organomet. Chem.*, 1993, 458, C8.

244. A. K. Mukerjee and R. Ashare, *Chem. Rev.*, 1991, 91, 1.

245. J. A. E. Gibson and M. Cowie, *Organometallics*, 1984, 3, 984.

246. C. Bianchini, D. Masi, C. Mealli and A. Meli, *Inorg. Chem.*, 1984, 23, 2838.

247. C. Bianchini, D. Masi, C. Mealli and A. Meli, *J. Organomet. Chem.*, 1983, 247, C29.

248. I. R. Beaumont, M. J. Begley, S. Harrison and A. H. Wright, *J. Chem. Soc., Chem. Commun.*, 1990, 1713.

249. P. Jernakoff and N. J. Cooper, *J. Am. Chem. Soc.*, 1989, 111, 7424.

250. W. Bertleff and H. Werner, *Chem. Ber.*, 1982, 115, 1012.

251. H. Werner, *Coord. Chem Rev.*, 1982, 43, 165.

252. R. O. Harris, J. Powell, A. Walker and P. V. Yaneff, *J. Organomet. Chem.*, 1977, 141, 217.

253. M. C. Baird and G. Wilkinson, *J. Chem. Soc. (A)*, 1967, 865.

254. H. G. Raubenheimer, L. Linford, G. Kruger and A. Lombard, *J. Chem. Soc., Dalton Trans.*, 1991, 2795.

255. E. P. Cullen, J. Fortune, A. R. Manning, P. McArdle, D. Cunningham and F. S. Stephens, *Organometallics,* 1990, 9, 1443.

256. R. Rossi, A. Marchi, A. Duatti, L. Magon, U. Casellato and R. Graziani, *J. Chem. Soc., Dalton Trans.,* 1987, 2299.

257. C. Bianchini, C. A. Ghilardi, A. Meli, S. Midollini and A. Orlandini, *Inorg. Chem.,* 1985, 24, 932.

258. H. Brunner, H. Buchner and J. Wachter, *J. Organomet. Chem.,* 1983, 244, 247.

259. W. P. Fehlhammer and A. Mayr, *J. Organomet. Chem.,* 1980, 191, 153.

260. K. J. Edwards, J. S. Field, R. J. Haines, B. Homann, J. Sundermeyer and S. F. Woollam, *J. Organomet. Chem.,* 1990, 386, C1.

261. W. Mei, L. Shiwei, B. Meizhi and G. Hefu, *J. Organomet. Chem.,* 1993, 447, 227.

262. R. Rossi, A. Marchi, A. Duatti, L. Magon, U. Casellato and R. Graziani, *J. Chem. Soc., Dalton Trans.,* 1988, 1857.

263. S. P. Abraham, N. Narasimhamurthy, M. Nethaji and A. G. Samuelson, *Inorg. Chem.,* 1993, 32, 1739.

264. R. M. Silverstein, G. C. Bassler and T. C. Morrill, "Spectrometric Identification of Organic Compounds", John Wiley and Sons, New York, 1981.

265. R. J. Restivo, G. Ferguson, D. J. O'Sullivan and F. J. Lalor, *Inorg. Chem.,* 1975, 14, 3046.

266. A. J. Blake, J. D. Fotheringham and T. A. Stephenson, *Acta. Cryst.,* 1992, C48, 1485.

267. A. R. Hendrickson, R. L. Martin and D. Taylor, *Aust. J. Chem.,* 1976, 29, 269.

268. S. C. Abrahams, *Quart. Rev., (London),* 1956, 10, 407.

269. A. H. Guenther, *J. Chem. Phys.,* 1959, 31, 1095.

270. S. P. Abraham, N. Narasimhamurthy, M. Nethaji and A. G. Samuelson, *Inorg. Chem.,* 1993, 32, 1739.

271. M. Kato, M. Kawano, H. Taniguchi, M. Funaki, H. Moriyama, T. Sato and K. Matsumoto, *Inorg. Chem.,* 1992, 31, 26.

272. H. Werner, O. Kolb, R. Feser and U. Schubert, *J. Organomet. Chem.*, 1980, 191, 283.

273. A. A. Newman, "Chemistry and Biochemistry of Thiocyanic Acid and its Derivatives", Academic Press, London, 1975.

274. A. Kjekshus and T. Rakke, *Acta. Chem. Scand.*, 1974, A28, 99.

275. G. Bombieri, R. Graziani, C. Panattoni, L. Volponi, R. J. H. Clark and G. Natile, *J. Chem. Soc. (A)*, 1970, 14.

276. A. M. Arif, R. A. Jones, M. H. Seeberger, B. R. Whittlesey and T. C. Wright, *Inorg. Chem.*, 1986, 25, 3943.

277. M. A. Petrie, M. M. Olmstead, H. Hope, R. A. Bartlett and P. P. Power, *J. Am. Chem. Soc.*, 1993, 115, 3221.

278. A. J. Blake, J. D. Fotheringham, T. A. Stephenson, S. G. Hambling and L.Sawyer, *Acta Cryst.*, 1991, C47, 648.

279. G. Ferguson, S. Coughlan and T. R. Spalding, *Acta. Cryst.*, 1993, C49, 957.

280. M. DiVaira, D. Rovai and P. Stoppioni, *Polyhedron*, 1993, 12, 13.

281. D. J. Cole-Hamilton and T. A. Stephenson, *J. Chem. Soc., Dalton Trans.*, 1974, 1818.

282. G. Ferguson, Faridoon and T. R. Spalding, *Acta Cryst.*, 1988, C44, 1368.

283. H. L. M. Van Gaal, J. W. Diesveld, F. W. Pijpers and J. G. M. Van Der Linden, *Inorg. Chem.*, 1979, 18, 3251.